On the assessment of multiaxial fatigue resistance of welded steel joints in marine structures when exposed to non-proportional constant amplitude loading

van Lieshout, P.S.

DOI
10.4233/uuid:afd39f40-7569-4cc6-ac1a-659342b45f9a

Publication date
2020

Document Version
Final published version

Citation (APA)
van Lieshout, P. S. (2020). *On the assessment of multiaxial fatigue resistance of welded steel joints in marine structures when exposed to non-proportional constant amplitude loading*. [Dissertation (TU Delft), Delft University of Technology]. https://doi.org/10.4233/uuid:afd39f40-7569-4cc6-ac1a-659342b45f9a

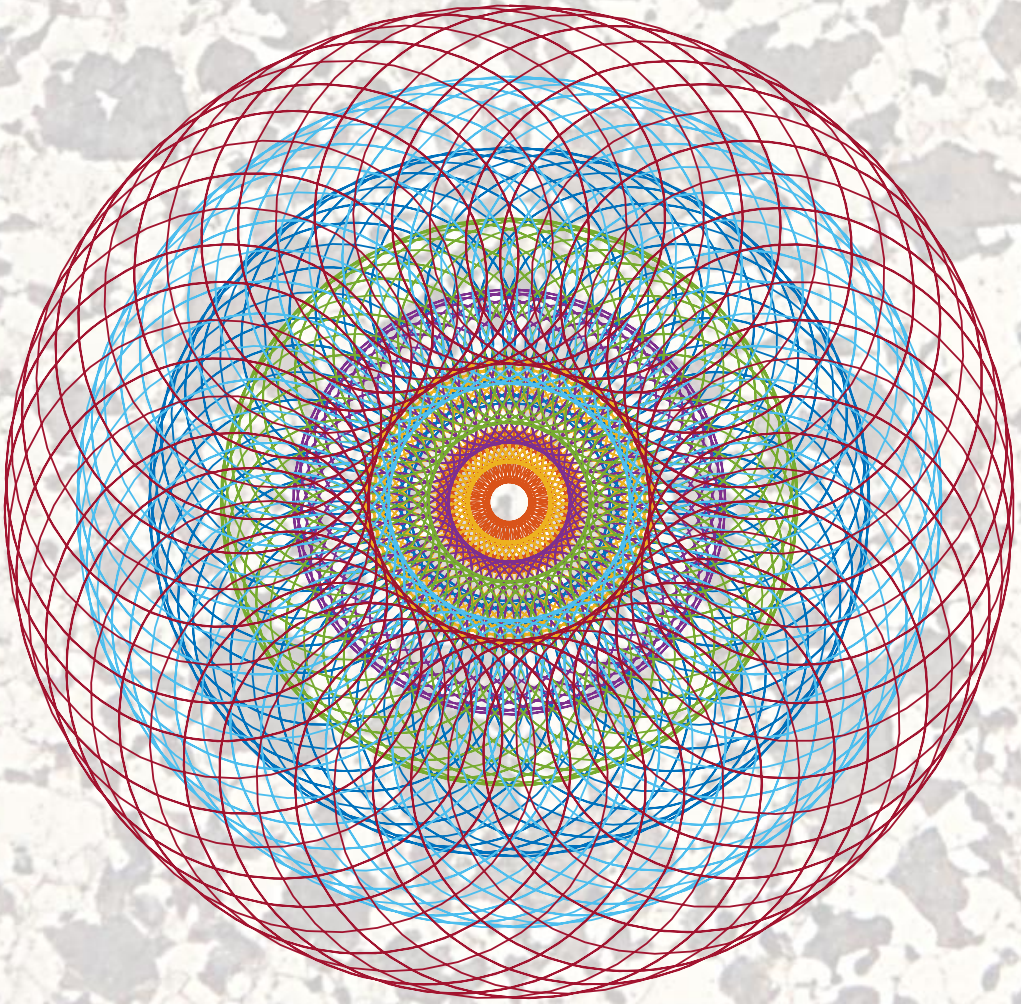

On the assessment of multiaxial fatigue resistance of welded steel joints in marine structures when exposed to non-proportional constant amplitude loading

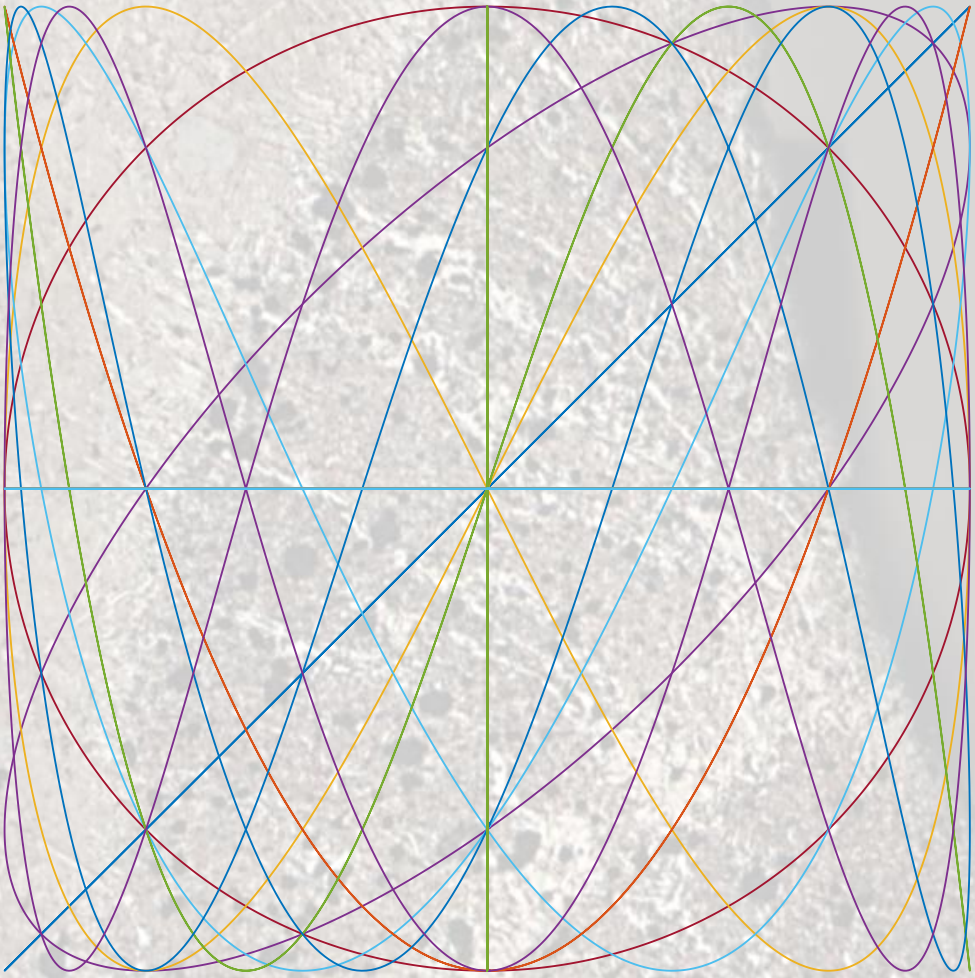

by P.S. van Lieshout

On the assessment of multiaxial fatigue resistance of welded steel joints in marine structures when exposed to non-proportional constant amplitude loading

Dissertation

for the purpose of obtaining the degree of doctor
at Delft University of Technology
by the authority of the Rector Magnificus Prof.dr.ir. T.H.J.J. van der Hagen
Chair of the Board for Doctorates
to be defended publicly on
Wednesday the 22nd of January 2020 at 15:00.

by

Paula Suzanne van LIESHOUT

Master of Science in Offshore and Dredging Engineering
Delft University of Technology, the Netherlands
born in Breda, the Netherlands

This dissertation has been approved by the promotor.

Composition of the doctoral committee:

Rector Magnificus	Chairperson
Prof. Dr. Ir. M.L. Kaminski	Delft University of Technology, promotor
Dr. Ir. J.H. den Besten	Delft University of Technology, copromotor
Independent members:	
Prof. Dr. C.M. Sonsino	Fraunhofer Institute for Structural Durability and System Reliability LBF, Darmstadt, Germany
Dr. S. Mahérault-Mougin	Bureau Veritas, Paris, France
Prof. Dr. Ir. J. Maljaars	Eindhoven University of Technology
Prof. Dr. M. Veljkovic	Delft University of Technology
Dr. V. Popovich	Delft University of Technology
Reserve member:	
Prof. Dr. Ir. R.H.M. Huijsman	Delft University of Technology

This research was supported and funded by the 4D-Fatigue Joint Industry Project (JIP), Nederlandse Organisatie voor Wetenschappelijk Onderzoek (NWO) and Delft University of Technology.

Keywords: marine structures, multiaxial fatigue, steel, welded joints, non-proportional, constant amplitude loading

ISBN:
Printed by: Multicopy Den Haag

“Apparently, once the seed has been sown, you see nothing for about five years, apart from a tiny shoot. All the growth takes place underground, where a complex root system reaching upward and outward is being established. Then, at the end of the fifth year, the bamboo suddenly shoots up to a height of twenty-five meters.”

Paulo Coelho -Aleph

Table of Contents

Abstract

Structural geometry and stochastic loads such as swell and wind seas can typically induce multiaxial stress states in welded details of marine structures. It is known that such complex time varying stress states determine the fatigue resistance of welded steel joints. Therefore, it is of importance to account for them in fatigue lifetime assessment. Over the past few decades, a wide variety of design codes and guidelines have been developed for performing fatigue assessments in engineering practice. In particular for multiaxial fatigue lifetime assessment, additional methods have been developed. These multiaxial fatigue methods are typically developed within academia.

A consensus on the most suitable approach for the assessment of multiaxial fatigue in marine structures is lacking. This requires thorough investigation of all different approaches, and equitable comparison and validation with experimental data. Establishing a test setup that enables to test multiaxial fatigue of welded marine structures, is however time and cost intensive. Therefore, experimental multiaxial fatigue data is scarce.

An extensive literature study was performed to obtain a clear overview of the state-of-the-art of multiaxial fatigue assessment. This study was particularly focussed on multiaxiality, non-proportionality and fatigue in welded steel joints with representative configurations and/or dimensions for marine structures. From this study, approaches and methods were selected that are most suitable for the assessment of high cycle fatigue with intact geometry parameters.

Since experimental multiaxial fatigue data is scarce and often not representative for marine structures, a unique test facility was procured by Delft University of Technology. The design and engineering of this test rig was performed such that it enables to perform complex and representative loads (i.e. the rig is a hexapod with six degrees of freedom). As such, a consistent and controlled experimental data set could be collected from testing welded tubular specimens with maritime representation (i.e. dimensions, type of material – S355, welding procedure). All the data that has been collected with the hexapod, was obtained under multiaxial constant amplitude loading from mixed Mode I (bending) and Mode III (torsion). The considered load cases were pure Mode I loading, pure Mode III loading, combined proportional (in-phase) loading, combined phase shift induced non-proportional (out-of-phase) loading and combined frequency induced non-proportional (out-of-phase) loading. For relative comparison, experimental data of similar geometries (i.e. welded tube-to-flange connections) and load cases was selected from literature.

Both the experimentally obtained hexapod data and the literature data were compared to lifetime estimates from a selection of multiaxial fatigue methods. These methods were selected from the literature study, based on the consideration of their applicability to multiaxial fatigue problems in welded joints. Only constant amplitude load cases were taken into consideration. The selected methods are the Modified Wöhler Curve Method (MWCM), the Modified Carpinteri Spagnoli Method (MCSM), the Structural Stress Critical Plane method (SSCP), the Projection-by-Projection (PbP) method and the Effective Equivalent Stress Hypothesis (EESH). Three recommendations, that are widely accepted and applied in engineering practice, were considered as reference material; IIW, DNV-GL and Eurocode3.

The process of welding introduces not only welding induced defects in the material but also different material zones and residual stresses. In addition, stress is raised locally at the notch of the weld. In order to obtain more insight into the effect of welding deffects, bar specimens were

experimentally tested under pure Mode I loading (tension). These bar specimens had the same material properties (S355) and notched geometry as the welded tubular specimens that were tested in the hexapod but instead of being welded they had a laser induced elliptically shaped surface defect at the notch. Surface defects of various sizes were tested (i.e. defect sizes ranging from $100\ x\ 400\ um$ to $500\ x\ 2000\ um$).

Analysis of the bar specimen results clearly demonstrated that increasing defect size contributes to a reduction in fatigue lifetime. The selected dimensions of the elliptically shaped surface defects show a close resemblance with the fatigue resistance that is typically considered (in engineering practice) for welded joints. For reference, the bar specimen results were compared to the fatigue resistance of its base material that was found in literature. A change in inverse slope of the fatigue resistance curve indicated a difference in damage mechanism. When the Mode I hexapod data was added to this comparison, it became apparent that the welding quality of the tubular specimens was of higher value than what is typically considered in engineering practice.

The recommended practice from IIW, Eurocode and DNV-GL for multiaxial fatigue assessment were compared to the selected multiaxial fatigue methods. For this comparative study two different data sets were considerd: the collected data from literature and the test results from the hexapod. Comparison of the hexapod data with the considered recommendations from guidelines/codes demonstrated that the hexapod based uniaxial SN curves are not in agreement with the in the guidelines recommended reference SN curves. This can be attributed to the significantly high welding quality of the tubular specimens which affects the slope of their SN curve.

When recommendations from IIW, Eurocode and DNV-GL considered reference SN curves that were based on the selected literature data, the fatigue lifetime estimates became less conservative as with their recommended SN curves. This demonstrated that there are discrepancies between the selected literature data and the data that was used to establish these recommended SN curves in the guidelines. It indicates that the selected data set from literature originates from the upper bound of the data set that was used to generate the recommended SN curves for engineering practice.

When dealing with non-proportionality, IIW consistently provided conservative lifetime estimates and DNV-GL under-conservative lifetime estimates. IIW however makes a conservative assumption by reducing the CV value from 1.0 to 0.5 for non-proportional load cases. Disregarding this CV reduction provides lifetime estimates that are less conservative and with a better correspondence to the selected experimental data.

The selected multiaxial fatigue methods showed significant discrepancies amongst each other under proportional and non-proportional multiaxial loading. The PbP method provides most conservative lifetime estimates and the MWCM most under-conservative.

The comparative study presented in this dissertation, emphasizes the need for further experimental data collection under complex multiaxial loadings. From the discrepancies between the hexapod data and the selected data from literature, it becomes apparent that specimen quality (i.e. welding, manufacturing) should be taken into consideration. For conservative lifetime estimation, IIW should be followed. Further investigation of the selected multiaxial fatigue models is needed in order to improve their correspondence with experimental data and to trace whether discrepancies are the result of the model basis or the reference data for model development.

List of symbols

σ	Normal stress
$\sigma_{eq,a}$	Equivalent stress amplitude
σ_{max}	Maximum stress
σ_{min}	Minimum stress
σ_a	Stress amplitude
$\sigma_{n,max}$	Maximum normal stress
$\sigma_{a,f-1}$	Fatigue stress amplitude limit under fully reversed tension-compression
$\sigma_{a,N_{CAT}}$	Fatigue strength stress amplitude according to Eurocode CATegory
$\sigma_{a,N_{FAT}}$	Fatigue strength stress amplitude according to IIW FAT class
σ_{VM}	Von Mises equivalent stress
$\sigma_{1,2}$	Principal stress
σ_s	Structural stress
σ_m	Membrane stress
σ_b	Bending stress
$\sigma_{a,ref}$	Stress amplitude in accordance with the used reference SN curve
σ_{avg}	Average/Mean stress
σ_{UTS}	Ultimate Tensile Stress
$\sigma_f{}'$	Fatigue strength coefficient
σ_H	Hydrostatic stress
σ_{eff}	Effective stress
σ_{actual}	Actual measured stress
σ_y	Yield stress
k_σ	Stress concentration factor
K_σ	Structural stress concentration factor

ε	Strain
ε^e	Elastic strain
ε^p	Plastic strain
$\varepsilon_f{}'$	Fatigue ductility coefficient
τ	Shear stress
$\tau_{a,f-1}$	Fatigue stress amplitude limit under fully reversed torsional loading
τ_a	Shear stress amplitude
τ_{eq}	Equivalent shear stress
$\tau_{a,ref}$	Shear stress amplitude in accordance with the used reference SN curve
τ_{actual}	Actual measured shear stress
τ_s	Shear structural stress
$\tau_f{}'$	Shear fatigue strength coefficient
γ	Shear strain
γ^e	Elastic shear strain
γ^p	Plastic shear strain
$\gamma_f{}'$	Shear fatigue ductility coefficient
ϵ^e	Elastic strain
ϵ^p	Plastic strain
n'	Cyclic strain hardening exponent
K'	Cyclic strength coefficient
k_τ	Shear stress concentration factor
K_τ	Structural shear stress concentration factor
I_1	First stress invariant
J_2	Second invariant of deviatoric stress
$f_x{}'$	Nodal line forces
$m_x{}'$	Nodal line moments

ρ	Stress amplitude ratio between normal and shear critical plane stresses
ρ_{lim}	Limit value of the critical plane stress amplitude ratio
β	Stress amplitude ratio between normal and shear stress
W_{eq}	Equivalent strain energy density
N_f	Number of cycles to failure
N_{ref}	Number of cycles to failure at the considered reference stress
m	Inverse slope of the fatigue resistance SN curve
α	Non-proportionality sensitivity parameter
γ	Walker mean stress model calibration coefficient
E	Young's Modulus
G	Shear Modulus
t	Plate thickness
δ	Phase shift
FR	Frequency ratio
LR	Load ratio
H_v	Vickers hardness

Abbreviations

IP	In-Phase loading (i.e. Proportional loading)
OP	Out-of-Phase loading (i.e. Non-Proportional loading
CA	Constant Amplitude
VA	Variable Amplitude
MWCM	Modified Wöhler Curve Method
EESH	Effective Equivalent Stress Method
MCSM	Modified Carpinteri Spagnoli Method
PbP	Projection-by-Projection
SSCP	Structural Stress Critical Plane
EM	Energy Method
PDMR	Path Dependent Maximum Range
MLP	Moment of Load Path
RFL	Random Fatigue Limit
SCF	Stress Concentration Factor
SSCF	Structural Stress Concentration Factor
SIF	Stress Intenstiy Factor
LCF	Low Cycle Fatigue
HCF	High Cycle Fatigue

1 Introduction

"Problems that remain persistently insoluble should always be suspected as questions asked in the wrong way." – Alan Watts

Any type of structure at sea, either it be a ship or an offshore structure, is exposed to cyclic wave loading. Marine structures are exposed to such wave loads as a result of a combination of sea states which each consist of their own wave systems. Wind seas and swells generally dominate these wave systems. Cyclic wave loads induce fatigue damage which accumulates over time and which can eventually lead to crack nucleation, initiation and growth. In welded structures, the fatigue critical locations occur at the weld toe or weld root. This is the result of a local stress raise and changing material characteristics (see Figure 1.1). For operators it is of importance to know when fatigue cracks impair the structural integrity to an unacceptable level of damage and/or risk. Once the critical amount of fatigue damage has been reached, intervention such as maintenance or repair will be required in order to avoid eventual failure.

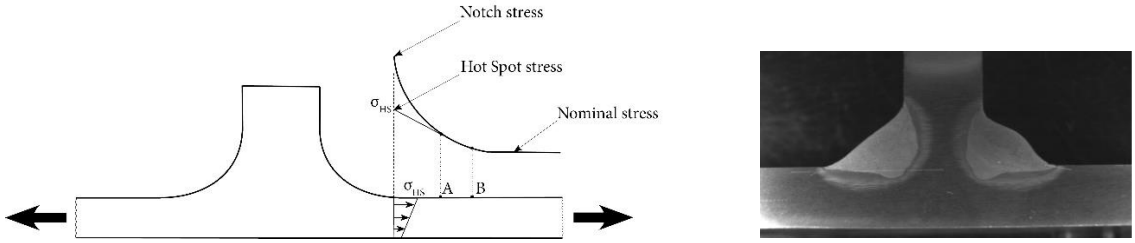

Figure 1.1: Local stress state at the weld toe that can be considered by membrane stress, hot spot stress and notch stress (left) and changes in the microstructure at a weld showing the base material, Heat Affected Zone (HAZ) and weld material (right)

Analysing the fatigue performance of a marine structure comprises of several main steps. First, a metocean analysis is executed using site-specific environmental data. From spectral density functions the wave systems of all sea states are described. Then, complex accelerations and pressures are calculated in a hydrodynamic analysis. The accelerations and pressures can be applied to the global structural model in order to obtain the transfer functions at fatigue sensitive locations. The time trace or spectral density function of different stress or strain components can be extracted and used as an input for the fatigue analysis. Marine structures typically deal with high cycle fatigue whereby fatigue crack initiation dominates the total fatigue life. This fatigue regime is governed by stress due to elastic deformation of the material (Suresh, 1998). Elastic-plastic deformations induce low cycle fatigue which is governed by strain.

Most welds in structural details of marine structures are predominantly subjected to uniaxial stresses due to the stiffness distributions in typical structural member assemblies like stiffened panels, frames and trusses. However, there are also welds which could be subjected to multiaxial stresses induced either by geometry or loading (Hong & Forte, 2014; Maddox, 2010). Such stresses may lead to a significant reduction of the fatigue resistance of welded steel joints as can be seen in Figure 1.2 (Sonsino & Kueppers, 2001). Considering that the majority of marine structures are (relatively thick)

plated structures, such fatigue lifetime reductions are generally caused by the combined effect of a dominant normal and shear stress (mixed Mode-I and Mode-III).

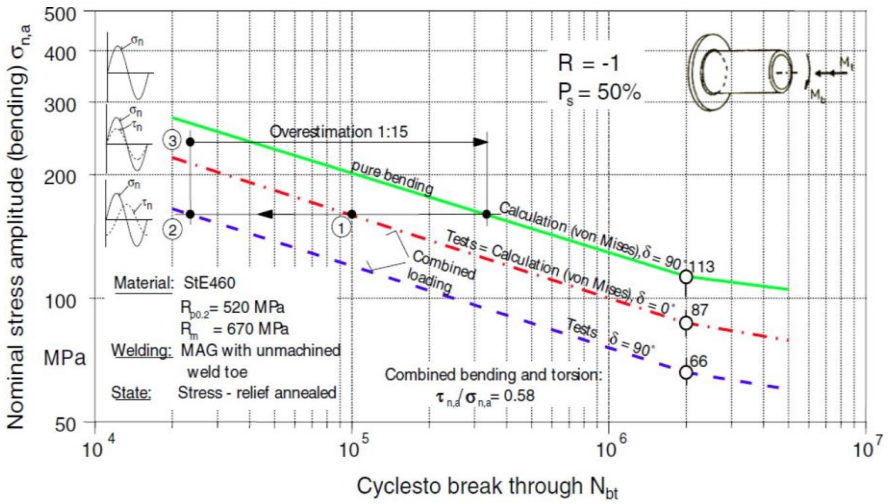

Figure 1.2: Multiaxial fatigue resistance SN-curves resulting from pure bending, proportional and non-proportional experimental testing of a welded plate-to-tube specimen

One of the difficulties with multiaxial fatigue in welded marine structures is that the phenomenon of fatigue in welded joints cannot be scaled. Plenty of research on multiaxial fatigue has been executed for the automotive and aerospace industry but this knowledge, concerning thin plated structures, cannot be directly transferred to relatively thick plated marine structures. As elaborated in (den Besten, 2015), fatigue resistance decreases with increasing plate thickness due to an increase in welded material volume, residual stress effects, surface quality and a larger stressed material volume. A total stress concept was developed to incorporate these effects (den Besten, 2015, 2018). However, this concept was developed for welded aluminium joints subjected to uniaxial fatigue and are being extended to steel joints facing multiaxial fatigue (Qin et al., 2019).

A multiaxial fatigue analysis is not a procedure with a univocal set of instructions. In fact, different decisions can be made at three elementary levels. In the first place it is of importance to identify the physical features, such as joint type (welded or non-welded), material characteristics (ductile, semi-ductile or brittle) and scale (macro, meso or micro). This leads to the second level of decision making where it has to be decided whether an intact geometry parameter is chosen, wherefore SN-curves are used, or a crack damaged parameter, whereby fracture mechanics is used. Since an intact geometry parameter is most commonly applied for the fatigue design of welded joints in marine structures, the presented overview will not elaborate further on the different approaches of fracture mechanics. With an intact geometry parameter, a distinction can be made between those who lead to a fatigue lifetime estimate (i.e. finite lifetime) and those who identify a ‘safe region’ without fatigue crack initiation (i.e. an infinite lifetime). This ‘safe region’ is then identified by a fatigue boundary definition. An example of such a definition is the Dang Van criterion (Callens & Bignonnet, 2012; Dang Van, 2014; Lieshout, den Besten, & Kaminski, 2016; Radaj, Sonsino, & Fricke, 2006). At the third level, four sequential steps lead to a fatigue lifetime estimate, expressed in number of cycles. These steps can be executed in the time domain or the frequency domain. In the first step, the fatigue damage parameter should be identified. This parameter can be formulated from stress, strain or

energy - a product of stress and strain. Four different approaches can be used to determine a fatigue damage parameter: an equivalent stress or strain, a damage parameter based on a critical damage plane, a damage parameter based on an invariant formulation or an integral formulation. Then, the cycle counting procedure (uniaxial or multiaxial), damage accumulation rule (linear of non-linear) and the reference SN-curve (considering separate modes or mixed modes) have to be chosen. In Figure 1.3 a schematic overview is provided of this decision making process in the fatigue analysis of marine structures, indicating de different options.

1.1 Motivation

Fatigue design of marine structures is predominantly based on uniaxial fatigue criteria assuming a governing Mode-I. These criteria are then used in combination with a damage accumulation hypothesis (e.g. Miner's rule) and cycle counting method (e.g. rainflow counting) to determine the fatigue lifetime. However, such an approach can be non-conservative for structural details where the welds are subjected to multiaxial stresses, especially when these are non-proportional, i.e. out-of-phase (OP).

Over the last few decades intensive efforts have been made to develop multiaxial fatigue approaches which are able to deal with difficulties of multiaxiality such as mixed mode loading, (random) variable amplitude (VA) loading and non-proportionality. This has resulted, amongst others, in multiaxial cycle counting methods (Anes, Reis, Li, Fonte, & De Freitas, 2014; Meggiolaro, Tupiassú, & De Castro, 2012; Wei & Dong, 2014), critical plane based criteria (Carpinteri, Spagnoli, & Vantadori, 2008; Sonsino & Kueppers, 2001; Susmel & Tovo, 2004), invariant based criteria (Cristofori, Susmel, & Tovo, 2007) and energy based criteria (Macha & Sonsino, 1999). Furthermore, spectral methods have been developed to assess multiaxial fatigue in the frequency domain, instead of the time domain (Denis Benasciutti, Sherratt, & Cristofori, 2016; Nieslony, 2009; Nieslony & Macha, 2007).

Numerous multiaxial fatigue assessment methods have been developed with the intention to improve the accuracy of fatigue lifetime estimates under multiaxial stress states. However, they often have limited applicability and compatibility due to their complexity, lacking or limited experimental validation and non-scalability of the phenomenon of fatigue in welded joints. Therefore, a consensus is still lacking regarding the most suitable approach for the assessment of multiaxial fatigue in welded joints whereby non-proportionality and variable amplitude loading can be accounted for. An important aspect here is the limited availability of proper experimental data and the difficulties in multiaxial fatigue testing of welded marine structures.

1.2 Research outline

1.2.1 Research objectives

The objective of this research is the identification and validation of an appropriate method for the assessment of multiaxial fatigue in welded joints in marine structures, under non-proportional constant amplitude loading. The work seeks to improve the accuracy of fatigue lifetime estimates for fillet welded joints, representative for the maritime industry. Therefore, a unique test setup is used to collect experimental (multiaxial fatigue) data for model validation. In order to improve the fundamental understanding of the different phenomena affecting multiaxial fatigue damage accumulation, the deliberate choice was made to separate non-proportionality from variable amplitude loading.

Consideration of a crack damaged geometry introduces the concept of fracture mechanics. Fracture mechanics is a good approach to assess fatigue but in order to account for multiaxiality, and in

particular to distinguish non-proportionality from proportionality, SN based approaches are further developed. Furthermore, the SN based approach is a typically applied engineering practice in the maritime industry for the fatigue assessment of fatigue lifetime of welded plated structures. Therefore, this work follows the SN based approach for fatigue lifetime assessment.

1.2.2 Scope of work and the 4D-Fatigue project

The scope of this research was part of the Joint Industry Project (JIP) 4D-Fatigue. The 4D-Fatigue project involved three working scopes: fundamental, experimental and numerical.

The fundamental scope of work beholds investigation and interpretation of the state-of-the-art of multiaxial fatigue methods. For the experimental scope of work, a dedicated multiaxial test facility was built. With this test facility, the fatigue resistance of a large scale welded structural joint was experimentally examined under different (multiaxial) loading conditions. In addition to these large scale tests, small scale fatigue tests were performed to investigate the contribution of the weld(ing defects) on fatigue resistance. The numerical scope of work merely served to identify typical locations in a marine structure that are prone to multiaxial fatigue. This scope was established as a justification of the project initiative to the industrial partners. It also provided insights into the contribution of geometry and loading to a multiaxial stress state. The project deliverables aim to contribute to the improvement of (multiaxial) fatigue design and the optimization of maintenance & repair strategies of welded joints in marine structures.

The work that is presented in this thesis covers the fundamental and experimental scope of work of the 4D-Fatigue project.

1.2.3 Research questions

As a guidance and framework throughout this research, the following research questions have been established:

Main research question: "*Which model basis is most suitable for the assessment of multiaxial fatigue, induced by proportional and non-proportional constant amplitude loading, in fillet welded steel joints in marine structures?*"

Subquestion 1: "What are the different approaches and methods that can be used for the assessment of multiaxial fatigue, induced by proportional and non-proportional constant amplitude loading?"

Subquestion 2: "What are the effects of a fillet welded steel joint in combination with characteristics of a marine structure on the validity of these methods?"

Subquestion 3: "How does non-proportionality under constant amplitude loading influence the fatigue resistance in a fillet welded steel joint?"

Subquestion 4: "To what extend and in what manner are the different approaches and methods for multiaxial fatigue assessment able to capture the influences of non-proportional constant amplitude loading on the fatigue resistance of a fillet welded steel joint?"

1.2.4 Thesis outline

This dissertation consists of five Chapters. Chapter 1 presents the research topic and provides background information about the motivation, project structure, scope of work and research outline. Chapter 2 provides an overview of the progresses in academia and engineering practice in relation to the multiaxial fatigue assessment of welded joints in marine structures. The experimental scope of work is subdivided into two additional Chapters. The large scale experiments have been performed in a unique hexapod which is presented in Chapter 3. Small scale experiments were performed with the objective to represent the fatigue resistance of a welded joint through a notched geometry with an artificial laser induced surface defect. Chapter 4 elaborates further upon these small scale testing activities. Finally, a comparative study is presented in Chapter 5. This Chapter shows to what extend a selection of state-of-the-art multiaxial fatigue methods matches with experimentally obtained test data from literature and from the hexapod.

Figure 1.3: Schematic overview of the decision making process in the fatigue analysis of marine structures

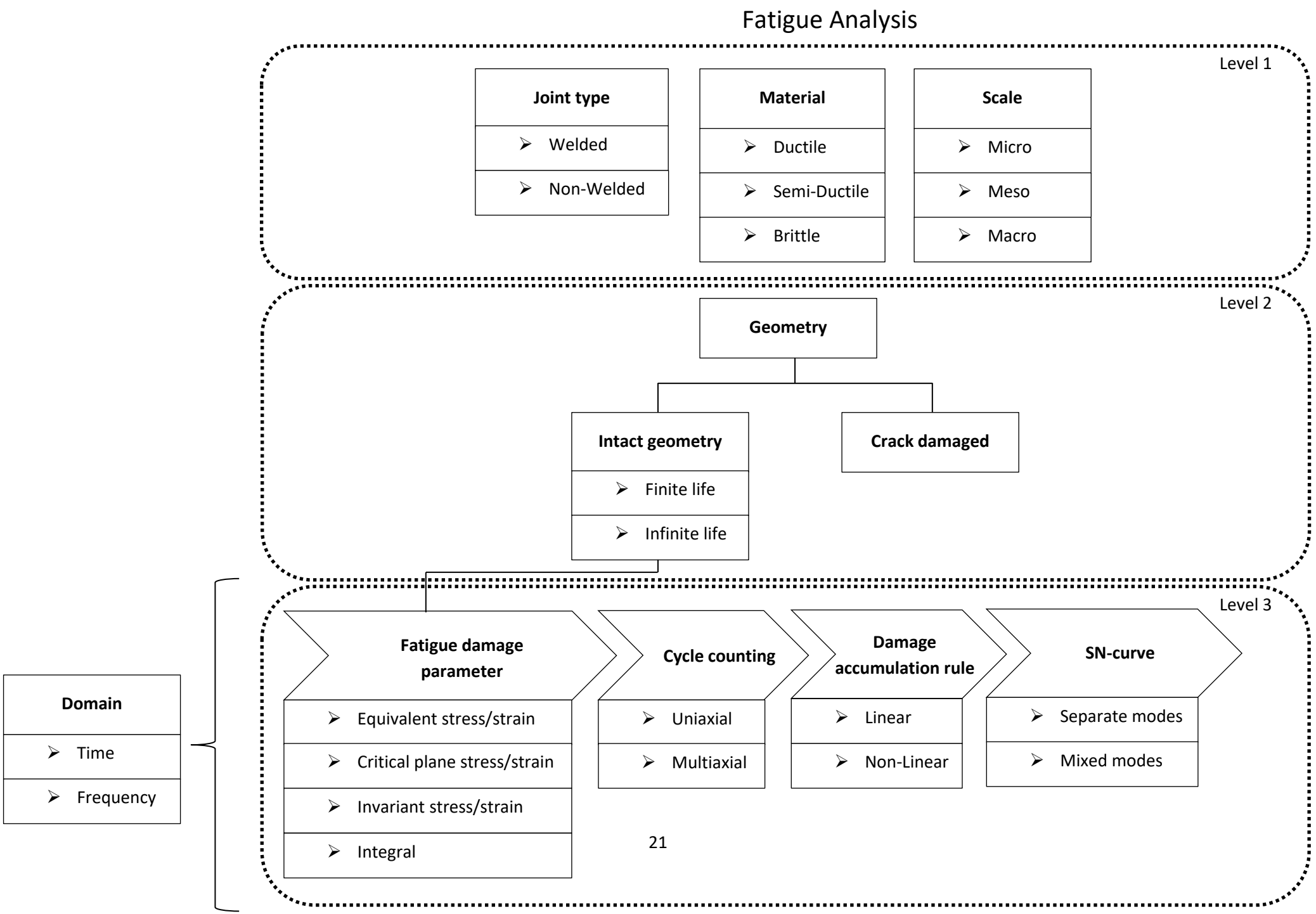

1.3 References

Anes, V., Reis, L., Li, B., Fonte, M., & De Freitas, M. (2014). New approach for analysis of complex multiaxial loading paths. *International Journal of Fatigue*, *62*, 21–33. https://doi.org/10.1016/j.ijfatigue.2013.05.004

Benasciutti, D., Sherratt, F., & Cristofori, A. (2016). Recent developments in frequency domain multi-axial fatigue analysis. *International Journal of Fatigue*, *91*, 397–413. https://doi.org/10.1016/j.ijfatigue.2016.04.012

Besten, J. H. den. (2015). *A total stress concept*. Delft University of Technology.

Besten, J. H. den. (2018). Fatigue damage criteria classification, modelling developments and trends for welded joints in marine structures. *Ships and Offshore Structures*, *13*(8), 787–808. https://doi.org/10.1080/17445302.2018.1463609

Callens, A., & Bignonnet. (2012). Fatigue design of welded bicycle frames using a multiaxial criterion. *Procedia Engineering*, *34*, 640–645. https://doi.org/10.1016/j.proeng.2012.04.109

Carpinteri, A., Spagnoli, A., & Vantadori, S. (2008). Multiaxial fatigue life estimation in welded joints using the critical plane approach. *International Journal of Fatigue*, *31*, 188–196. https://doi.org/10.1016/j.ijfatigue.2008.03.024

Cristofori, A., Susmel, L., & Tovo, R. (2007). A stress invariant based criterion to estimate fatigue damage under multiaxial loading. *International Journal of Fatigue*, *30*, 1646–1658. https://doi.org/10.1016/j.ijfatigue.2007.11.006

Dang Van, K. (2014). *On a unified fatigue modelling for structural analysis based on the shakedown concept*. *Mecamix, X-Tech*. Paris, France. https://doi.org/10.1007/s13398-014-0173-7.2

Hong, J. K., & Forte, T. P. (2014). Fatigue evaluation procedures for multiaxial loading in welded structures using the Battelle Structural Stress approach. In *ASME 2014 33rd International Conference on Ocean, Offshore and Arctic Engineering* (pp. 1–9). San Fransisco, USA.

Lieshout, P. S. van, Besten, J. H. den, & Kaminski, M. L. (2016). Comparative study of multiaxial fatigue methods applied to welded joints in marine structures. *Frattura Ed Integrità Strutturale*, *37*, 173–192. https://doi.org/http://dx.doi.org/10.3221/IGF-ESIS.37.24

Macha, E., & Sonsino, C. M. (1999). Energy criteria of multiaxial fatigue failure. *Fatigue and Fracture of Engineering Materials and Structures*, *22*, 1053–1070.

Maddox, S. J. (2010). *Fatigue assessment of welds not oriented either normal or parallel to the direction of loading*. *IIW document*. Cambridge, UK.

Meggiolaro, M. A., Tupiassú, J., & De Castro, P. (2012). An improved multiaxial rainflow algorithm for non-proportional stress or strain histories - Part II: The Modified Wang-Brown method. *International Journal of Fatigue*, *42*, 194–206. https://doi.org/10.1016/j.ijfatigue.2011.10.012

Nieslony, A. (2009). Determination of fragments of multiaxial service loading strongly influencing the fatigue of machine components. *Mechanical Systems and Signal Processing*, *23*, 2712–2721. https://doi.org/10.1016/j.ymssp.2009.05.010

Nieslony, A., & Macha, E. (2007). *Spectral Method in Multiaxial Random Fatigue* (Vol. 33). Springer.

Qin, Y., Besten, H., Palkar, S., & Kaminski, M. L. (2019). Fatigue design of welded double-sided T-joints

and double-sided cruciform joints in steel marine structures: A total stress concept. *Fatigue & Fracture of Engineering Materials & Structures*. https://doi.org/10.1111/ffe.13089

Radaj, D., Sonsino, C. M., & Fricke, W. (2006). *Fatigue assessment of welded joints by local approaches*. *Woodhead Publishing Limited* (Vol. 53). https://doi.org/10.1017/CBO9781107415324.004

Sonsino, C. M., & Kueppers, M. (2001). Multiaxial fatigue of welded joints under constant and variable amplitude loadings. *Fatigue and Fracture of Engineering Materials and Structures*, *24*, 309–327.

Suresh, S. (1998). *Fatigue of materials* (Second edi). Cambridge, UK: Cambridge University Press.

Susmel, L., & Tovo, R. (2004). On the use of nominal stresses to predict the fatigue strength of welded joints under biaxial cyclic loading. *Fatigue & Fracture of Engineering Materials & Structures*, *27*, 1005–1024. https://doi.org/10.1111/j.1460-2695.2004.00814.x

Wei, Z., & Dong, P. (2014). A generalized cycle counting criterion for arbitrary multi-axial fatigue loading conditions . *Journal of Strain Analysis for Engineering Design*, *49*, 325–341.

2 A literature overview of progresses in academia and engineering practice for the multiaxial fatigue assessment of welded joints in marine structures

This Chapter is based on the following publication:
"Multiaxial Fatigue Assessment of Welded Joints in Marine Structures
– Literature Overview of Progresses in Academia and Engineering Practice- "
P.S. van Lieshout, J.H. den Besten, M.L. Kaminski
International Shipbuilding Progress 65(4):1-43, 2017
DOI: 10.3233/ISP-170141

"Blind believe in authority is the greatest enemy of truth."
– Albert Einstein

2.1 Introduction

Fatigue is a well-known phenomenon in a variety of applications in different industries e.g. aerospace, automotive, railway and nuclear. Typically it occurs in mechanical components dealing with cyclic loadings such as rotating parts (e.g. bearings, crankshafts, turbines, wheel-rail contacts) or components subjected to thermal or other types of mechanical cyclic loadings (e.g. nuclear pressure vessels, airplane wings). Many research and experimental work has been dedicated to investigate the fatigue behaviour and evolution in such applications. This has resulted in a fairly good understanding of uniaxial fatigue nowadays. However, there are still unresolved issues concerning the more complex form: multiaxial fatigue.

Understanding of multiaxial fatigue is of relevance for the lifetime assessment of ship and offshore structures (henceforth referred to as marine structures). Marine structures can encounter multiaxiality due to the stochastic load characteristics which are mainly dominated by a combination of wind seas and swells. Generally such complex loadings induce multiaxial stress states which are non-proportional (i.e. out-of-phase). However, multiaxiality can also be induced by structural geometry which is predominantly proportional (i.e. in-phase) (den Besten, 2015; Erny, Thevenet, Cognard, & Körner, 2010b; Maddox, 2010).

As a result of its mechanical properties, structural steel is generally used for the construction of marine structures. This material is also used throughout a wide variety of other industries (e.g. civil, automotive, railway, nuclear). However, fatigue behaviour is affected by size, material characteristics (e.g. chemical composition, material properties) and welding effects (e.g. non-uniform material characteristics, welding induced defects, residual stresses) (Sonsino, 1995, 2011). Therefore, the knowledge transfer between these different industries remains limited.

Experimental data is requisite for validation of existing multiaxial fatigue methods but only a limited amount of data is currently available for welded joints. Various experimental data sets which have been frequently used to validate multiaxial fatigue methods have been reviewed in (Papuga, 2013; Papuga, Parma, & Růžička, 2016). From these reviews it was concluded that the data sets are often not suitable for validation purposes due to their incompleteness and incompatibility. Moreover,

fatigue failure is not univocally defined. Some experimental studies define it as complete breakage of the specimen whilst in others studies the tests are stopped when a macroscopic crack is detected (affecting the specimen's stiffness). These discrepancies impede clear and fair judgement of the different multiaxial fatigue methods. In (Bäckstrom & Marquis, 2004; Bäckström & Marquis, 2001; den Besten, 2015; Dong & Hong, 2004) it is shown that large scatter bands exist amongst the (different) experimental data sets.

An extensive amount of literature was selected and studied, focussing on multiaxiality and non-proportionality in welded steel joints (in marine structures). For the fatigue lifetime assessment of such joints an intact geometry or a crack damaged geometry can be considered. In case of the latter, fatigue lifetime is typically assessed using fracture mechanics. This study focusses on the assessment of high cycle fatigue using intact geometry parameters and therefore the fracture mechanics approach is not incorporated in the scope of work. External environmental conditions such as thermal effects and corrosion will not be addressed.

The overview starts with Section 2.2 which discusses the effects of multiaxiality on fatigue crack evolution in welded steel in terms of material, geometry and loading. Section 2.3 provides an overview of current guidelines and recommendations for engineering practice. This is followed by Section 2.4 where different multiaxial fatigue methods are audited, focussing on their application to multiaxial fatigue problems in welded joints. This Section is categorized by: critical plane based, invariant based and integral based methods. Section 2.5 and 2.6 elaborate upon the different cycle counting techniques and damage accumulation rules that can be used for multiaxial fatigue assessment. In Section 2.7 two schematic overviews are provided which serve as a supplement to Section 2.4, 2.5 and 2.6. One overview indicates the required input parameters for each audited multiaxial fatigue method and the other overview demonstrates the application domain of each method. Finally, a discussion and conclusions are provided in Section 2.8 and 2.9.

2.2 Effects of multiaxiality on fatigue crack evolution in welded steel

2.2.1 Fundamentals of fatigue

Typically, four stages are defined in crack evolution namely nucleation, initiation (i.e. early growth), growth and propagation. However, not all stages are always part of the crack evolution. This is the case for example in welded joints where the presence of welding induced crack-like defects exclude the nucleation phase of a crack (Remes, Lehto, & Romanoff, 2014). If crack initiation is considered as early (small) crack growth, fatigue lifetime can indeed be considered growth dominant although the majority of fatigue lifetime is spent in the weld notch affected region (den Besten, 2015; Remes et al., 2014). In the studied literature, different definitions of crack initiation were found. For example, in (Castelluccio & Mcdowell, 2016) the nucleation and initiation stage are defined over an area of several grains whereas in (Hobbacher, 2015; Sonsino, 1997; Sonsino et al., 2012) crack initiation is defined by a crack depth of 0.5-1 mm. However, in engineering practice, crack initiation is generally defined as the minimal detectable macroscopic crack size (T. Lassen & Recho, 2006; Radaj, Sonsino & Fricke, 2008; Sonsino et al., 2012). It can thus be concluded that the definition of the different stages of crack evolution are dependent on the considered scale, i.e. microscopic, mesoscopic, macroscopic. Important to note is that the transition between these different scales is not univocal and often arbitrarily defined (den Besten, 2018; Mikulski & Lassen, 2019).

The theory of cyclic deformation in a single crystal distinguishes two phases in the crack evolution of High Cycle Fatigue (HCF). The first phase (i.e. crack nucleation and initiation) is driven by laminar flow of dislocations along Persistent Slip Bands (PSBs) whilst the second phase (i.e. crack growth and propagation) is driven by crack opening or closing. The material behaves elastically on macroscopic scale whilst on a more local meso- or microscopic scale elastic/plastic behaviour leads to fatigue damage. Due to this behaviour, HCF is typically described by a (macroscopic) stress driven fatigue parameter. On the other hand, Low Cycle Fatigue (LCF) is characterized by macroscopic plastic behaviour which is typically described by a (macroscopic) strain driven fatigue parameter.

Fatigue cracks follow the path of the least resistance. This means that under cyclic loading, the microscopic stress concentration moves with the crack tip until it reaches and activates another slip band. Shear can develop under two angles and therefore a zig-zag shape is typically observed on microscopic level (Schijve, 1989). Interestingly, under pure tensile loading (Mode I), the macroscopic crack growth direction is perpendicular to the loading direction (i.e. the first principal stress) whilst the microscopic crack is initiated on the material plane with a ±45 degrees inclination. See for clarification Figure 2.1. Under pure torsional loading (Mode III) microscopic cracks initiate on the material plane which corresponds with the macroscopic crack growth plane of Mode I. The Mode III macroscopic crack growth plane then corresponds with the material plane of Mode I crack initiation. See Figure 2.2.

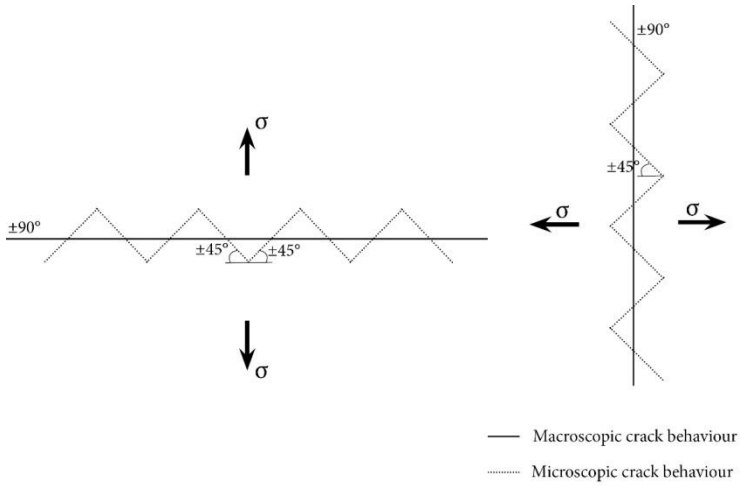

Figure 2.1: Macroscopic and microscopic crack behaviour of Mode I loading

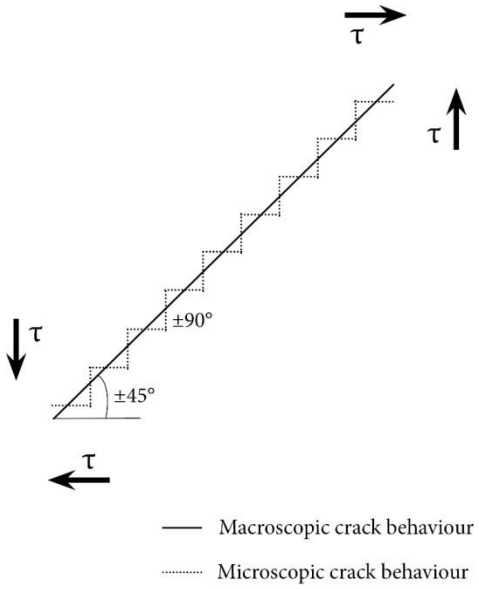

Figure 2.2: Macroscopic and microscopic crack behaviour of Mode III loading

2.2.2 Material effects on multiaxial fatigue resistance of welded joints

Extensive experimental work has been performed by Sonsino et al. whereby welded joints of various material types (e.g. wrought steel, cast steel, cast iron, magnesium alloy, aluminium alloy) were tested under multiaxial loadings induced by (non-) proportional constant and or variable amplitude loading (Exel & Sonsino, 2014; Sonsino, 2008b, 2011; Wiebesiek & Sonsino, 2010). A correlation was found between material ductility and fatigue resistance under non-proportional loading conditions. Ductile materials show a decrease in fatigue resistance under non-proportional loading, semi-ductile materials show negligible differences between non-proportional and proportional loading whilst brittle materials show an increase in fatigue resistance. The reduction in fatigue resistance under non-proportional loading in ductile materials is often attributed to cyclic hardening (Fatemi & Shamsaei, 2010; Shamsaei, 2010; Sonsino, 2011). Cyclic hardening is the result of interactions between different dislocations caused by the rotating easy glide plane (i.e. cross hardening). These interactions cause dislocations to block each other's movement. This means that locally higher stress concentrations will occur which facilitates flow of Persistent Slip Bands (PSBs) and impedes the fatigue resistance. However, in (semi-)brittle materials the finer grained material structure facilitates annihilation of dislocations. Interactions are reduced, which leads to higher fatigue resistance (i.e. cyclic softening) (Chai & Laird, 1987).

2.2.3 Geometry effects on multiaxial fatigue resistance

Geometry beholds the type of joint connection (e.g. plated, tubular), type of weld (e.g. groove weld, fillet weld) and plate thickness. These geometrical features affect the fatigue resistance and crack evolution through a stress raise at the joint connection, i.e. notched geometry. Generally, such notched geometries are distinguished from plane geometries. A notched geometry can induce multiaxiality even though a uniaxial load is applied (Maddox, 2010). Therefore, loading and geometry induced multiaxiality can and should be distinguished. Precaution should thus be taken with application of assessment methods which originate from plane geometries to notched geometries.

2.2.4 Loading effect on multiaxial fatigue resistance

In (Liu & Zenner, 1993, 2003) an interesting comparison is presented of the different effects of loading on multiaxial fatigue resistance. This work compares various experimental results of smooth specimens subjected to combined bending/tension and torsion under constant amplitude loading. For the metals, 42CRMo4, 34Cr4, St35 and 25CrMo4 the fatigue resistance was compared considering different phase shifts, frequency ratios and wave forms. The results are considered valuable despite the fact that non-welded specimens were used because the influences of frequency and wave form on multiaxial fatigue resistance are seldomly investigated.

2.2.4.1 Frequency induced non-proportionality

Non-proportionality which is induced by a difference in frequency amongst the governing stress components, hereafter referred to as frequency induced non-proportionality, has been less frequently addressed in literature as phase shift induced non-proportionality. When addressed, the contribution of frequency to non-proportional fatigue damage is typically investigated in base materials and partly focussed on low cycle fatigue (i.e. strain governed fatigue damage) (Fujczak, 1994; Liu & Zenner, 2003).

Although applicable to low cycle fatigue, Pejkowski et al. (2018) concluded from an experimental study that frequency induced non-proportionality affects the fatigue behaviour of materials differently than phase shift induced non-proportionality. Different materials were investigated (aluminium, ferritic-pearlitic steel, austenitic stainless steel) and exposed to both phase shift induced non-proportional loading and frequency induced non-proportional loading. All materials showed a reduction in fatigue resistance through increased cyclic hardening, as a result of the non-proportionality of the loading.

Under frequency induced non-proportional loadings, both an increase and a decrease in fatigue resistance can be observed (Liu & Zenner, 1993, 2003). This is also seen in the experimental results collected by Sonsino et al. and can be attributed to the correlation between ductility and the susceptibility to non-proportional hardening (Sonsino, 2008b, 2011; Sonsino & Kueppers, 2001). In work from (Liu & Zenner, 2003) the fatigue resistance decreased with increasing frequency ratios (investigated up to a ratio of 10), for frequency induced non-proportionality under alternating combined normal and shear stresses. Interestingly, this effect appeared insensitive to the definition of the frequency ratio, i.e. f_τ/f_σ or f_σ/f_τ.

Apart from testing frequency, the shape of the load signal plays a role in fatigue resistance (Schijve, 1989). In (Liu & Zenner, 2003) the effect of three different wave forms (i.e. sinusoidal, trapezoidal and triangular) was investigated. In the two investigated load combinations (i.e. two perpendicular normal stresses vs. normal and shear stress) the triangular wave form appeared to be the least detrimental whilst the trapezoidal wave form appeared the most detrimental.

2.2.4.2 Testing frequency

The frequency used to perform fatigue tests can influence the fatigue resistance (Fujczak, 1994; Schijve, 1989). For ASTM A723 steel it was found that the test frequency of a fully reversed bending test hardly affected the fatigue resistance at frequencies ranging from 0-15 Hz and frequencies ranging from 30-75 Hz, but at the intermediate frequencies ranging from 15-30 Hz there appeared a consistent influence on fatigue resistance. The test results indicated a change in damage mechanism at these intermediate test frequencies.

Apart from consideration of the effect of testing frequency on fatigue resistance, the environmental conditions should also be taken into consideration since aggressive and corrosive environments can affect crack initiation and growth. In contrast to the behaviour in ambient (air), test frequencies ranging between 0.1 Hz and 10 Hz have a significant detrimental effect on fatigue resistance of steel in corrosive environments (Fujczak, 1994). This can be attributed to corrosion induced surface damage and corrosion enhanced crack growth (Schijve, 1989).

2.2.4.3 Residual stresses

Residual stress is induced by fabrication techniques such as for example machining or welding. Such fabrications can cause a stress raise in the material due to a local input of high temperature and relatively rapid cooling which cause thermal stresses and strains (Radaj et al., 2006). Residual stress and mean stress should not be confused with each other because in contrast to mean stresses, the residual stresses can encounter relaxation as a result of heat treatment and/or cyclic loading. This is not the case for mean stresses which may result from mounting, dead weight and stress fluctuations.

The welding process induces a high tensile residual stress at the weld toe region and therefore experimental studies with welded joints often discard mean stress effects (Sonsino, Lagoda, & Demofonti, 2004). It is important to note that small scale specimens contain a significantly lower level of residual stress than joints in real maritime applications. SN-curves which are generated with small scale welded specimens should thus be corrected for the higher residual stresses present in the actual application (Hobbacher, 2015; Radaj et al., 2006).

In the work of (Bäckstrom & Marquis, 2004; Sonsino, 2008a), (non-)proportional multiaxial loadings were applied to welded joints with different levels of residual stresses (resulting from heat treatment and machining). Both under constant and variable amplitude loadings, it was observed that residual stress affects the fatigue resistance. However, to draw clear conclusions the effect of residual stress (relaxation) on fatigue lifetime still requires further investigation (Farajian, Nitschke-Pagel, Boin, & Wimpory, 2013; Sonsino, 2008b).

2.2.4.4 Mean stresses and mean stress correction

In literature, two synonyms are used for the ratio between the maximum and minimum stress value during a load cycle: stress ratio and load ratio. However, stress ratio implies that the ratio is response governed whilst load ratio implies that it is loading governed. Although not consistently used, both definitions refer to the same load characteristic. Henceforth load ratio will be used as it is considered a less ambiguous definition.

The load ratio indicates the level of mean stress during a load cycle. Interestingly, the normal mean stresses are typically considered to be affecting fatigue resistance whilst the shear mean stress effect is considered negligible (for as long as it remains below yield) (Schijve, 1989). This is for example the case in (Susmel, 2010). However, caution should be taken with this assumption as it is based on a limited amount of experimental data of non-welded specimens, of the particular material type (39NiCrMo3) (Davoli, Bernasconi, Filippini, Foletti, & Papadopoulos, 2003). See for example (Kluger & Lagoda, 2016; G. Marquis, 2000; Muhs, Wittel, Becker, Jannasch, & Vossiek, 2008) where shear mean stress effects are demonstrated.

Experimental data can be converted with a mean stress correction so that it represents a structural detail with increased mean stress induced load levels, residual stress and heat treatment (affecting residual stress relaxation) (Ince & Glinka, 2011). Most well-known are the (empirical)

correction models of Gerber, Goodman, Soderberg and Morrow which are typically depicted in a Haigh diagram (i.e. σ_{avg} vs. σ_a). The correction model of Walker and Smit-Watson-Topper (SWT) can also be considered but are seldomely used for welded joints, despite the fact that they can accurately account for relatively low stress amplitudes and high mean stress (den Besten, 2015). This would make them suitable candidates for welded joints. The SWT model considers equal contribution of mean stress and stress amplitude whilst the Walker model considers an unequal contribution governed by a material dependent calibration coefficient γ. See Equations 2.1 and 2.2.

Smith-Watson-Topper:

$$\sigma_{eq,a} = \sigma_{max}^{\frac{1}{2}} \cdot \sigma_a^{\frac{1}{2}} \tag{2.1}$$

Walker:

$$\sigma_{eq,a} = \sigma_{max}^{1-\gamma} \cdot \sigma_a^{\gamma} \tag{2.2}$$

2.3 Review of current engineering practices

The fatigue assessment of marine structures generally consists of several main steps. First, a metocean analysis is executed using site-specific environmental data. This data typically represents a combination of stationary sea states which consist of a certain amount of wave systems described by spectral density functions. Two types of wave systems can be distinguished, namely wind seas and swell. Reference is made to (Zou & Kaminski, 2016) for further characterization of wave data. Secondly, complex accelerations and pressures are calculated in the hydrodynamic analysis. These accelerations and pressures act on the rigid hull structure and are defined for each unit wave of a given length and direction. Transfer functions at fatigue sensitive locations are obtained by application of the accelerations and pressures on the global structural model, either directly or using a sub-structuring technique. This global model includes a refined mesh at the fatigue sensitive locations. Finally, the Power Spectral Density (PSD) functions of different stress components can be obtained by employing a spectral analysis. At this step, in uniaxial fatigue assessment, the fatigue damage can be directly calculated with a relevant SN-curve and the spectral moments of the probability density functions of stress. This Section elaborates upon the different approaches that can be chosen for the multiaxial fatigue assessment of marine structures.

2.3.1 Calculation domains

Time histories of stress or strain components can be obtained directly from the time domain through FE analysis or experimental testing but can also be generated with PSD functions. Time traces are generally the inputs for existing multiaxial fatigue methods. However, if stress/strain histories are obtained in time domain the statistical convergence and data scatter of the fatigue results depend on the considered time interval and chosen sampling rate (Benasciutti, Sherratt, & Cristofori, 2015).

In the spectral domain the stress state is not described by a time history for each individual stress component but by PSD functions. If needed, these can be determined relatively easily from time traces using Fast Fourier Transform (FFT) of relatively short time histories (Benasciutti et al., 2015).

This saves computational efforts in comparison to the time domain calculations. The spectral moments of the PSD functions are valuable parameters in fatigue assessment. They enable to determine e.g. variance, expected number of zero crossing and expected rate of peaks. Non-proportionality is typically captured in the correlation coefficient. Spectral methods are based on the assumption of stationary (Gaussian) stochastic processes meaning that the statistical properties such as mean (square), variance and standard deviation are presumed independent of time. Mean stress fluctuations and non-linearity's cannot be accounted for. For application to marine structures it should be verified whether this assumption can be made for combined and confused sea states.

Spectral methods for the assessment of multiaxial fatigue generally represent the PSD functions in a matrix of auto/cross-spectral density functions. This matrix is used in combination with a particular multiplication matrix to determine an equivalent PSD function. The representation of this multiplication matrix depends on the considered multiaxial fatigue approach. See for example (Carpinteri, Fortese, Ronchei, Scorza, & Vantadori, 2016; Cristofori et al., 2007; Macha & Niesłony, 2012; Mrsnik, Slavic, & Boltezar, 2016). The equivalent PSD function is eventually used for damage estimation. This estimate depends on the probability distribution of the Rainflow counted equivalent stress cycles. Over the years various approximations have been formulated for this distribution, e.g. Wirsching-Light, Dirlik, Zhao-Baker, Tovo-Benasciutti (D. Benasciutti & Tovo, 2006; Carpinteri et al., 2016; Niesłony et al., 2012). The accuracy of these approximations depends on the considered scenario as demonstrated in (Carpinteri et al., 2016; Lagoda & Sonsino, 2004; Macha & Niesłony, 2012; Niesłony, 2010; Niesłony et al., 2012).

2.3.2 Fatigue resistance and (in)finite life

Wöhler curves, often referred to as SN-curves, are most commonly used to describe fatigue resistance. The curves describe a loglog-linear relationship between stress range S and number of load cycles N, depending on the (welded) joint geometry, environmental conditions (e.g. presence of cathodic protection, seawater, ambient air) and level of stress information (i.e. nominal, structural hot spot, notch). In design codes and guidelines for marine structures different annotations are used for standardized SN-curves. For example, IIW assigns FAT(igue) classes, Eurocode 3 assigns (detail) CAT(egories) and DNV assigns Classes (DNV-GL, 2005; European Standard, 2005; Hobbacher, 2015).

Under variable amplitude loading, the fatigue resistance can be described by Gassner curves. These curves consider load spectra instead of CA loads (Sonsino et al., 2004). Therefore they result into higher fatigue resistances in comparison to the (CA based) Wöhler curves. Gassner curves are often unfavoured in (multiaxial) fatigue assessments because most experimental data has been obtained under CA loading. However, some work can be found where Gassner curves were used in the multiaxial fatigue assessment of welded joints (Bolchoun, Wiebesiek, Kaufmann, & Sonsino, 2014; Lagoda & Sonsino, 2004; Sonsino, 2008a; Sonsino & Kueppers, 2001; Sonsino, Kueppers, Gath, Maddox, & Razmjoo, 1999).

SN-curves account for finite or infinite fatigue life by means of their slope. Experimental data typically shows an asymptotic behaviour towards the high cycle fatigue regime. From the standpoint of today's knowledge this behaviour is characterized by a slope change at a so-called knee-point, but in the past, engineering practice simplified this asymptotic behaviour by a horizontal slope at $1 \cdot 10^7$ number of cycles. Infinite fatigue life was then defined by the so-called fatigue limit which equalled the fatigue resistance at $1 \cdot 10^7$ number of cycles. None of the stress ranges below this fatigue limit were considered contributing to fatigue damage (implicating infinite life). However, significant experimental

evidence has shown that steel welded joints show a finite slope change towards the high cycle fatigue regime when exposed to constant and variable amplitude loading. The number of cycles where the knee-point (i.e. slope change) occurs depends on material, loading mode, residual stress and manufacturing and is therefore not explicitly defined in most of the studied literature.

2.3.3 Multiaxial fatigue assessment using interaction equations

Many multiaxial fatigue models make use of a fatigue criterion in the form of an interaction equation. Infinite life is considered if the interaction equation remains within specific bounds. If the bounds are exceeded it is presumed that fatigue damage is encountered. These type of equations typically have a phenomenological basis and are thus generated from experimental data. It is a relatively easy way of modelling although the model performance depends on the completeness of the data sets that were used. Moreover, knowledge of the fatigue sensitive parameters and mechanisms that drive the fatigue damage process are essential.

2.3.3.1 Gough-Pollard relationship

Investigation of multiaxial fatigue in metals was initiated by Gough and Pollard who developed, based on extensive experimental research, the well-known empirical Gough-Pollard equation (Equation 2.3) (Gough, 1950; Gough & Pollard, 1935). Under combined reversed bending and torsional loading the equal-life curve showed an ellipse shape for ductile materials whilst a parabola shape (i.e. often referred to as ellipse-arc shape) for brittle materials (Gaier & Dannbauer, 2006; Gough & Pollard, 1935; Li, Jiang, Han, & Li, 2015; I. V. Papadopoulos & Panoskaltsis, 1996).

Even nowadays, many multiaxial fatigue criteria are based on the Gough-Pollard interaction equation. The equation defines the interaction at stress level and not at damage level meaning that different damage mechanisms (i.e. slope differences) are not incorporated. If the stress state remains within the boundaries of the ellipse shape (or ellipse-arc shape) it is believed that fatigue life is infinite, i.e. no fatigue damage is encountered. Furthermore, it is important to note that this equation was developed for constant amplitude loading based on (far-field) nominal stress.

An important aspect of the Gough-Pollard equation is that it was derived from reversed cyclic loading ($R = -1$) . The denominators in the equation are the presumed fatigue limits under fully reversed torsion and bending. Although not explicitly stated in the studied literature, this implies that the nominator and denominator should have the same load ratio (Gough, 1950; Gough & Pollard, 1935). This could require a correction using a mean stress model, cf. Section 2.4.2.

Gough-Pollard equation:

$$\left(\frac{\sigma_a}{\sigma_{a,f-1}}\right)^2 + \left(\frac{\tau_a}{\tau_{a,f-1}}\right)^2 = 1 \tag{2.3}$$

2.3.3.2 Recommendations in design guidelines

For the multiaxial fatigue assessment of welded marine structures, design codes such as Eurocode 3 and the International Institute of Welding (IIW) suggest a Gough-Pollard based interaction equation (European Standard, 2005; Hobbacher, 2015). See Equations 2.4-2.5. The combination of a normal and shear stress term are based on the dominating Mode I and Mode III contributions in weld toe failures

(Maddox, 2001). These modified Gough-Pollard based equations are applicable to nominal, (structural) hot-spot and notch stress concepts.

Eurocode accounts for different damage mechanisms by introducing different exponents for the normal and shear stress terms. The denominator in the equation is defined as the fatigue strength at $2{\cdot}10^6$ cycles (i.e. characteristic detail category). At or beyond this number of cycles, fatigue resistance typically shows a slope change. Therefore, many approaches for fatigue assessment make use of the fatigue strength at this particular knee-point. The Eurocode guideline can be applied to VA loading by converting the VA loading of the individual stress components (σ_a, τ_a) into a CA equivalent stress which provides the same amount of damage at $2{\cdot}10^6$ cycles. These equivalent stress values are then used as numerator in Equation 2.4.

IIW guidelines distinguish between CA loading (Equation 2.5) and VA loading (Equation 2.6). Both under CA and VA loadings the Critical Value (CV) of the criterion is set to 1 for proportional load cases and 0.5 for non-proportional load cases. This reduction of CV value is caused by load sequence effects under variable amplitude loading. With fluctuating mean stresses the allowable damage sum D is even advised to be further reduced to a value of 0.2. Under VA loading the numerator in Equation 2.5 is defined as an equivalent stress which represent the VA loading by a CA load. For further details see (Hobbacher, 2015). It should be noted that the IIW guidelines for multiaxial non-proportional loading are still under development and therefore rather conservative (Podgornik, 2017; Sonsino & Wiebesiek, 2007). Just like in Eurocode the denominators are defined as the fatigue strength at $2{\cdot}10^6$ cycles, using the dedicated FAT class (Hobbacher, 2015).

Eurocode:

$$\left(\frac{\sigma_a}{\sigma_{a,N_{CAT}})}\right)^3 + \left(\frac{\tau_a}{\tau_{a,N_{CAT}}}\right)^5 \leq 1 \tag{2.4}$$

IIW – CA loading:

$$\left(\frac{\sigma_a}{\sigma_{a,N_{FAT}}}\right)^2 + \left(\frac{\tau_a}{\tau_{a,N_{FAT}}}\right)^2 \leq CV \tag{2.5}$$

IIW – VA loading:

$$\left(\frac{\sigma_{eq}(D)}{\sigma_{a,N_{FAT}}}\right)^2 + \left(\frac{\tau_{eq}(D)}{\tau_{a,N_{FAT}}}\right)^2 \leq CV \tag{2.6}$$

In the DNV-GL recommendations (i.e. recommendations for fatigue design of offshore steel structures) the maximum principal stress is used for multiaxial fatigue assessment, and under some conditions this is also recommended by IIW and Eurocode 3 (i.e. maximum principal stress range approach). The use of this equivalent stress is based on experimental observations which demonstrate that (on a macroscopic level) fatigue cracks tend to grow perpendicular to the maximum principal stress (Schijve, 1989). Under uniaxial and proportional multiaxial loading the principal stress changes value but remains with a fixed direction. Characteristic for non-proportionality is a changing direction of the maximum principal stress. Therefore, principal stress vectors are often used to detect locations in a structure which are prone to non-proportional multiaxial fatigue.

DNV-GL advises different fatigue resistance curves depending on the angle of the maximum principal stress range to the weld seam (DNV-GL, 2005). See Figure 2.3. It is reasoned that the weld toe notch is more of a fatigue critical location when the maximum principal stress acts perpendicular to the weld seam (i.e. a lower SN-curve should be used). However, guidance is lacking for situations where the principal stress orientation changes during a load cycle, which typically occurs in (welded) joints which are subjected to non-proportional multiaxial stresses.

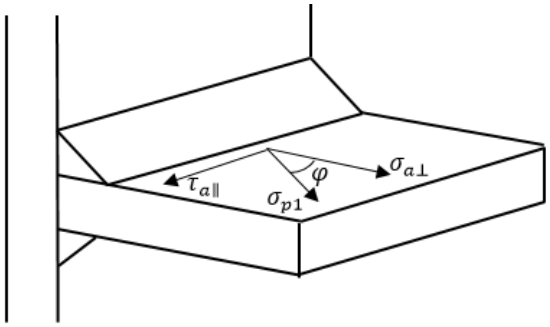

Figure 2.3: Illustration clarifying how angle ϕ is used to determine the maximum principal stress direction σ_p1 with respect to the weld toe; Reproduced from (DNV-GL, 2005)

2.3.3.3 Interaction equations for finite lifetime estimation

Interaction equations need to be formulated as a function of N (number of cycles) in order to determine the encountered fatigue damage and corresponding finite lifetime estimate. Examples of such interaction equations are the Findley criterion (Findley, 1959), Matake criterion (Matake, 1977) and McDiarmid criterion (McDiarmid, 1991). They can be described by the generic equation provided in Equation 2.7 where a and b are material dependent constants which serve as scaling factors between the shear and normal stress components.

$$\sigma_{eq}(N) = a \cdot f(\tau) + b \cdot f(\sigma) \tag{2.7}$$

In many multiaxial fatigue criteria de ratio of the normal and shear stress fatigue resistance is incorporated in scaling factors (Anes et al., 2014; Anes, Reis, Li, Freitas, & Sonsino, 2014). However, experimental tests demonstrated that the multiaxial damage mechanism is not well described by such (constant) factors as it varies with stress amplitude (ratio) and non-proportionality (Anes, Reis, & De Freitas, 2014; Anes et al., 2014). Anes et al. suggest to describe the stress scale factor as a function of stress amplitude σ_a and stress amplitude ratio r (Anes, Reis, & De Freitas, 2014; Anes et al., 2014). This function can be obtained from a regression analysis of experimental data under known uniaxial and multiaxial loading conditions, resulting in a polynomial function. Remarkable however is their choice for a shear stress based formulation. See Equation 2.8. Parameter Y represents non-proportionality and the load block is defined as the time interval between two zero-upcrossings. Shear stress is considered as most governing for fatigue crack initiation (Anes et al., 2014). Disadvantageous of this choice is that a pure torsional fatigue resistance curve is then required for which significantly less standardized curves are available (Anes, Reis, & De Freitas, 2014). This so called Stress-Scale-Factor (SSF) approach was validated with experimental data of plane geometries exposed to non-proportional and multiaxial load cases with CA and VA loading (Anes, Caxias, Freitas, & Reis, 2017; Anes et al., 2014).

$$\tau_{eq,block}(N) = Y \cdot \max(\tau_a + f(r, \sigma_a) \cdot \sigma_a)_{block} \tag{2.8}$$

The most well-known interaction equation for finite life calculations of ductile materials is generally known as the von Mises equivalent stress (Radaj et al., 2006). See Equation 2.9. Von Mises stress can be physically interpreted as the distortional strain energy. Looking at the existing literature and engineering practice, the von Mises equivalent is remarkably often used in multiaxial fatigue assessments. This is peculiar because this stress formulation was originally not designed for application to fatigue problems. It was developed by Huber, Mises and Hencky as an equivalent yield stress definition under static loading (Hencky, 1924; Huber, 1904; Mises, 1913). Therefore, some of its deficiencies should be carefully considered in multiaxial fatigue assessment. One of these deficiencies is the non-conservatism that results from non-proportionality. A severe overestimation of fatigue lifetime was observed under combined out-of-phase bending and torsion (Fatemi & Shamsaei, 2011; Sonsino, 2008b). The formulation appears to be insensitive for phase shifts between the normal and shear stress components (Nieslony, 2016). Similar issues are encountered in the frequency domain (Bonte, de Boer, & Liebregts, 2007; Nieslony, 2016). Interestingly, none of the studied literature discusses the application of von Mises stress to cases with a frequency induced non-proportionality. Further research on this matter could add valuable knowledge. Moreover, a point of attention is the sign loss due to the squared formulation. This is extensively discussed in (Sonsino, 1997) where it is suggested to account for the sign of the maximum load component (i.e. shear or normal stress). Von Mises equivalent stress considers a constant ratio (i.e. √3) between the uniaxial fatigue resistances of Mode I and Mode III. However, this ratio does not hold for various materials and the curves for uniaxial fatigue resistance (normal and shear) are not (always) parallel to each other (Anes & Reis, 2017; Carpinteri, Spagnoli, & Vantadori, 2003; Nieslony, 2016).

$$f\big(\sigma(N)\big) = \sigma_{VM}(N) = \sqrt{\sigma^2 + 3\tau^2} \tag{2.9}$$

2.3.4 Local stress information

The three most commonly used levels of local stress are nominal stress, (structural) hot spot stress and (effective) notch stress (Radaj et al., 2008). The nominal stress only considers the far-field response as a result of the macroscopic joint geometry. Although the use of nominal stresses requires low computational efforts it is known that additional local stress information improves the accuracy of fatigue lifetime estimates (i.e. less scatter in fatigue strength and higher confidence levels) (den Besten, 2015). In Figure 2.4 it is clearly demonstrated that nominal stress based lifetime estimates show significant data scatter. More local stress information is incorporated by the (structural) hot spot stress which also accounts for the structural geometry induced stress concentrations. The effect of a notch (for example at the weld toe) can be accounted for through the (effective) notch stress which encompasses the notch peak stress at the weld toe.

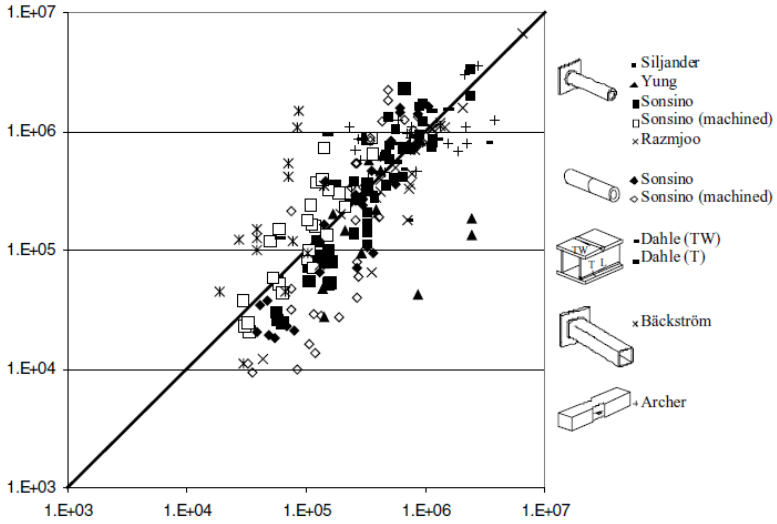

Figure 2.4: Scatter shown between experimental (vertical axis) and estimated (horizontal) fatigue lifetimes of welded joints based on nominal stress; Figure taken from (Bäckstrom & Marquis, 2004)

2.3.4.1 Structural hot spot stress

In welded joints, fatigue failure most commonly occurs at the weld toe (Maddox, 2001). Through linear extrapolation towards the weld toe, the hot spot stresses can be obtained based on particular reference points. However, the position of these reference points (i.e. location P and Q in Figure 2.5) are not univocally defined. Depending on the type of joint and hot spot (A, B or C) different positions are recommended in current engineering codes and guidelines (DNV-GL, 2005; European Standard, 2005; Hobbacher, 2015). A solution to this issue is provided by Dong et al. (Dong, 2001, 2005; Dong & Hong, 2006). They developed a mesh insensitive structural stress definition presuming an equilibrium-equivalent structural stress part and a self-equilibrating notch stress part acting on the vertical crack plane at the weld toe (Dong, 2001). The structural stress part (σ_s) is subdivided into a membrane (σ_m) and bending component (σ_b) as shown in Equation 2.10.

$$\sigma_s = \sigma_m + \sigma_b \tag{2.10}$$

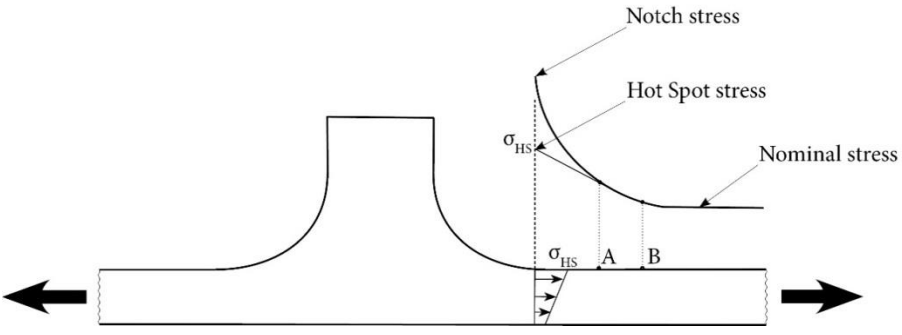

Figure 2.5: Illustration of nominal, (structural) hot spot and notch peak stress with respect to the weld toe

2.3.4.2 Notch stress

In engineering practice, stress raise at the weld toe is generally accounted for by the SN-curve (i.e. correction at the fatigue resistance side) or by Stress Concentration Factors (SCFs) (Radaj et al., 2006). SCFs describe the stress raise caused by the geometry of the notch. The ratio of the notch peak stress value over the nominal stress value corresponds to the SCF for that particular notch. Difficulties are however encountered at sharp corner notches and crack tips because the SCF could go to an infinitely high value, i.e. stress singularity. Stress Intensity Factors (SIFs) were developed to describe this stress singularity at crack tips (Radaj & Vormwald, 2013). They are commonly used in fracture mechanics. Unlike SCFs, SIFs are dependent on joint geometry, the particular size and location of the notch and the type of loading. The concept of SIFs is extended by Notch Stress Intensity Factors (N-SIF) which enable to describe the notch peak stress intensity at corner notches and amongst them weld toe notches (Radaj & Vormwald, 2013). Further details and references can be found in (Radaj et al., 2006; Radaj & Vormwald, 2013).

An essential feature of the notch stress approaches is the so-called Neubers microstructural support effect (Berto, Lazzarin, & Radaj, 2008; Radaj et al., 2006; Radaj & Vormwald, 2013). This effect enables to describe the physical mechanism behind the underestimation of the fatigue strength using elastic notch stress concentration. See Figure 2.6 for further clarification. A microstructural length parameter ρ^* is determined (i.e. microstructural support length) which indicates the distance, perpendicular to the notch, over which the notch stress should be averaged. Not the maximum notch stress but this effective averaged notch stress is considered for fatigue. The averaging procedure can be circumvented by assumption of a fictitious notch radius ρ_f that corresponds to a maximum notch stress value equal to the effective averaged notch stress. The fictitious radius can be found by adding the microstructural support length multiplied with a particular support factor s to the original notch radius. This microstructural support length is a characteristic material dependent parameter whilst the support factor is dependent on geometry (i.e. notch opening angle), loading mode and multiaxiality (Berto et al., 2008).

As an alternative to the Neuber concept, Strain Energy Density can be used (SED) (Radaj, Berto, & Lazzarin, 2009). The amount of strain energy is then considered in a particular elementary material volume (note the parallel to microstructural support length) at the notch tip. Just like stress, the strain energy density shows a singularity at the notch. However, once this density is averaged over a local elementary volume it becomes finite. This averaged SED is considered to be a representative fatigue resistance criterion for fatigue lifetime. Even though extensive work has already been performed, further research on the fatigue analysis of welded joints using N-SIFs or SED is still needed.

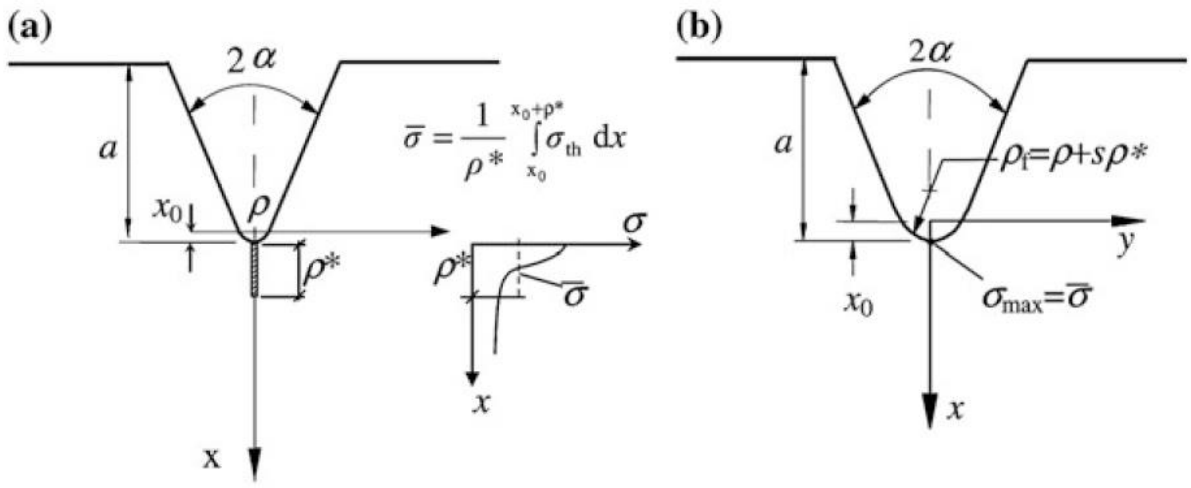

Figure 2.6: Illustration of the effective notch stress approach based on a fictitious notch stress radius ρ_f (b) presuming a microstructural support length ρ^*(a); Figure taken from (Radaj et al., 2009)

2.3.5 Fatigue damage parameters

For HCF the relatively low load amplitudes leading to macroscopically elastic deformations are characterizing. Therefore, stress is typically chosen as fatigue damage parameter in HCF criteria describing fatigue lifetime by a Basquin-like equation: $log(N) = log(C) - m \cdot log(S)$. On the other hand, LCF occurs under relatively high load amplitudes leading to plasticity. Therefore, strain is typically chosen as fatigue damage parameter and fatigue lifetime is described by a strain based Basquin-like equation referred to as the Manson-Coffin equation. However, (non-proportional) cyclic hardening cannot be accounted for by strain terms only. Combining stress and strain damage parameters results into an energy parameter. The advantage of an energy parameter is its ability to describe the constitutive material behaviour of HCF and LCF by accounting for the interaction between stress and strain, and thus path dependency of the material response.

The elastic and plastic strain energy densities (i.e. W^e and W^p) are described as a function of the normal and shear strain energies (Jahed et al., 2007; Macha & Sonsino, 1999; Noban et al., 2012). See Equation 2.11-2.13 where C^e and C^p represent empricial fitting factors. These terms represent the microscopic cyclic dissipation of strain energy and are related to the cylic hysteresis loops. Strain energy density is then related to fatigue lifetime using a Basquin- and Manson-Coffin-like relationship as shown in Equation 2.14 (Ahmadzadeh & Varvani-Farahani, 2016b; Macha & Sonsino, 1999).

$$\Delta W = \Delta W^e + \Delta W^p \tag{2.11}$$

$$\Delta W^e = \Delta\sigma^e \cdot \Delta\varepsilon^e + C^e \cdot \Delta\tau^e \cdot \Delta\gamma^e \tag{2.12}$$

$$\Delta W^p = \Delta\sigma^p \cdot \Delta\varepsilon^p + C^p \cdot \Delta\tau^p \cdot \Delta\gamma^p \tag{2.13}$$

$$\Delta W = \frac{\sigma_f'}{E}(2N_f)^b + \varepsilon_f'(2N_f)^c \tag{2.14}$$

For energy based damage parameters it is vital to know the material's cyclic stress-strain response. Ramberg-Osgood's equation, given in Equation 2.15, is often used to describe such cyclic stress-strain behaviour (Stephens et al., 2000). The cyclic strain hardening exponent n' and the cyclic strength coefficient K' can be derived from stable cyclic stress-strain data. Moreover, they can be expressed as a function of the parameters in the Manson-Coffin equation, see Equations 2.16-2.17 and Figure 2.7.

$$\frac{\Delta\varepsilon_n}{2} = \left(\frac{\Delta\sigma_n}{2E}\right) + \left(\frac{\Delta\sigma_n}{2K\prime}\right)^{1/n\prime} \tag{2.15}$$

$$K' = \frac{\sigma_f'}{\varepsilon_f'^{b/c}} \tag{2.16}$$

$$n' = \frac{b}{c} \tag{2.17}$$

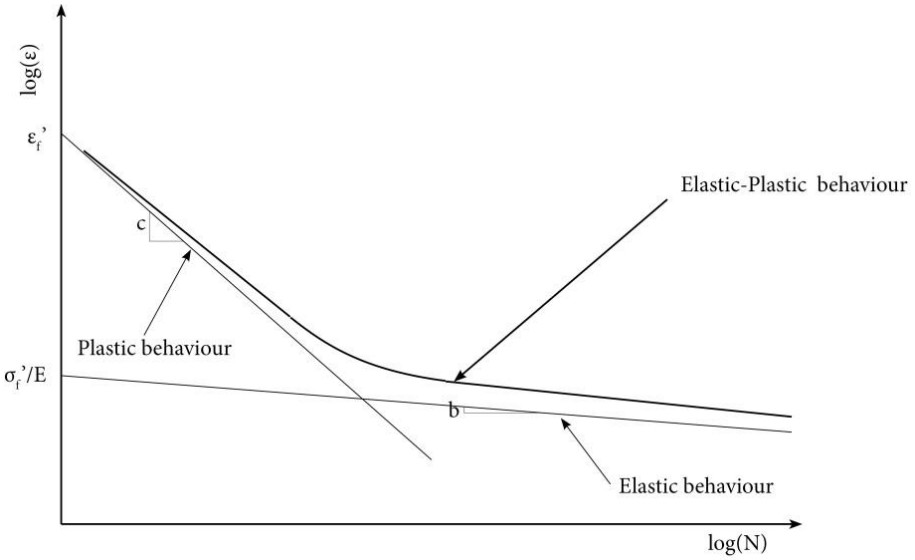

Figure 2.7: Fatigue life – strain curve showing the regions of elastic and plastic behaviour

Plasticity models enable to describe the cyclic elastic-plastic stress-strain behaviour under complex loadings by a yield condition, flow rule, consistency condition and hardening rule (Garud, 1981; Jahed et al., 2007; Noban et al., 2012). The yield function enables to differentiate between elastic and plastic behaviour. The flow rule, also referred to as the normality rule, describes the plastic strain rate internal variable whilst hardening (either isotropic and/or kinematic) is incorporated to describe the yield surface evolution. Finally, a consistency equation is required to solve all constitutive equations.

Macha & Sonsino (1999) executed an extensive review of multiaxial fatigue methods which make use of an energy based fatigue damage parameter. Interestingly, none of the investigated methods was recommended for application in engineering practice because further experimental validation is required. Particularly, difficulties arise when the plastic strain energy under complex random/VA loading has to be determined.

2.4 Audit of multiaxial fatigue assessment methods

An extensive amount of literature has been reviewed to identify multiaxial fatigue methods which are or could be suitable for the fatigue lifetime assessment of welded joints in marine structures exposed to (non-)proportional CA and VA loading. An audit of the selected approaches is presented here, focussing on application in the high cycle fatigue regime.

2.4.1 Critical plane methods

Experimental observations have shown that fatigue cracks tend to occur on particular material planes (Bäckström & Marquis, 2001; Fatemi & Shamsaei, 2011) and this has led to the development of critical plane based fatigue methods. The physical mechanism behind fatigue crack initiation and early crack growth is related to laminar flow in combination with crack opening/closing in the easy glide plane. Critical plane methods typically consider that high cycle fatigue damage is proportional to the macroscopic shear stress acting at the material plane of easy gliding (Susmel & Lazzarin, 2002). This assumption can be found at the basis of various critical plane based methods such as the ones proposed by Findley (Findley, 1959), Matake (Matake, 1977), Mc Diarmid (McDiarmid, 1991) and Fatemi-Socie (Fatemi & Socie, 1988). This fundamental basis explains why shear amplitude or range are typically used as model input. Fatigue crack evolution is affected by crack opening and closure which can be characterized by a normal or hydrostatic component (I. V. Papadopoulos & Dang Van, 1997; Susmel & Lazzarin, 2002). Therefore, critical plane based methods generally account for the combined damaging effect of a shear and normal stress/strain.

Critical plane methods consider a fatigue criterion at all possible plane orientations, through an iterative procedure (using an arbitrarily defined interval). The critical plane is typically found through one of the following characteristics: the maximum shear stress amplitude or range acting on the plane, the maximum damage parameter (often governed by the combined effect of a shear and normal stress component) acting on the plane, or by a specific inclination towards another fracture plane (Fatemi & Shamsaei, 2011; Papuga, 2011; Susmel, 2008; Weber, Kenmeugne, Clement, & Robert, 1999). The latter originates from the experimental observation of cracks initiating and growing/propagating on differently oriented material planes. Specific reference to a fracture plane is made for example in (Bedkowski & Macha, 1992; Macha, 1991) whilst in (Carpinteri et al., 2016) the critical plane is considered as the dominant failure plane. As discussed in (Papuga, 2011), the material characteristics determine the deviation between the plane of fatigue crack initiation/early growth and the plane of macroscopic fracture.

Different critical plane based methods were compared with experimental data in (Bäckström & Marquis, 2001; Fatemi & Shamsaei, 2011; Papuga, 2011) but only few methods have been developed and applied to notched geometries like welded joints encountering multiaxial fatigue. An interesting overview study was provided in (Fatemi & Shamsaei, 2011) where it is claimed that critical plane based methods can capture non-proportionality best by accounting for stress and strain terms in their damage parameter. Another interesting publication is (Bäckström & Marquis, 2001) where multiaxial fatigue data of various welded joints is compared with a Findley based critical plane approach. From the studied literature it can be concluded that the critical plane definition appears most successful with a maximum damage parameter. Such a damage parameter enables to account for damage mechanism and fatigue strength which are both needed to determine fatigue resistance correctly. In the following

there will be elaborated on a selection of critical plane methods which appear to be, or show potential, for application to multiaxial fatigue problems in welded joints.

2.4.1.1 Modified Wöhler Curve (MWC) Method

For estimation of fatigue lifetime under multiaxial loading conditions the MWC method constructs a shear stress based, loading specific fatigue resistance curve (i.e. modified $\tau_{eq} - N$ Wöhler curve). This curve is described by a linear Basquin-like relationship which uses characteristic values of the uniaxial fatigue resistance. See Equation 2.18-2.22 and Figure 2.9. The reference value N_{ref} is considered at $2{\cdot}10^6$ cycles because it corresponds to the class definition of various design codes and guidelines and avoids problems with typical slope changes at the knee-point.

The Maximum Variance Method (MVM) is used to identify the direction of the critical plane. An advantageous feature of this method is that once the (co)variances have been determined the proceeding calculations are independent of length of the input signal, i.e. time trace (Susmel, 2014). This saves significant computational efforts (Susmel, 2010). The MVM is applicable to CA and VA time traces and originates from experimental observations (Susmel, Tovo, & Benasciutti, 2009). Crack initiation is considered at the material plane which endures the maximum variance of shear stress (i.e. the maximum shear stress range). The degree of multiaxiality is then determined through the stress amplitude ratio ρ of the shear and normal stress component acting on the critical plane. The governing equations can be clarified using Mohr's circle as depicted in Figure 2.8. It should be noted that this formulation is valid for a load ratio of -1.

The MWC method has been applied successfully for the assessment of multiaxial fatigue in welded joints under VA loading (Susmel, 2014). However, high mean stresses or large stress amplitudes can lead to over-conservative results due to high stress amplitude ratios. Under these conditions a limit value for ρ is proposed, i.e. ρ_{lim}. This limitation is based on the assumption that normal stress no longer affects fatigue damage once the crack is fully opened (Susmel, 2008).

$$\rho = \frac{\sigma_{n,max}}{\tau_a} = \frac{\sigma_a}{(\tau_{max} - \tau_{min})/2} \tag{2.18}$$

$$\tau_{eq}(\rho) = \left(\frac{\sigma_{a,ref}}{2} - \tau_{a,ref}\right) \cdot \rho + \tau_{a,ref} \tag{2.19}$$

$$k(\rho) = \left(k_{\rho=1} - k_{\rho=0}\right) \cdot \rho + k_{\rho=0} \tag{2.20}$$

$$N_f = N_{ref} \left(\frac{\tau_{eq}(\rho)}{\tau_a}\right)^{k(\rho)} \tag{2.21}$$

$$\rho_{lim} = \frac{\tau_{a,ref}}{2 \cdot \tau_{a,ref} - \sigma_{a,ref}} \tag{2.22}$$

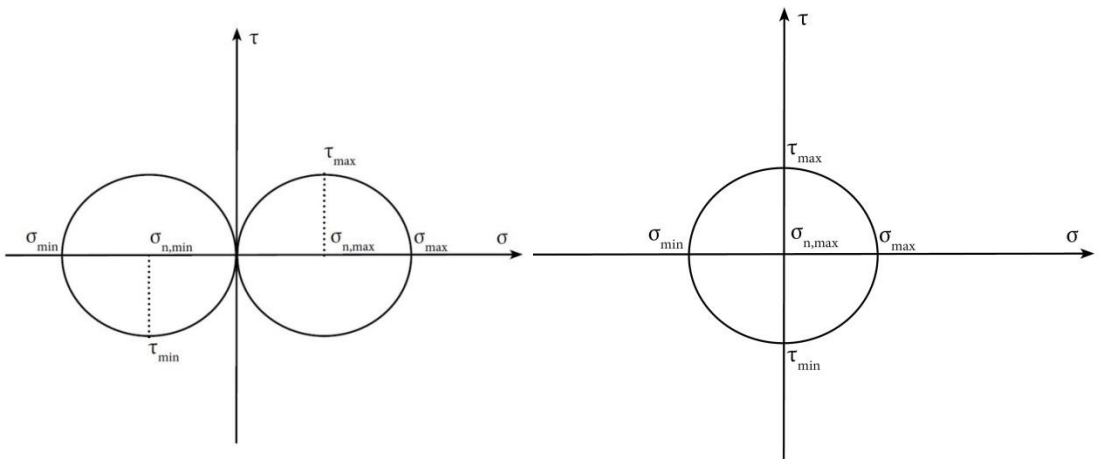

Figure 2.8: Mohr's circle for cyclic reversed sinusoidal loading in pure tension/bending (left) and pure torsion (right)

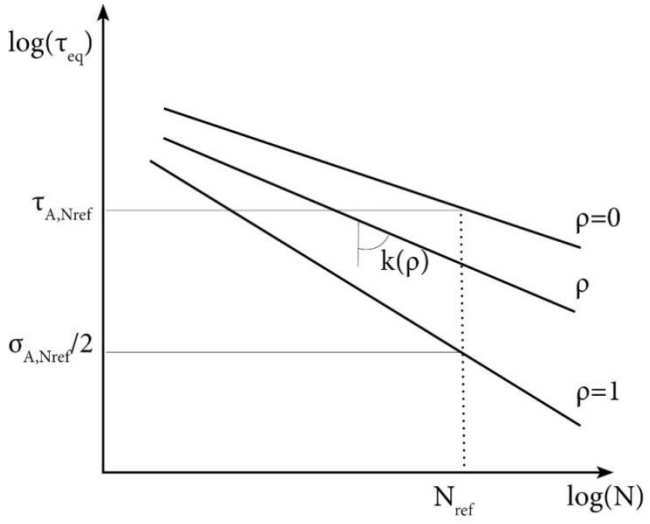

Figure 2.9: Illustration of the linear relationship between the modified Wohler curve and the uniaxial fatigue resistance curves (ρ = 0,ρ = 1)

2.4.1.2 Modified Carpinteri Spagnoli (MCS) Method

The MCS method is based on work showing a strong dependence between the fracture plane, the principal stress direction and maximum shear stress (Carpinteri, Brighenti, Macha, & Spagnoli, 1999). Principal stress directions change under (complex) cyclic loading and therefore the MCS method considers their average values and direction (i.e. $\hat{1}$, $\hat{2}$, $\hat{3}$), described by Euler angles (i.e. θ, ϕ, ψ). From a parametric study it was observed that the direction of the average principal stress axes corresponds closely to the direction of the principal axes when the maximum principal stress is experienced (i.e. the fracture plane) (Carpinteri et al., 2008). The direction of the critical plane is determined by a rotational angle with respect to this (observable) fracture plane (Carpinteri, Macha, Brighenti, & Spagnoli, 1999). An expression for this rotational angle has been proposed in the form given in Equation 2.23 (Carpinteri & Spagnoli, 2001). The expression provides a zero angle (i.e. δ = 0) for very brittle materials (i.e. $\frac{\tau_{a,f-1}}{\sigma_{a,f-1}} = 1$) and an angle of 45 degrees (i.e. δ = π/4) for ductile materials (i.e.

$\frac{\tau_{a,f-1}}{\sigma_{a,f-1}} = \frac{1}{\sqrt{3}}$). Therefore, the Equation is applicable for as long as the ratio $\frac{\tau_{a,f-1}}{\sigma_{a,f-1}}$ remains within the bounds of zero to one.

$$\delta = 45 \cdot \frac{3}{2}\left(1 - \left(\frac{\tau_{a,f-1}}{\sigma_{a,f-1}}\right)^2\right) \tag{2.23}$$

Interestingly, the MCS method uses a Gough-Pollard-like equation as fatigue criterion (see Equation 2.24). Input parameters for this criterion are the mean normal and shear stress component acting on the critical plane. Under non-proportional and multiaxial loading the shear stress τ_a, acting on a material plane, changes in value and direction unlike the normal stress σ_n which does not change in direction. To identify the shear stress amplitude or range acting on a particular material plane, various methods have been developed. Examples are the Minimum Circumscribed Circle (MCC), Minimum Circumscribed Ellipse (MCE) and Prismatic Hull (PH) (Mamiya, Araújo, & Castro, 2008; I. V. Papadopoulos, 1998; I. V. Papadopoulos & Dang Van, 1997). An advantageous feature of the latter two is that the ratio of their major and minor axis can be used as indicator for the degree of non-proportionality. See Appendix A for further details about the Prismatic Hull method. The MCS method performs a Goodman based mean stress correction on the normal stress (see Equation 2.25) (Carpinteri et al., 2008) and a Basquin-like equation is proposed for finite-lifetime estimation (see Equation 2.26) (Carpinteri et al., 2008; Carpinteri, Spagnoli, Vantadori, & Bagni, 2013a).

Under CA loading conditions normal Rainflow counting can be used (Carpinteri, Spagnoli, Vantadori, & Bagni, 2013b) whilst under VA or random loading, an alternative cycle counting is required. In (Carpinteri et al., 2003) an alternative rainflow counting procedure is suggested which considers two signals (i.e. normal and shear stress acting on the critical plane). One signal is considered primary (normal stress) and the other (shear stress amplitude) auxiliary. For each counted cycle of the primary signal the maximum value of the auxiliary signal is also stored. This counting technique shows similar basis as multiaxial Rainflow counting (Langlais, Vogel, & Chase, 2003), cf. Section 5.1.

Specifically for VA and random loading the MCS method was reformulated in spectral domain which resulted in a significant decrease of computational efforts (Carpinteri, Ronchei, Spagnoli, & Vantadori, 2014). However, this spectral approach has only been validated with plane geometries and therefore requires some further validation for its application to notched geometries like welded joints. In time-domain the MCS method has been applied to multiaxial fatigue problems in welded joints with satisfactory results (Carpinteri et al., 2008).

$$\left(\frac{\sigma_a^*}{\sigma_{a,f-1}}\right)^2 + \left(\frac{\tau_a}{\tau_{a,f-1}}\right)^2 = 1 \tag{2.24}$$

$$\sigma_a^* = \sigma_a + \sigma_{a,f-1}\left(\frac{\sigma_{avg}}{\sigma_{UTS}}\right) \tag{2.25}$$

$$\sigma_{eq} = \sqrt{(\sigma_a^*)^2 + \frac{\sigma_{a,f-1}}{\tau_{a,f-1}}\tau_a^2} \tag{2.26}$$

2.4.1.3 Structural Stress Critical Plane (SSCP) Method

The Structural Stress Critical Plane (SSCP) method has been developed specifically for the fatigue lifetime assessment of multiaxially loaded and welded joints (Jiang, Liu, Wang, Zhang, & Long, 2015).

It is based on structural (hot-spot) stress following a combination of the methodologies used in the MCS and the MWC method. Stress Concentration Factors (SCF) are used in order to account for the local structural normal and shear stress components acting at the weld toe. With these stress terms an equivalent shear stress is formulated which is then used in a fatigue criterion similar to the one in MCS method. See Equation 2.27. This enables to determine fatigue life using Equation 2.28 in combination with the Modified Wöhler Curve.

The SSCP method has been validated with experimental tests of welded StE460 specimens subjected to uniaxial and (non-)proportional multiaxial CA loadings. The results were compared to the hot-spot stress approach recommended in IIW guidelines (Hobbacher, 2015). The SSCP performed more satisfactory but on the conservative side and thus further research is needed, particularly looking into its application to complex VA/random loadings (Jiang et al., 2015).

$$\tau_{eq} = \sqrt{(k_\sigma \cdot \sigma_a)^2 + \left(\frac{\sigma_{A,f-1}}{\tau_{A,f-1}}\right)^2 \cdot (k_\tau \cdot \tau_a)^2} \tag{2.27}$$

$$N_f = N_{ref} \left(\frac{\tau_{ref}}{\tau_{eq}}\right)^{k(\rho)} \tag{2.28}$$

2.4.1.4 Stress-Strain (SS) Method

Over the years a variety of methods has been developed which use an energy based fatigue parameter in combination with a critical plane approach for multiaxial fatigue assessment. In (Fatemi & Shamsaei, 2011) it is also stated that critical plane based methods can capture non-proportionality best by accounting for stress and strain terms in their damage parameter. In the work of (Ince & Glinka, 2013) such methods have been thoroughly evaluated addressing the important features for a multiaxial fatigue damage parameter.

In recent work of (Ahmadzadeh & Varvani-Farahani, 2016a, 2016b), Mohrs circles of normal and shear stress and strain are used for multiaxial fatigue assessment under complex loading (see Equation 2.29-2.30). Multiaxial Wang-Brown cycle counting is used to determine the Mohr circles. Fatigue life is defined by a combination of a Basquin-like and Mason-Coffin-like relationship and the required parameters (e.g. b_1, b_2, c_1, c_2) can be obtained from the fatigue life-strain curves. This approach was validated with experimental data of plane geometries under non-proportional VA loading but showed conservative results. Further validation with experimental data is still needed, also with fatigue data of welded joints.

$$W_{eq} = \frac{1}{\sigma_f' \varepsilon_f'} (\Delta\sigma \Delta\varepsilon) + \frac{1}{\tau_f' \gamma_f'} (\Delta\tau_{max} (\gamma_a)_{max}) \tag{2.29}$$

$$W_{eq} = \left(\frac{\sigma_f'}{E} (2N_f)^b + \varepsilon_f' (2N_f)^c\right) + \left(\frac{\tau_f'}{G} (2N_f)^d + \gamma_f' (2N_f)^e\right) \tag{2.30}$$

To determine the stress-strain response of a material as a result of a particular load path, the the Garud multi-surface hardening rule can be used (Ahmadzadeh & Varvani-Farahani, 2016b; Ince & Glinka, 2013). However, this calculation requires a significant amount of computational efforts. In (Ince & Glinka, 2016) a relatively simple and fast modelling technique is suggested for the local elastoplastic stress-strain response. The stress-strain response at the notched area is then used as an input for a

damage parameter which is evaluated at all planes. The critical plane is the one experiencing the maximum damage. The damage parameter assumes the contribution of plastic normal strain in opening the crack, plastic shear strain in inducing dislocation movement, elastic normal strain in assisting crack opening and elastic shear strain in overcoming sliding friction of crack surfaces (Ince & Glinka, 2016). See equation 2.31. Multiaxial fatigue data (proportional and non-proportional) of a notched geometry (SAE 1045) was compared with the described approach (Ince & Glinka, 2016). A good correlation was found but further investigation is still needed for the application to welded joints.

$$f(N) = \frac{\tau_{max}}{\tau_f'}\frac{\Delta\gamma^e}{2} + \frac{\Delta\gamma^p}{2} + \frac{\sigma_{n,max}}{\sigma_f'}\frac{\Delta\epsilon_n^e}{2} + \frac{\Delta\epsilon_n^p}{2} \tag{2.31}$$

2.4.2 Invariant methods

Contrary to the physical grounds which have led to the development of critical plane based methods computational advantages have led to the development of invariant based fatigue methods. The use of stress invariants significantly reduces computational efforts and model complexity. There exist different formulations but invariant based multiaxial fatigue models typically use a term which accounts for dilation (i.e. volume change) and a part which accounts for distortion (i.e. yielding). Dilation is represented by hydrostatic stress σ_H or the first stress invariant I_1 whilst distortion is represented by the second invariant of the deviatoric stress J_2, see Equations 2.32-2.33 (cf. Appendix B).

Crossland and Sines were one of the first who proposed an invariant based approach for multiaxial fatigue assessment (Crossland, 1956; Sines, 1959). They suggested a fatigue criterion which can be described by the generic equation provided in Equation 2.34. Material parameter k represents a function of the uniaxial fatigue strengths (I. V. Papadopoulos & Dang Van, 1997). The equation represents a fatigue limit criterion meaning that infinite fatigue life is considered. For finite fatigue lifetime estimation the left-hand-side can be represented by a Basquin-like equation (Cristofori et al., 2007).

$$I_1 = \sigma_x + \sigma_y + \sigma_z \tag{2.32}$$

$$J_2 = \frac{1}{6}\left(\left(\sigma_x - \sigma_y\right)^2 + \left(\sigma_y - \sigma_z\right)^2 + \left(\sigma_z - \sigma_x\right)^2\right) + \tau_{xy}^2 + \tau_{yz}^2 + \tau_{zx}^2 \tag{2.33}$$

$$f(\tau(N)) = \sqrt{J_2} + k\sigma_H \tag{2.34}$$

2.4.2.1 Projection-by-Projection (PbP) Method

This invariant based method accounts for the load path of the deviatoric stress in its five dimensional Euclidean space (i.e. deviatoric space) (Cristofori et al., 2007). It is hypothesized that the total fatigue damage can be represented by the sum of the individual damage contributions of each projected load path. As a result of the load path projection on the axes of the reference frame, uncorrelated signals are generated. Therefore, the method is named the Projection-by-Projection method (PbP). For each projection the accumulated fatigue damage is determined through multiaxial rainflow counting where deviatoric stress is considered as primary signal and hydrostatic stress as auxiliary signal (Cristofori et al., 2007; Langlais et al., 2003). For further details on this counting procedure see Section 5.1. For each projection (i) the mean amplitude of the deviatoric stress ($J_{2a,i}$) is determined. In addition, the overall

mean hydrostatic stress ($\sigma_{H,avg}$) is defined. See Equations 2.35 and 2.36 where j represents the counted cycle and i the projection.

$$\sqrt{J_{2a,i}} = \frac{\sum_j \sqrt{J_{2a,ij}}}{j_{max}} \tag{2.35}$$

$$\sigma_{H,avg} = \frac{\sum_{ij} \sigma_{H,ij}}{i_{max} \cdot j_{max}} \tag{2.36}$$

For finite fatigue lifetime estimation a load specific fatigue resistance curve is constructed ($\sqrt{J_{2a}} - N$). This is done using the same linearization as proposed in the MWC method, cf. Section 4.1.1 (Cristofori et al., 2007). Stress ratio ρ is based on the deviatoric and hydrostatic stress components as can be seen in Equation 2.37. It should be noted, that just like in the MWC method, the ρ value has a limit value (Susmel, 2008). Fatigue damage is defined for each load cycle in each projection, see Equation 2.38.

The PbP method has been validated in the time domain for non-proportional CA loading, and its spectral formulation (Benasciutti, Zanellati, & Cristofori, 2019; Cristofori, Benasciutti, & Tovo, 2011) for random loading. Experimental data of plane geometries was used (Benasciutti et al., 2019; Cristofori et al., 2011, 2007). Accurate results were found and the spectral formulation resulted in reduced computational efforts. So far, the generated results have been promising and therefore the PbP method is incorporated in this study. However, further research is required in both domains (i.e. time and frequency). In the time domain the method has not yet been validation for non-proportional VA loadings. Both in the time and frequency domain, further investigation is needed for the application and validation with welded joints.

$$\rho = \sqrt{3} \cdot \frac{\sigma_{H,avg}}{\sqrt{\sum_i \left(\sqrt{J_{2a,i}}\right)^2}} \tag{2.37}$$

$$D_{ij} = \left(\frac{\sqrt{J_{2,ij}}}{\sqrt{J_{2,\rho}}}\right)^{k_\rho} \cdot \frac{1}{N_{ref}} \tag{2.38}$$

2.4.3 Integral methods

Integral based methods have been developed to circumvent the difficulties of critical plane based methods with non-proportionality induced lifetime reduction in ductile materials. By integration of a particular fatigue parameter, over a specified (elementary) material volume, it is tried to account for non-proportionality induced interaction effects. This requires significant computational efforts since optimization of such a calculation procedure is limited. The integration has to be executed over all material planes within an acceptable level of accuracy (Papuga & Ruzicka, 2007). Therefore, integral methods are generally considered more computational intensive, and thus less favourable, than critical plane or invariant based methods.

2.4.3.1 Effective Equivalent Stress Hypothesis (EESH)

The EESH is based on von Mises equivalent stress and considers local stress, in order to overcome the deficiency of a Von Mises equivalent under non-proportional loadings (cf. Section 3.3.3). It is an

extension of the critical plane approach, with the intention to account for the interactions resulting from non-proportional fatigue loading of ductile materials. This hypothesis considers the interaction between slip bands (caused by non-proportionality) by integration of the shear stresses acting on each material plane (Sonsino, 1997, 2008b; Sonsino & Kueppers, 2001). This results into an effective shear stress F which can be used to correct the von Mises equivalent stress $\sigma_{VM} = \sigma_{eq}(\delta = 0)$ as shown in Equations 2.39-2.40. Originally, the EESH considered a square root term in the equation of σ_{eq} for which reference is made to (Sonsino, 2008b; Sonsino & Kueppers, 2001). However, the term appeared unsuccessful and eventually it was removed from the governing equations.

Promising results were obtained in comparison to experimental data of welded joints under multiaxial CA loading (Sonsino, 2008b; Sonsino & Kueppers, 2001). The hypothesis can also be applied to more complex VA loadings for which suggestions can be found in (Sonsino & Kueppers, 2001; Sonsino et al., 1999; Sonsino & Maddox, 2001). However, difficulties are encountered with time varying phase differences and the hypothesis requires a realistic damage sum. For this purpose representative multiaxial fatigue data has to be available. Further investigation and validation are therefore still needed.

$$F(\delta) = \frac{1}{\pi}\int_0^{\pi} f(\varphi)d\varphi \begin{cases} f(\varphi) = \tau_a(\varphi);\ CA\ loading \\ f(\varphi) = \frac{1}{L}\sum_{i=1}^{L}\tau_{a,i}(\varphi)\ ; VA/stochastic\ loading \end{cases} \tag{2.39}$$

$$\sigma_{eq}(\delta) = \sigma_{eq}(\delta = 0) \cdot \frac{F(\delta)}{F(\delta=0)} \tag{2.40}$$

2.4.3.2 Energy Method (EM)

In (Saintier, Palin-Luc, Bénabes, & Cocheteux, 2013) an integral based approach is formulated using an energy based fatigue parameter. Henceforth, this method will be referred to as the Energy Method (EM). It is a generic assumption that material behaves elastically in the HCF regime and therefore the EM considers the elastic strain energy density as fatigue parameter. From an FE model the (rates of) stresses and strains are evaluated and used as inputs for the method, which describes an incremental damage parameter. Advantageous of this formulation is that cycle counting is circumvented.

The EM considers local maxima of strain energy density (W) at critical points C_i. The surrounding material points (M) that encounter damaging work are identified using a threshold concept. The average strain energy density W_{eq}, which corresponds to this volume V_i, is then found by integration over a certain period t (for CA loading) or time duration t (for VA loading). In (Saintier et al., 2013) stress triaxiality T is taken into account through an empirical expression which was derived from experimental multiaxial fatigue data of plane geometries. The generalized governing equations are provided in Equations 2.41-2.42. Fatigue lifetime is determined by conversion of the uniaxial fatigue resistance curves into a so-called Master SN-curve (Saintier et al., 2013).

The EM has been validated with various experimental data sets of plane geometries exposed to complex multiaxial load cases (i.e. VA and non-proportional) (Saintier et al., 2013). Promising results were obtained but further investigation is still required for notched geometries and welded joints encountering such complex loads.

$$W(M,t) = \frac{1}{2}\sigma(M,t) \cdot \tau(M,t) \tag{2.41}$$

$$W_{eq}(C_i) = \frac{1}{V_i}\int_{V_i} f(T,W)\, dV \tag{2.42}$$

2.4.4 Damage models

For the description of (multiaxial) fatigue behaviour, damage mechanics can also be used instead of the commonly used (empirically based) SN-approach. The fundamentals of damage mechanics are described by the thermomechanical behaviour of solids. Reference is made to the following background literature (Francois, Pineau, & Zaoui, 2012; Lemaitre & Chaboche, 1990; Lemaitre & Desmorat, 2005; Lemaitre & Marquis, 1992).

Local plasticity eventually leads to crack initiation. Therefore, damage is typically coupled to local stress/strain. The constitutive equations of damage models originate from the laws of thermodynamics for irreversible processes. The thermodynamic state of a material at a certain time instant is described by observable and (not directly measurable) internal state variables at that same instant. This so-called state potential is described by state laws and associated variables. For dissipative processes, a dissipation potential $F\ (\sigma, X, R, Y)$ is considered which is a function of the associated variables listed in Table 2.1. Dissipative behaviour is then described by evolution laws of the flux of these internal variables. Damage evolution is governed by a so-called yield function f which describes the relationship between local plasticity and damage (Lemaitre, 1996; Lemaitre, Sermage, & Desmorat, 1999). An advantageous feature of damage mechanics is that it uses a continuous damage variable so that cycle counting is circumvented. Moreover, the model can be adjusted depending on the material characteristics and load conditions (e.g. brittle/ductile materials, isotropic/anisotropic behaviour, crack closure/opening).

Variable	*Symbol*	*Flux of internal variable*	*Symbol*
Stress	σ	Plastic strain rate	$\dot{\varepsilon^p}$
Kinematic hardening	X	Kinematic hardening	$\dot{\alpha}$
Isotropic hardening	R	Isotropic hardening	$\dot{r}$
Damage energy release rate	Y	Damage rate	$\dot{D}$

Table 2.1: Associated variables to dissipative processes and the flux of their corresponding internal variables

2.4.4.1 Application of damage mechanics to marine structures

Damage mechanics has been applied specifically to marine (i.e. naval) structures in (Erny, Thevenet, Cognard, & Körner, 2010a), (Lautrou, Thevenet, & Cognard, 2009) and (Thevenet, Erny, Cognard, & Korner, 2009). In (Lautrou et al., 2009) a strategy was developed and validated to assess fatigue in a butt-welded plate of S355 steel which is typically used in the maritime industry. The strategy was subdivided into two steps. Firstly, a shakedown study was performed by executing a FE analysis. Weld toe geometry (obtained from laser measurements), residual stresses, material zone dependent yield stresses (i.e. base material, weld material, heat affected zone) and elastic-plastic material behaviour were all incorporated in this model. Secondly, fatigue crack initiation was studied by post-processing of the results in a damage model. The approach showed promising results but was only applied to CA and VA uniaxial fatigue problems.

The same strategy has been applied to a structural detail of a stiffened panel and a cruciform joint (Erny et al., 2010a; Thevenet et al., 2009). Experimental data was collected by testing a transversal and longitudinal stiffened panel and cruciform joints under cyclic tensile loading conditions (Erny et

al., 2010a). In the stiffened panel, three locations where identified which showed multiaxial stresses. However, due to orthogonality of the structure these multiaxial stress states must have been proportional. The model parameters were obtained from a monotonic stress-strain curve, a cyclic tension-compression test and two uniaxial SN-curves determined by self-heating tests. By minimizing the difference between the model results and the experiments the model parameters were identified (Erny et al., 2010b). Numerical and experimental results showed agreement but no concrete conclusions could be drawn yet (Erny et al., 2010a). Particularly for more complex multiaxial load cases (e.g. VA and non-proportional) further research is needed.

2.5 Multiaxial cycle counting

The majority of the approaches for (multiaxial) fatigue assessment require cycle counting. The most commonly applied cycle counting technique is rainflow counting. This technique defines load cycles by the closed hysteresis loops in their cyclic stress-strain behaviour. For as long as there is one (equivalent) input parameter, this counting procedure can be used to identify the number of load cycles and corresponding stress/strain ranges or amplitudes. If there are multiple fluctuating input parameters ($\sigma\ (t), \tau\ (t)$) a multiaxial cycle counting techniques is required.

2.5.1 Multiaxial Rainflow counting

Bannantine & Socie were one of the first to identify cycles under multiaxial variable amplitude loading by making use of rainflow counting (Shamsaei, 2010). They consider the projected strain path on a plane and counted the normal and shear component of this projection individually. Using the Fatemi-Socie and Smit-Watson-Topper parameters they then determine damage. Two failure modes are considered (i.e. tensile and shear failure) and damage is thus determined for each failure mode (i.e. axial or shear damage). The Bannantine & Socie counting procedure has several deficiencies which are addressed in (Anes et al., 2014; Langlais et al., 2003).

Langlais et al. developed an extension to traditional rainflow counting for multiaxial variable amplitude loadings which overcomes the deficiencies in the Bannantine & Socie counting procedure (Langlais et al., 2003). In the counting procedure of Langlais et al. two individual load signals are introduced. One primary signal which is considered governing for fatigue damage and a second auxiliary signal of which the fluctuations are registered for each counted primary cycle. In (Cristofori et al., 2007) the counting procedure was applied in combination with the PbP method (cf. Section 4.2.1). In their procedure, Langlais et al. choose the deviatoric stress as the primary signal and the hydrostatic stress as the auxiliary signal. The maximum hydrostatic stress is then identified for each counted cycle of deviatoric stress.

2.5.2 Modified Wang-Brown cycle counting

In (Meggiolaro et al., 2012) the Wang-Brown multiaxial cycle counting procedure was modified to overcome its deficiencies with load sign (loss) and starting point definition (which is not univocally defined). This Modified Wang-Brown (MWB) counting procedure considers the relative Von Mises equivalent strain in the five dimensional deviatoric Euclidean space. An advantageous feature of the Euclidean working space is that computational complexity is reduced because the distance between two points directly corresponds to the relative Von Mises stress/strain range. The procedure can be easily converted from strain into Von Mises equivalent stress if preferred.

To determine the mean and amplitude of each load cycle an enclosed surface procedure should be used. A so-called Moments of Inertia (MOI) method has been developed to account for the actual shape of the load path and not only its extremes (Meggiolaro, Tupiassú, & De Castro, 2015). The load path is assigned a unit mass so that the centre of mass corresponds with the mean. The moments of inertia can then be used to define the equivalent stress/strain range. Advantageous of this MOI method is that it can account for non-convexity and load path dependency. However, in the studied literature, no work could be found wherein the MWB counting procedure has been applied in multiaxial fatigue assessment.

2.5.3 Virtual cycle counting

Anes et al. claim that many cycle counting procedures are incapable of relating the maximum damage parameter in a particular time interval to the encountered total damage during this interval (Anes, Reis, & Freitas, 2015). Therefore, they developed a new so-called virtual cycle counting procedure. This cycle counting procedure derives its name from the fact that it does not consider hysteresis loops like conventional rainflow counting. A load block is defined as the time interval between two zero up-crossings of the equivalent shear stress. Within this block, the number of virtual load cycles are counted based on an equivalent shear stress which is defined in accordance with the Stress Scale Factor (SSF) method (cf. Section 3.3.3).

For damage calculation a reference SN-curve is required which describes fatigue resistance in pure torsion (i.e. Mode III). The counting procedure has been compared to other techniques and validated with multiaxially loaded plane geometries. Satisfactory results were obtained although the considered load cases did not account for mean stress effects (i.e. all load cases had a zero mean stress) (Anes, Reis, & De Freitas, 2014). Important to note is that this counting procedure can only be applied in accordance with the SSF method. It is not applicable in combination with other multiaxial fatigue methods.

2.5.4 Path-Dependent-Maximum Range (PDMR) cycle counting

The shape of a load path is correlated to plastic dissipation and therefore characterizes a load cycle. The Path-Dependent-Maximum-Range (PDMR) method accounts for complex load histories (i.e. variable amplitude, non-proportional) in stress space ($\sigma_s - \sqrt{\beta}\tau_s$), by consideration of the maximum stress range and the load path corresponding to this range (Dong, Wei, & Hong, 2009; Mei & Dong, 2016; Wei & Dong, 2014).

Typically, PDMR counting considers a Von Mises based stress space. Therefore, parameter β is set to √3. Counting is performed on a structural stress level (cf. Section 3.4) generally considering Mode I and Mode III as governing modes in welded joints (i.e. plated or shell structures). If needed, the procedure can be converted to strain space (i.e. $\varepsilon - \sqrt{\beta}\gamma$ for LCF) or extended to three dimensional space (i.e. including Mode II as well). However, the latter will significantly increase the already complex and time intensive computation.

PDMR cycle counting requires an appropriate fatigue resistance curve for damage calculation. A Master SN-curve was developed for fatigue lifetime estimation of welded joints. This so-called Master SN-curve is compatible with Von Mises based PDMR cycle counting (Hong & Forte, 2014). A large experimental data set was used to determine the characteristic values of the Master curve. All data was captured in a narrow scatter band. Amongst the data were welded joints of different

geometries and dimensions subjected to various types of (complex) loading (i.e. uniaxial, proportional and non-proportional). Two sets of characteristics were determined depending on a dominant Mode I or Mode III (Dong, Hong, Osage, & Prager, 2002; Hong & Forte, 2014). PDMR cycle counting has been validated in various studies and was applied successfully in the multiaxial fatigue assessment of welded joints (Dong et al., 2009; Wei & Dong, 2010, 2011, 2014).

2.6 Fatigue damage accumulation

Cycle counting provides the number of (half) cycles at a given stress range/amplitude. This knowledge can be used to determine the amount of accumulated fatigue damage and corresponding fatigue lifetime. For this purpose, a damage accumulation rule is typically used. In literature, various rules can be found which distinguish themselves in how they describe the evolution of fatigue damage. Typically the critical damage sum (corresponding to fatigue failure) is $D_c = 1$. However, it should be kept in mind that this value originates from an average based on experimental results ranging from a damage value of 0.01 to 10 (Schijve, 1989; Sonsino & Wiebesiek, 2007). For complex load cases (e.g. variable amplitude loading, mean stress and non-proportionality), the critical damage sum is often reduced. In (Sonsino, 2008b) it is demonstrated that a critical damage sum of 1 appears non-conservative for welded steel and aluminium joints subjected to multiaxial loads. Based on this, a design value of $D_c = 0.5$ is recommended in IIW guidelines (Hobbacher, 2015).

2.6.1 Palmgren-Miner rule

The most well-known damage rule is the linear Palmgren-Miner rule, which is often referred to as Miner rule. It presumes a linear accumulation of fatigue damage by consideration of a single sloped fatigue resistance, up to a kneepoint. See Figure 2.10. From experimental observations it is seen that constant amplitude load cycles show a significant slope change beyond the kneepoint (i.e. towards the high cycle regime). The damage contributions at the stress ranges beyond this kneepoint were initially disregarded through consideration of a horizontal fatigue limit. Fatigue damage is formulated by Equation 2.43, where n_i stands for the endured number of cycles (at a specific stress range) and N_i for the fatigue resistance (at this particular stress range). Due to its straightforward expression, Miners rule is (still) widely used in scientific research and engineering practice.

$$D = \sum_i n_i / N_i \tag{2.43}$$

2.6.2 Haibach

One of the first modifications of Miners rule was made by Haibach who considered a bilinear (i.e. double sloped) fatigue resistance. See Figure 2.10. This changes the course of the Wöhler curve after the kneepoint and thus introduces a change in damage mechanism. The damage formulation remains equal to Equation 2.43 but the damage contributions of stress amplitudes/ranges below the kneepoint are no longer neglected and accounted for.

2.6.3 Corten-Dolan

The damage rule of Corten-Dolan considers that each load cycle induces fatigue damage. In the damage rule of Haibach this is accounted for through a slope change after the kneepoint. The damage

rule of Corten-Dolan on the other hand, considers a slope change for the entire Wöhler curve. The damage rule considers a single-sloped fatigue resistance which is described by a powerlaw relationship (see Figure 2.10 and Equation 2.44) (Macha & Niesłony, 2012; G. B. Marquis & Socie, 2003; Zhu, Huang, Liu, He, & Liao, 2012). In this relationship the exponent d is material and load dependent. It is claimed that this experimentally defined parameter can account for the interaction between low(er) and high(er) stress cycles. However, its physical interpretation is not straightforward and from the reviewed literature it is not clear how it is experimentally defined. In (Marquis & Socie, 2003) and (Zhu et al., 2012) it is mentioned that (field) experience is required to correctly assign a value to exponent d. This is a drawback because it greatly affects fatigue lifetime estimation. The Corten-Dolan damage rule is rarely used in engineering practice.

$$D = \sum_i \frac{n_i}{N_{max}} \left(\frac{\sigma_i}{\sigma_{max}}\right)^d \tag{2.44}$$

2.6.4 Serensen-Kogayev

In the reviewed literature, only marginal information could be found about the physical interpretation and fundamental basis of the Serensen-Kogayev damage rule. This can be attributed to the fact that the original article was written in Russian (Nieslony & Macha, 2007). The governing equations of the Serensen-Kogayev damage rule are provided in Equation 2.45-2.47 (Karolczuk & Blacha, 2011). Palmgren-Miners rule is considered when b = 1. This is shown in Figure 2.10 and Equation 2.45. Parameter a determines a threshold stress such that all stress ranges below this value are disregarded in the fatigue damage accumulation. In that respect, a sort of fatigue limit is being considered. Typically, a is set to a value of 0.5 but why this value is chosen as such is not supported by argumentation in any of the reviewed literature (Łagoda, Macha, & Niesłony, 2005; Macha & Niesłony, 2012; Nieslony & Macha, 2007). Like the The Corten-Dolan damage rule, Serensen-Kogayev damage rule is rarely used in engineering practice.

$$D = \sum_i \frac{n_i}{b \cdot N_i} \tag{2.45}$$

$$b = \sum_i \frac{\sigma_i \cdot t_i - a \cdot \sigma_{a,f-1}}{\sigma_{max} - a \cdot \sigma_{a,f-1}} \tag{2.46}$$

$$t_i = \frac{n_i}{\sum_i n_i} \tag{2.47}$$

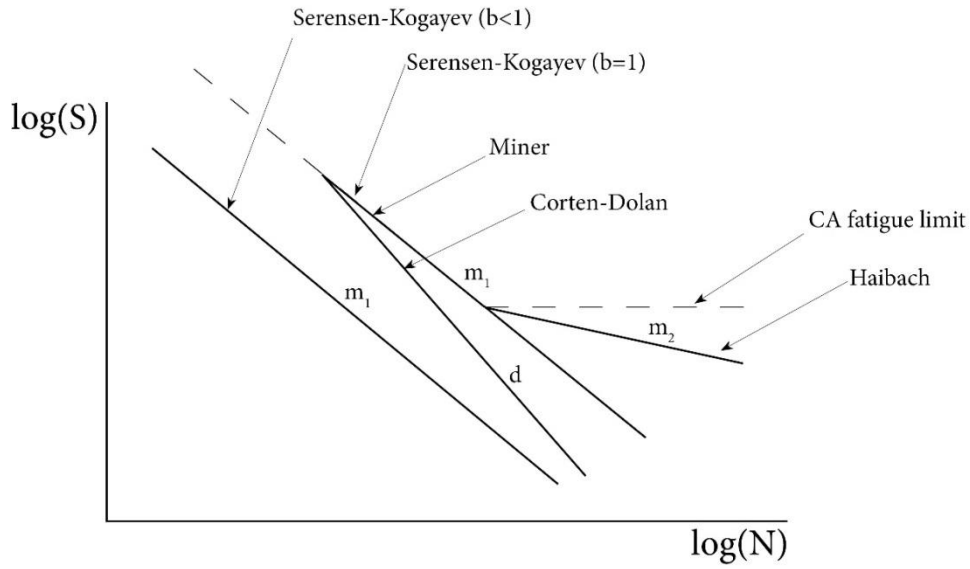

Figure 2.10: Fatigue resistance behaviour corresponding to the damage accumulation rules of Miner, Haibach, Corten-Dolan and Serensen Kogayev

2.6.5 Moment of Load Path (MLP) concept

It has been shown that path length is an incomplete indicator of multiaxial fatigue damage for some specific load cases (Mei & Dong, 2016). Therefore, an accumulative Moment of Load Path (MLP) concept has been developed (Mei & Dong, 2016, 2017a, 2017b, 2017c). It is based on earlier work from (Itoh, Sakane, Socie, & Ohnami, 1995). A path-dependent parameter accounts for load path dependency whilst a material parameter accounts for the materials' sensitivity to non-proportional loading. Multiaxial fatigue damage is considered a linear summation of a proportional part and a non-proportional part. The proportional damage part corresponds to the (shortest/direct) path length between two points (i.e. A and B) in $\sigma - \sqrt{\beta}\tau$ stress space (i.e. $\Delta\sigma_{eff}$). The non-proportional damage part is related to the actual path length and therefore represented by an integral.

Using PDMR cycle counting, the equivalent MLP stress $\Delta\sigma_{eff,MLP}$ for each cycle is expressed as a function of the effective stress range $\Delta\sigma_{eff}$, a parameter of dimensionless path length g and a material dependent non-proportionality sensitivity parameter α. See Equation 2.48. For structural steel the sensitivity parameter α ≈ 1 provides reasonable correlation with multiaxial fatigue data of non-proportionally loaded welded joints (Mei & Dong, 2017a). However, it remains unclear at which specified number of cycles α should be determined and how to deal with slope differences between the two fatigue resistance curves of proportional and non-proportional loading.

In (Mei & Dong, 2016, 2017a, 2017b, 2017c) a substantial amount of experimental data was used to validate the MLP concept applied to complex load cases for welded joints of structural steel and aluminum alloys. Satisfactory results were obtained. An advantageous feature of this damage concept is its applicability to both LCF (strain based) and HCF (stress based).

$$\Delta\sigma_{eff,MLP} = \Delta\sigma_{eff}(1 + \alpha \cdot g) \tag{2.48}$$

2.7 State-of-the-Art of multiaxial fatigue assessment

The amount of information on (the different methods and approaches for) multiaxial fatigue assessment is abundant. For clarity, this Chapter provides two schematic overviews which show the required input parameters of the audited methods (Table 2.2) and their current application domain (Table 2.3).

	IIW	Eurocode	DNV-GL	Stress Scale Factor (SSF) Method	Modified Wöhler Curve (MWC) Method	Modified Carpinteri-Spagnoli (MCS) Method	Structural Stress Critical Plane (SSCP) Method	Stress-Strain (SS) Method	Projection-by-Projection (PbP) Method	Effective Equivalent Stress Hyposthesis (EESH)	Energy Method (EM)	Damage Model
Fatigue strenght at specified nr. of cycles - Mode I	✓	✓				✓	✓				✓	
Fatigue strenght at specified nr. of cycles - Mode IIII	✓	✓				✓	✓				✓	
Fatigue resistance behaviour Mode I	✓	✓			✓	✓	✓		✓	✓	✓	✓
Fatigue resistance behaviour Mode III	✓	✓		✓	✓	✓	✓		✓	✓	✓	✓
Fatigue resistance behaviour Mixed Mode I & III			✓									
Local weld toe information			✓				✓			✓		✓
Monotonic stress-strain behaviour						✓		✓			✓	✓
Cyclic stress-strain behaviour								✓			✓	✓

Table 2.2: Overview showing the required input parameters for the audited multiaxial fatigue methods

2.8 Discussion

Over the past few decades the complexity of structural designs in the maritime industry has increased, as well as the operational and environmental conditions they are facing. Furthermore, there is a growing interest in lifetime extension of existing marine structures. This requires investigation and development of new methods and approaches for multiaxial fatigue assessment. In current practice, SN-approaches are most commonly used. Such approaches identify the damage parameter(s) and then require cycle counting in combination with a damage (accumulation) rule and a reference SN-curve to come to a fatigue lifetime estimate. For each of these individual steps, methods have been developed specifically for multiaxial fatigue problems. However, these methods are not per definition compatible with one another. Examples are the SSF approach (cf. Section 3.3.3) which can only be used in combination with specific virtual cycle counting and PDMR cycle counting which is not compatible with standardized fatigue resistance curves (cf. Section 4.3).

	IIW	Eurocode	DNV-GL	Stress Scale Factor (SSF) Method	Modified Wöhler Curve (MWC) Method	Modified Carpinteri-Spagnoli (MCS) Method	Structural Stress Critical Plane (SSCP) Method	Stress-Strain (SS) Method	Projection-by-Projection (PbP) Method	Effective Equivalent Stress Hyposthesis (EESH)	Energy Method (EM)	Damage Model
Time domain	✓	✓	✓	✓	✓	✓	✓	✓	✓	✓	✓	✓
Spectral domain						✓			✓			
Uniaxial (Rainflow) cycle counting	✓	✓	✓		✓	✓	✓			✓		
Multiaxial cycle counting				✓		✓	✓	✓	✓			
Plane geometries		✓	✓	✓				✓	✓		✓	✓
Notched geometries	✓				✓	✓	✓			✓		
Non-proportionality	✓		✓	✓	✓	✓	✓	✓	✓	✓	✓	
Requires dedicated SN curve	✓	✓	✓	✓	✓	✓	✓	✓	✓	✓	✓	

Table 2.3: Overview showing the current domain of application for the audited multiaxial fatigue methods

Multiaxial fatigue methods were initially developed for the assessment of infinite life. Later on, these criteria have been developed towards finite life so that they could be used for fatigue lifetime estimation. Commonly, a Basquin-like equation is used which incorporates material dependency (i.e. fatigue strength) in the log(C) term. However, in this equation, the multiaxial load path dependent damage mechanism is not accounted for since slope m is considered a constant. New models were developed with the intention of overcoming these deficiencies such as the MLP concept (see Section 4.6.5) which suggests two individual parameters: a load path dependent non-proportionality factor and a material dependent sensitivity parameter.

From the reviewed literature it can be observed that discrepancies exist between the approaches and models applied in academia and engineering practice. The approaches and methods developed by academia are often found unfavourable for industrial practice due to their complexity (i.e. computational efforts) and need for further improvement and validation. Implementation and application sometimes requires (rarely) determined parameter(s). On the other hand, the design guidelines and recommendations which are used in engineering practice often lack a clear description on how to deal with more complex multiaxial load case, e.g. frequency induced non-proportionality and random loading.

The knowledge (through model validation) of multiaxial fatigue in welded joints of marine structures is affected by the scarcity and often incompleteness of experimental data. Furthermore, findings and test data which is obtained in other fields of expertise (e.g. aerospace, automotive) is not directly applicable to marine structures since different joint and weld geometries, loading conditions and materials are used. (Papuga et al., 2016) elaborates further upon these inconsistencies in experimental data sets for multiaxial fatigue assessment and model validation.

Multiaxial fatigue methods are typically validated individually or in comparison to a selection of other methods. Based on the findings in such studies, judgements are made about accuracy and validity. However, the experimental data sets in these kind of studies often originate from different sources. Complete and representative experimental data is needed to make a fair judgement of, and comparison between, the different methods and approaches that are currently available. Further experimental studies are therefore necessary to improve the understanding of multiaxial fatigue in welded joints, and to identify the strengths and weaknesses of the different methods in their application to marine structures.

2.9 Conclusion

There exist large differences between the approaches for multiaxial fatigue assessment in engineering practice and academia. Engineering practice prefers comprehensive and efficient calculation procedures with relatively simple models. Safety factors/margins are introduced in order to cover for uncertainties and data scatter. Typically, these approaches have an empirical basis and lack a strong physical (theoretical) background. Therefore, when they are applied to more complex multiaxial fatigue problems they can become untrustworthy and lead to under- or over-conservative results. Academia produce more refined but also more complex models, generally with the objective to incorporate a physical basis. However, these are often incomplete or have limitations in their application domain. Due to this situation, a consensus about multiaxial fatigue assessment is lacking, particularly for welded joints in marine structures. Experimental proof is needed to take away uncertainties and to help clarify which model(s) or approach(es) are capable of (the most) accurate lifetime estimation. It is important that such experimental data is not only obtained under conceptual CA loadings but also under VA and random loadings which represent realistic load conditions of marine structures. Until such experimental proofs have been generated, inspections and maintenance will be of high importance, especially for fatigue critical components and joints. In the following Chapters, work will be presented that contributes to the validation of multiaxial fatigue models for marine structures based on unique experimental data.

2.10 Appendix A: Prismatic Hull method

The prismatic hull-shape can be found by implementation of a procedure which considers three angles $(\varphi, \theta, \gamma)$ to describe a particular assessment plane orientation and the prismatic hull in this plane which encloses the considered load path projection, i.e. shear stress acting on the critical material plane. Through iteration the angles are determined whereby an optimum is reached.

First, the unity vector u of the normal to the critical plane is determined with respect to the Cartesian coordinate system. See equation A.1. Then, assuming that the z axis rotates with u, the rotation of the x and y axis is describe through vectors a and b. Again the Cartesian coordinate system is used as reference, cf. Figure A1. Then, a new coordinate system is determined for the prismatic hull enclosing the shear stress load path acting in the critical plane. See Figure A2. The major and minor axis of the prismatic plane are assigned $p1$ and $p2$ and are defined with respect to the axis a and b. Finally, the shear stress vector is projected along both axis of the prismatic hull (i.e. p_1 and p_2) in order to determine the shear stress amplitude.

$$u = \begin{cases} u_x = \sin\varphi\cos\theta \\ u_y = \sin\varphi\cos\theta \\ u_z = \cos\varphi \end{cases} \quad a = \begin{cases} a_x = \sin\theta \\ a_y = -\cos\theta \\ a_z = 0 \end{cases} \quad b = \begin{cases} b_x = \cos\varphi\cos\theta \\ b_y = \cos\varphi\sin\theta \\ b_z = -\sin\varphi \end{cases} \qquad \text{A.1}$$

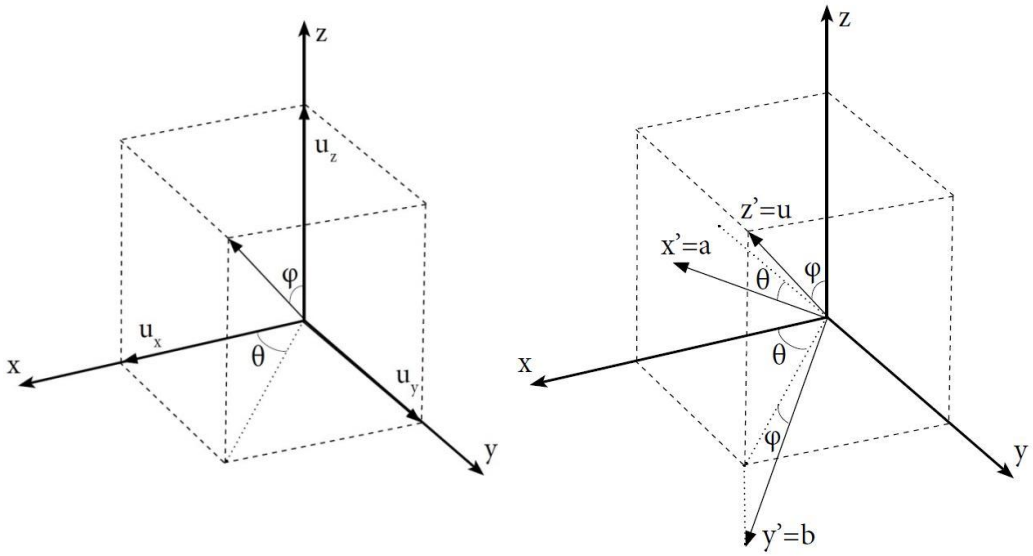

Figure A1: Illustration of the rotational angles φ and θ with which the unity vector u of the normal to the critical plane is described in the Cartesian coordinate system (left)

$$p_1 = \begin{cases} p_{1a} = \cos\gamma \\ p_{1b} = \sin\gamma \end{cases}$$

$$p_2 = \begin{cases} p_{2a} = -\sin\gamma \\ p_{2b} = \cos\gamma \end{cases}$$

$$a_1 = \frac{1}{2}(\max(\tau \cdot p_1) - \min(\tau \cdot p_1))$$
$$a_2 = \frac{1}{2}(\max(\tau \cdot p_2) - \min(\tau \cdot p_2))$$

$$\tau_a = \sqrt{a_1^2 + a_2^2}$$

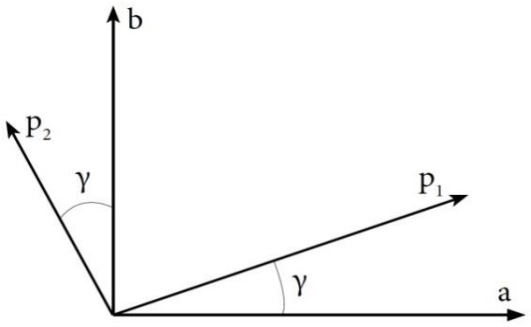

Figure A2: Illustration of how the reference system for the prismatic hull is determined from the rotated x' and y' axis (respectively a and b) and rotational angle γ.

2.11 Appendix B: Stress invariants

Any stress tensor can be expressed by its three principal stresses, i.e. $\sigma_1, \sigma_2, \sigma_3$, which describe the stress state solely by normal stress (see tensor S- Equation B.1). The characteristic equation that derives from this tensor is provided in Equations B.2-B.3. Three stress invariants can be found from this characteristic equation, namely I_1, I_2, I_3 (Francois *et al.,* 1988; Wolf, 2008). They are given in equation B.4-B.6.

$$S = \begin{bmatrix} \sigma_1 & 0 & 0 \\ 0 & \sigma_2 & 0 \\ 0 & 0 & \sigma_3 \end{bmatrix} \tag{B.1}$$

$$det(S - \lambda I) = 0 \tag{B.2}$$

$$-\lambda^3 + I_1\lambda^2 - I_2\lambda + I_3 = 0 \tag{B.3}$$

$$I_1 = \sigma_1 + \sigma_2 + \sigma_3 \tag{B.4}$$
$$I_2 = \sigma_1\sigma_2 + \sigma_2\sigma_3 + \sigma_1\sigma_3 \tag{B.5}$$
$$I_3 = \sigma_1\sigma_2\sigma_3 \tag{B.6}$$

Similar calculations can be done using the deviatoric stress tensor S^D which excludes the hydrostatic stress component σ_H (see Equations B.7-B.8). This leads to the three stress invariants of the deviatoric stress tensor, i.e. J_1, J_2, J_3 (Francois *et al.,* 1988; Wolf, 2008). These are provided in equation B.9-B.11.

$$S^D = \begin{bmatrix} \sigma_1 - \sigma_H & 0 & 0 \\ 0 & \sigma_2 - \sigma_H & 0 \\ 0 & 0 & \sigma_3 - \sigma_H \end{bmatrix} \tag{B.7}$$

$$\sigma_H = \frac{\sigma_1+\sigma_2+\sigma_3}{3} \tag{B.8}$$

$$J_1 = (\sigma_1 - \sigma_H) + (\sigma_2 - \sigma_H) + (\sigma_3 - \sigma_H) = 0 \tag{B.9}$$
$$J_2 = \frac{1}{6}[(\sigma_1 - \sigma_2)^2 + (\sigma_2 - \sigma_3)^2 + (\sigma_3 - \sigma_1)^2] = \frac{1}{2}Tr\left(S^{D^2}\right) \tag{B.10}$$
$$J_3 = (\sigma_1 - \sigma_H)(\sigma_2 - \sigma_H)(\sigma_3 - \sigma_H) = \frac{1}{3}Tr\left(S^{D^3}\right) \tag{B.11}$$

For a better comprehension of stress invariants there can be looked at in the principal stress space. If a diagonal is drawn in the principal stress space, such that $\sigma_1 = \sigma_2 = \sigma_3$, the load path will travel along this diagonal. The location on the diagonal is proportional to the first stress invariant I_1 and the hydrostatic stress σ_H. This is evident because $\sigma_H = \frac{I_1}{\sqrt{3}}$. In the plane perpendicular to the diagonal the distance towards the load path in this plane corresponds to the second deviatoric stress invariant J_2. Therefore, this invariant is used to define yield criteria. Like for example the Von Mises yield criterion: $\sigma_{VM} = \sqrt{3J_2}$. See Figure B1 for clarification.

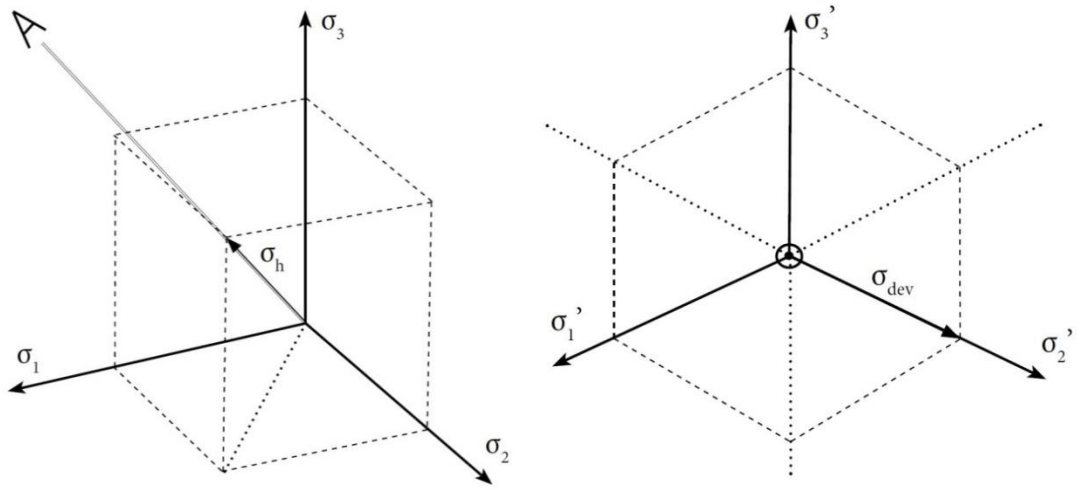

Figure B2: Illustration of the hydrostatic stress component σ_H in principal stress space (left) and the deviatoric stress component σ_{dev} looking down the diagonal passing through the hydrostatic stress vector (right).

2.12 References

Ahmadzadeh, G. R., & Varvani-Farahani, A. (2016a). Fatigue damage and life evaluation of SS304 and Al 7050-T7541 alloys under various multiaxial strain paths by means of energy-based Fatigue damage models. *Mechanics of Materials*, *98*, 59–70. https://doi.org/10.1016/j.mechmat.2016.04.007

Ahmadzadeh, G. R., & Varvani-Farahani, A. (2016b). Fatigue life assessment of steel samples under various irregular multiaxial loading spectra by means of two energy-based critical plane damage models. *International Journal of Fatigue*, *84*, 113–121. https://doi.org/10.1016/j.ijfatigue.2015.11.018

Anes, V., Caxias, J., Freitas, M., & Reis, L. (2017). Fatigue damage assessment under random and variable amplitude multiaxial loading conditions in structural steels. *International Journal of Fatigue*, *100*, 591–601. https://doi.org/10.1016/j.ijfatigue.2016.12.009

Anes, V., Reis, L., & De Freitas, M. (2014). A new criterion for evaluating multiaxial fatigue damage under multiaxial random loading conditions. *Advanced Materials Research*, *891–892*, 1360–1365. https://doi.org/10.4028/www.scientific.net/AMR.891-892.1360

Anes, V., Reis, L., & Freitas, M. (2015). Asynchronous Multiaxial Fatigue Damage Evaluation. *Procedia Engineering*, *101*, 421–429. https://doi.org/10.1016/j.proeng.2015.02.051

Anes, V., Reis, L., Li, B., Fonte, M., & De Freitas, M. (2014). New approach for analysis of complex multiaxial loading paths. *International Journal of Fatigue*, *62*, 21–33. https://doi.org/10.1016/j.ijfatigue.2013.05.004

Anes, V., Reis, L., Li, B., Freitas, M., & Sonsino, C. M. (2014). Minimum Circumscribed Ellipse (MCE) and Stress Scale Factor (SSF) criteria for multiaxial fatigue life assessment. *Theoretical and Applied Fracture Mechanics*, *73*, 109–119. https://doi.org/10.1016/j.tafmec.2014.08.008

Anes, V., & Reis, M. D. F. L. (2017). The damage scale concept and the critical plane approach. *Fatigue & Fracture of Engineering Materials & Structures*, (January), 1240–1250. https://doi.org/10.1111/ffe.12653

Bäckstrom, M., & Marquis, G. (2004). Interaction equations for multiaxial fatigue assessment of welded structures. *Fatigue and Fracture of Engineering Materials and Structures*, *27*, 991–1003. https://doi.org/10.1111/j.1460-2695.2004.00811.x

Bäckström, M., & Marquis, G. (2001). A review of multiaxial fatigue of weldments: Experimental results, design code and critical plane approaches. *Fatigue and Fracture of Engineering Materials and Structures*, *24*, 279–291. https://doi.org/10.1046/j.1460-2695.2001.00284.x

Bedkowski, W., & Macha, E. (1992). Fatigue Fracture Plane Loadings - Prediction by Based on the Stresses Variance Under Multiaxial Random of Equivalent Stress Maximum Shear and Normal. *Materialwissenschaft Und Werkstofftechnik*, *23*, 82–94.

Benasciutti, D., Sherratt, F., & Cristofori, A. (2015). Basic principles of spectral multi-axial fatigue analysis. *Procedia Engineering*, *101*, 34–42. https://doi.org/10.1016/j.proeng.2015.02.006

Benasciutti, D., & Tovo, R. (2006). Comparison of spectral methods for fatigue analysis of broad-band Gaussian random processes. *Probabilistic Engineering Mechanics*, *21*, 287–299. https://doi.org/10.1016/j.probengmech.2005.10.003

Benasciutti, D., Zanellati, D., & Cristofori, A. (2019). The “Projection-by-Projection” (PbP) criterion for multiaxial random fatigue loadings: Guidelines to practical implementation. *Frattura Ed Integrita Strutturale*, *47*, 348–366. https://doi.org/10.3221/IGF-ESIS.47.26

Berto, F., Lazzarin, P., & Radaj, D. (2008). Fictitious notch rounding concept applied to sharp V-notches : Evaluation of the microstructural support factor for different failure hypotheses . Part I : Basic stress equations. *Engineering Fracture Mechanics*, *75*, 3060–3072. https://doi.org/10.1016/j.engfracmech.2007.12.011

Besten, J. H. den. (2015). *A total stress concept*. Delft University of Technology.

Besten, J. H. den. (2018). Fatigue damage criteria classification, modelling developments and trends for welded joints in marine structures. *Ships and Offshore Structures*, *13*(8), 787–808. https://doi.org/10.1080/17445302.2018.1463609

Bolchoun, A., Wiebesiek, J., Kaufmann, H., & Sonsino, C. M. (2014). Application of stress-based multiaxial fatigue criteria for laserbeam-welded thin aluminium joints under proportional and non-proportional variable amplitude loadings. *Theoretical and Applied Fracture Mechanics*, *73*, 9–16. https://doi.org/10.1016/j.tafmec.2014.05.009

Bonte, M. H. A., Boer de, A., & Liebregts, R. (2007). Determining the von Mises stress power spectral density for frequency domain fatigue analysis including out-of-phase stress components. *Journal of Sound and Vibration*, *302*(1–2), 379–386. https://doi.org/10.1016/j.jsv.2006.11.025

Carpinteri, A., Brighenti, R., Macha, E., & Spagnoli, A. (1999). Expected principal stress directions under multiaxial random loading. Part II: numerical simulation and experimental assessment through the weight function method. *International Journal of Fatigue*, *21*, 89–96.

Carpinteri, A., Fortese, G., Ronchei, C., Scorza, D., & Vantadori, S. (2016). Spectral fatigue life estimation for non-proportional multiaxial random loading. *Theoretical and Applied Fracture Mechanics*, *83*, 67–72. https://doi.org/10.1016/j.tafmec.2015.12.019

Carpinteri, A., Macha, E., Brighenti, R., & Spagnoli, A. (1999). Expected principal stress directions under multiaxial random loading. Part I: theoretical aspects of the weight function method. *International Journal of Fatigue*, *21*, 83–88.

Carpinteri, A., Ronchei, C., Spagnoli, A., & Vantadori, S. (2014). On the use of the Prismatic Hull method in a critical plane-based multiaxial fatigue criterion. *International Journal of Fatigue*, *68*, 159–167. https://doi.org/10.1016/j.ijfatigue.2014.05.007

Carpinteri, A., & Spagnoli, A. (2001). Multiaxial high-cycle fatigue criterion for hard metals. *International Journal of Fatigue*, *23*, 135–145.

Carpinteri, A., Spagnoli, A., & Vantadori, S. (2003). A multiaxial fatigue criterion for random loading. *Fatigue and Fracture of Engineering Materials and Structures*, *26*(6), 515–522. https://doi.org/10.1046/j.1460-2695.2003.00620.x

Carpinteri, A., Spagnoli, A., & Vantadori, S. (2008). Multiaxial fatigue life estimation in welded joints using the critical plane approach. *International Journal of Fatigue*, *31*, 188–196. https://doi.org/10.1016/j.ijfatigue.2008.03.024

Carpinteri, A., Spagnoli, A., Vantadori, S., & Bagni, C. (2013a). Structural integrity assessment of metallic components under multiaxial fatigue : the C – S criterion and its evolution. *Fatigue and Fracture of Engineering Materials and Structures*, *36*, 870–883. https://doi.org/10.1111/ffe.12037

Carpinteri, A., Spagnoli, A., Vantadori, S., & Bagni, C. (2013b). Structural integrity assessment of metallic components under multiaxial fatigue: The C-S criterion and its evolution. *Fatigue and Fracture of Engineering Materials and Structures*, *36*(9), 870–883. https://doi.org/10.1111/ffe.12037

Castelluccio, G. M., & Mcdowell, D. L. (2016). Microstructure-sensitive small fatigue crack growth assessment : Effect of strain ratio , multiaxial strain state , and geometric discontinuities. *International Journal of Fatigue*, *82*, 521–529. https://doi.org/10.1016/j.ijfatigue.2015.09.007

Chai, H. F., & Laird, C. (1987). Mechanisms of cyclic softening and cyclic creep in low carbon steel. *Materials Science and Engineering*, *93*, 159–174. https://doi.org/10.1016/0025-5416(87)90421-6

Cristofori, A., Benasciutti, D., & Tovo, R. (2011). A stress invariant based spectral method to estimate fatigue life under multiaxial random loading. *International Journal of Fatigue*, *33*, 887–899. https://doi.org/10.1016/j.ijfatigue.2011.01.013

Cristofori, A., Susmel, L., & Tovo, R. (2007). A stress invariant based criterion to estimate fatigue damage under multiaxial loading. *International Journal of Fatigue*, *30*, 1646–1658. https://doi.org/10.1016/j.ijfatigue.2007.11.006

Crossland, B. (1956). Effect of large hydrostatic pressures on the torsional fatigue strength of an alloy steel. In *Proceedings of the International Conference on Fatigue of Metals* (pp. 138–145). London, UK: Institution of Mechanical Engineers.

Davoli, P., Bernasconi, A., Filippini, M., Foletti, S., & Papadopoulos, I. V. (2003). Independence of the torsional fatigue limit upon a mean shear stress. *International Journal of Fatigue*, *25*(6), 471–480. https://doi.org/10.1016/S0142-1123(02)00174-3

DNV-GL. (2005). *Fatigue design of offshore steel structures*. *Recommended Practice*.

Dong, P. (2001). A structural stress definition and numerical implementation for fatigue analysis of welded joints. *International Journal of Fatigue*, *23*, 865–876.

Dong, P. (2005). A Robust Structural Stress Method for Fatigue Analysis of Offshore/Marine Structures. *Journal of Offshore Mechanics and Arctic Engineering*, *127*, 68–74. https://doi.org/10.1115/1.1854698

Dong, P., & Hong, J. K. (2004). The master S-N curve approach to fatigue evaluation of offshore and marine structures. In *23rd Internation Conference on Offshore Mechanics and Arctic Engineering* (pp. 1–9). Vancouver, Canada.

Dong, P., & Hong, J. K. (2006). A Robust Structural Stress Parameter For Evaluation Of Multiaxial Fatigue Of Weldments. *Journal of ASTM International*, *3*(7), 18. https://doi.org/10.1520/JAI100348

Dong, P., Hong, J. K., Osage, D., & Prager, M. (2002). *Master SN-Curve Method for fatigue evaluation of welded components*. New York, USA.

Dong, P., Wei, Z., & Hong, J. K. (2009). A path-dependent cycle counting method for variable-amplitude multi-axial loading. *International Journal of Fatigue*, *32*, 720–734. https://doi.org/10.1016/j.ijfatigue.2009.10.010

Erny, C., Thevenet, D., Cognard, J. Y., & Körner, M. (2010a). Experimental and numerical analysis of fatigue behaviour of welded cruciform joints. *Journal of ASTM International*, *7*(4), 1–15. https://doi.org/10.1520/JAI102535

Erny, C., Thevenet, D., Cognard, J. Y., & Körner, M. (2010b). Fatigue assessment of naval welded assemblies. *Procedia Engineering*, *2*(1), 603–612. https://doi.org/10.1016/j.proeng.2010.03.065

European Standard. (2005). *Eurocode 3: Design of steel structures - Part 1-9: Fatigue*.

Exel, N., & Sonsino, C. M. (2014). Multiaxial fatigue evaluation of laserbeam-welded magnesium joints according to IIW-fatigue design recommendations. *Welding in the World*, *58*(4), 539–545. https://doi.org/10.1007/s40194-014-0139-6

Farajian, M., Nitschke-Pagel, T., Boin, M., & Wimpory, R. C. (2013). Relaxation of welding residual stresses in tubular joints under multiaxial loading. In *International Conference on Multiaxial Fatigue and Fracture*. ICMFF 10.

Fatemi, A., & Shamsaei, N. (2010). Multiaxial Fatigue Modeling and Some Simple Approximations. In *International Conference on Multiaxial Fatigue and Fracture* (pp. 7–24). ICMFF 9.

Fatemi, A., & Shamsaei, N. (2011). Multiaxial fatigue: An overview and some approximation models for life estimation. *International Journal of Fatigue*, *33*, 948–958. https://doi.org/10.1016/j.ijfatigue.2011.01.003

Fatemi, A., & Socie, D. F. (1988). a Critical Plane Approach To Multiaxial Fatigue Damage Including Out-of-Phase Loading. *Fatigue & Fracture of Engineering Materials and Structures*, *11*(3), 149–165. https://doi.org/10.1111/j.1460-2695.1988.tb01169.x

Findley, W. N. (1959). A theory for the effect of mean stress on fatigue of metals under combined torsion and axial load or bending. *Journal of Industrial and Engineering Chemistry*, *81*, 301–306.

Francois, D., Pineau, A., & Zaoui, A. (2012). *Mechanical Behaviour of Materials Volume 1: Micro-and Macroscopic Constitutive Behaviour*. *Springer-Verlag* (Vol. 1). Springer-verlag Berlin Heidelberg. https://doi.org/10.1016/B978-0-08-034912-1.50041-2

Fujczak, R. R. (1994). *The effects of fatigue loading frequency on fatigue life of high strength pressure vessel steels*. Watervliet, NY.

Gaier, C., & Dannbauer, H. (2006). An Efficient Critical Plane Method for Ductile , Semi- Ductile and Brittle Materials. In *Oral reference: FT436*. Elsevier Ltd.

Gough, H. J. (1950). Engineering Steels under Combined Cyclic and Static Stresses. *Journal of Applied Mechanics (ASME)*, *17*, 113–125.

Gough, H. J., & Pollard, H. V. (1935). The strength of metals under combined alternating stress. *Proceedings of the Institute of Mechanical Engineers*, *131*(1), 3–103.

Hencky, H. Z. (1924). Zur Theorie Plasticher Deformationen und der Hierdurch im Material Hervorgerufenen Nachspannungen. *Z. Angerw. Math. Mech.*, *4*, 323.

Hobbacher, A. (2015). *Recomendations for Fatigue Design of Welded Joints and Components*. *IIW document IIW-2259-15 ex XIII-2460-13/XV-1440-13* (Second Edi). https://doi.org/10.1007/978-3-319-23757-2

Hong, J. K., & Forte, T. P. (2014). Fatigue evaluation procedures for multiaxial loading in welded structures using the Battelle Structural Stress approach. In *ASME 2014 33rd International Conference on Ocean, Offshore and Arctic Engineering* (pp. 1–9). San Fransisco, USA.

Huber, M. T. (1904). Specific Deformation Work as a Measure of Material Damage. *Mechanik Czasopismo Techniczne*, *15*.

Ince, A., & Glinka, G. (2011). A modification of Morrow and Smith-Watson-Topper mean stress correction models. *Fatigue and Fracture of Engineering Materials and Structures*, *34*(11), 854–867. https://doi.org/10.1111/j.1460-2695.2011.01577.x

Ince, A., & Glinka, G. (2013). A numerical method for elasto-plastic notch-root stress-strain analysis. *The Journal of Strain Analysis for Engineering Design*, *48*, 229–244. https://doi.org/10.1177/0309324713477638

Ince, A., & Glinka, G. (2016). Innovative computational modeling of multiaxial fatigue analysis for notched components. *International Journal of Fatigue*, *82*, 134–145. https://doi.org/10.1016/j.ijfatigue.2015.03.019

Itoh, T., Sakane, M., Socie, D. F., & Ohnami, M. (1995). Non-proportional low cycle fatigue criterion for type 304 stainless steel. *Journal of Engineering Materials and Technology*, *117*, 285–292.

Jiang, C., Liu, Z. C., Wang, X. G., Zhang, Z., & Long, X. Y. (2015). A structural stress-based critical plane method for multiaxial fatigue life estimation in welded joints. *Fatigue and Fracture of Engineering Materials and Structures*, *39*(3), 372–383. https://doi.org/10.1111/ffe.12369

Karolczuk, A., & Blacha, L. (2011). Fatigue life estimation under variable amplitude bending using the non-local damage parameter and multisurface plasticity model. *International Journal of Fatigue*, *33*(10), 1376–1383. https://doi.org/10.1016/j.ijfatigue.2011.05.003

Kluger, K., & Lagoda, T. (2016). Fatigue life estimation for selected materials in multiaxial stress states with mean stress. *Journal of Theoretical and Applied Mechanics*, *54*(2), 385–396. https://doi.org/10.15632/jtam-pl.54.2.385

Łagoda, T., Macha, E., & Niesłony, A. (2005). Fatigue life calculation by means of the cycle counting and spectral methods under multiaxial random loading. *Fatigue and Fracture of Engineering Materials and Structures*, *28*(4), 409–420. https://doi.org/10.1111/j.1460-2695.2005.00877.x

Łagoda, T., & Sonsino, C. M. (2004). Comparison of different methods for presenting variable amplitude loading fatigue results. *Materialwissenschaft Und Werkstofftechnik*, *35*. https://doi.org/10.1002/mawe.200300692

Langlais, T. E., Vogel, J. H., & Chase, T. R. (2003). Multiaxial cycle counting for critical plane methods. *International Journal of Fatigue*, *25*, 641–647. https://doi.org/10.1016/S0142-1123(02)00148-2

Lassen, T., & Recho, N. (2006). *Fatigue life analyses of welded structures*. *ISTE USA* (Vol. 143). ISTE Ltd. https://doi.org/10.1002/9780470612149

Lautrou, N., Thevenet, D., & Cognard, J.-Y. (2009). Fatigue crack initiation life estimation in a steel welded joint by the use of a two-scale damage model. *Fatigue & Fracture of Engineering Materials & Structures*, *32*(5), 403–417. https://doi.org/10.1111/j.1460-2695.2009.01344.x

Lemaitre, J. (1996). *A course on damage mechanics*. *Springer-Verlag* (Vol. 1). Berlin, Germany: Springer-verlag Berlin Heidelberg. https://doi.org/10.1017/CBO9781107415324.004

Lemaitre, J., & Chaboche, J. L. (1990). *Mechanics of solid materials*. Cambridge University Press.

Lemaitre, J., & Desmorat, R. (2005). *Engineering Damage Mechanics*. *Springer*. Paris, France: Springer. https://doi.org/10.1007/s13398-014-0173-7.2

Lemaitre, J., & Marquis, D. (1992). Modeling Complex Behavior of Metals by the "State-Kinetic Coupling Theory." *ASME J. Eng. Mater. Tech.*, *114*(July 1992), 250–254.

Lemaitre, J., Sermage, J. P., & Desmorat, R. (1999). A two scale damage concept applied to fatigue. *International Journal of Fracture*, *97*(1), 67-81–81. https://doi.org/10.1023/A:1018641414428

Li, B. C., Jiang, C., Han, X., & Li, Y. (2015). A new approach of fatigue life prediction for metallic materials under multiaxial loading. *International Journal of Fatigue*, *78*, 1–10. https://doi.org/10.1016/j.ijfatigue.2015.02.022

Liu, J., & Zenner, H. (1993). Berechnung der Dauerschwingfestigkeit bei mehrachsiger Beanspruchung — Teil 1. *Materialwissenschaft Und Werkstofftechnik*, *24*(8), 240–249. https://doi.org/10.1002/mawe.19930240808

Liu, J., & Zenner, H. (2003). Fatigue limit of ductile metals under multiaxial loading. *European Structural Integrity Society*, *31*, 147–164. https://doi.org/10.1016/S1566-1369(03)80009-2

Macha, E. (1991). Generalized Fatigue Criterion of Maximum Shear and Normal Strains on the Fracture Plane for Materials under Multiaxial Random Loadings. *Materialwissenschaft Und Werkstofftechnik*, *22*, 203–210.

Macha, E., & Niesłony, A. (2012). Critical plane fatigue life models of materials and structures under multiaxial stationary random loading: The state-of-the-art in Opole Research Centre CESTI and directions of future activities. *International Journal of Fatigue*, *39*, 95–102. https://doi.org/10.1016/j.ijfatigue.2011.03.001

Maddox, S. J. (2001). Recommended Hot-Spot Stress Design S-N Curves for Fatigue Assessment of FPSOs. In *11th International Offshore and Polar Engineering Conference*. Stavanger, Norway.

Maddox, S. J. (2010). *Fatigue assessment of welds not oriented either normal or parallel to the direction of loading*. *IIW document*. Cambridge, UK.

Mamiya, E. N., Araújo, J. A., & Castro, F. C. (2008). Prismatic hull: A new measure of shear stress amplitude in multiaxial high cycle fatigue. *International Journal of Fatigue*, *31*, 1144–1153. https://doi.org/10.1016/j.ijfatigue.2008.12.010

Marquis, G. (2000). Mean Stress in Long-Life Torsion Fatigue. *Fatigue and Fracture of Engineering Materials and Structures*, *23*(4), 293–300.

Marquis, G. B., & Socie, D. F. (2003). *Multiaxial Fatigue*. Elsevier. https://doi.org/10.1016/b0-08-043749-4/04030-1

Matake, T. (1977). An explanation on fatigue limit under combined stress. *Bulletin of Japan Societ of Mechanical Engineers*, *20*, 257–263.

McDiarmid, D. L. (1991). A general criterion for high cycle multiaxial fatigue failure. *Fatigue and Fracture of Engineering Materials and Structures*, *14*, 429–453.

Meggiolaro, M. A., Tupiassú, J., & De Castro, P. (2012). An improved multiaxial rainflow algorithm for non-proportional stress or strain histories - Part II: The Modified Wang-Brown method. *International Journal of Fatigue*, *42*, 194–206. https://doi.org/10.1016/j.ijfatigue.2011.10.012

Meggiolaro, M. A., Tupiassú, J., & De Castro, P. (2015). The moment of inertia method to calculate equivalent ranges in non-proportional tension–torsion histories. *Journal of Materials Research and Technology*, *4*(3), 229–234. https://doi.org/10.1016/j.jmrt.2015.01.004

Mei, J., & Dong, P. (2016). A new path-dependent fatigue damage model for non-proportional multi-axial loading. *International Journal of Fatigue*, *90*, 210–221. https://doi.org/10.1016/j.ijfatigue.2016.05.010

Mei, J., & Dong, P. (2017a). An equivalent stress parameter for multi-axial fatigue evaluation of welded components including non-proportional loading effects. *International Journal of Fatigue*, *101*, 297–311. https://doi.org/10.1016/j.ijfatigue.2017.01.006

Mei, J., & Dong, P. (2017b). Analysis of Nonproportional Multiaxial Fatigue Test Data of Various Aluminum Alloys Using a New Damage Parameter. *Fatigue and Fracture Test Planning, Test Data Acquisitions and Analysis*, *ASTM STP15*, 278–298. https://doi.org/10.1520/STP159820160079

Mei, J., & Dong, P. (2017c). Modeling of path-dependent multi-axial fatigue damage in aluminum alloys. *International Journal of Fatigue*, *95*, 252–263. https://doi.org/10.1016/j.ijfatigue.2016.10.031

Mikulski, Z., & Lassen, T. (2019). Fatigue crack initiation and subsequent crack growth in fillet welded steel joints. *International Journal of Fatigue*, *120*(August 2018), 303–318. https://doi.org/10.1016/j.ijfatigue.2018.11.014

Mises, R. von. (1913). Mechanik der festen Korper im plastisch deformablen Zustand. *Nachr. Ges. Wiss. Gottingen*, (1), 582–592.

Mrsnik, M., Slavic, J., & Boltezar, M. (2016). Multiaxial vibration fatigue - A theoretical and experimental comparison. *Mechanical Systems and Signal Processing*, *76–77*, 409–423. https://doi.org/10.1016/j.ymssp.2016.02.012

Muhs, D., Wittel, H., Becker, M., Jannasch, D., & Vossiek, J. (2008). *Roloff/Matek Machine-onderdelen* (4th ed.). Den Haag, the Netherlands: Sdu Uitgevers bv.

Nieslony, A. (2016). A Critical Analysis of the Mises Stress Criterion Used in Frequency Domain Fatigue Life Prediction. *Frattura Ed Integrità Strutturale*, *38*, 177–183. https://doi.org/10.3221/IGF-ESIS.38.24

Niesłony, A. (2010). Comparison of some selected multiaxial fatigue failure criteria dedicated for spectral method. *Journal of Theoretical and Applied Mechanics*, *48*(1), 233–254.

Nieslony, A., & Macha, E. (2007). *Spectral Method in Multiaxial Random Fatigue* (Vol. 33). Springer.

Niesłony, A., Ruzička, M., Papuga, J., Hodr, A., Balda, M., & Svoboda, J. (2012). Fatigue life prediction for broad-band multiaxial loading with various PSD curve shapes. *International Journal of Fatigue*, *44*, 74–88. https://doi.org/10.1016/j.ijfatigue.2012.05.014

Papadopoulos, I. V. (1998). Critical plane approaches in high-cycle fatigue: on the definition of the amplitud and mean value of the shear stress acting on the critical plane. *Fatigue and Fracture of Engineering Materials and Structures*, *21*, 269–285.

Papadopoulos, I. V., & Dang Van, K. (1997). *Multiaxial Fatigue Limit Criterion of Metals: a Mesoscopic Scale Approach*. *High-cycle Metal Fatigue From Theory to applications*. Udine, Italy.

Papadopoulos, I. V., & Panoskaltsis, V. P. (1996). Gradient-Dependent Multiaxial High-Cycle Fatigue Criterion. In A. Pineau, G. Cailletaud, & T. C. Lindley (Eds.), *Multiaxial Fatigue and Design* (ESIS 21, Vol. 1, pp. 349–364). London: Mechanical Engineering Publications.

Papuga, J. (2011). A survey on evaluating the fatigue limit under multiaxial loading. *International Journal of Fatigue*, *33*(2), 153–165. https://doi.org/10.1016/j.ijfatigue.2010.08.001

Papuga, J. (2013). Quest for fatigue limit prediction under multiaxial loading. *Procedia Engineering*, *66*, 587–597. https://doi.org/10.1016/j.proeng.2013.12.110

Papuga, J., Parma, S., & Růžička, M. (2016). Systematic validation of experimental data usable for verifying the multiaxial fatigue prediction methods. *Frattura Ed Integrità Strutturale*, *38*, 106–113. https://doi.org/10.3221/IGF-ESIS.38.14

Papuga, J., & Ruzicka, M. (2007). Two new multiaxial criteria for high cycle fatigue computation. *International Journal of Fatigue*, *30*, 58–66. https://doi.org/10.1016/j.ijfatigue.2007.02.015

Podgornik, B. (2017). Validation of linear damage rules using random loading. *International Journal of Damage Mechanics*, *26*(3), 463–479. https://doi.org/10.1177/1056789515605881

Radaj, D., Berto, F., & Lazzarin, P. (2009). Local fatigue strength parameters for welded joints based on strain energy density with inclusion of small-size notches. *Engineering Fracture Mechanics*, *76*(8), 1109–1130. https://doi.org/10.1016/j.engfracmech.2009.01.009

Radaj, D., Sonsino, C. M., & Fricke, W. (2006). *Fatigue assessment of welded joints by local approaches*. *Woodhead Publishing Limited* (Vol. 53). https://doi.org/10.1017/CBO9781107415324.004

Radaj, D., Sonsino, C. M., & Fricke, W. (2008). Recent developments in local concepts of fatigue assessment of welded joints. *International Journal of Fatigue*, *31*, 2–11. https://doi.org/10.1016/j.ijfatigue.2008.05.019

Radaj, D., & Vormwald, M. (2013). *Advanced Methods of Fatigue Assessment*. Springer. https://doi.org/10.1007/978-3-642-30740-9

Remes, H., Lehto, P., & Romanoff, J. (2014). Microstructure and Strain-Based Fatigue Life Approach for High-Performance Welds. *Advanced Materials Research*, *891–892*, 1500–1506. https://doi.org/10.4028/www.scientific.net/AMR.891-892.1500

Saintier, N., Palin-Luc, T., Bénabes, J., & Cocheteux, F. (2013). Non-local energy based fatigue life calculation method under multiaxial variable amplitude loadings. *International Journal of Fatigue*, *54*, 68–83. https://doi.org/10.1016/j.ijfatigue.2012.12.013

Schijve, J. (1989). *Fatigue of Structures and Materials*. *Springer* (Vol. 53). Springer. https://doi.org/10.1017/CBO9781107415324.004

Shamsaei, N. (2010). *Multiaxial fatigue and deformation including non-proportional and variable amplitude loading effects*. University of Toledo.

Sines, G. (1959). Behaviour of metals under complex stresses. In G. Sines & J. L. Waisman (Eds.), *Metal Fatigue* (pp. 145–169). Mc Graw Hill.

Sonsino, C. M. (1995). Multiaxial fatigue of welded joints under in-phase and out-of-phase local strains and stresses. *International Journal of Fatigue*, *17*(1), 55–70.

Sonsino, C. M. (1997). *Fatigue behaviour of welded components under complex Elasto-Plastic*

multiaxial deformations. Darmstadt, Germany: Fraunhofer Institute for Structural Durability LBF.

Sonsino, C. M. (2008a). Effect of residual stresses on the fatigue behaviour of welded joints depending on loading conditions and weld geometry. *International Journal of Fatigue*, *31*, 88–101. https://doi.org/10.1016/j.ijfatigue.2008.02.015

Sonsino, C. M. (2008b). Multiaxial fatigue assessment of welded joints – Recommendations for design codes. *International Journal of Fatigue*, *31*, 173–187. https://doi.org/10.1016/j.ijfatigue.2008.06.001

Sonsino, C. M. (2011). Influence of material's ductility and local deformation mode on multiaxial fatigue response. *International Journal of Fatigue*, *33*, 930–947. https://doi.org/10.1016/j.ijfatigue.2011.01.010

Sonsino, C. M., Fricke, W., De Bruyne, F., Hoppe, A., Ahmadi, A., & Zhang, G. (2012). Notch stress concepts for the fatigue assessment of welded joints - Background and applications. *International Journal of Fatigue*, *34*, 2–16. https://doi.org/10.1016/j.ijfatigue.2010.04.011

Sonsino, C. M., & Kueppers, M. (2001). Multiaxial fatigue of welded joints under constant and variable amplitude loadings. *Fatigue and Fracture of Engineering Materials and Structures*, *24*, 309–327.

Sonsino, C. M., Kueppers, M., Gath, N., Maddox, J., & Razmjoo, G. R. (1999). *Fatigue behaviour of welded high strength components under combined multiaxial variable amplitude loading*. *LBF-Report*. Darmstadt, Germany.

Sonsino, C. M., Lagoda, T., & Demofonti, G. (2004). Damage accumulation under variable amplitude loading of welded medium- and high-strength steels. *International Journal of Fatigue*, *26*, 487–495. https://doi.org/10.1016/j.ijfatigue.2003.10.001

Sonsino, C. M., & Maddox, J. (2001). Multiaxial Fatigue of Welded Structures - Problems and Present Solutions. In *Proceedings of the 6th International Conference of Multiaxial/Biaxial Fatigue* (pp. 3–15).

Sonsino, C. M., & Wiebesiek, J. (2007). *Assessment of Multiaxial Spectrum Loading of Welded Steel and Aluminium Joints By Modified Equivalent Stress and Gough-Pollard Algorithms*. *IIW document*. Darmstadt, Germany.

Susmel, L. (2008). Multiaxial fatigue limits and material sensitivity to non-zero mean stresses normal to the critical planes. *Fatigue and Fracture of Engineering Materials and Structures*, *31*(3–4), 295–309. https://doi.org/10.1111/j.1460-2695.2008.01228.x

Susmel, L. (2010). A simple and efficient numerical algorithm to determine the orientation of the critical plane in multiaxial fatigue problems. *International Journal of Fatigue*, *32*, 1875–1883. https://doi.org/10.1016/j.ijfatigue.2010.05.004

Susmel, L. (2014). Four stress analysis strategies to use the Modified Wöhler Curve Method to perform the fatigue assessment of weldments subjected to constant and variable amplitude multiaxial fatigue loading. *International Journal of Fatigue*, *67*, 38–54.

Susmel, L., & Lazzarin, P. (2002). A bi-parametric Wöhler curve for high cycle multiaxial fatigue assessment. *Fatigue and Fracture of Engineering Materials and Structures*, *25*(1), 63–78. https://doi.org/10.1046/j.1460-2695.2002.00462.x

Susmel, L., Tovo, R., & Benasciutti, D. (2009). A novel engineering method based on the critical plane concept to estimate the lifetime of weldments subjected to variable amplitude multiaxial fatigue loading. *Fatigue and Fracture of Engineering Materials and Structures*, *32*, 441–459. https://doi.org/10.1111/j.1460-2695.2009.01349.x

Thevenet, D., Erny, C., Cognard, J. Y., & Korner, M. (2009). Modélisation du comportement en fatigue d ' assemblages soudés de type naval. In *19eme Congres Français de Mécanique* (pp. 24–28). Marseille, France: 19eme Congres Français de Mécanique.

Weber, B., Kenmeugne, B., Clement, J. C., & Robert, J. L. (1999). Improvements of multiaxial fatigue criteria computation for a strong reduction of calculation duration. *Computational Materials Science*, *15*, 381–399.

Wei, Z., & Dong, P. (2010). Multiaxial fatigue life assessment of welded structures. *Engineering Fracture Mechanics*, *77*, 3011–3021. https://doi.org/10.1016/j.engfracmech.2010.03.045

Wei, Z., & Dong, P. (2011). A rapid path-length searching procedure for multi-axial fatigue cycle counting. *Fatigue and Fracture of Engineering Materials and Structures*, *35*, 556–571. https://doi.org/10.1111/j.1460-2695.2012.01649.x

Wei, Z., & Dong, P. (2014). A generalized cycle counting criterion for arbitrary multi-axial fatigue loading conditions . *Journal of Strain Analysis for Engineering Design*, *49*, 325–341.

Wiebesiek, J., & Sonsino, C. M. (2010). *New results in multiaxial fatigue of welded aluminium joints*. *IIW document*. Darmstadt, Germany.

Zhu, S. P., Huang, H. Z., Liu, Y., He, L. P., & Liao, Q. (2012). A practical method for determining the Corten-Dolan exponent and its application to fatigue life prediction. *International Journal of Turbo and Jet Engines*, *29*(2), 79–87. https://doi.org/10.1515/tjj-2012-0013

Zou, T., & Kaminski, M. L. (2016). Validation of WaveWatch-III wave model for investigation of climate change effects on fatigue lifetime of offshore floating structures 2 Wave data formats. *Ocean Dynamics*, *66*(9), 1099–1108. https://doi.org/https://doi.org/10.1007/s10236-016-0977-4

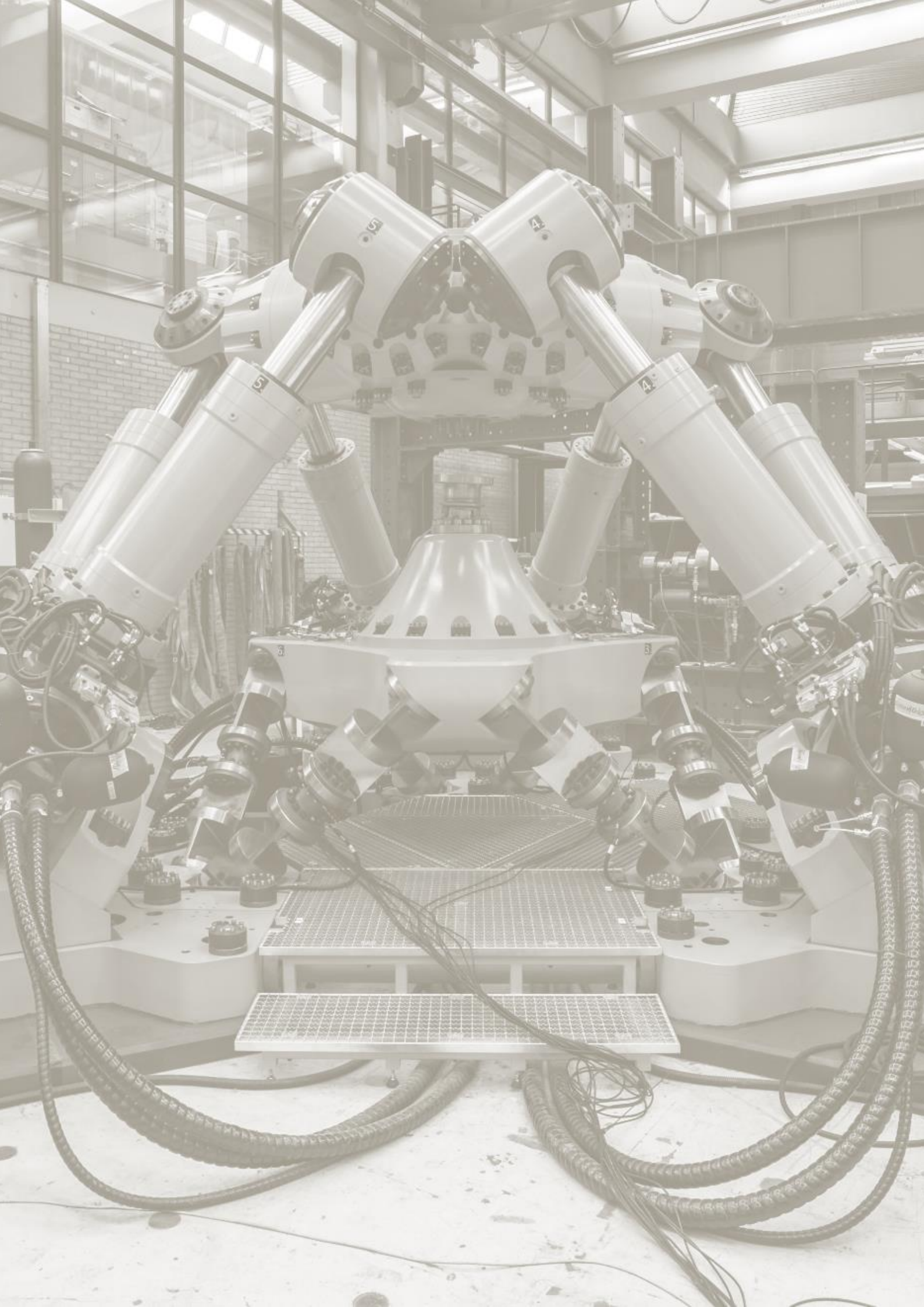

3 A hexapod for multiaxial fatigue testing of marine structural details under non-proportional constant and variable amplitude loading

" A creative artist works on his next composition because he was not satisfied with the previous one."
– Dimitri Shostakovich

Marine structures are continuously exposed to cyclic actions of waves which are stochastic in nature with varying directions, heights, periods and phases. Such actions result in multiaxial stress states in some structural joints and this necessitates their lifetime estimation by applying multiaxial fatigue assessment methods. The availability of experimental fatigue data under multiaxial loading conditions is of vital importance for validation, improvement and development of these methods.

In this Chapter, a unique hexapod is presented which was designed and used to collect multiaxial fatigue data with a structural detail that is representative for a joint in a marine structure. This hexapod can perform fatigue tests at a maximum test frequency of 30 Hz and a maximum vertical load of 1 MN. The full workability in terms of test frequency and loading are dependent on the specimen stiffness and geometry, position in the hexapod, and available oil flow.

The experimental data that has been collected and presented in this thesis merely consist of constant amplitude fatigue test results. However, the intrinsic features of a hexapod enable to operate in 6 Degrees of Freedom (DoFs) which provides the opportunity to also test variable and random amplitude loading. These particular features allow for realistic load scenarios; The actual loads that are encountered by marine structures can be experimentally mimicked by this hexapod. Being able to collect this type of experimental data will improve and facilitate the expansion of knowledge and understanding of multiaxial fatigue as a phenomenon, and enable to advance assessment methods (for marine structures) through model validation.

3.1 Introduction

In marine structures, the global structural response induces predominantly uniaxial fatigue but in some structural details the local stress state could be multiaxial with a detrimental effect on fatigue lifetime (Sonsino, 1995). The severity of multiaxial fatigue damage is characterised by various features, namely material characteristics, load ratio, stress amplitude, number of load cycles and non-proportionality. This makes it a challenging topic which is still not fully understood. Although many research has been done with regard to this subject, knowledge gaps and uncertainties remain. This can be attributed to various features amongst which uncertainties in the encountered loads on the structure, different material characteristics, weld effects and the lack of sufficient experimental data.

A typical complication in multiaxial fatigue assessment is the validation of lifetime estimates due to scarcity of experimental data under variable or random amplitude loading. If available, such tests are generally performed through resonance testing which does not realistically represent the characteristic load spectrum of a marine structure. Furthermore, the investigation of non-proportionality is strongly focussed on phase shift induced non-proportionality using academic load scenarios (i.e. sinusoidal constant amplitude loading), see for example (Anes et al., 2014; Carpinteri et

al., 2008; Sonsino, 1995; Susmel & Tovo, 2004; Wei et al., 2013).

In marine structures the technique of welding is indispensable and materials with distinct characteristics show a different fatigue resistance under multiaxial loading (Sonsino, 2008a, 2011; Sonsino *et al.*, 2004). Therefore, it is of importance to take welding parameters and post-welding treatments into consideration as they considerably affect the fatigue lifetime of a welded connection. Both for academia and industrial practice, more research beyond the effects of loading on fatigue resistance would be valuable.

When experimental fatigue tests on welded joints are conducted, it is important to clearly document the loading conditions but also the type of material and welding process. This information enables to identify and analyse also other features such as residual and mean stress effects, root vs. toe failures, heat treatments and the effect of different material types. If vital details are missing uncertainties and errors are introduced, especially when evaluating experimental data sets originating from different sources.

3.2 Multiaxial fatigue testing

It has been mentioned by numerous researchers in the field of multiaxial fatigue that the currently available experimental data is scarce and incomplete, see i.e. (Anes et al., 2014; Benasciutti et al., 2015; Papuga, 2011; Saintier et al., 2013; Sonsino, 2008b; Susmel, 2010). Multiaxial fatigue models often lack validation, particularly for the more complex load scenarios (e.g. random loading, non-proportionality). Therefore, both academia and industrial practice lack a consensus and agreement on the quality of the different approaches and methods for multiaxial fatigue assessment. This emphasizes the need and relevance of advanced test programs for the collection of multiaxial fatigue data.

So far, in particular for the maritime industry, the collection of representative experimental data under multiaxial loading conditions has been very limited. This can be mainly attributed to the fact that multiaxial fatigue testing is time consuming, costly and more complex than uniaxial fatigue testing. The majority of fatigue test equipment is designed for uniaxial fatigue tests. Multiaxial fatigue test facilities are rare and scarce and are typically limited to biaxial testing. Equipment that could be thought of are the ASTREE for in-plane tension (Figure 3.1a) and the INSTRON ElectroPulse for tension-torsion (Figure 3.1b) (Doudard et al., 2007; Instron, 2017). In the test facilities of SINTEF, TWI and OCAS it is possible to perform rotating bending tests where a static (mean) stress component is added through internal pressure (Figure 3.1c) (Johnston, 2017). However, such tests remain uniaxial when the internal pressure is non-fluctuating.

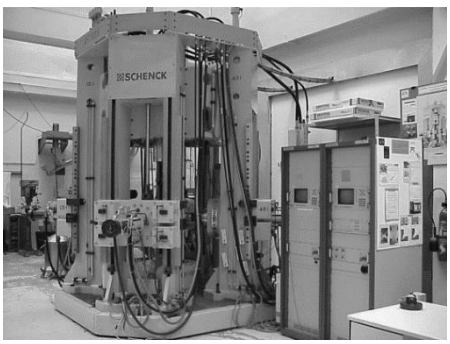


Figure 3.1: a) ASTREE biaxial tension-tension test bench at LMT Cachan (Paris, FR); b) INSTRON ElectroPulse tension-torsion test bench; c) Facility at TWI (UK) for rotating bending tests with internal pressure

A seldomly used but suitable configuration for multiaxial fatigue testing is a hexapod, also known as Stewart platform. Such a structure features 6 DoFs due to its six legs which are each able to vary in length independently. Only few hexapods have been built for the purpose of multiaxial fatigue testing. A hexapod for closed loop load application was custom made by FGB (FGB, 2018) for the University of Paderborn (Germany) (Kohlstedt et al., 2017) and the technical university of Hamburg (TUHH, Germany) (TUHH, 2015). A similar device is located at the University of Cachan (France) (Nierenberger et al., 2012), and also available as the Multi-Axial simulation table of MTS (MTS, 2017) which focusses on vibration simulation. See Figure 3.2a-d.

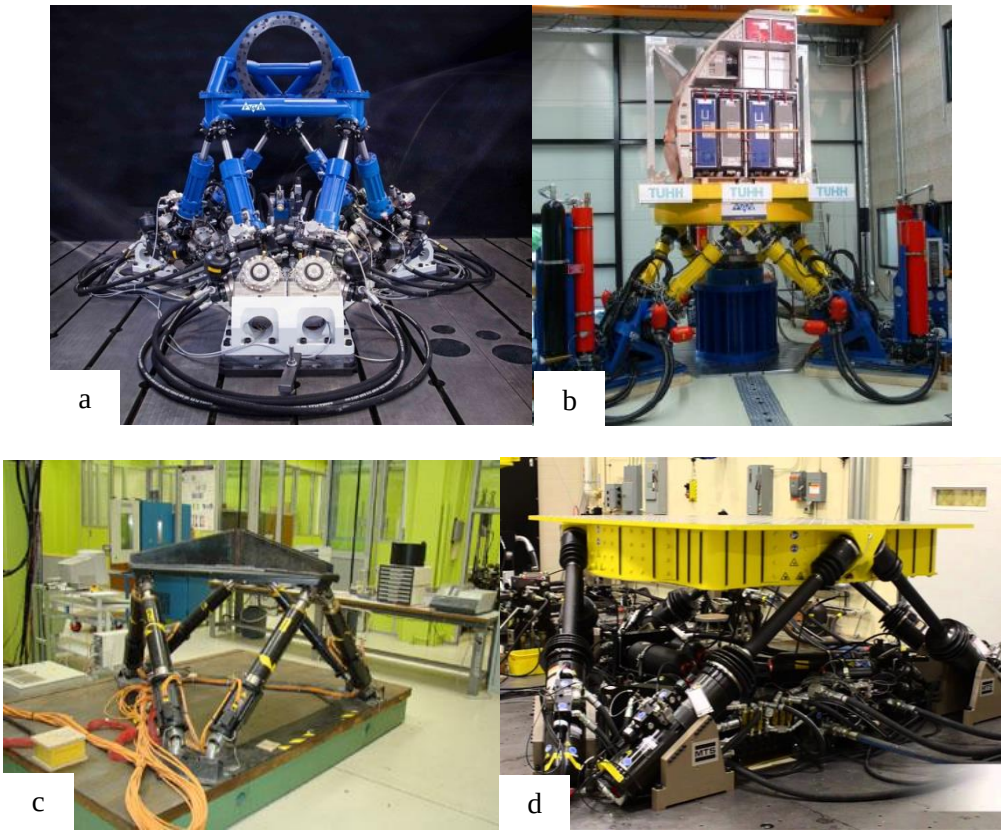

Figure 3.2: Existing hexapods with specific purpose of multiaxial fatigue testing; a) FGB hexapod of the University of Paderborn b) FGB hexapod at TUHH c) hexapod at Cachan LMT d) Simulation table of MTS

3.3 Kinematics of a hexapod

The kinematic equations of a hexapod can be described through inverse kinematics, meaning that the actuator displacements are obtained from the displacements of the traverse with respect to the base plate of the hexapod (Hsu & Fong, 2001). The orientation and position of the traverse is described by xyz coordinates and three Euler angles θ, φ, ψ. The length of leg i (L_i) can be described by Equation 1 where T_i and B_i refer to the coordinates of the leg at the travers (T) and at the base (B). The leg vector can then be described considering the coordinates of the leg at the base (B_i) and at the traverse (T_i) with respect to the origin of the traverse O. See Equation 3.2-3.4 and Figure 3.3. The rotations of

the traverse are taken into account through a rotational matrix M, using the Euler angles θ for pitch (rotation around y-axis), φ for roll (rotation around x-axis), ψ for yaw (rotation around z-axis).

$$L_i = \sqrt{\left(T_{x,i} - B_{x,i}\right)^2 + \left(T_{y,i} - B_{y,i}\right)^2 + \left(T_{z,i} - B_{z,i}\right)^2} \tag{3.1}$$

$$\overline{L_\iota} = \overline{O_\iota} + M(\theta, \varphi, \psi) \cdot \overline{T_\iota} - \overline{B_\iota} \tag{3.2}$$

$$O = \begin{bmatrix} O_x \\ O_y \\ O_z \end{bmatrix}, T_i = \begin{bmatrix} T_{ix} \\ T_{iy} \\ T_{iz} \end{bmatrix}, B_i = \begin{bmatrix} B_{ix} \\ B_{iy} \\ B_{iz} \end{bmatrix} \tag{3.3}$$

$$M(\theta, \varphi, \psi) = \begin{bmatrix} \cos(\psi)\cos(\theta) & \cos(\psi)\sin(\theta)\sin(\varphi) - \sin(\psi)\cos(\varphi) & \cos(\psi)\sin(\theta)\cos(\varphi) + \sin(\psi)\sin(\varphi) \\ \sin(\psi)\cos(\theta) & \sin(\psi)\sin(\theta)\sin(\varphi) + \cos(\psi)\cos(\varphi) & \sin(\psi)\sin(\theta)\cos(\varphi) - \cos(\psi)\sin(\varphi) \\ -\sin(\theta) & \cos(\theta)\sin(\varphi) & \cos(\theta)\cos(\varphi) \end{bmatrix} \tag{3.4}$$

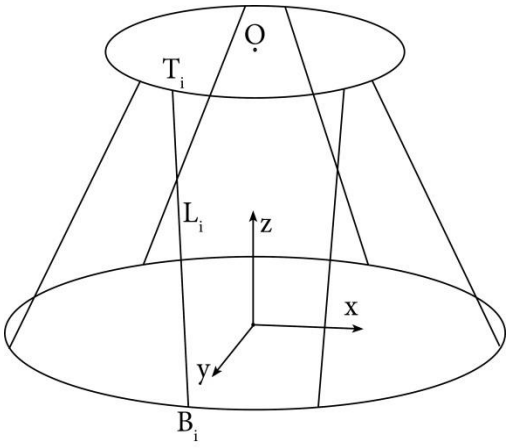

Figure 3.3: Schematic illustration of the reference system and coordinates used in the kinematic equations of a hexapod

3.4 Experimental test setup

In particular for the assessment of marine structures, with a predominance of welded connections, it is of importance that data is collected on a representative scale. In order to achieve this goal the Technical University of Delft has specified and purchased a unique hexapod from FGB. See Figure 3.4.

The hexapod of TU Delft has been designed for (high cycle) fatigue testing of marine structures and is thus able to apply relatively high loads with small displacements. The main characteristics of the hexapod are listed in Table 3.1. This hexapod distinguishes itself by its capacity to test large structures under complex fatigue loading at relatively high frequencies and its potential for other fields of research such as ultimate strength (e.g. buckling, impact loads) and dynamic behaviour.

3.4.1 Hexapod capacity

In Figure 3.6 the global dimensions of the hexapod are provided. The machine has been designed for a maximum oil flow of 750 l/min at 280 bar. For higher test flows (i.e. frequencies) modifications can be made (i.e. replacement of valves) which enable to increase the oil flow up to 1500 l/min. The hexapod has been recently equipped with its own HPU unit.

Table 3.1: Main characteristics of the hexapod

Description	Capacity
Displacement in X	± 150 mm
Displacement in Y	± 150 mm
Displacement in Z	± 150 mm
Rotation around X, Y, Z	± 5 deg.
Maximum force in X, Y	± 400 kN
Maximum force in Z	± 1000 kN
Moment around X, Y	± 400 kNm
Moment around Z	± 1000 kNm
Test frequency	0-30 Hz
Gross weight	60 tons
Weight of the traverse	13 tons

Figure 3.4: FGB hexapod in the laboratory of Delft University of Technology (NL)

Figure 3.5: Specially designed calibration device for the load cell

The hexapod has a gross weight of 60 tons of which 13 tons is contributed by the traverse. This is caused by the large weight of the bearings which are contained inside the traverse. Due to its weight and capacity the hexapod requires a fixed connection to a heavy weight floor.

To measure the applied loads (forces and moments), an additional hexapod configuration is used as 6 DoF load cell. This loadcel has static legs containing a uniaxial load cell each with a capacity of 500 kN each. The load cell is calibrated using a specially designed and manufactured calibration device. See Figure 3.5. The loadcell was calibrated before testing. Its upper part is called the pedestal. Orthogonal gusset plates are attached to both ends of the load cells in order to assure that each leg is predominantly axially loaded, i.e. transfer of remaining load components such as bending moments is minimized without jeopardizing buckling strength.

The casing of the traverse is a forged 42CrMoS4 steel. Rather than a casting, this production technique enables to meet a high microscopic material quality, i.e. minimized amount and size of microscopic defects. In a numerical analysis it has been checked that the maximum stress concentrations under extreme loading conditions remain below the fatigue limit.

Although the design allows for modification, the system is currently designed for a bolted connection of a specimen between the traverse and the pedestal. Specimen specific interfaces are required to facilitate such a connection. Both the traverse and load cell have a circular bolt pattern such that customized interfaces can be attached. The traverse also permits a bolted connection on the

top. Moreover, the traverse and the pedestal contain circular openings in the middle (with a diameter of 450 mm) which allows to stick a specimen through.

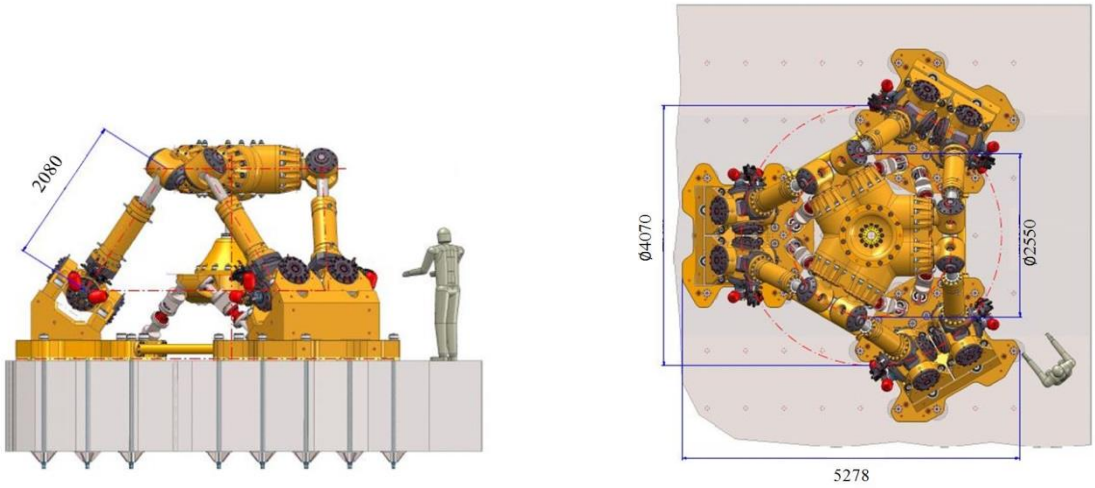

Figure 3.6: Main dimensions of the hexapod with mounted test specimen and some auxiliary fixation between load cell and traverse

3.4.2 Natural frequencies

The behaviour of the hexapod is predominantly described by its kinematics and the crosstalk between the different DOFs. The eigenfrequencies of the hexapod itself (without connection between the load cell and the traverse) are 13 Hz in x and y direction, 27 Hz in z direction and around the z axis, and 39 Hz around the x and y axis. See also Figure 3.7. The used coordinate system accounts for the x and y-axis in the horizontal plane, and the z-axis vertically upwards and perpendicular to the horizontal xy-plane. Once a specimen is connected between the load cell and the traverse, the overall stiffness will be changed. With an increased stiffness (e.g. specimen induced) the eigenfrequencies will become higher whilst the eigenfrequencies will reduce when mass is added (e.g. added mass on top of the traverse).

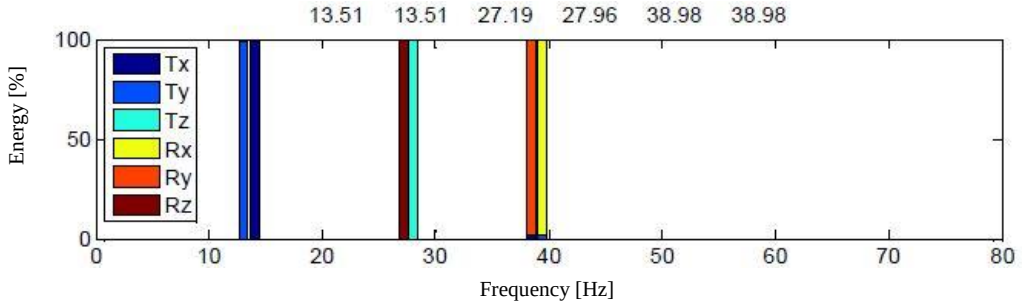

Figure 3.7: Eigenfrequencies of the hexapod without connection between the load cell and the traverse

3.4.2.1 Crosstalk between the different degrees of freedom

An important characteristic of the system performance of a hexapod is the amount of crosstalk between the different DoFs. This crosstalk is a measure of the accuracy of the system. Table 3.2 lists the crosstalk of the hexapod of TU Delft, expressed as a percentage of the target values for acceptance. The results were obtained from displacement controlled tests.

Table 3.2: Crosstalk of the hexapod in free motion using displacement control

Frequency [Hz]	Target translation in x-direction [mm]	Translation in x-direction	Translation in y-direction	Translation in z-direction
0.1	150	100% ± 0.1 %	0.1 %	0.1 %
5	5	100% ± 4.0 %	1.6 %	1.6 %
10	2.5	100% ±4.0%	3.0%	3.0%

Frequency [Hz]	Target translation in y-direction [mm]	Translation in y-direction	Translation in x-direction	Translation in z-direction
0.1	150	100% ± 0.1 %	0.1 %	0.1 %
5	5	100% ± 2.5 %	2.5 %	1.6 %
10	2.5	100% ±5.0%	4.0%	2.5%

Frequency [Hz]	Target translation in z-direction [mm]	Translation in z-direction	Translation in x-direction	Translation in y-direction
0.065	150	100% ± 0.1 %	0.1 %	0.1 %
5	1.25	100% ± 5 %	5 %	5 %
10	2	100% ± 10 %	5.0 %	4.0 %

Frequency [Hz]	Target rotation around x-axis [deg]	Rotation around x-axis	Rotation around y-axis	Rotation around z-axis
0.1	5	100% ± 0.2 %	0.2 %	0.2 %
10	0.125	100% ± 3.0%	4.0 %	4.0 %

Frequency [Hz]	Target rotation around y-axis [deg]	Rotation around y-axis	Rotation around x-axis	Rotation around y-axis
0.1	5	100% ± 0.2 %	0.2 %	0.2 %
10	0.125	100% ± 4.0 %	4.0 %	3.0 %

Frequency [Hz]	Target rotation around z-axis [deg]	Rotation around z-axis	Rotation around x-axis	Rotation around y-axis
0.1	5	100% ± 0.05 %	0.07 %	0.02 %
10	0.125	100% ± 2.0 %	4.0 %	3.0 %

In addition to the characterization of crosstalk in free motion, the system behaviour was investigated under (combined) loading conditions. For this purpose, a dedicated specimen was mounted and attached between the traverse and the load cell, using two bell-shaped interfaces. See Figure 3.8 for the test setup and Table 3.3 for the main characteristics of the used test specimen. The specimen design is in accordance with the dimensions of the specimens for fatigue testing (see Chapter 5). In Figure 3.9 the maximum load that can be applied to this particular specimen is plotted as a function of the frequency of a sinusoidal loading signal, considering a hydraulic oil supply of 750 /min. As mentioned in Section 2.3.3.2, Mode I and Mode III dominate multiaxial fatigue damage in weld toes. Therefore, the graphs in Figure 3.9 are made for vertical tension (Mode I) and torsion around the vertical axis (Mode III). It can be seen in Figure 3.9 that the relatively low torsional stiffness strongly affects the relation between maximum test frequency and maximum torsional load. An overview of the crosstalk under uniaxial loading conditions is shown in Table 3.4. Under these uniaxial loading conditions the crosstalk remains below ten percent of the maximum governing stress.

Figure 3.8: Detailed view of the mounted specimen (left), Overview of the test specimen mounted in the hexapod between the two bell-shaped interfaces (right)

Table 3.3: Main characteristics of tested tubular specimen

Characteristic	Value
Material	S690
Outer diameter of tube	170 mm
Wall thickness	10 mm
Height	260 mm
Flange thickness	35 mm

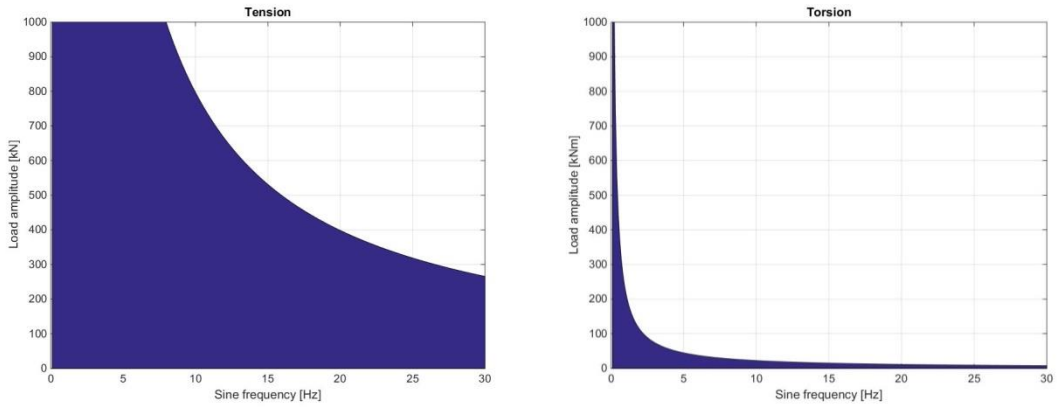

Figure 3.9: Working envelopes of the hexapod considering 750 l/min oil flow and a sinusoidal loading signal; Left)Maximum tensile load as a function of test frequency; Right) Maximum torsional load as a function of test frequency

Table 3.4: Crosstalk of the hexapod with the tubular test specimen connected to the load cell and the traverse (considering load control)

Frequency [Hz]	Target force in x-direction [kN]	Force x-direction	Force y-direction	Force z-direction	Moment around x and y – axis
0.1	200	100% ± 0.5 %	2.0 %	6.0 %	± 2 kNm
5	200	100% ± 2.5 %	2.5 %	4.0 %	± 1.5 kNm
10	200	100% ± 2.5 %	2.5 %	2.5 %	± 1 kNm

Frequency [Hz]	Target force in y-direction [kN]	Force y-direction	Force x-direction	Force z-direction	Moment around x and y – axis
0.1	200	100% ± 0.5 %	3.0 %	5.0 %	± 4 kNm
5	200	100% ± 2.5 %	2.5 %	4.0 %	± 1 kNm
10	200	100% ± 1.5 %	4.0 %	4.0 %	± 1 kNm

Frequency [Hz]	Target force in z-direction [kN]	Force z-direction	Force x-direction	Force y-direction	Moment around x and y – axis
0.1	1000	100% ± 0.2 %	1.0 %	1.0 %	± 2 kNm
5	1000	100% ± 2.0 %	0.5 %	0.5 %	± 0.5 kNm

Frequency [Hz]	Target moment around z-axis [kNm]	Moment around z-axis	Moment around x- axis	Moment around y- axis	Force x,y,z-direction
0.1	10	100% ± 1.0 %	2.0 %	2.0 %	± 5 kN
0.1	50	100% ± 0.5 %	0.5 %	0.5 %	± 3 kN
2.5	50	100% ± 0.4 %	0.4 %	0.4 %	± 3 kN
10	10	100% ± 0.1 %	2.0 %	2.0 %	± 3 kN

The performance of the hexapod under combined loading conditions was analysed for the Mode I – Mode III load combination induced by cyclic tension and cyclic torsion around the vertical axis. A trajectory error was used in accordance with Equation 3.5 . This error considers the reference stress (σ_{ref}/τ_{ref}) and actual measured stress ($\sigma_{actual}/\tau_{actual}$) for each trajectory i. Eight different load cases were determined considering proportional Constant Amplitude (CA) loading, two types of non-proportional CA loading (i.e. phase difference and frequency difference) and a random load trajectory based on a JONSWAP spectrum. See Table 3.5. The resulting load paths for the CA load cases are depicted in Table 3.6. It shows the load paths in stress space: normal stress (plotted along the horizontal axis) versus shear stress (plotted along the vertical axis). Figure 3.10 and Figure 3.11 show the time traces and corresponding Power Spectral Densities (PSD) of random load case 7.

$$\epsilon = \frac{\sqrt{\sum_i \epsilon_{\sigma,i}^2 + \epsilon_{\tau,i}^2}}{\sqrt{\sum_i \sigma_{ref,i}^2 + \tau_{ref,i}^2}} \tag{3.5}$$

$$\epsilon_{\sigma,i} = \sigma_{ref,i} - \sigma_{actual,i}$$

$$\epsilon_{\tau,i} = \tau_{ref,i} - \tau_{actual,i}$$

Table 3.5: The combined load cases which have been used to investigate the Hexapod's crosstalk under combined tension and torsion

Load case	1	2	3	4	5	6
Description	CA IP	CA IP	CA OP (phase)	CA OP (phase)	CA OP	CA OP
Frequency	0.1 Hz	10 Hz	0.1 Hz	10 Hz	0.1Hz (σ) 0.05 Hz (τ)	10Hz (σ) 5 Hz (τ)
Trajectory error [%]	2.12	7.98	3.77	6.99	2.8	5.5

Table 3.6: Load paths of the CA load cases which were used for the crosstalk check of the hexapod under combined loading (i.e vertical tension in combination with torsion around the vertical z-axis)

Loadcase 1	Loadcase 2	Loadcase 3	Loadcase 4	Loadcase 5	Loadcase 6
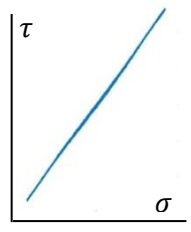	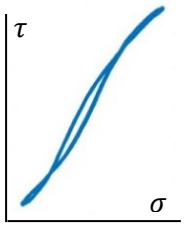	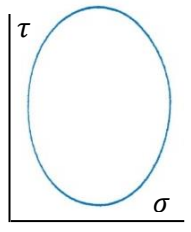	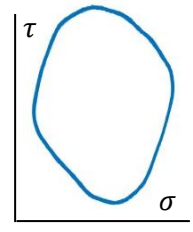	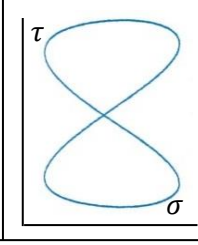	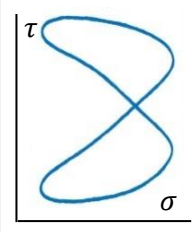

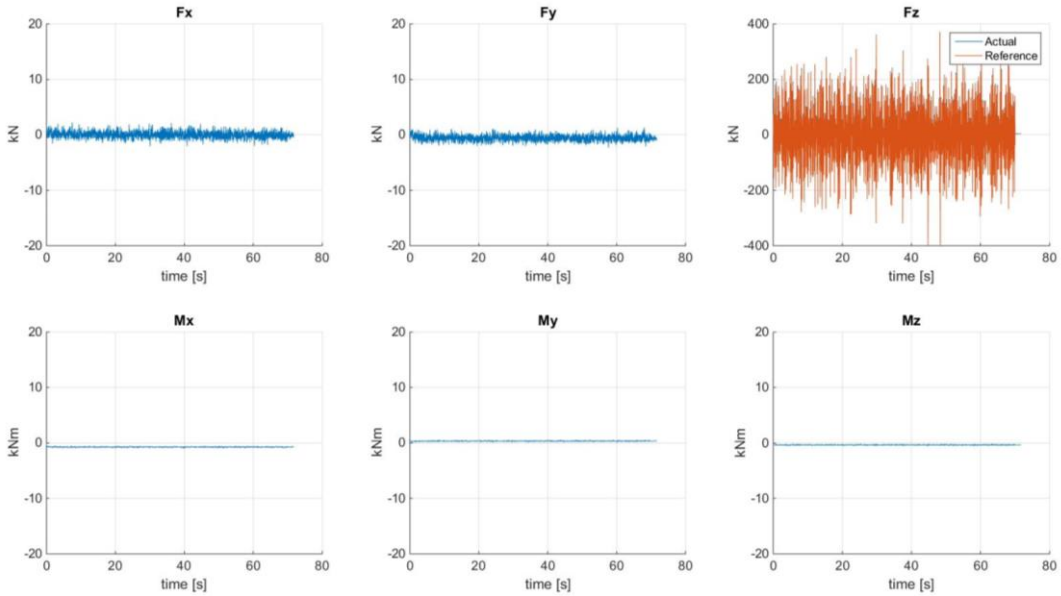

Figure 3.10: Time traces of the forces and moments acting on the tubular test specimen under random loading

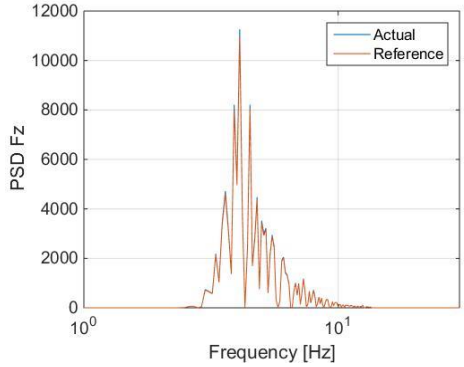

Figure 3.11: The power spectral density (PSD) distribution of random loading

3.5 Discussion

The presented amount of crosstalk in the hexapod has been quantified and characterized based on free motions (i.e. no specimen connected) but since this particular investigation requires testing in the predominantly elastic (high cycle fatigue) regime, load controlled tests were also performed. The system behaviour was analysed for (multiaxial) Mode I - Mode III load controlled tests, considering the attachment of the dedicated tubular specimen for this research. The accuracy of the system was then judged based on load path and stress. The discussed results are applicable to the scope of this particular research. However, for each new test setup the accuracy, working range and settings of the PID controller of the hexapod have to be established anew since they are dependent on load combination, hydraulic oil supply and tested specimen (i.e. geometry, stiffness).

3.6 Conclusions

A unique test rig (i.e. hexapod) is presented which has been specifically designed and engineered for multiaxial fatigue testing of marine structural details. Currently, experimental data under such loading conditions are lacking. In particular for joints and loading-and-response conditions that are representative for the maritime industry, the experimental data is scarce. However, such data is prerequisite in order to improve the understanding of multiaxial fatigue as a phenomenon and to make further steps and advances in multiaxial fatigue assessment. With the presented hexapod, academic load scenarios can be investigated and supplemented by more complex scenarios with stochastic/random loadings that represent real loading conditions of marine structures. The test facility can be used for the investigation of (multiaxial) fatigue in different materials, but also provides means to achieve research goals beyond the scope of fatigue (such as ultimate strength and dynamics/vibrations) and even outside the scope of the maritime sector. In Chapter 5, fatigue test results will be presented and analysed that were generated with the in this Chapter presented hexapod.

3.7 References

Anes, V., Reis, L., Li, B., & De Freitas, M. (2014). New cycle counting method for multiaxial fatigue. *International Journal of Fatigue*. https://doi.org/10.1016/j.ijfatigue.2014.02.010

Anes, V., Reis, L., Li, B., Fonte, M., & De Freitas, M. (2014). New approach for analysis of complex multiaxial loading paths. *International Journal of Fatigue*, *62*, 21–33. https://doi.org/10.1016/j.ijfatigue.2013.05.004

Benasciutti, D., Sherratt, F., & Cristofori, A. (2015). Basic principles of spectral multi-axial fatigue analysis. *Procedia Engineering*, *101*, 34–42. https://doi.org/10.1016/j.proeng.2015.02.006

Carpinteri, A., Spagnoli, A., & Vantadori, S. (2008). Multiaxial fatigue life estimation in welded joints using the critical plane approach. *International Journal of Fatigue*, *31*, 188–196. https://doi.org/10.1016/j.ijfatigue.2008.03.024

Doudard, C., Poncelet, M., Calloch, S., Boue, C., Hild, F., & Galtier, A. (2007). Determination of an HCF criterion by thermal measurements under biaxial cyclic loading. *International Journal of Fatigue*, *29*(4), 748–757. https://doi.org/10.1016/j.ijfatigue.2006.06.009

Hsu, C., & Fong, I. (2001). Motion control of a hydraulic Stewart platform with computed force feedback. *Journal of the Chinese Institute of Engineers*, *24*(6), 709–721. https://doi.org/10.1080/02533839.2001.9670667

Instron. (2017). ElectroPuls. Retrieved December 18, 2017, from http://www.instron.us/en-us/products/testing-systems/dynamic-and-fatigue-systems/electropuls-systems

Johnston, C. (2017). Full-Scale Fatigue Testing using the Resonance Method. Retrieved December 18, 2017, from https://www.twi-global.com/technical-knowledge/job-knowledge/full-scale-fatigue-testing-using-the-resonance-method-141/

Kohlstedt, A., Olma, S., Traphöner, P., Jäker, K. P., & Trächtler, A. (2017). Kinematics-based force/position control of a hexapod in a HiL axle test rig. In *Internationales Stuttgarter Symposium, Proceedings*. https://doi.org/10.1007/978-3-658-16988-6_92

MTS. (2017). MAST™ (Multi-axial Simulation Table) Systems. Retrieved January 10, 2018, from https://www.mts.com/cs/groups/public/documents/library/dev_002251.pdf

Nierenberger, M., Poncelet, M., Pattofatto, S., Hamouche, A., Raka, B., & Virely, J. M. (2012). Multiaxial Testing of Materials Using a Stewart Platform: Case Study of the Nooru-Mohamed Test. *Experimental Techniques*, *38*, 74–83. https://doi.org/10.1111/j.1747-1567.2012.00807.x

Papuga, J. (2011). A survey on evaluating the fatigue limit under multiaxial loading. *International Journal of Fatigue*, *33*(2), 153–165. https://doi.org/10.1016/j.ijfatigue.2010.08.001

Saintier, N., Palin-Luc, T., Bénabes, J., & Cocheteux, F. (2013). Non-local energy based fatigue life calculation method under multiaxial variable amplitude loadings. *International Journal of Fatigue*, *54*, 68–83. https://doi.org/10.1016/j.ijfatigue.2012.12.013

Sonsino, C. M. (1995). Multiaxial fatigue of welded joints under in-phase and out-of-phase local strains and stresses. *International Journal of Fatigue*, *17*(1), 55–70.

Sonsino, C. M. (2008a). Effect of residual stresses on the fatigue behaviour of welded joints depending on loading conditions and weld geometry. *International Journal of Fatigue*, *31*, 88–101. https://doi.org/10.1016/j.ijfatigue.2008.02.015

Sonsino, C. M. (2008b). Multiaxial fatigue assessment of welded joints – Recommendations for design codes. *International Journal of Fatigue*, *31*, 173–187. https://doi.org/10.1016/j.ijfatigue.2008.06.001

Sonsino, C. M. (2011). Influence of material's ductility and local deformation mode on multiaxial fatigue response. *International Journal of Fatigue*, *33*, 930–947. https://doi.org/10.1016/j.ijfatigue.2011.01.010

Sonsino, C. M., Lagoda, T., & Demofonti, G. (2004). Damage accumulation under variable amplitude loading of welded medium- and high-strength steels. *International Journal of Fatigue*, *26*, 487–495. https://doi.org/10.1016/j.ijfatigue.2003.10.001

Susmel, L. (2010). A simple and efficient numerical algorithm to determine the orientation of the critical plane in multiaxial fatigue problems. *International Journal of Fatigue*, *32*, 1875–1883. https://doi.org/10.1016/j.ijfatigue.2010.05.004

Susmel, L., & Tovo, R. (2004). On the use of nominal stresses to predict the fatigue strength of welded joints under biaxial cyclic loading. *Fatigue & Fracture of Engineering Materials & Structures*, *27*, 1005–1024. https://doi.org/10.1111/j.1460-2695.2004.00814.x

TUHH. (2015). Prüfanlage HEXAPOD. Retrieved January 10, 2018, from https://www.tuhh.de/hexapod/news.html

Wei, Z., Dong, P., Batra, R. C., & Nikbin, K. (2013). Analysis of multi-axial fatigue test data using a path-dependent effective stress/strain definition. In *ASME 2013 Pressure Vessels and Piping Conference*. Paris, France: ASME 2013 Pressure Vessels and Piping Conference.

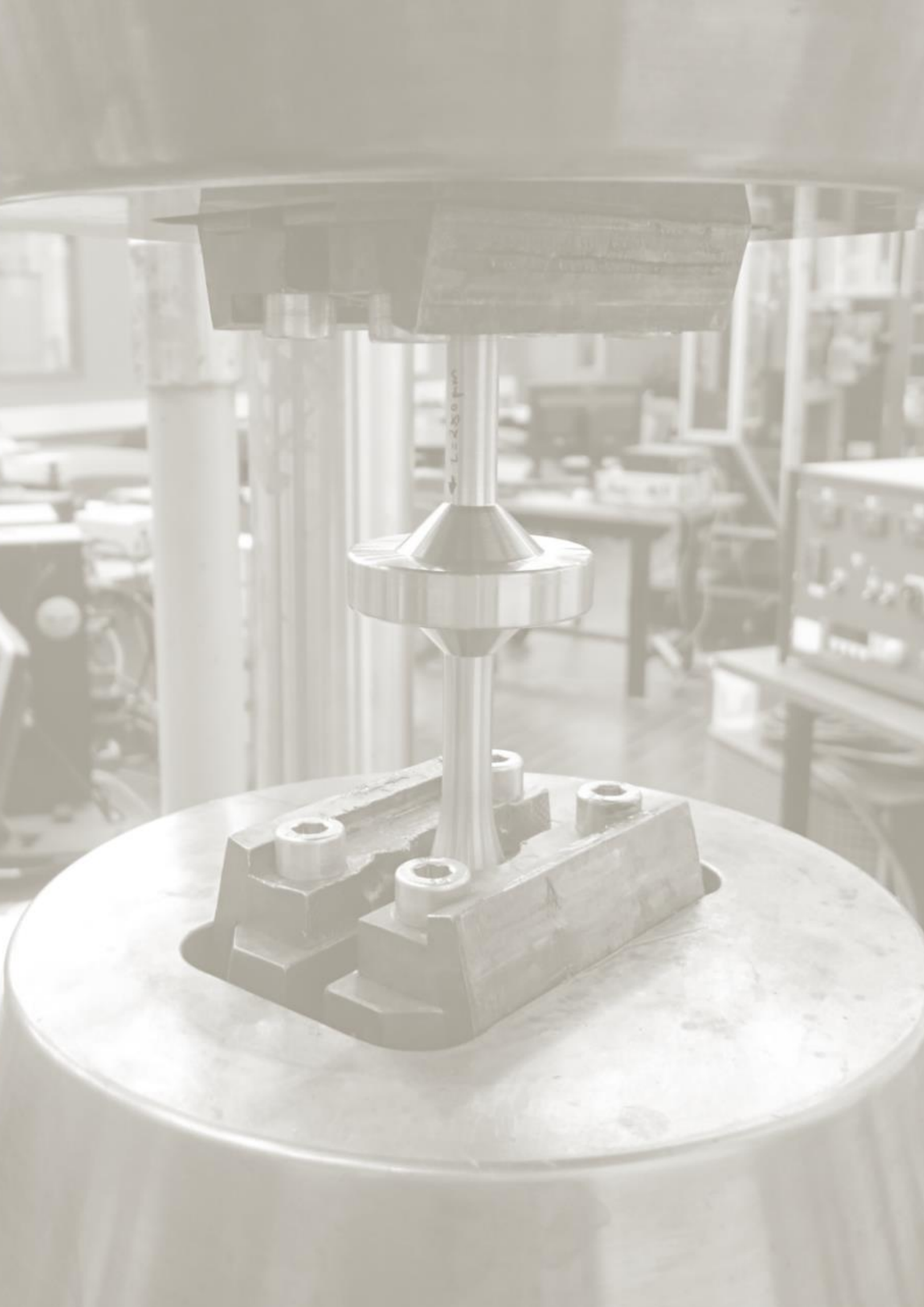

4 On the representation of the fatigue resistance of a welded joint through a notched geometry with an artificial laser induced surface defect

"If we are to achieve things never before accomplished we must employ methods never before attempted"
- Francis Bacon

4.1 Introduction

To systematically investigate the effect of multiaxial fatigue in a welded joint, the experimental scope of work has been executed in two stages. The first stage will be treated in this Chapter 4, whilst the second stage will be addressed in the next Chapter 5. See also Table 4.1.

This Chapter aims to investigate the contribution of welding induced defects on fatigue resistance. A notched geometry is still considered but welding effects such as residual stresses or welding induced material zones (base material, weld material, HAZ) are not present. A bar specimen with a laser induced elliptical surface defect in a notched geometry, is subjected to experimental fatigue testing in cyclic tension. The geometry of this small scale specimen is in accordance with the specimen geometry for large scale testing in the hexapod (cf. Chapter 5).

Next Chapter presents the experimentally obtained test results with the hexapod. Fatigue tests were performed with as-welded large scale tubular specimens that were exposed to multiaxial constant amplitude loading. These results are then used in a comparative study with a selection of state-of-the-art multiaxial fatigue methods.

Table 4.1: Overview of the sub-division of the experimental scope of work in small scale and large scale testing

Experimental Scope of Work	
Chapter 4 – Small scale	Chapter 5 – Large scale
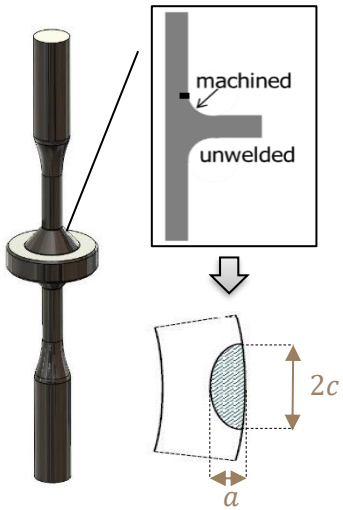	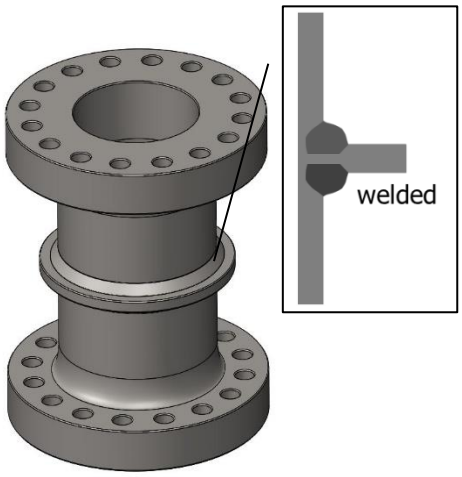

4.2 Welding defects

In regard to welded joints, the definition of the different crack growth phases (i.e. initiation, early growth, macro growth, propagation) is arbitrary. See for example (den Besten, 2015; Mikulski & Lassen, 2019). Experiments have indicated that a crack initiation (and early growth) phase is existent (Lassen, 1990; Verreman & Nie, 1996), and for welded joints a transition from initiation to growth is typically considered at a crack depth between 0.05 and $0.1\ mm$ (Darcis, Lassen, & Recho, 2006). In high cycle fatigue, this part of fatigue life typically dominates the total lifetime (up to failure). According to (Verreman & Nie, 1996) the lifetime up until a crack depth of $0.05\ mm$ accounts for $25 - 50\ \%$ of the total lifetime.

In fracture mechanics, the initial defect size is based on a theoretical concept. The initiation and early crack growth phase in marine structures is typically considered up to a crack depth of $0.1\ mm$. This explains that an initial crack depth of $0.1\ mm$ is often considered in their fracture mechanics calculations. Another more practical aspect that plays a role, is the minimal detectable defect size with Non-Destructive methods (e.g. X-Ray, Ultrasone, MPI).

The initial crack depth for fatigue lifetime assessment is often ranging between $0.05\ mm$ and $0.1\ mm$ (Lassen, 1990). However, such initial defect sizes do not directly correspond to the size of physical welding induced defects (Darcis et al., 2006). In reality, fatigue cracks in welded joints initiate at various locations along the weld toe. These small (elliptical) surface cracks start to grow at a depth of less than $0.1\ mm$ and then coalescence (Darcis et al., 2006). Typically, they grow from the toe into the fine microstructure of the HAZ. The Canadian Offshore Corrosion Fatigue Research Program demonstrated this crack behaviour for manually fillet (as-)welded cruciform joints of structural steel (Verreman & Nie, 1996).

For weld toe failures, a semi-elliptical surface crack can be considered as initial defect shape. The development of the shape of such a crack is governed by its initial shape, the stress gradient and the local material characteristics. It could be argued that these aspects are governed by the welding procedure through welding induced defect size, weld geometry and HAZ. However, from a linear regression analysis of 75 semi-elliptical surface cracks it was found that any initial crack shape tends towards a stable aspect ratio of 1:3 (i.e. $a/2c$) (Lassen, 1990). In (Verreman & Nie, 1996) there is also referred to an experimental study of manually fillet (as-)welded cruciform structural steel plates. This study showed that elliptical surface cracks, exposed to relatively low stress ranges at a load ratio of zero, reach aspect ratios of $0.5 - 0.6$ (i.e. a/c) and maintained this aspect ratio up until several millimetres of crack depth.

4.3 Experimental testing

The fatigue resistance of the considered weld geometry (i.e. filet welded T-joint), has been investigated through experimental testing of a bar specimen with different artificial defect size. Failure was defined as total rupture. In Figure 4.1 the geometry of this bar specimen is shown. The chemical composition and material characteristics were tested in laboratory conditions by MME. Results are given in Table 4.2. The Stress Concentration Factors (SCFs) for this specimen correspond with the SCFs of the large scale tubular specimen (cf. Section 5.3). The Stress Concentration Factor (SCF) in pure Mode I is $k_\sigma = 2.1$ and $k_\tau = 1.5$ in pure Mode III. An elliptically shaped surface defect has been created at the notch of the weld toe geometry. For this purpose an Ultra Short Pulse (USP) laser was used. See Figure 4.3. This laser uses pulse lengths in the range of $10\ ps$ – $100\ fs$ and is typically used for cutting, drilling, marking or surface treatments. The pulse length of an USP laser is considerably short so that energy cannot diffuse in the atomic lattice so that local heat effects are avoided.

Uniaxial tensile (Mode I) fatigue tests were executed on an MTS 350 kN fatigue test bench, considering a load ratio of 0.1. See Figure 4.2 for the test setup. Different aspect ratios and defect sizes were tested in order to investigate their effect on the fatigue resistance of the notched weld geometry. Table 4.3 lists which aspect ratios were considered for the elliptically shaped defects, and at which load levels they were tested. In Table 4.4 further details are provided of the lifetimes that were achieved with the respective aspect ratios. Figure 4.4 shows an image of the typical fracture surface. As reference data, four specimens without artificial defect (i.e. intact geometry) were tested in addition to this test matrix.

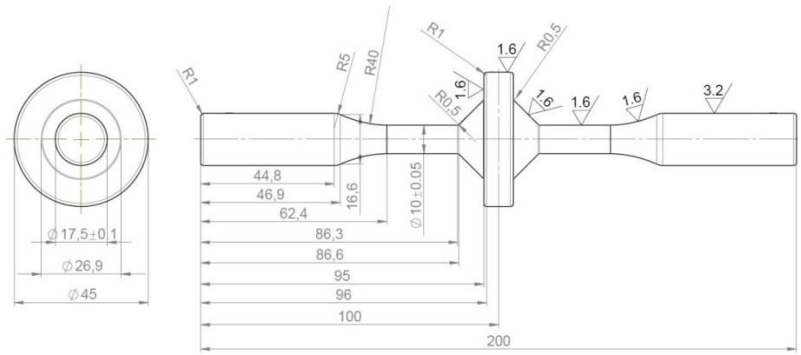

Figure 4.1: Technical drawing of the experimentally tested bar specimen

Figure 4.2: Test setup showing the bar specimen clamped in a uniaxial MTS fatigue test bench

Table 4.2: Chemical composition and material characteristics of the considered bar specimens (S355J2 steel)

C [%]	Si [%]	Mn [%]	P [%]	S [%]	Cr [%]	Mo [%]	Ni [%]	Al [%]	Cu [%]	Ti [%]	V [%]
0.16	0.29	1.20	0.016	0.007	0.09	0.02	0.10	0.022	0.22	<0.01	<0.01
Yield strength = 370 MPa Tensile strength = 511 MPa E- Modulus = 203 GPa											

Table 4.3: Overview of the test matrix for the bar specimens

Minor axis a[µm]	**Major axis $2c$ [µm]**	**Load level $\Delta\sigma$ [MPa]**	**Nr. of specimens**
100	400	150, 200, 300	1x, 2x, 2x
200	800	150, 200, 300	2x, 2x, 2x
250	800	200	2x
300	800	200	2x
300	1200	150, 200, 300	2x, 2x, 2x
500	2000	150, 200, 300	2x, 2x, 2x
Reference data		**Load level $\Delta\sigma$ [MPa]**	**Nr. of specimens**
Intact geometry		200, 300	2x, 2x

Table 4.4: Lifetimes corresponding to the tested bar specimens with their respective defect size

Minor axis a [µm]	Major axis $2c$ [µm]	Lifetime at load level $\Delta\sigma$ 150 MPa	Lifetime at load level $\Delta\sigma$ 200 MPa	Lifetime at load level $\Delta\sigma$ 300 MPa
100	400	1.4E6	1.1E6 9.8E5	1.5E5 1.9E5
200	800	1.5E6 1.9E6	4.9E5 4.7E5	1.1E5 9.5E4
250	800		4.6E5 4.6E5	
300	800		5.0E5 4.6E5	
300	1200	1.3E6 1.0E6	4.8E5 4.4E5	6.3E4 1.0E5
500	2000	9.7E5 7.3E5	3.1E5 3.5E5	6.6E4 7.1E4
Reference data		**Lifetime at load level $\Delta\sigma$ 150 MPa**	**Lifetime at load level $\Delta\sigma$ 200 MPa**	**Lifetime at load level $\Delta\sigma$ 300 MPa**
Intact geometry			1.1E7 1.0E7	2.1E5 2.7E5

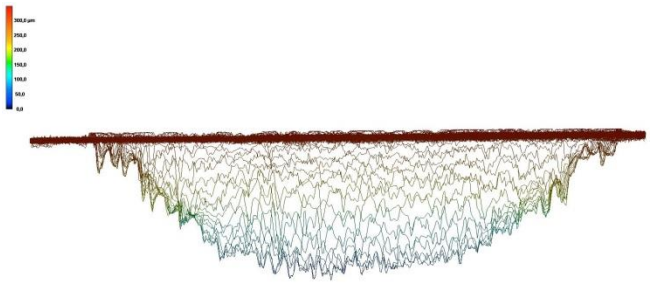

Figure 4.3: Profile scan of a laser induced artificial defect (size: 300 µm deep and 1200 µm wide)

Figure 4.4: Fracture surface of a failed bar specimen with artificial defect

4.4 Bar specimen data analysis

The fatigue lifetimes of all tested bar specimens are shown in Figure 4.5. Based on this data, a linear regression has been established using the least-squares method. Runouts are conservatively considered as failures. For the characterization of the fatigue resistance curves, a Basquin-like equation is considered (cf. Section 2.3.5). The resulting SN curve parameters (slope m and $log(C)$) are taken into consideration for the data analysis and are included in the legend.

The effect of a notched geometry in combination with an artificial defect is demonstrated through a comparison of the bar specimen results with two data sets from literature.These data sets emanate from (Margetin, Ďurka, & Chmelko, 2016) and (R. Ulewicz, P. Szataniak, 2014). Margetin et al. tested conventional bar specimens applying uniaxial cyclic loading in tension-compression with a load ratio $LR = -1$. The bar specimens were made of S355J2+C structural steel and had a diameter of $12.5\ mm$. The tests were stopped at a crack depth of $0.5 - 1\ mm$ since in engineering practice this

crack depth is typically associated with the crack initiation phase (i.e. minimum detectable crack size). Ulewicz et al. also tested an unnotched bar specimen of S355J2 structural steel with a diameter of 7 mm in rotated bending with a load ratio of $LR = -1$. The specimens were tested until failure.

For each data set, the characterizing SN curve parameters have been established. It can however be seen in Figure 4.6 and Figure 4.5 that the regression analyses are strongly affected by the consideration of runouts. In Table 4.5 the SN curve parameters are listed for each data set, including and excluding runout data. From this table it becomes clear that runout data can have a significant impact on the data analysis. When the data set of Ulewicz et al. *discards* runouts, its linear regression corresponds best with the linear regression of the data set of Margetin et al. with runouts *included* as failures.

A slope change can be observed towards the high cycle fatigue region. As a refinement of the presented regression analysis, the Random Fatigue Limit (RFL) model from Pascal & Meekers has been considered (Pascual & Meeker, 1999). This RFL model accounts for the increased data scatter at decreasing stress levels and the slope change associated with the consideration of a fatigue limit. The amount of data is however insufficient to successfully make use of a RFLM.

The bar specimen results show consistency with limited data scatter. Only the specimens with defect size $250\,x\,800\,\mu m$ showed a large difference in fatigue lifetime at stress range $\Delta\sigma = 200\,MPa$. One specimen resulted in an outlier at a significantly higher number of cycles. This specimen was however exposed to several tensile overloads (with about $30\,kN$) due to problems with the grip settings for clamping. This could have introduced a pre-loading or ratcheting effect. Therefore this data point was exclude from the data analysis.

Table 4.5: Overview of the SN curve parameters with and without consideration of runouts for the bar specimen results and two data sets from literature (for base material S355).

Source of Mode I data	m		$Log(C)$	
	With runouts	*Without runouts*	*With runouts*	*Without runouts*
Bar specimens with artificial defect	4.7	3.6	16.6	14.1
Bar specimens with intact geometry	9.5	NA*	28.8	NA*
Margetin et al, 2016	7.9	18.1	27.2	49.9
Ulwicz et al, 2014	11.8	8.8	36.0	28.2

* insufficient test results to make a linear regression analysis

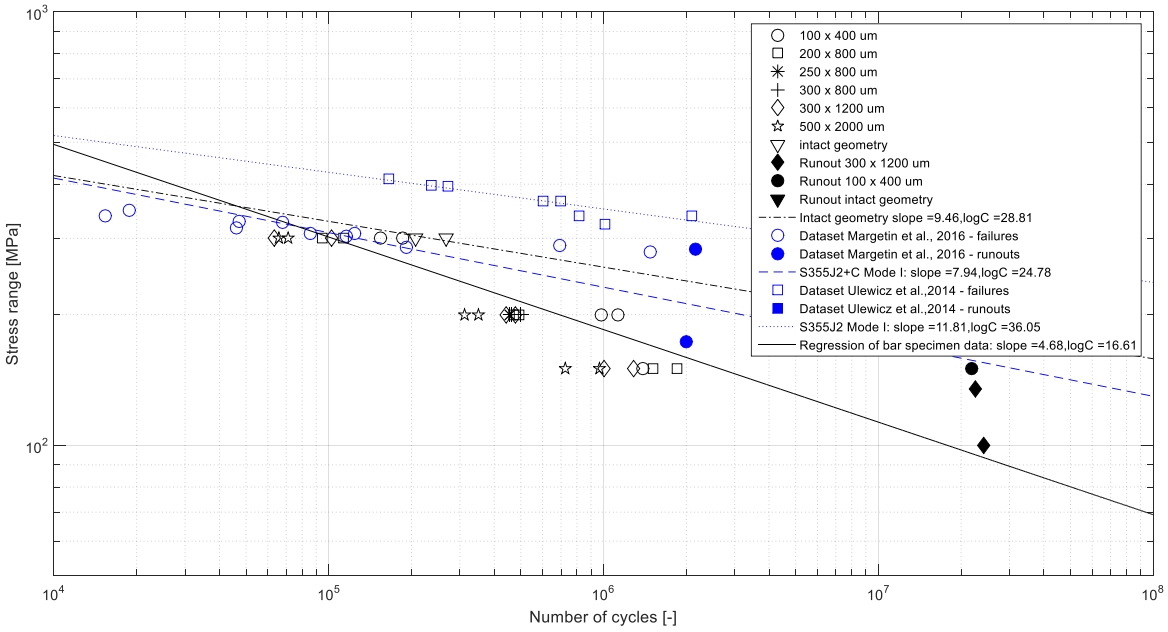

Figure 4.5: Uniaxial tensile fatigue test results of bar specimens with varying size of elliptically shaped artificial defect, compared to the fatigue lifetime of intact bar specimens from literature; runouts included.

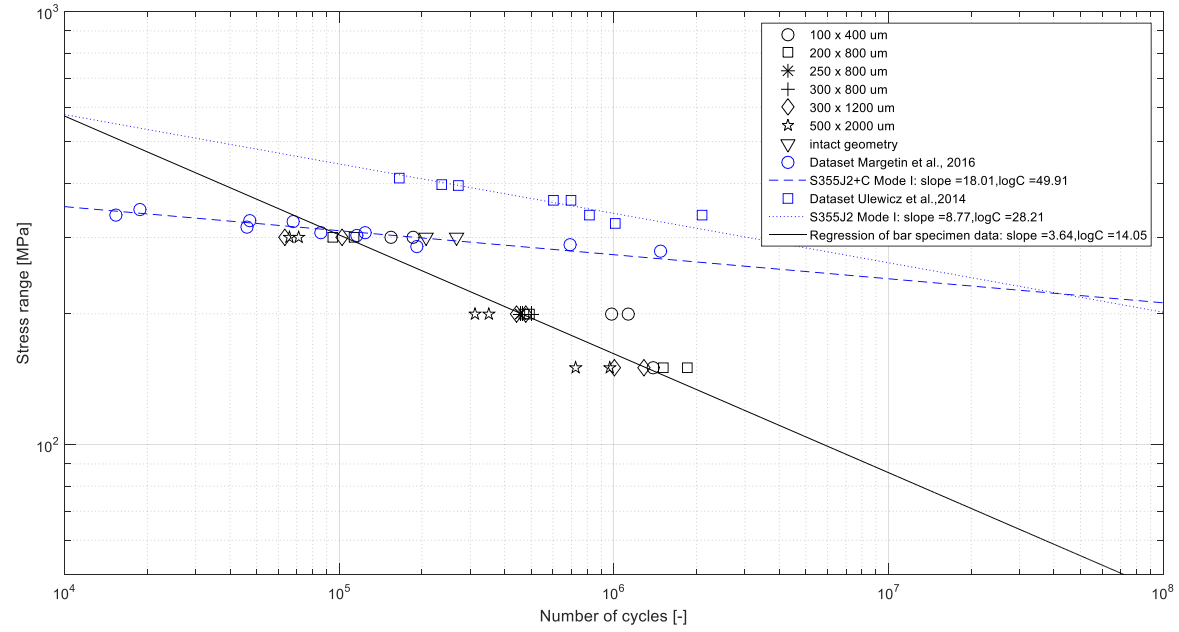

Figure 4.6: Uniaxial tensile fatigue test results of bar specimens with varying size of elliptically shaped artificial defect, compared to the fatigue lifetime of intact bar specimens from literature; runouts excluded

4.5 Discussion and Conclusion

The tested bar specimens show that the fatigue lifetime reduces with increasing defect size. This is clearly visible when the linear regressions (using least squares) are plotted. See Figure 4.7. There are insufficient test results for the defect sizes $250\ x\ 800$ and $300\ x\ 800\ \mu m$. Therefore, only four linear regression curves are shown. These regression curves demonstrate that increasing defect size has a detrimental effect on fatigue resistance, i.e. the SN curve drops with increasing defect size. Another remarkable observation is that the slopes remain very close to each other, ranging from $m = 3.4$ to $m = 4$. This indicates similarity with what is typically considered for as-welded joints in Mode I: a slope of $m = 3$.

The fatigue resistance of the tested bar specimens is significantly lower than that of base material, i.e. data from (Margetin et al., 2016) and (R. Ulewicz, P. Szataniak, 2014). In Figure 4.7 it can be seen that the base material data has a higher fatigue resistance and larger slope m. This is also to be expected since the bar specimens contain a sharp notch in combination with an elliptical surface defect of significant size. Four bar specimens were tested without artificial defect (i.e. intact geometry). These test results demonstrate the main contribution of the notch effect to the decrease in fatigue strength (i.e. $log(C)$). Unfortunately, there is no sufficient data available to generate a linear regression curve for these intact geometries. This could confirm the expected influence of defect size on the damage mechanism (i.e. inverse slope m).

In the following chapter the effect of welding will be investigated. From the tested bar specimens it could be observed how fatigue resistance is affected by the geometrical presence of a notch, and the presence of a surface defect (representing a welding induced defect). By adding also data from welded joints, insights are obtained in the additional welding induced effects.

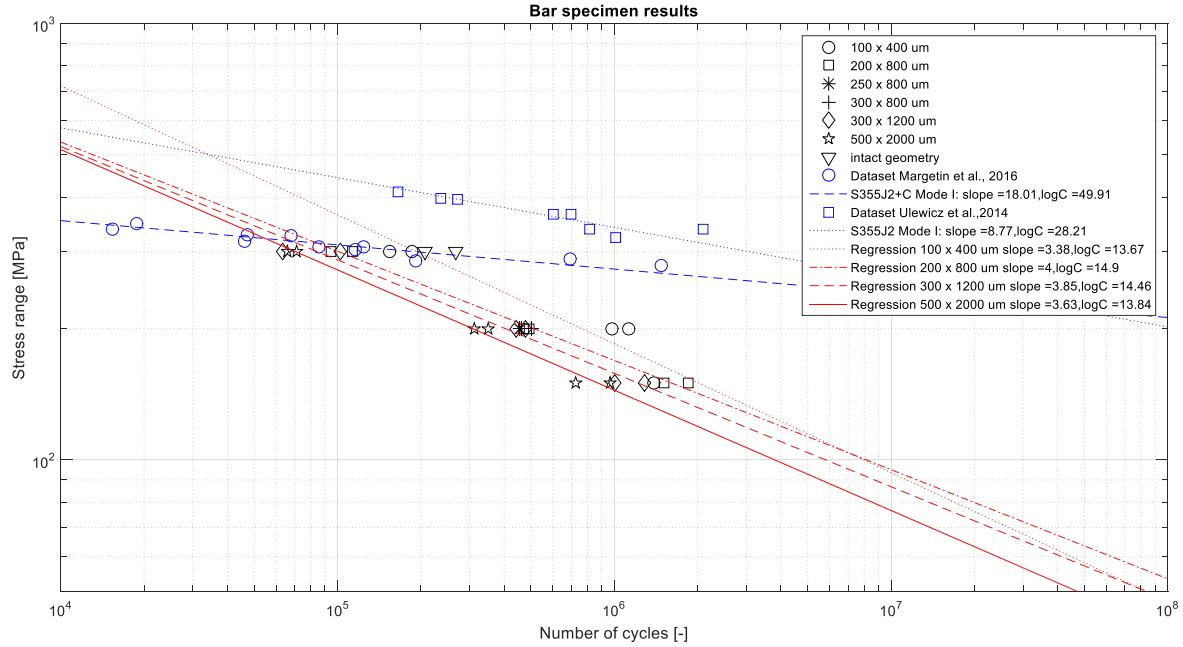

Figure 4.7: Linear regression curve of bar specimens with varying size of elliptically shaped artificial defect, compared to fatigue lifetime of intact bar specimens from literature; runouts excluded

4.6 References

Besten, J. H. den. (2015). *A total stress concept*. Delft University of Technology.

Darcis, P., Lassen, T., & Recho, N. (2006). Fatigue Behavior of Welded Joint Part 2- Physical Modeling of the Fatigue Process. *Welding Journal*, *85*(1), 19–25. https://doi.org/10.1111/j.1559-3584.1936.tb03841.x

Dong, P., Hong, J. K., & Cao, Z. (2003). Stresses and stress intensities at notches: "anomalous crack growth" revisited. *International Journal of Fatigue*, *25*, 811–825. https://doi.org/10.1016/S0142-1123(03)00130-0

Lassen, T. (1990). The effect of the welding process on the fatigue crack growth in welded joints. *Welding Journal*, *February*, 75s-85s.

Margetin, M., Ďurka, R., & Chmelko, V. (2016). Multiaxial fatigue criterion based on parameters from torsion and axial S-N curve. *Frattura Ed Integrita Strutturale*, *10*(37), 146–152. https://doi.org/10.3221/IGF-ESIS.37.20

Mikulski, Z., & Lassen, T. (2019). Fatigue crack initiation and subsequent crack growth in fillet welded steel joints. *International Journal of Fatigue*, *120*(August 2018), 303–318. https://doi.org/10.1016/j.ijfatigue.2018.11.014

Pascual, F. G., & Meeker, W. Q. (1999). Estimating Fatigue Curves with the Random Fatigue-Limit Model. *Technometrics*, *41*(4), 277–290. https://doi.org/10.2307/1271342

R. Ulewicz, P. Szataniak, F. N. (2014). Fatigue properties of wear resistant martensitic steel. In *Metal*. Brno, Czech Republic.

Schijve, J. (1989). *Fatigue of Structures and Materials*. *Springer* (Vol. 53). Springer. https://doi.org/10.1017/CBO9781107415324.004

Verreman, Y., & Nie, B. (1996). Early development of fatigue cracking at manual fillet welds. *Fatigue and Fracture of Engineering Materials and Structures*, *19*(6), 669–681. https://doi.org/10.1111/j.1460-2695.1996.tb01312.x

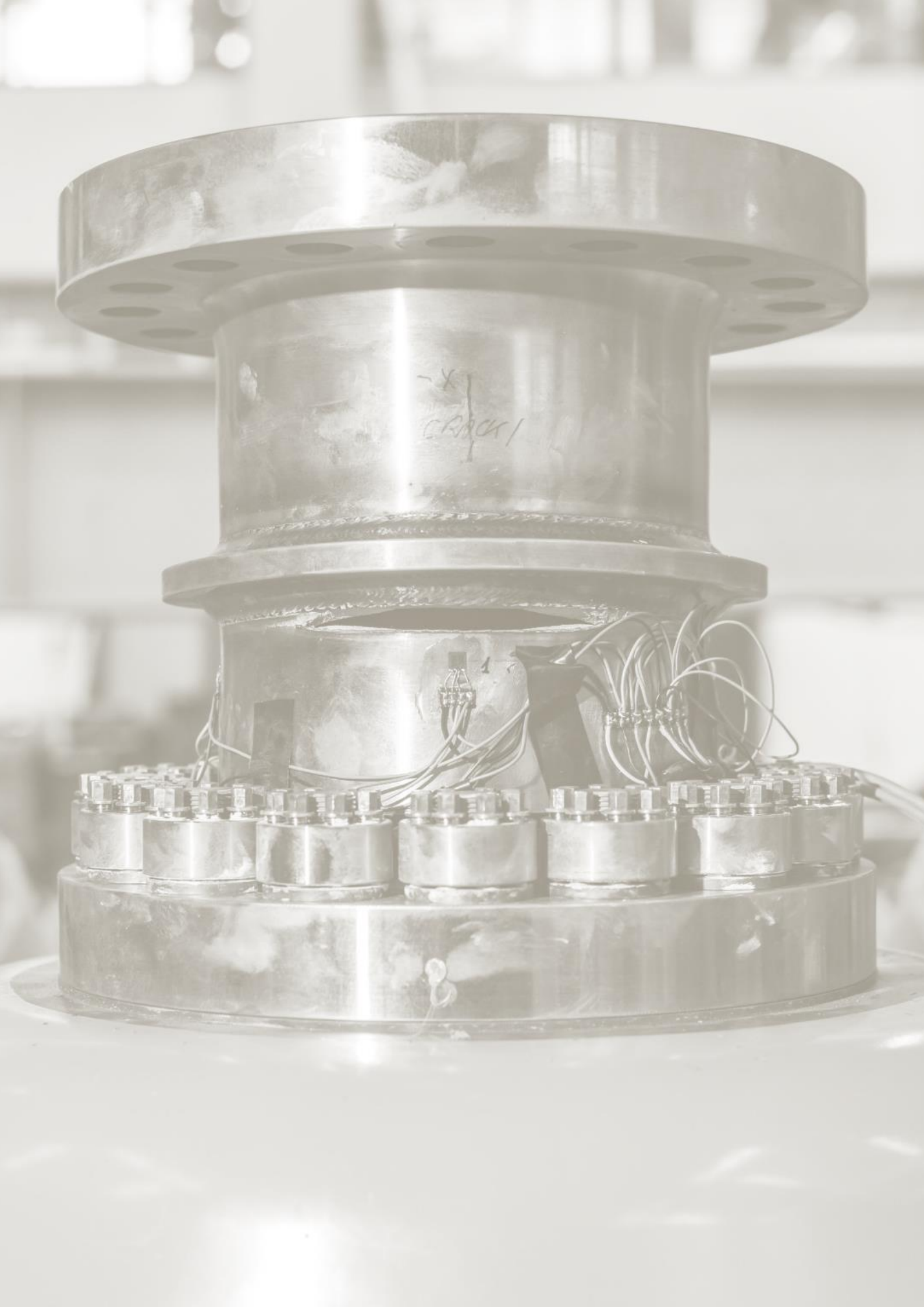
CRACK

5 Comparative study of state-of-the-art multiaxial fatigue methods.

This Chapter is partly based on the following publication:
"Comparative study of multiaxial fatigue methods applied to welded joints in marine structures"
P.S. van Lieshout, J.H. den Besten, M.L. Kaminski
Conference paper ICMFF 11 2016
Frattura ed Integrità Strutturale 10(37):173-192, 2016
DOI: 10.3221/IGF-ESIS.37.24

"All truths are easy to understand once they are discovered; the point is to discover them."
– Galileo Galilei

5.1 Introduction

This Chapter is dedicated to presenting the experimental test results that were collected with the hexapod (cf. Chapter 3). Furthermore, this data will be compared with fatigue lifetime estimates from a selection of multiaxial fatigue methods. In Chapter 2 an overview has been provided of the variety of methods that can be used for multiaxial fatigue assessment. On the basis of this study, a selection of methods was made. This selection was based on the consideration that the methods are applicable to welded joints:

- Critical plane method
    - Modified Wohler Curve (MWC) method
    - Structural Stress Critical Plane (SSCP) method
    - Modified Carpinteri-Spagnoli (MCS) method
- Invariant method
    - Projection-by-Projection (PbP) method
- Integral method
    - Effective Equivalent Stress Hypothesis (EESH)

An appropriate cycle counting technique and damage rule have been selected accordingly:

- Cycle counting technique
    - Rainflow
    - Multiaxial rainflow
- Damage rule
    - Palmgren-Miner

For reference to engineering practice, the following recommendations and guidelines have been added to the comparative study:

- IIW 2016: Recommendations for fatigue design of welded joints and components
- EN 1993-1-9: Eurocode 3: Design of steel structures - Fatigue
- DNV-GL-RP-C203: Fatigue design of offshore steel structures

5.2 Specimen design and manufacturing

For validation of the selection of multiaxial fatigue methods, experimental data has been collected with the unique and specially developed hexapod for multiaxial fatigue testing. The considered test specimen is that of a tubular geometry with fillet welded circumferential attachment. See Figure 5.2. The tubular is machined from one piece of axis material of S355J2G3+N structural steel. See Table 5.1 for details about the chemical composition and material characteristics that were tested in laboratory conditions by MME.

A fillet weld was later introduced in the rectangular corner on both sides of the circumferential attachment. This study considers weld toe failures and thus weld root failures should be avoided. Therefore, the weld does not serve as a connector between two separate parts.

Two batches of tubular specimens have been machined and welded. First a batch of ten specimens was ordered, followed by an additional batch of specimens. The welding procedure has been certified according to offshore quality standards (EN 10204-2004) and was checked by MPI (Standard: NEN-EN-ISO 17638, Acceptance criteria: NEN-EN-ISO 23278) and visual inspection (Standard: NEN-EN-ISO 17637, Acceptance criteria: NEN-EN-ISO 5817). A shielding gas of 80%Ar20%Co_2 was used with SM-70 1.2 mm x 15 kg welding consumable. The welding procedure was automated by using a fixed welding torch and rotating table. In Figure 5.1 the weld setup is shown.

The tubular specimens are as-welded without heat treatment or stress relief. Residual stresses are present but are considered of a negligible influence on the fatigue resistance due to the notch radius induced stress raise (i.e presence of a notch radius of 0.5 mm) and testing at a load ratio of LR=0.1 (cf. Section 5.4).

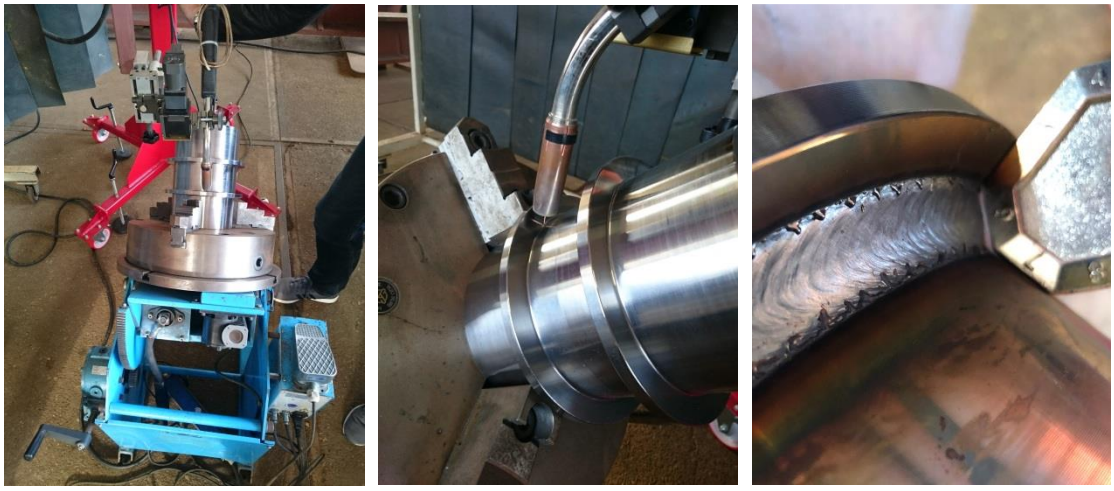

Figure 5.1: Overview of the used setup for automatic welding of the tubular specimens

Table 5.1: Chemical composition and material characteristics of the tubular specimens (S355J2G3+N)

Yield strength = 340 MPa Tensile strength = 506 MPa E-modulus = 258 GPa											
C [%]	Si [%]	Mn [%]	P [%]	S [%]	Cr [%]	Mo [%]	Ni [%]	Al [%]	Cu [%]	Ti [%]	V [%]
0.19	0.38	1.47	0.013	0.001	0.05	0.03	0.08	0.053	0.06	<0.01	<0.01

5.3 Weld quality characterization

The welding quality between the two different batches of tubular specimens has been investigated so that any significant influence on fatigue resistance can be excluded. For this purpose Vickers hardness has been measured (at the three different material zones of the weld), and microscopic inclusions have been evaluated. Vickers hardness measurement is a relatively simple means to characterize the different material zones of a weld, since sampling from the three different material zones of the weld is not needed. The measured hardness can be linearly correlated to yield strength, which provides information about the level of ductility, and thus microstructure.

Three samples were taken from two different tubular specimens. The first two samples were taken from the first tubular that originated from the first batch, and the third sample was taken from a tubular from the second batch. The first two samples were investigated with the objective to examine any differences in weld quality and material characteristics at the start and stop of the weld. See Figure 5.3. The third sample was studied to evaluate that the welding procedure had been performed consistently, and resulted in similar quality of the microstructure (in terms of hardness, material zones, and size and number of inclusions). This third sample was also taken at the weld start-stop location.

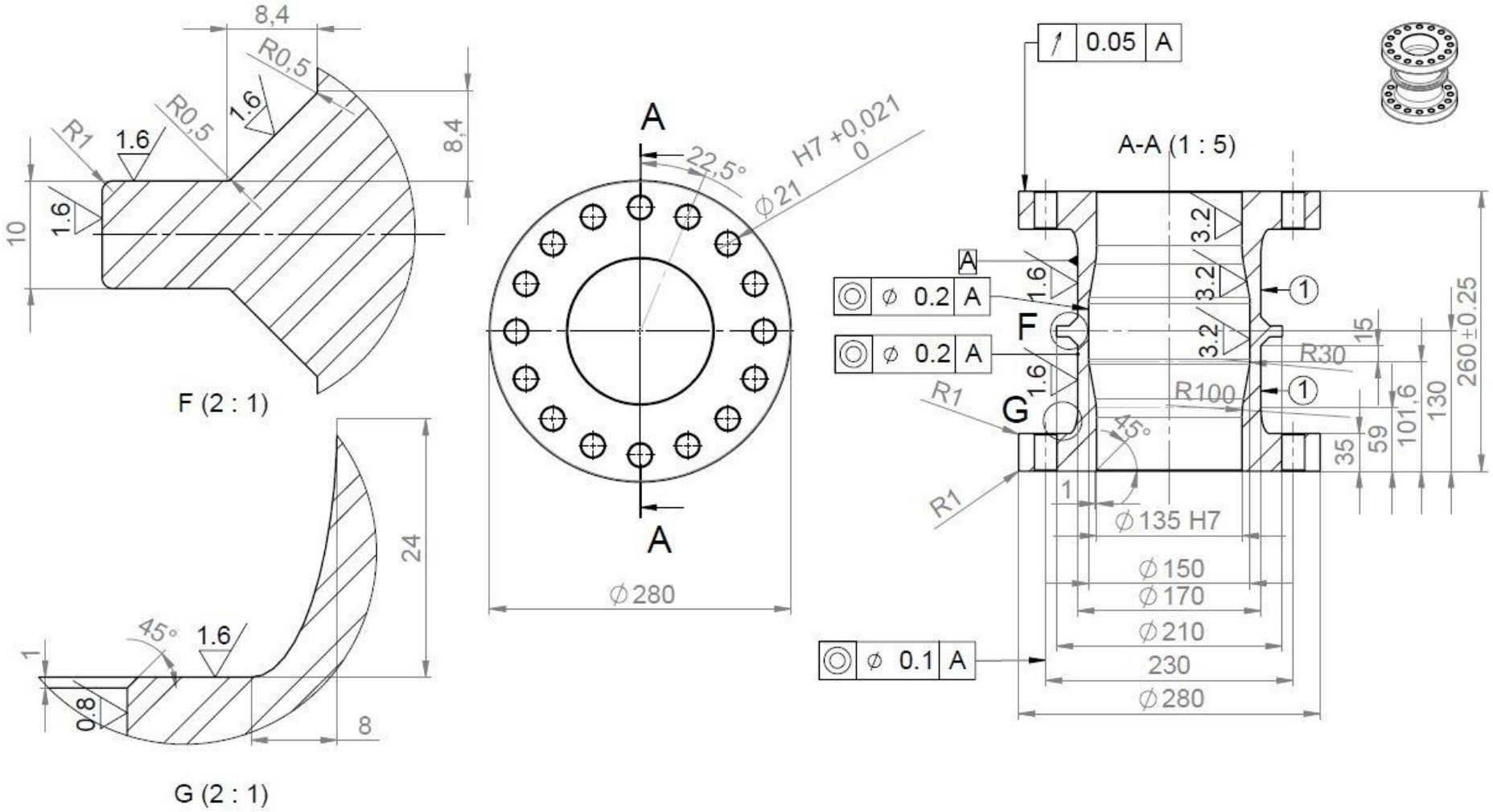

Figure 5.2: Technical drawing of the experimentally tested tubular specimen

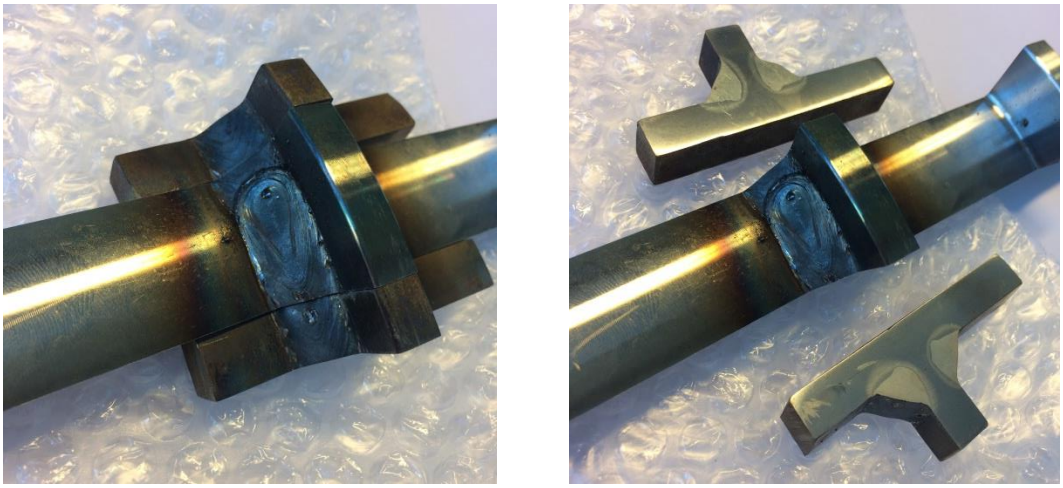

Figure 5.3: Overview of the two sampled specimens at the weld start-stop location

Vickers hardness measurements are a measure of plastic deformation. The pressure over the indenter can be related to the plastic properties of the material, which can again be related to yield stress (see references made in (Busby et al., 2005) about previous work of Tabor, Prandtl and Hencky). Based on the well-known Von Mises yield criterion, a relationship can be established for the two dimensional case of plastic deformation. See Equation 5.1. In this relationship k is the critical value of the maximum shear stress. The pressure P acting perpendicular to the sides of the (pyramidal shaped) indenter tip, can be described by Equation 5.2. By combination of Equation 5.1 and 5.2, a relationship can be found between the contact pressure and yield stress.

Vickers hardness is proportional to the ratio of load (or pressure) L, and the contact area A of the indenter (See Equation 5.3). This enables to establish a linear relationship between Vickers hardness and yield stress, using a correction factor C as shown in Equation 5.4. The correction factor accounts for the ratio of the projected area (i.e. the base of the pyramidal indenter tip) to the contact area (i.e. sides of the pyramidal indenter tip). A similar linear relationship was found between Vickers hardness and yield stress, for various materials (such as aluminium, copper and mild steels) and has been validated using finite element analysis (Busby et al., 2005).

$$2 \cdot k = 1.15 * \sigma_y \tag{5.1}$$

$$P = 2 \cdot k(1 + \frac{\pi}{2}) \tag{5.2}$$

$$H_v \sim \frac{L}{A} \tag{5.3}$$

$$H_v \sim C \cdot P \text{ or } H_v \sim C \cdot \sigma_y \tag{5.4}$$

The correlation factor C has been established for the in this dissertation considered S355 structural steel. The hardness measurements in the base material have been averaged and are correlated to the yield strength resulting from a tensile test. In Table 5.2 these results have been listed for two samples, each taken from a different production batch of tubulars. Vickers hardness was measured at four

locations: in the base material (sample 1 and 3), across the left and right weld toe (sample 1-3) and through the weld from toe to root (sample 1 and 3). In Figure 5.4 the indentations of the measurement points are shown for sample 1 and sample 3.

Before any hardness measurements were performed, the microstructure was analysed at the different material zones of the weld. Figure 5.5 shows images of the microstructure in base material, in the Heat Affected Zone (HAZ) and in the weld material. Furthermore, the distribution and size of the inclusions were inspected in the weld material. Table 5.3 lists the range of sizes of a randomly selected number of inclusions at the weld toe and root.

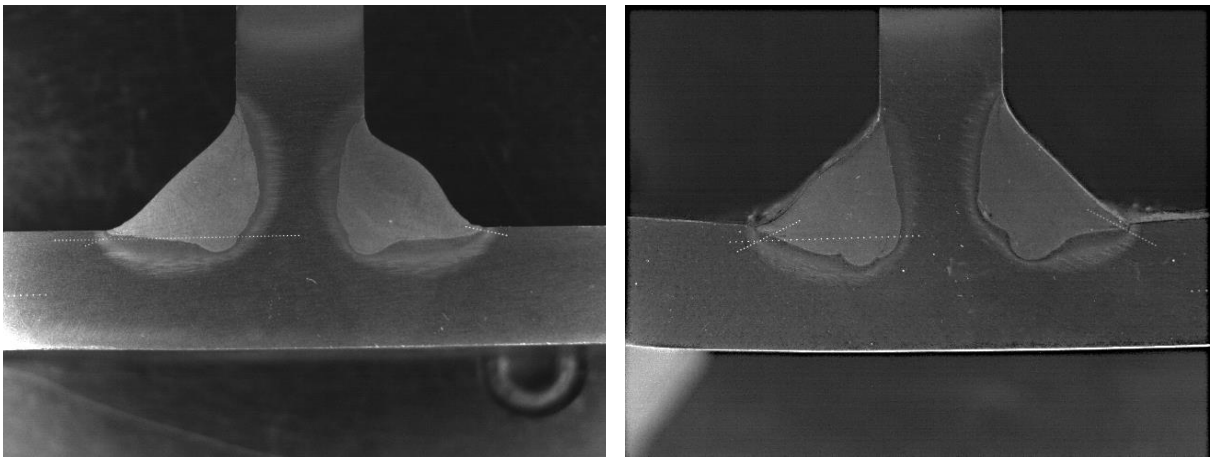

Figure 5.4: Sample 1 (left) and sample 3 (right) showing the indentations from Vickers hardness measurements

Table 5.2: The empirically determined correlation factor for Vickers hardness and yield strength

Sample	Batch	Averaged Vickers Hardness [HV]	Measured yield strength* [MPa]	Correlation factor C [-]
1	1	164.4	340	2.07
3	2	187.6	340	1.81

* Result of a tensile test with a sample of the S355J2G3+N base material, performed by MME (third party)

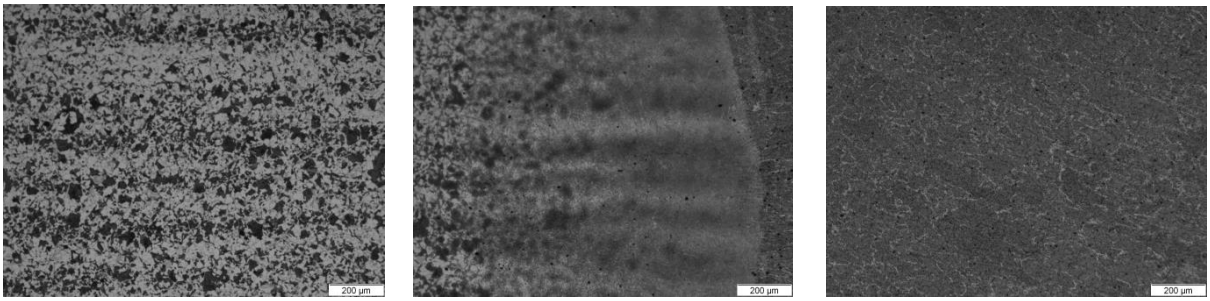

Figure 5.5: Microstructure from left to right: base material with ferritic microstructure, HAZ showing lighter and darker bands of ferrite-pearlite microstructure, weld material showing a distinct grained microstructure.

Table 5.3: Sizes of the random selection of inclusions at the weld toe and root

Sample	Batch	Lower bound diameter of selected inclusions [µm]	Upper bound diameter of selected inclusion [µm]
1	1	8.62	30.36
2	1	4.48	14.14
3	2	6.90	13.80

The hardness distribution was measured in base material and across the weld (from toe to root). Results were compared for sample 1 and sample 3, considering the two different production batches. For all samples the hardness distribution was measured locally at the weld toe. In Figure 5.6 - Figure 5.8 the measurements are shown, expressed in Vickers hardness. In Figure 5.9 - Figure 5.11 the same results are shown in yield stress, based on the linear relationship of Equation 5.4 and the empirically established correction factor (Table 5.2). No abnormalities were found in the microstructure, inclusions (size and/or distribution) or hardness measurements.

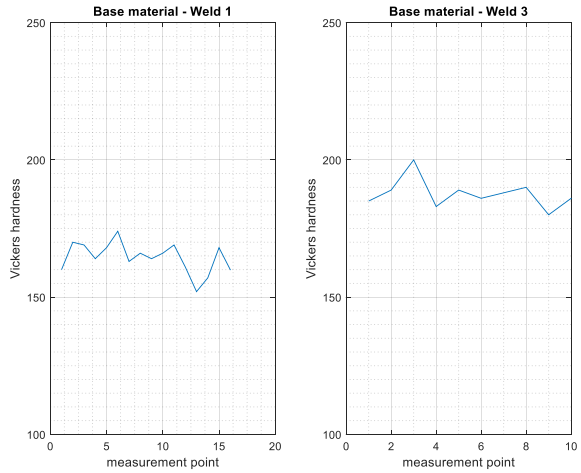

Figure 5.6: Hardness measurements in the base material of sample 1 (left) and sample 3 (right)

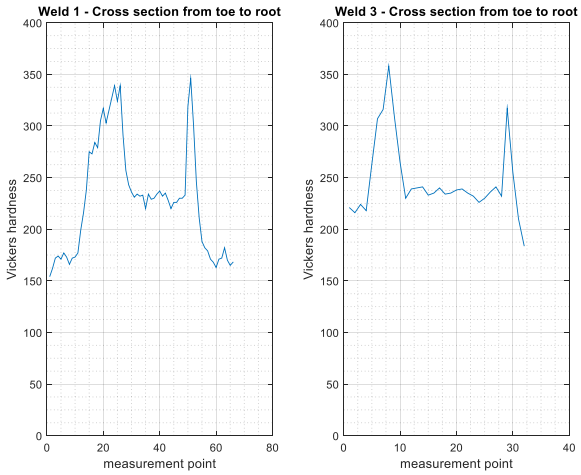

Figure 5.7: Hardness measurements in sample 1 (left) and sample 3 (right), through the weld from toe to root

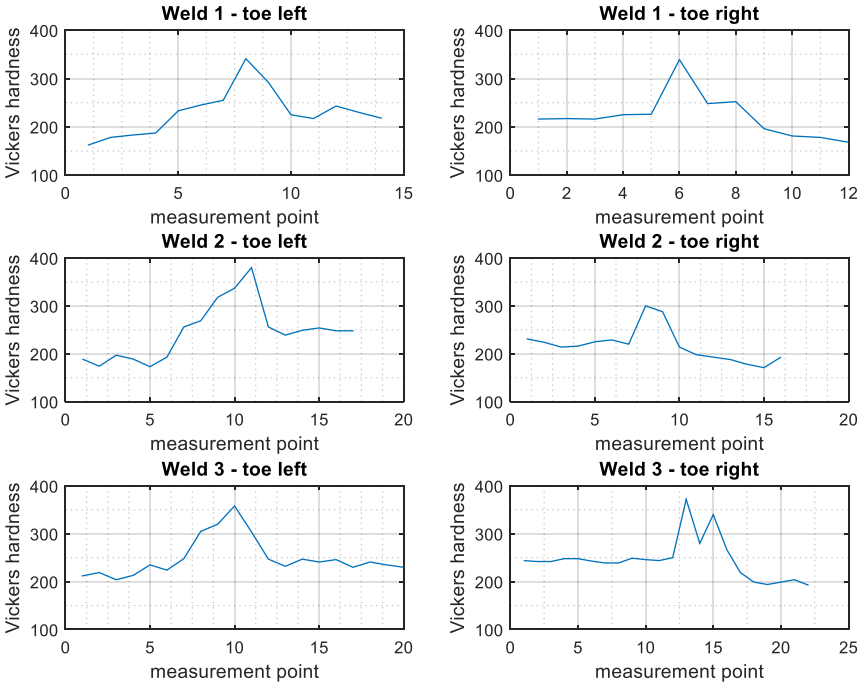

Figure 5.8: Hardness measurements in sample 1, 2 and 3 through the weld toe

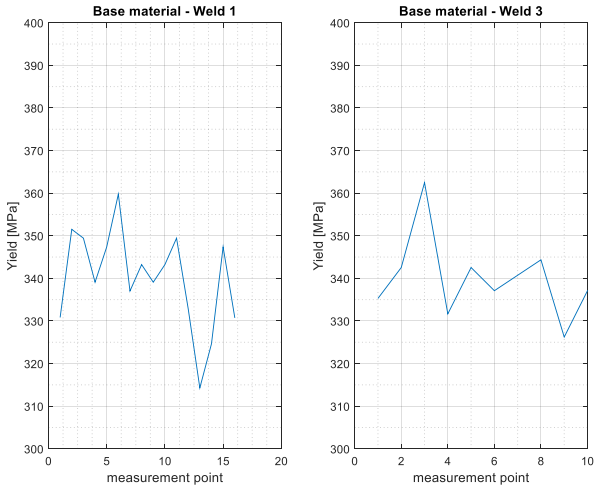

Figure 5.9: Empirically determined yield strength in the base material of sample 1 (left) and sample 3 (right)

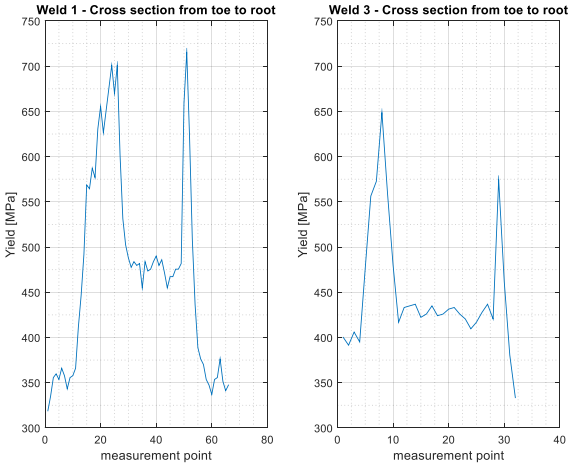

Figure 5.10: Empirically determined yield strength in sample 1 (left) and sample 3 (right), through the weld from toe to root

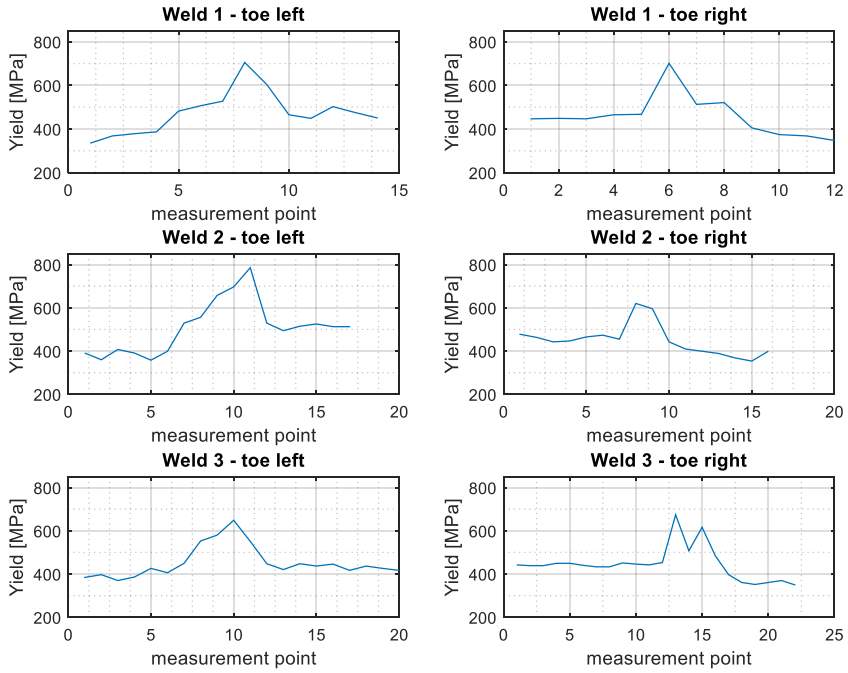

Figure 5.11: Empirically determined yield strength in sample 1, 2 and 3 through the weld toe

5.4 Numerical analysis of specimen design

The specimen design was examined using the finite element software ANSYS. The load transfer and strength were analysed, not only for the specimen but also for the bolted connection between the specimen and the hexapod. The bolted connection was included in the analysis so that the non linear contact behaviour could be accounted for. Pre-tension and maximum allowable surface pressure were taken into consideration. The tubular specimen was modelled using eight noded solid185 elements (for 3D modelling of solid structures). Loading is applied to the model through spiders of rigid links and MPS184 universal joint elements in the bolt holes. Figure 5.12 shows an image of the created ANSYS model. Due to the symmetry of the specimen, it was sufficient to model only half of the geometry.

With Equations 5.5 and 5.6, the structural stress at the weld toe could be determined. The structural stress is mesh insensitive since it makes us of the nodal line forces and line moments of all nodes along the weld line (cf. Section 2.3.4.1). For the tubular specimens, the considered Structural Stress Concentration Factor (SSCF) in pure Mode I is $K_\sigma = 1.2$ and in pure Mode III $K_\tau = 1.1$. The notch Stress Concentration Factors (SCF) in pure Mode I is $k_\sigma = 2.1$ and in pure Mode III $k_\tau = 1.8$.

$$\sigma_s = \frac{f_y'}{t} - \frac{6m_x'}{t^2} \tag{5.5}$$

$$\tau_s = \frac{f_x'}{t} + \frac{6m_y'}{t^2} \tag{5.6}$$

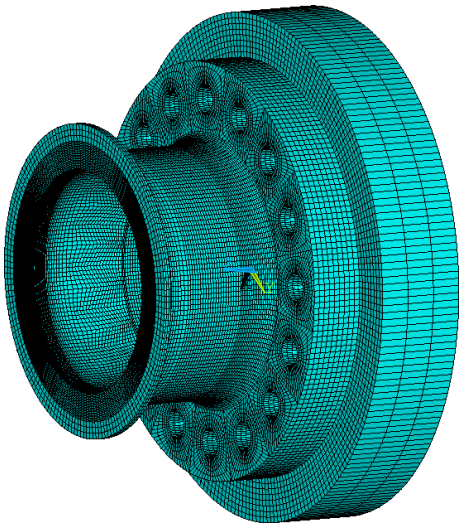

Figure 5.12: Visualization of the ANSYS model of the tested tubular specimen

5.5 Reference data from literature

Before any experimental tests were performed, a study was made of relevant experimental data already published in literature. Data was selected with a focus on multiaxial fatigue resistance (combined Mode I & Mode III), fillet welded tube-to-plate geometries and similar dimensions as the tubular specimen (e.g. wall thickness and weld size). Table 5.8 provides an overview of the experimental data sets that were selected. Later in this Chapter, this data will be used as reference data. This reference data allows to evaluate the quality of the test results from the hexapod and can be used to assess the quality of the selected multiaxial fatigue methods.

5.5.1 Uniaxial fatigue resistance of welded tubular joints

Multiaxial fatigue methods typically describe an interaction or combined effect of the Mode I and Mode III fatigue damage mechanisms. Therefore, conventional SN curves can be used as a reference for fatigue lifetime estimation. These SN curves are based on a profound amount of experimental data of various welded joints and are well documented in guidelines and recommended practices. For the welded tubular joint that is under consideration in this dissertation, IIW and Eurocode 3 both recommend FAT 71 with slope $m = 3$ for normal stress (σ) and FAT 80 with slope $m = 5$ for shear stress (τ) (European Standard, 2005; Hobbacher, 2015). DNV-GL works with classes and recommends Class F for principal stress direction normal to the weld (DNV-GL, 2005). See Figure 5.13.

The data listed in Table 5.8 contains not only multiaxial fatigue resistance data but also uniaxial fatigue resistance data. For a fair judgement of the multiaxial fatigue models it should be verified whether the uniaxial fatigue resistance of the reference data is in agreement with the SN curves that formed the basis for the models. Figure 5.14 shows this uniaxial fatigue resistance, based on a least square linear regression analysis. Only fatigue failures were considered. The slope of $m = 4.4$ in pure Mode I is higher than the expected slope of $m = 3$. This could be an indication of conservatism in the guidelines. For pure Mode III the slope of $m = 4.8$ is in alignment with the expected slope of $m = 5$. Overall, the fatigue resistance curve for Mode I governs over the one for Mode III, indicating a stronger contribution of cyclic normal stress to fatigue damage.

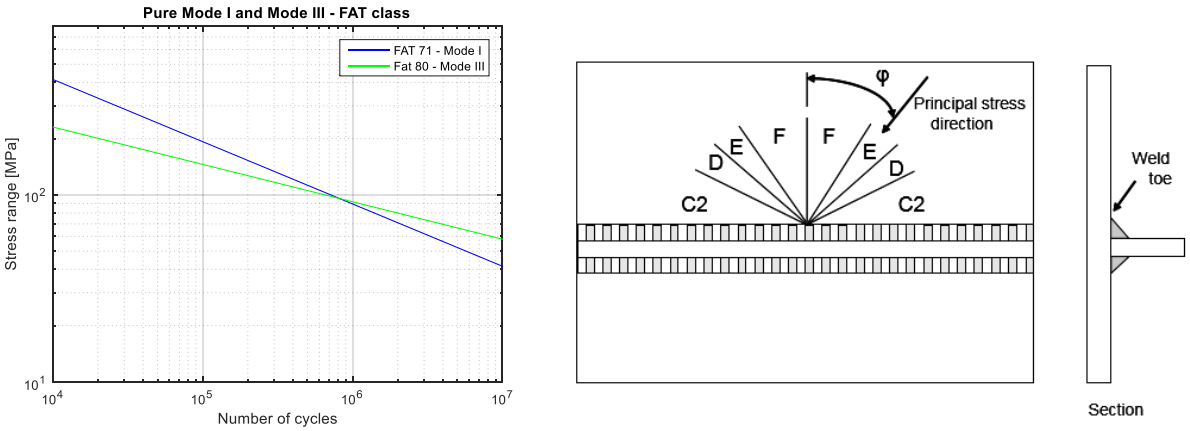

Figure 5.13: Uniaxial fatigue resistance curves for the considered welded tubular specimen in accordance with IIW and Eurocode (left), and in accordance with DNV-GL (right) (DNV-GL, 2005).

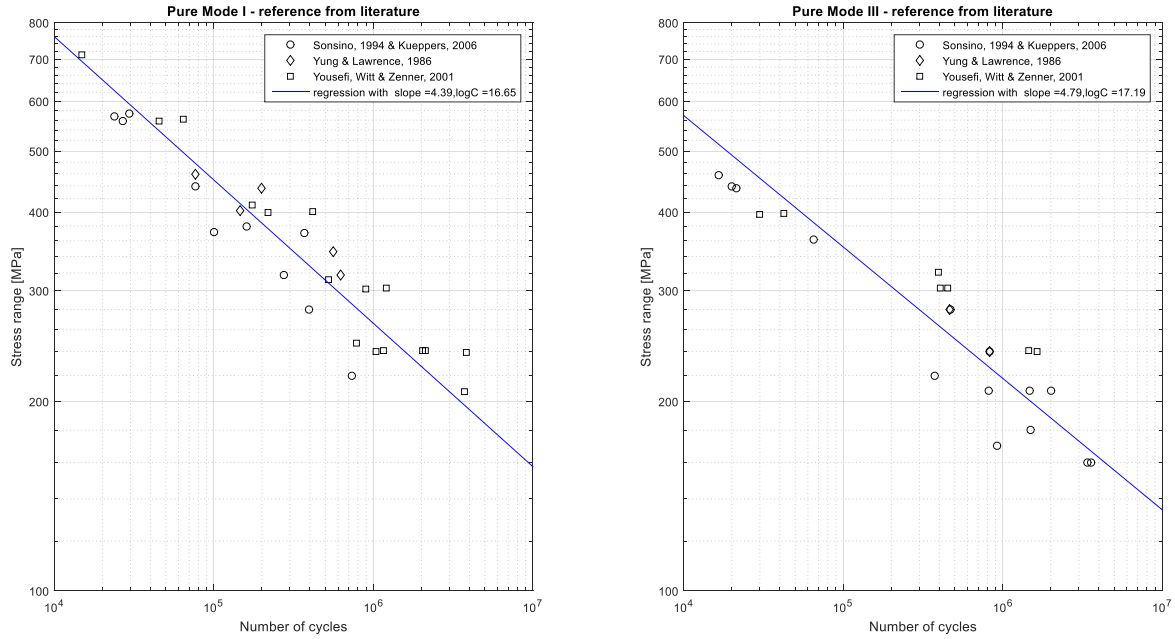

Figure 5.14: Nominal stress based uniaxial fatigue resistance curves of the selected reference data for pure Mode I (left) and pure Mode III (right)

5.5.2 Uniaxial fatigue resistance of base material

A data set of fatigue test results with conventional specimens of base material S355J2+C is added to the reference data set. This data is selected from literature, since it contains both Mode I data (pure tension/compression) and Mode III data (pure torsion) (cf. Section 4.4) for *un-welded* S355 material (Margetin et al., 2016). Especially the latter, Mode III fatigue resistance data, is hard to find.

By comparing the fatigue resistance curves of the base material with those of the selection of welded tubular joints, a clear insight can be obtained into the mechanism of Mode I and Mode III. In Figure 5.15 it can be seen that base material shows a different damage mechanism (i.e. slope change) in comparison to the welded tubular joints (Figure 5.13 and Figure 5.14).

An interesting observation that can be made is that the slope ratio (m_τ/m_σ), the damage mechanisms between Mode I and Mode III, are similar for the base material reference data and

guidelines for welded joints from IIW and Eurocode. The base material reference data has a slope ratio of $18.01/13.23 = 1.4$. IIW and Eurocode recommend a slope ratio of $5/3 = 1.7$.

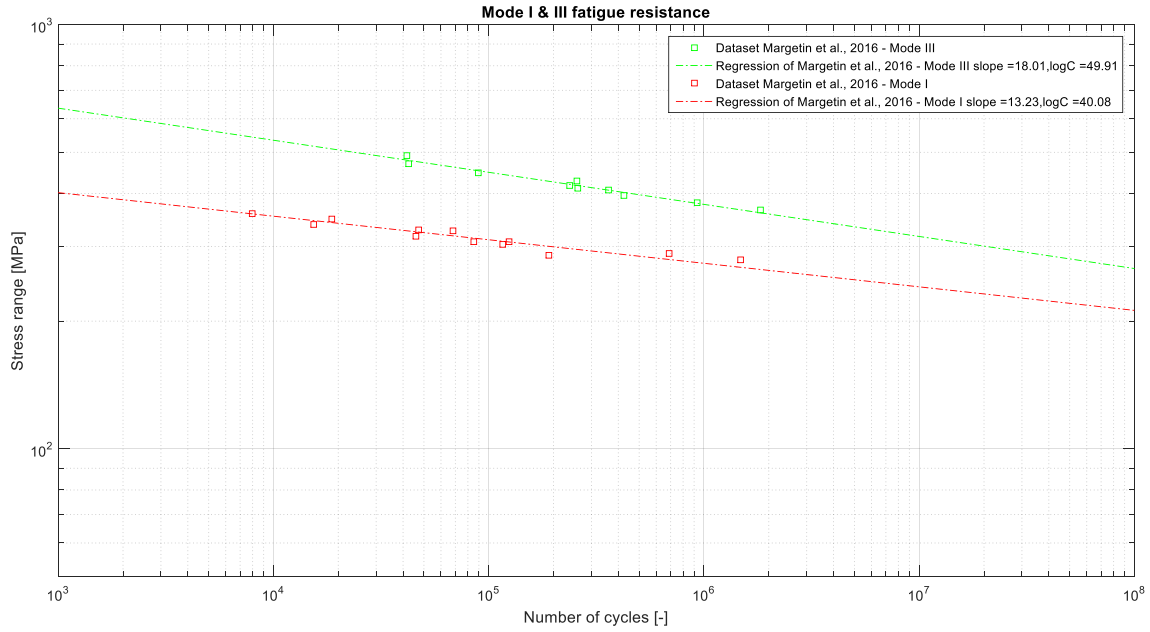

Figure 5.15: Nominal stress based fatigue resistance curves of base material S355J2+C failures in pure Mode I (tension/compression) and pure Mode III loading

5.6 Experimental multiaxial fatigue testing

The experimental tests that are presented in this work solely contain fatigue tests performed at constant amplitude loading. In Table 5.4 an overview is provided of the five distinguished load cases: pure Mode I, pure Mode III, combined proportional (in-phase) loading and two combined non-proportional (out-of-phase) load cases (i.e. phase shift induced and frequency induced). Multiaxiality was introduced by a combination of bending and torsion. Initially, the objective was to combine tension and torsion. Both these load components create a constant stress distribution over the cross sectional area. This however lead to fatigue failures at the critical start-stop location of the weld. Therefore, bending has been applied instead. Bending causes a stress gradient over the cross sectional area and thus one critical location for fatigue failure. Failure at the start-stop of the weld can be avoided by selecting the bending axes accordingly. This will also provide more representative results with respect to engineering practice since weld start-stops are typically removed by grinding.

Table 5.4: Considered load cases in the test matrix

Load case 1 *- Pure Mode I -*	**Load case 2** *- Pure Mode III -*	**Load case 3** *- Mode I & III - In-phase*	**Load case 4** *- Mode I & III - Out-of-phase*	**Load case 5** *- Mode I & III - Out-of-phase*
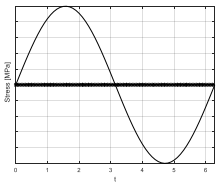	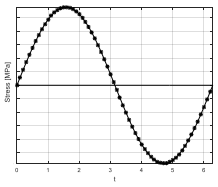	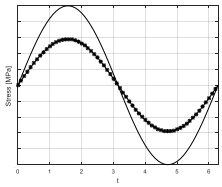	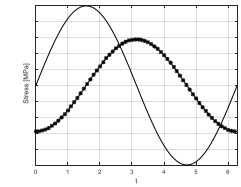	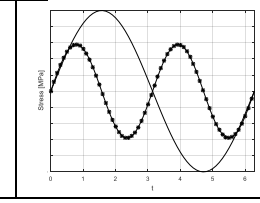

The multiaxial load cases are composed of in-phase and out-of-phase bending and torsion. The out-of-phase load cases are subdivided into two different categories: non-proportionality introduced by a 90 degrees phase shift and non-proportionality introduced by a frequency ratio $f_\sigma: f_\tau = 1:3$. Each load case was tested at three different load levels and all failures were once repeated.

All experiments, including the selected experimental data from literature, have been collected at test frequencies below 10 Hz in ambient air. Environmental conditions and its effect on the investigated fatigue behaviour are thus not included, neither testing frequency effects.

The tested tubular specimens are as-welded and all tests with exception of the torsion tests (Pure Mode III) have been performed at a load ratio LR=0.1. On one hand, the growth rates in as-welded joints tend to be higher in comparison to stress relieved joints due to the presence of residual stresses. On the other hand, notch plasticity and residual stress effects are typically less pronounced when the load ratio is higher or equal to zero, i.e. R≥0 (Verreman & Nie, 1996). This is however not the focus for this dissertation. This work presents a relative comparison between the different load cases and multiaxial fatigue models. Therefore, the debate about the absolute influence of residual stress and stress relaxation effect is circumvented.

5.6.1 Test matrix

Both load components (i.e. bending and torsion) were described by sinusoidal constant amplitude loading with a load ratio of $LR = 0.1$. See Equations 5.7 and 5.8 where A stands for the maximum amplitude, FR for the frequency ratio $f_\tau: f_\sigma$ and δ for the phase angle. The stress amplitude ratio σ_a/τ_a has been considered constant at a ratio of $1/\sqrt{3}$, based on consideration of the Von Mises yield criterion.

$$\sigma(t) = A \cdot \sin(t) + \left[\frac{(\sigma_{max} - \sigma_{min})}{2} + \sigma_{min}\right] \tag{5.7}$$

$$\tau(t) = A \cdot \sin((t \cdot FR) - \delta) + \left[\frac{(\tau_{max} - \tau_{min})}{2} + \tau_{min}\right] \tag{5.8}$$

$$\sigma_{min} = \frac{LR \cdot \Delta\sigma}{1 - LR}$$

$$\sigma_{max} = \sigma_{min} + \Delta\sigma$$

$$\sigma_{max} = \frac{\Delta\sigma}{1 - LR}$$

In Table 5.5 an overview is provided of the completed test matrix with tubular specimens in the hexapod. The test matrix is represented by stress equivalents so that the load cases can be equally compared with each other. Equivalent Von Mises and principal stress were considered, in accordance with Equations 5.9 and 5.10. Table 5.6 provides additional details, i.e. sequence of testing, stress

ranges of the individual components, load case, failure location at upper or lower weld.

$$\sigma_{VM}(t) = \sqrt{\sigma(t)^2 + 3 \cdot \tau(t)^2} \tag{5.9}$$

$$\sigma_{1,2}(t) = \frac{\sigma(t)}{2} + \sqrt{\left(\frac{\sigma(t)}{2}\right)^2 + \tau(t)^2} \tag{5.10}$$

Table 5.5: Test matrix of the tubular specimens expressed in equivalent Von Mises stress and principal stress

	Mode I			
	Pure bending			Pure tension
$\Delta\sigma_{VM}$ [MPa]	320	305	240	175
$\Delta\sigma_{1,2}$ [MPa]	320	305	240	175
Nr. of specimens	2	2	2	2
	Mode III			
	Pure torsion			
$\Delta\sigma_{VM}$ [MPa]	700	545	475	240(runout)
$\Delta\sigma_{1,2}$ [MPa]	405	315	275	130(runout)
Nr. of specimens	1	1	1	1
	Mode I & Mode III			
	Multiaxial in-phase			
$\Delta\sigma_{VM}$ [MPa]	340	310	280	240 (runout)
$\Delta\sigma_{1,2}$ [MPa]	305	280	250	215 (runout)
Nr. of specimens	2	2	2	1
	Mode I & Mode III			
	Multiaxial out-of-phase $\delta = 90\ deg$			
$\Delta\sigma_{VM}$ [MPa]	255	240	200	170 (runout)
$\Delta\sigma_{1,2}$ [MPa]	240	225	185	160 (runout)
Nr. of specimens	2	2	2	1
	Mode I & Mode III			
	Multiaxial frequency ratio $f_\sigma : f_\tau = 1:3$			
$\Delta\sigma_{VM}$ [MPa]	260	240	220	200 (runout)	180 (runout)
$\Delta\sigma_{1,2}$ [MPa]	215	200	190	170 (runout)	150 (runout)
Nr. of specimens	2	2	2	1	1

5.6.2 Load cases

The load cases listed in Table 5.5 and Table 5.6 correspond to different stress fluctuations. Fatigue is governed by the variations in stress over time (i.e. load cycles). When multiaxial loading is experienced, the interaction of the individual load components can have a different influence on the fatigue resistance. This is a consequence of (non-)proportionality and stress amplitude.

The consideration of an equivalent stress can lead to different stress fluctuations than the individual stress components. This affects the stress amplitude and number of load cycles. Therefore, the (equivalent) stress fluctuations per load cycle have been plotted for each tested tubular in Table 5.7. Since the level of multiaxiality and (non-)proportionality becomes apparent when the load path is plotted in stress space, the load path has also been listed in Table 5.7.

Table 5.6: Detailed overview of the tested tubular specimens in the hexapod

Test	Pure Mode I	Pure Mode III	Multiaxial IP	Multiaxial OP 90 deg	Multiaxial OP freq 1:3	$\Delta\sigma$ [MPa]	$\Delta\tau$ [MPa]	Crack location
1	X					175	0	Lower
2	X					175	0	Lower
3	X					320	0	Lower
4	X					240	0	Lower
5	X					305	0	Lower
6*				X		170	98	NA
7				X		240	139	Lower
8				X		240	139	Upper
9*			X			170	98	NA
10					X	240	139	Lower
11					X	240	139	Lower
12	X					240	0	Lower
13*		X				0	139	NA
14*					X	170	98	NA
15			X			240	139	Upper
16			X			240	139	Lower
17				X		200	115	Lower
18				X		200	115	Lower
19			X			200	115	Lower
20				X		260	150	Lower
21				X		260	150	Upper
22			X			220	127	Lower
23	X					320	0	Lower
24			X			220	127	Lower
25	X					305	0	Upper
26					X	225	130	Upper
27					X	190	110	NA*
28			X			200	115	Upper
29					X	225	130	Lower
30					X	210	121	Lower
31					X	210	121	Upper
32	X					320	0	Upper
33	X					305	0	Lower
34	X					240	0	Lower
35”		X				0	405	Lower
36”		X				0	315	Upper
37”		X				0	275	Upper

* Runout

” $LR = -1$

Table 5.7: Overview of the stress fluctuations and load paths of all tested tubular specimens in the hexapod

Plot of the stress fluctuations per load cycle	Plot of the loadpath in $\sigma - \tau$ stress space
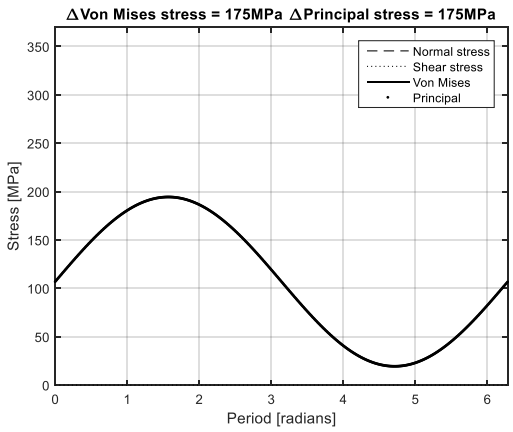	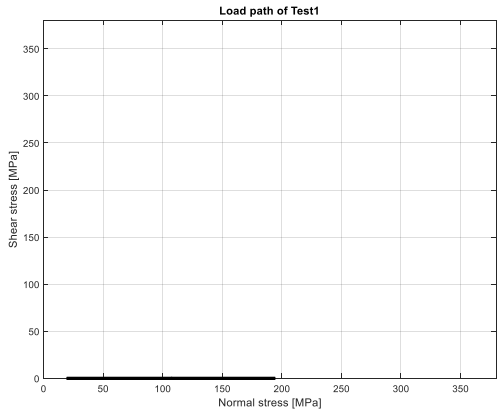
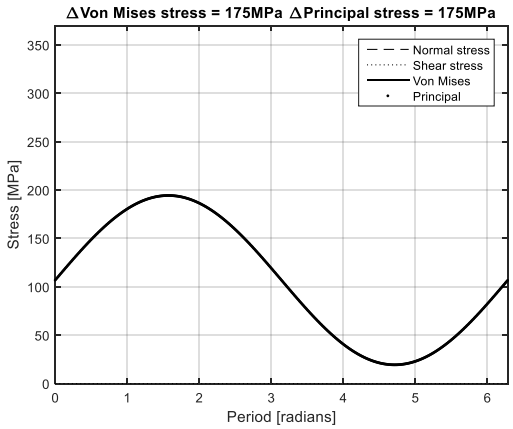	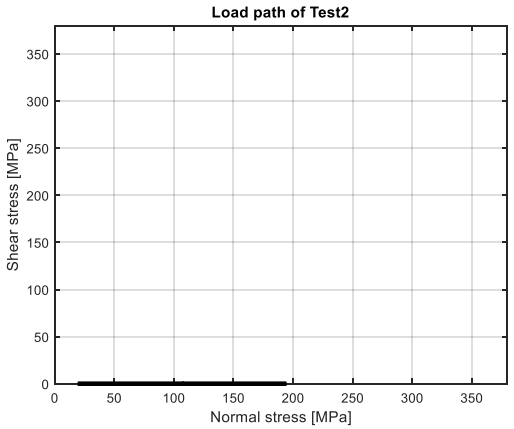
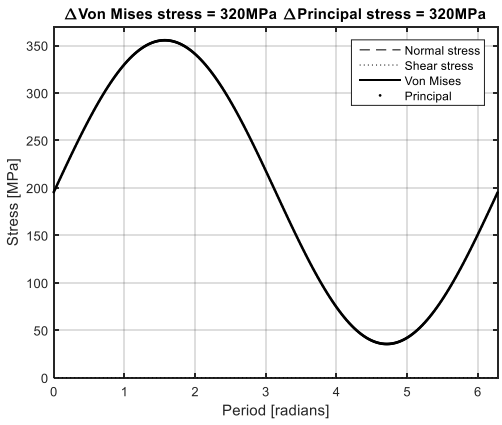	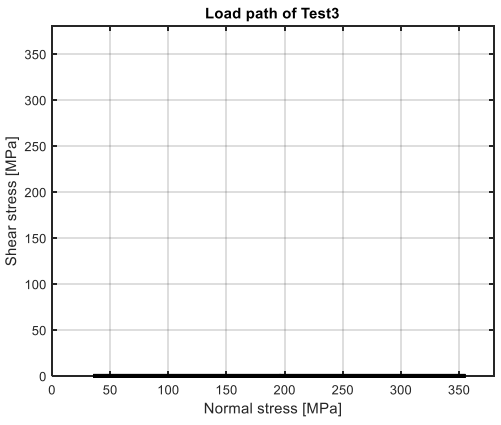

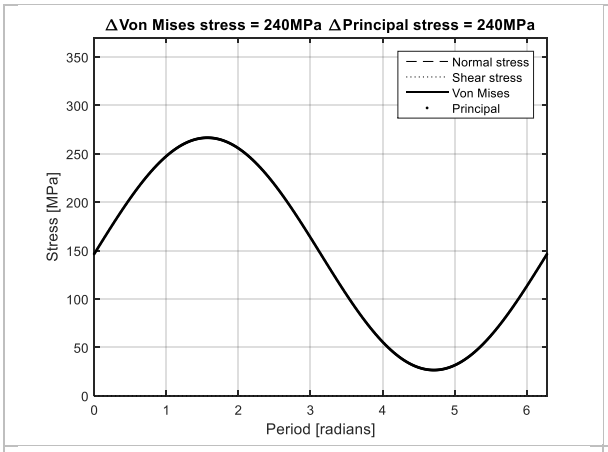
ΔVon Mises stress = 240MPa ΔPrincipal stress = 240MPa
Normal stress
Shear stress
Von Mises
Principal
Stress [MPa]
Period [radians]

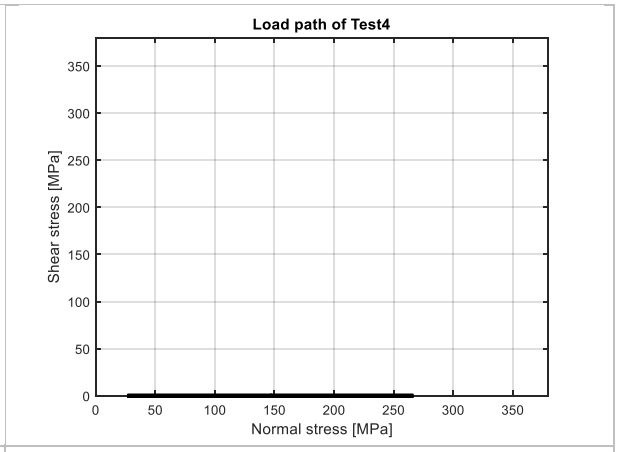
Load path of Test4
Shear stress [MPa]
Normal stress [MPa]

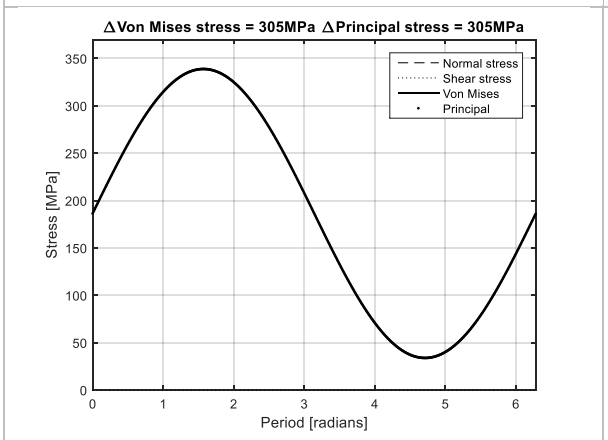
ΔVon Mises stress = 305MPa ΔPrincipal stress = 305MPa
Normal stress
Shear stress
Von Mises
Principal
Stress [MPa]
Period [radians]

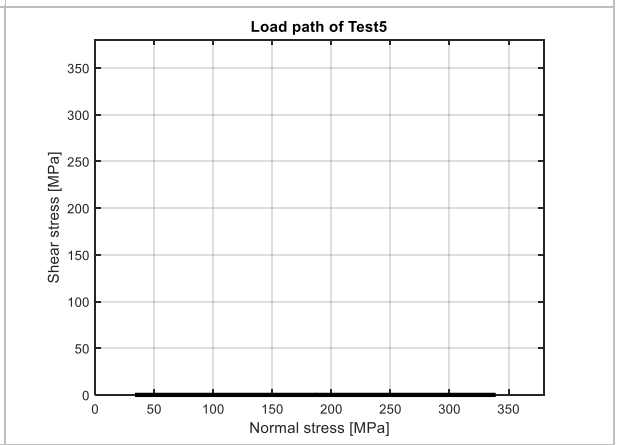
Load path of Test5
Shear stress [MPa]
Normal stress [MPa]

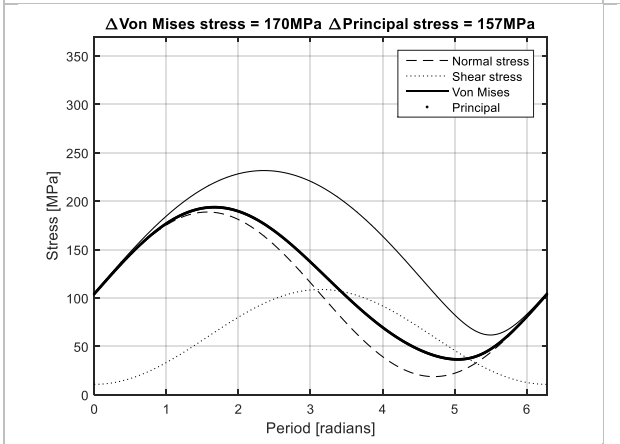
ΔVon Mises stress = 170MPa ΔPrincipal stress = 157MPa
Normal stress
Shear stress
Von Mises
Principal
Stress [MPa]
Period [radians]

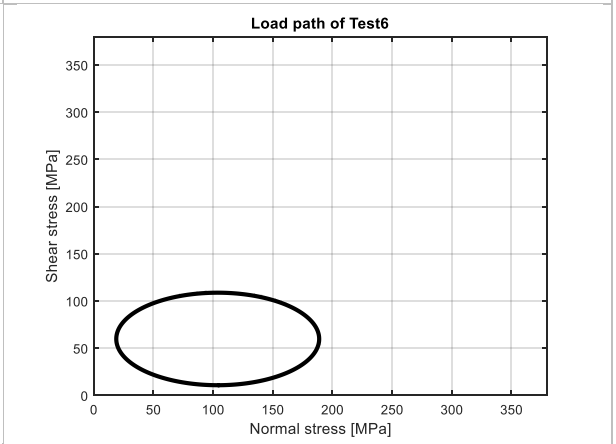
Load path of Test6
Shear stress [MPa]
Normal stress [MPa]

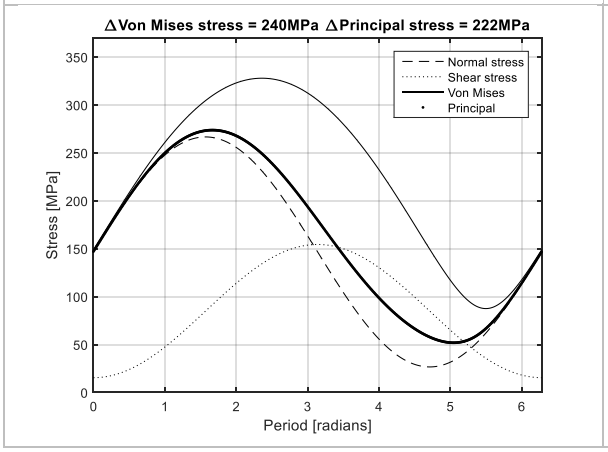
ΔVon Mises stress = 240MPa ΔPrincipal stress = 222MPa
Normal stress
Shear stress
Von Mises
Principal
Stress [MPa]
Period [radians]

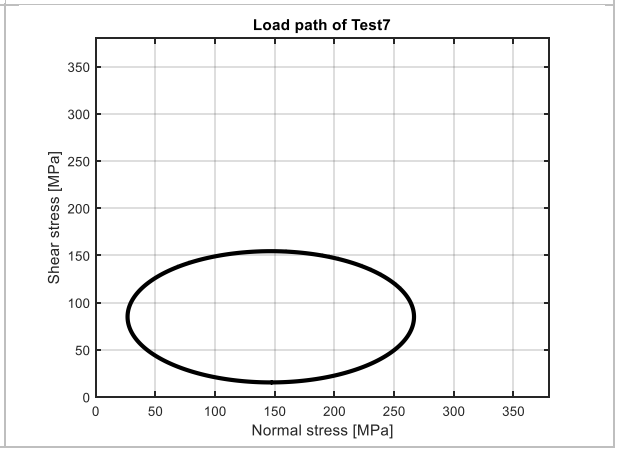
Load path of Test7
Shear stress [MPa]
Normal stress [MPa]

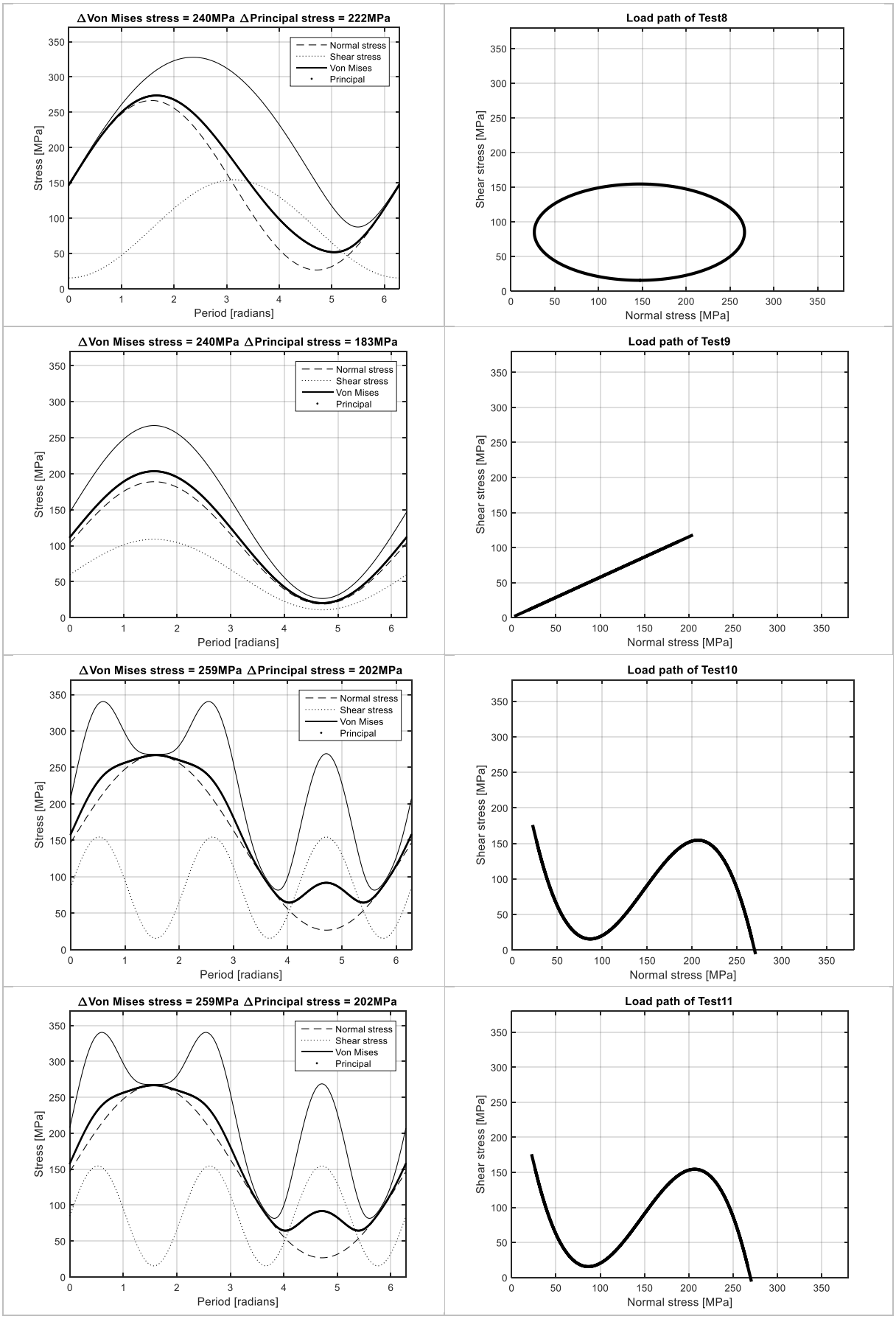
ΔVon Mises stress = 240MPa ΔPrincipal stress = 222MPa
Normal stress
Shear stress
Von Mises
Principal
Stress [MPa]
Period [radians]
Load path of Test8
Shear stress [MPa]
Normal stress [MPa]
ΔVon Mises stress = 240MPa ΔPrincipal stress = 183MPa
Load path of Test9
ΔVon Mises stress = 259MPa ΔPrincipal stress = 202MPa
Load path of Test10
ΔVon Mises stress = 259MPa ΔPrincipal stress = 202MPa
Load path of Test11

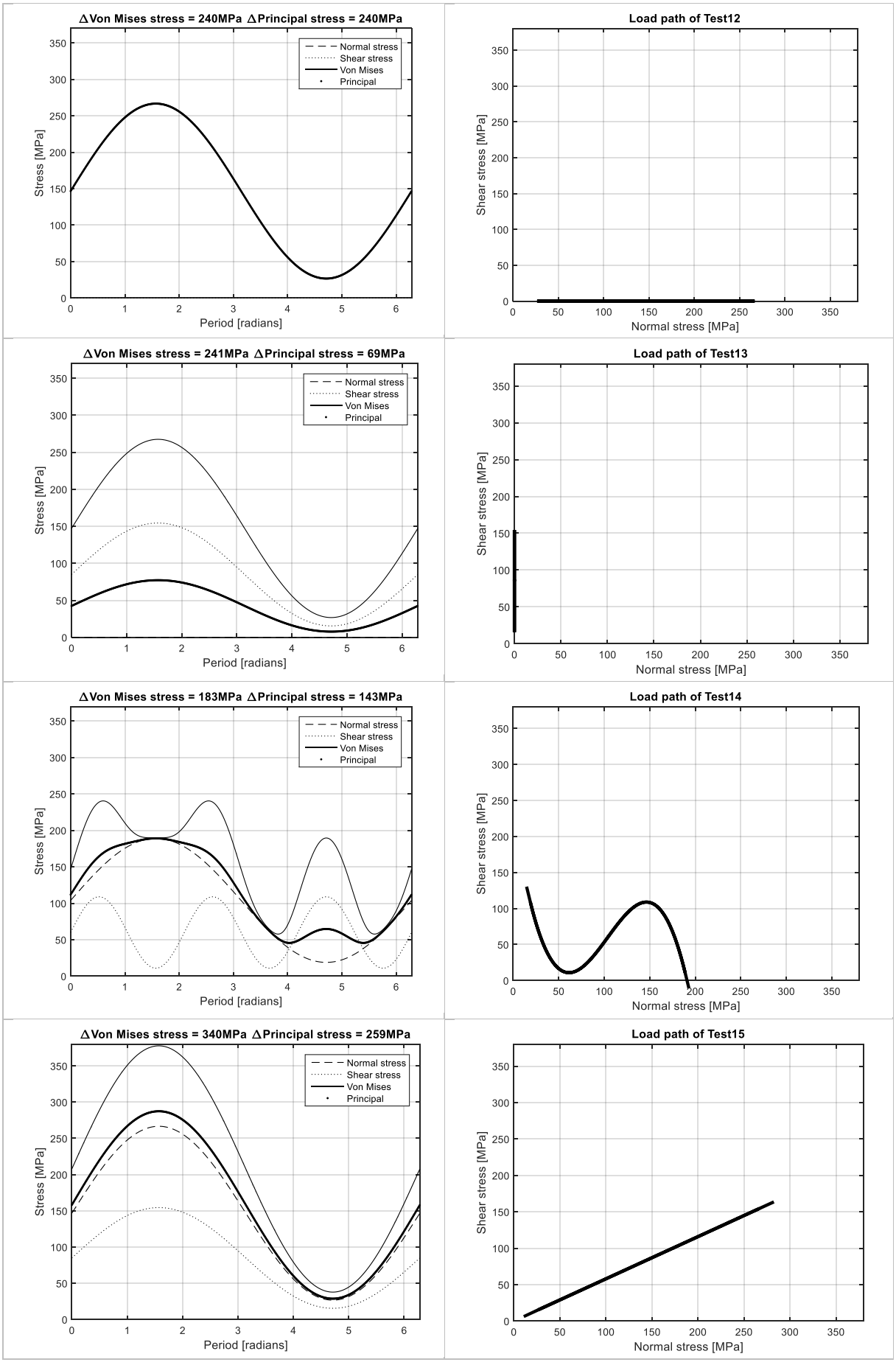
ΔVon Mises stress = 240MPa ΔPrincipal stress = 240MPa
Normal stress
Shear stress
Von Mises
Principal
Stress [MPa]
Period [radians]
Load path of Test12
Shear stress [MPa]
Normal stress [MPa]
ΔVon Mises stress = 241MPa ΔPrincipal stress = 69MPa
Load path of Test13
ΔVon Mises stress = 183MPa ΔPrincipal stress = 143MPa
Load path of Test14
ΔVon Mises stress = 340MPa ΔPrincipal stress = 259MPa
Load path of Test15

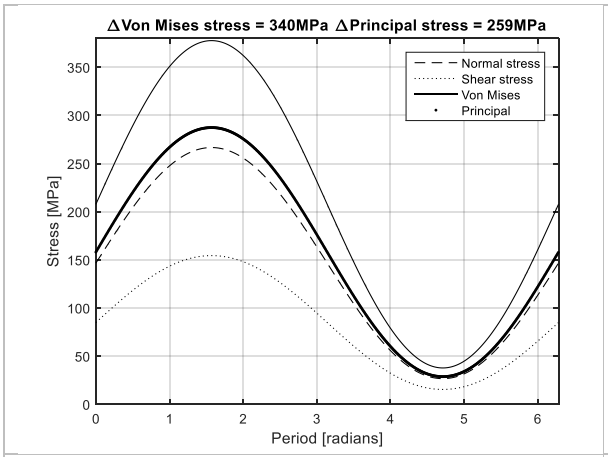
ΔVon Mises stress = 340MPa ΔPrincipal stress = 259MPa
Normal stress
Shear stress
Von Mises
Principal
Stress [MPa]
Period [radians]

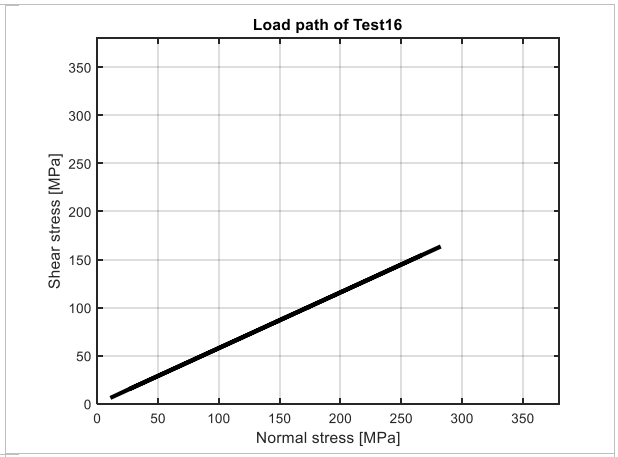
Load path of Test16
Shear stress [MPa]
Normal stress [MPa]

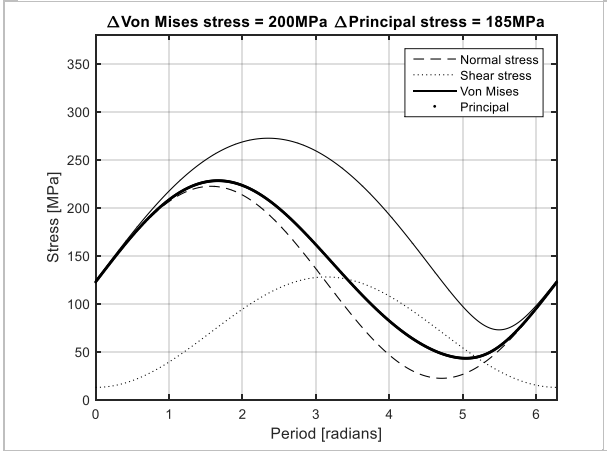
ΔVon Mises stress = 200MPa ΔPrincipal stress = 185MPa
Normal stress
Shear stress
Von Mises
Principal
Stress [MPa]
Period [radians]

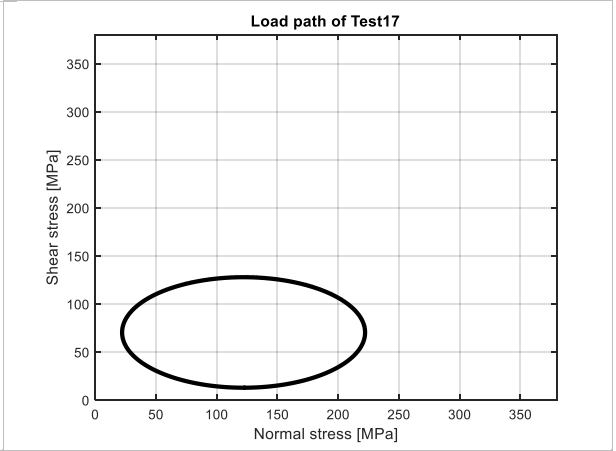
Load path of Test17
Shear stress [MPa]
Normal stress [MPa]

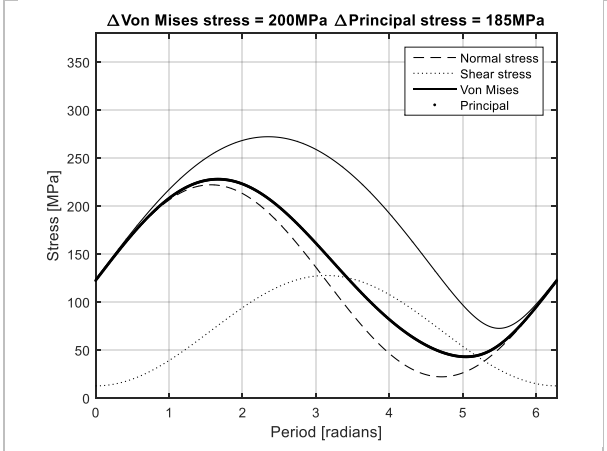
ΔVon Mises stress = 200MPa ΔPrincipal stress = 185MPa
Normal stress
Shear stress
Von Mises
Principal
Stress [MPa]
Period [radians]

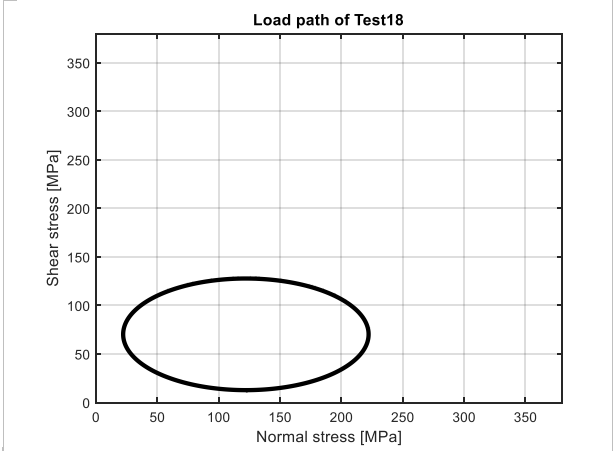
Load path of Test18
Shear stress [MPa]
Normal stress [MPa]

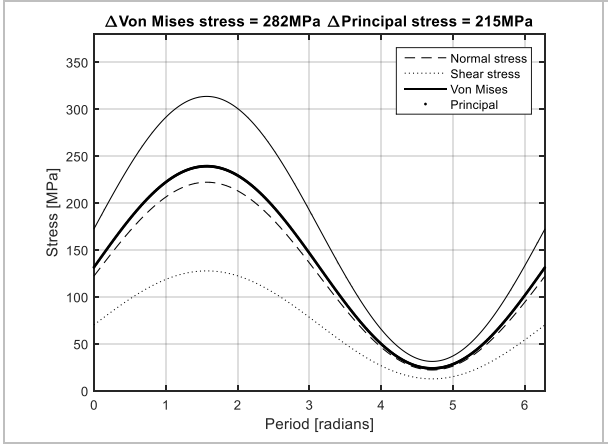
ΔVon Mises stress = 282MPa ΔPrincipal stress = 215MPa
Normal stress
Shear stress
Von Mises
Principal
Stress [MPa]
Period [radians]

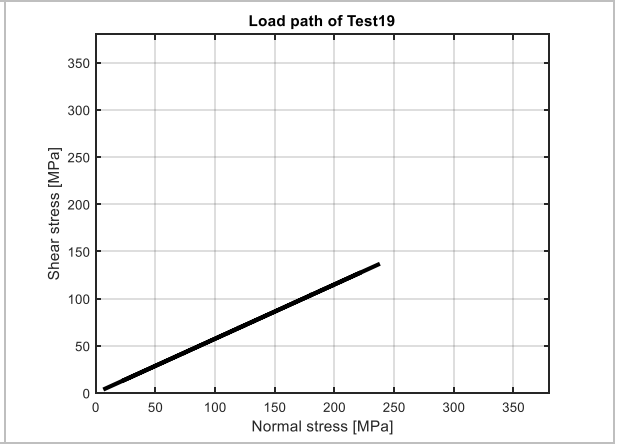
Load path of Test19
Shear stress [MPa]
Normal stress [MPa]

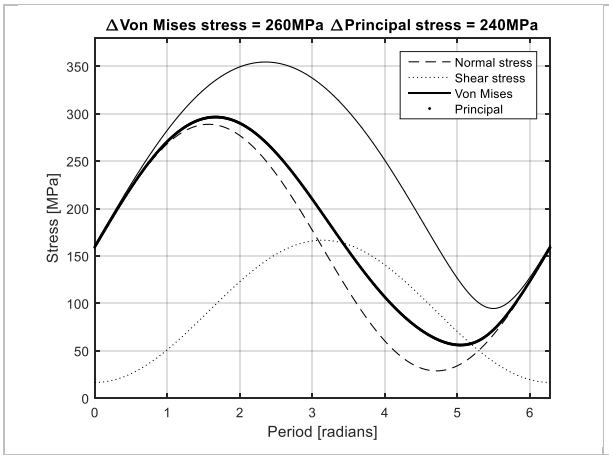
ΔVon Mises stress = 260MPa ΔPrincipal stress = 240MPa
Normal stress
Shear stress
Von Mises
Principal
Stress [MPa]
Period [radians]

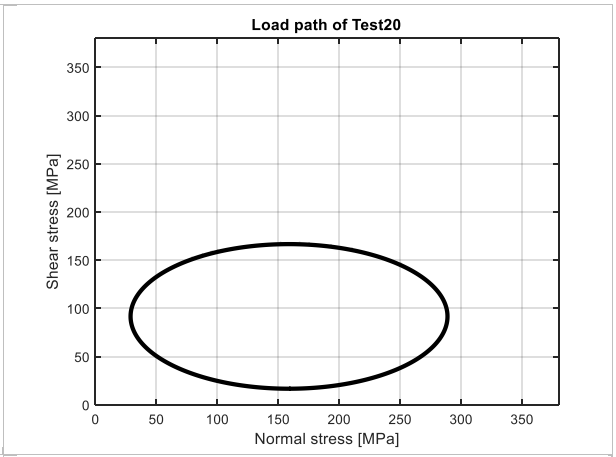
Load path of Test20
Shear stress [MPa]
Normal stress [MPa]

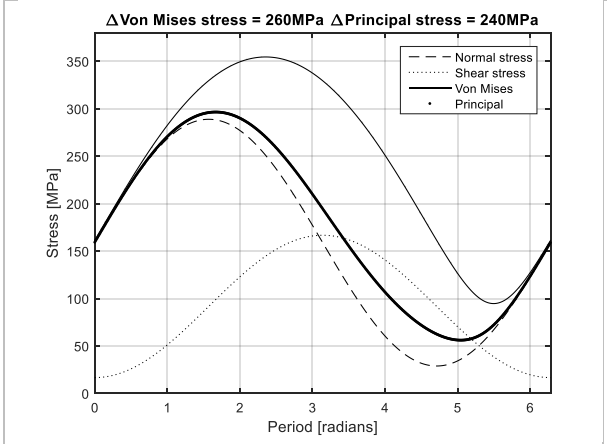
ΔVon Mises stress = 260MPa ΔPrincipal stress = 240MPa
Normal stress
Shear stress
Von Mises
Principal
Stress [MPa]
Period [radians]

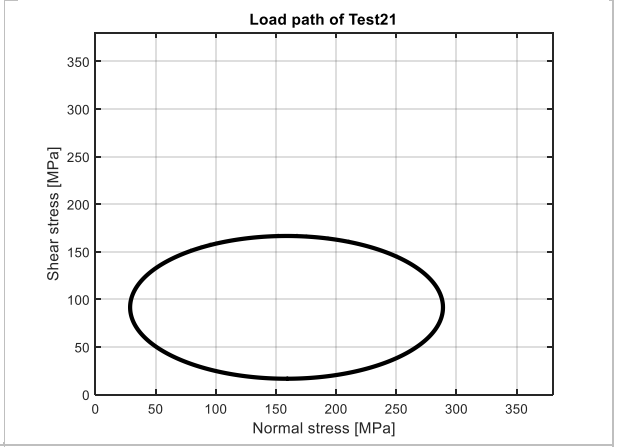
Load path of Test21
Shear stress [MPa]
Normal stress [MPa]

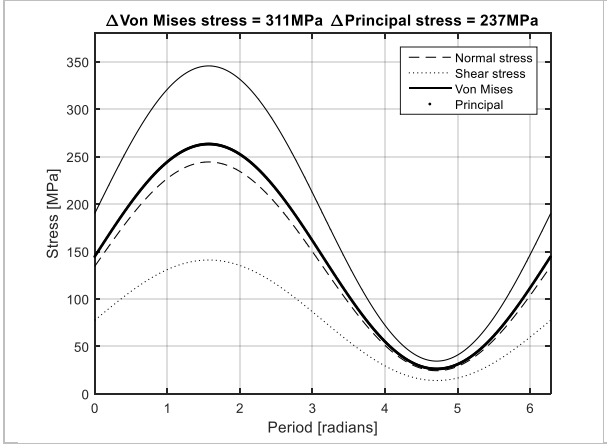
ΔVon Mises stress = 311MPa ΔPrincipal stress = 237MPa
Normal stress
Shear stress
Von Mises
Principal
Stress [MPa]
Period [radians]

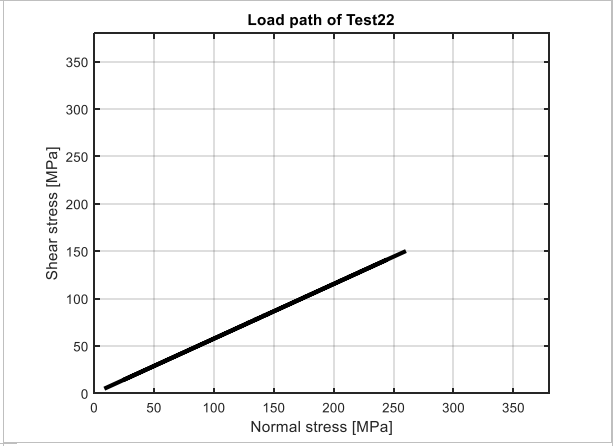
Load path of Test22
Shear stress [MPa]
Normal stress [MPa]

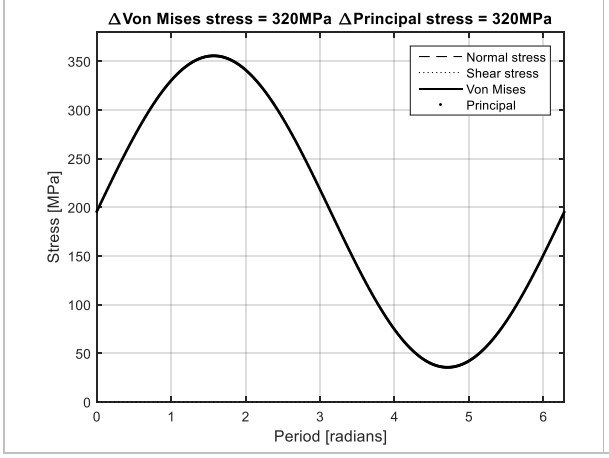
ΔVon Mises stress = 320MPa ΔPrincipal stress = 320MPa
Normal stress
Shear stress
Von Mises
Principal
Stress [MPa]
Period [radians]

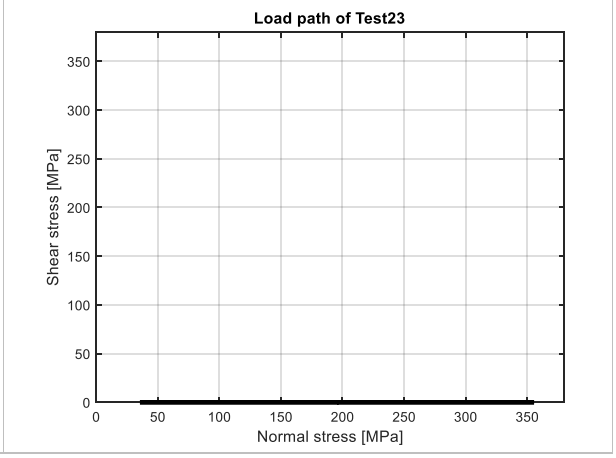
Load path of Test23
Shear stress [MPa]
Normal stress [MPa]

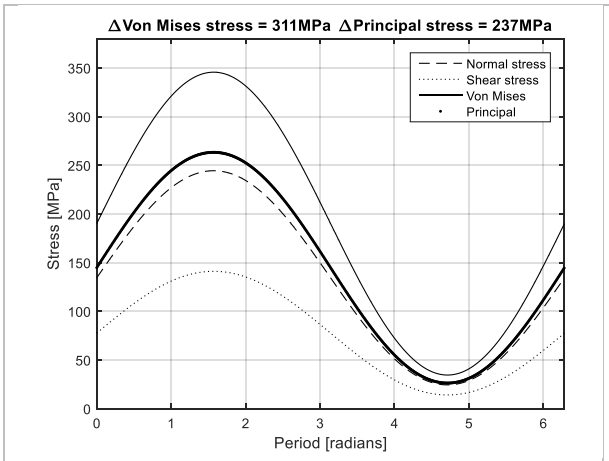
ΔVon Mises stress = 311MPa ΔPrincipal stress = 237MPa
Normal stress
Shear stress
Von Mises
Principal
Stress [MPa]
Period [radians]

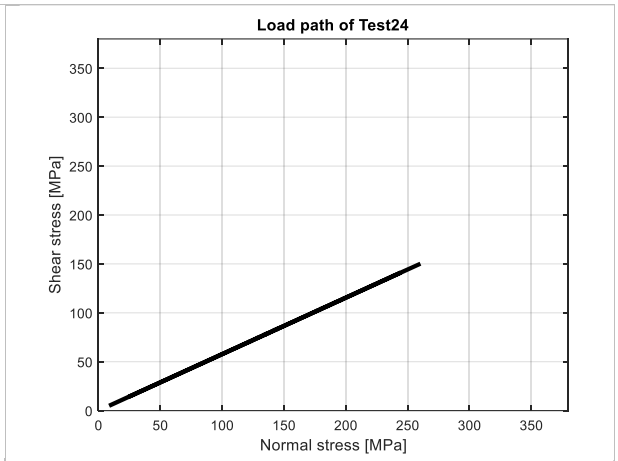
Load path of Test24
Shear stress [MPa]
Normal stress [MPa]

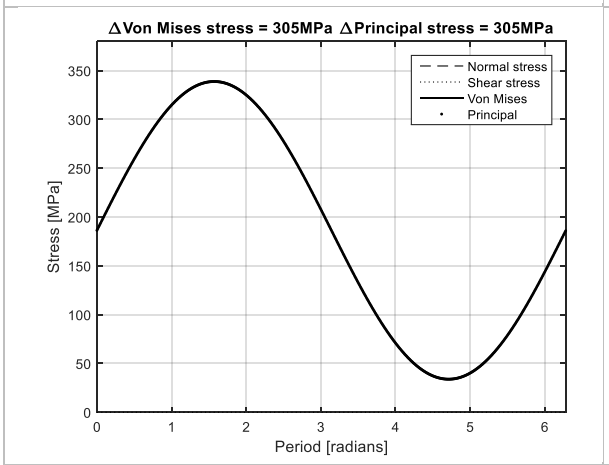
ΔVon Mises stress = 305MPa ΔPrincipal stress = 305MPa
Normal stress
Shear stress
Von Mises
Principal
Stress [MPa]
Period [radians]

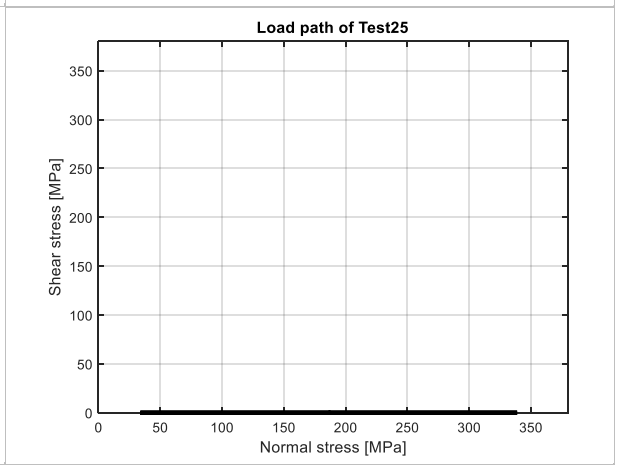
Load path of Test25
Shear stress [MPa]
Normal stress [MPa]

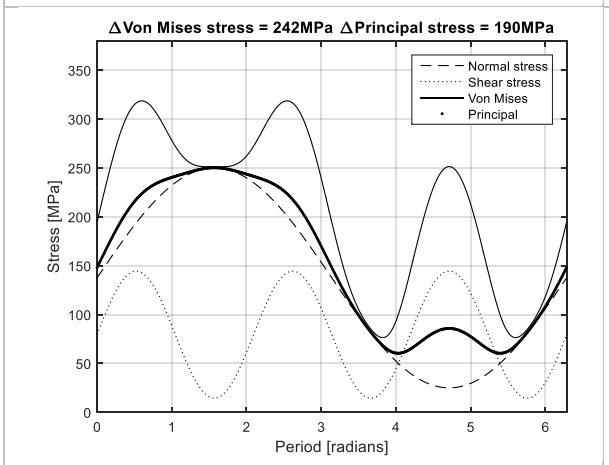
ΔVon Mises stress = 242MPa ΔPrincipal stress = 190MPa
Normal stress
Shear stress
Von Mises
Principal
Stress [MPa]
Period [radians]

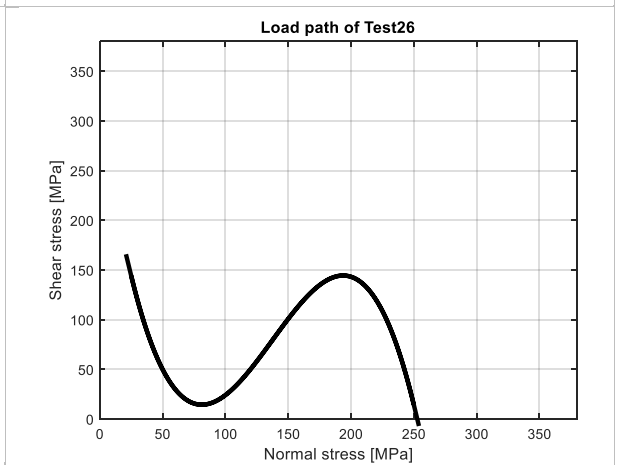
Load path of Test26
Shear stress [MPa]
Normal stress [MPa]

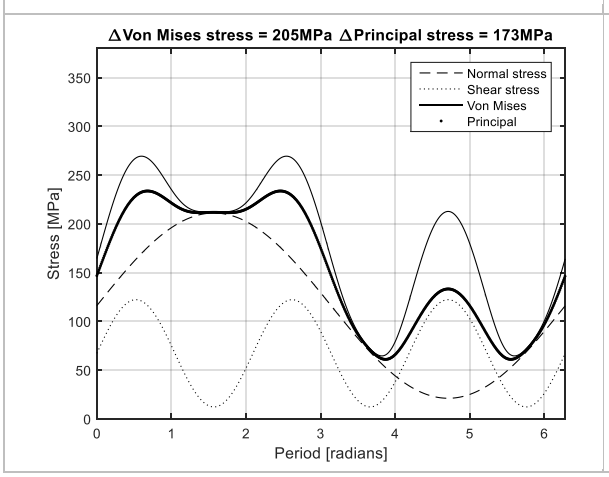
ΔVon Mises stress = 205MPa ΔPrincipal stress = 173MPa
Normal stress
Shear stress
Von Mises
Principal
Stress [MPa]
Period [radians]

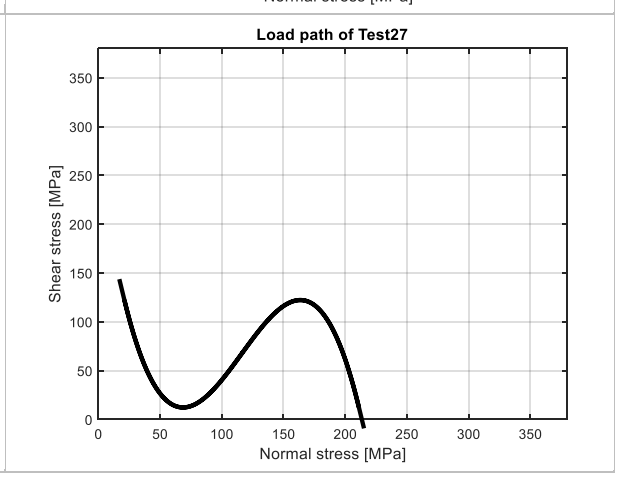
Load path of Test27
Shear stress [MPa]
Normal stress [MPa]

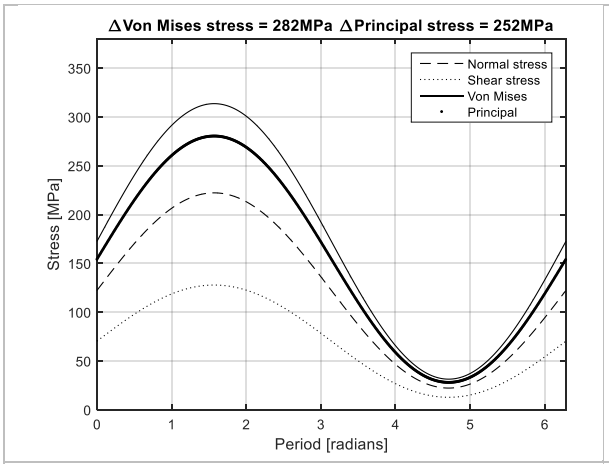
ΔVon Mises stress = 282MPa ΔPrincipal stress = 252MPa
Normal stress
Shear stress
Von Mises
Principal
Stress [MPa]
Period [radians]

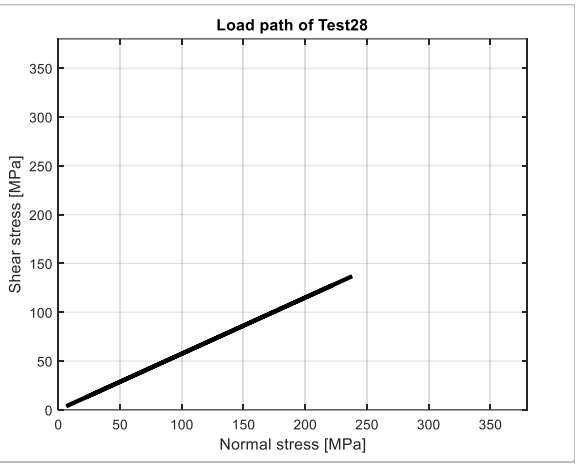
Load path of Test28
Shear stress [MPa]
Normal stress [MPa]

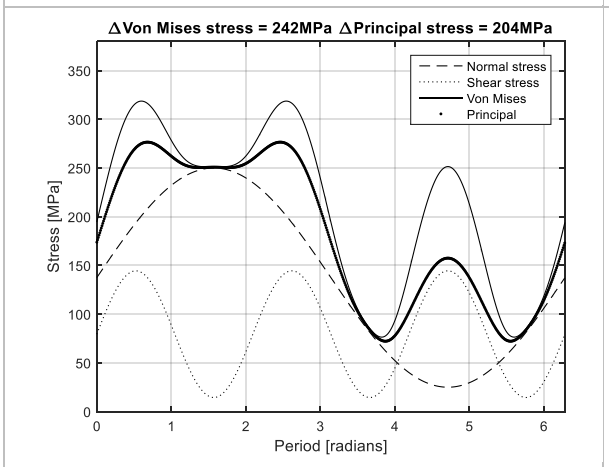
ΔVon Mises stress = 242MPa ΔPrincipal stress = 204MPa
Normal stress
Shear stress
Von Mises
Principal
Stress [MPa]
Period [radians]

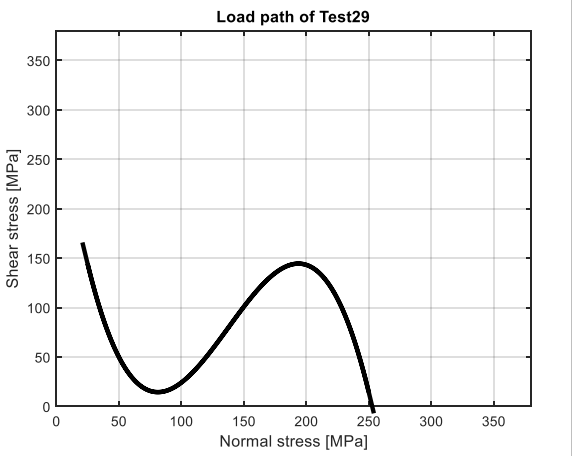
Load path of Test29
Shear stress [MPa]
Normal stress [MPa]

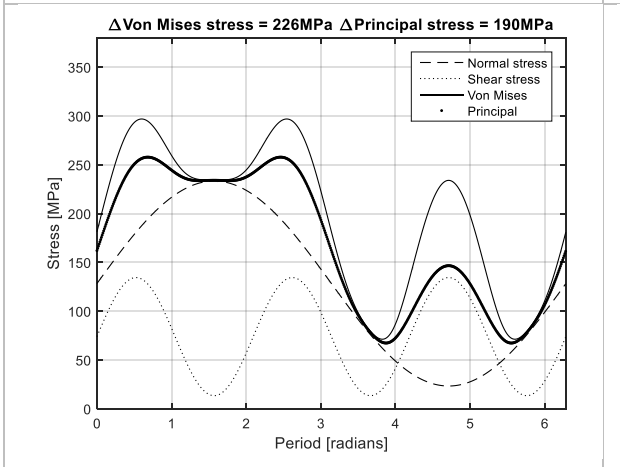
ΔVon Mises stress = 226MPa ΔPrincipal stress = 190MPa
Normal stress
Shear stress
Von Mises
Principal
Stress [MPa]
Period [radians]

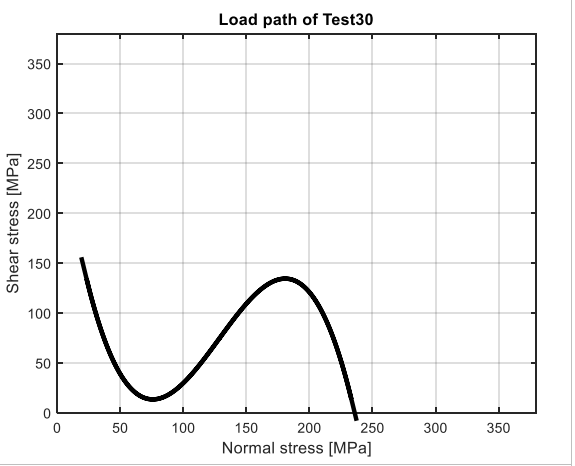
Load path of Test30
Shear stress [MPa]
Normal stress [MPa]

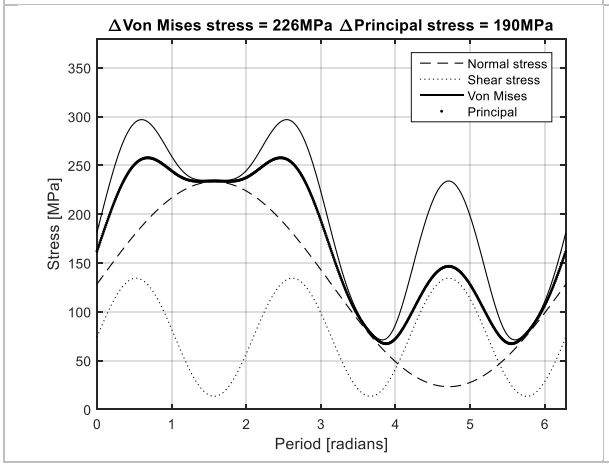
ΔVon Mises stress = 226MPa ΔPrincipal stress = 190MPa
Normal stress
Shear stress
Von Mises
Principal
Stress [MPa]
Period [radians]

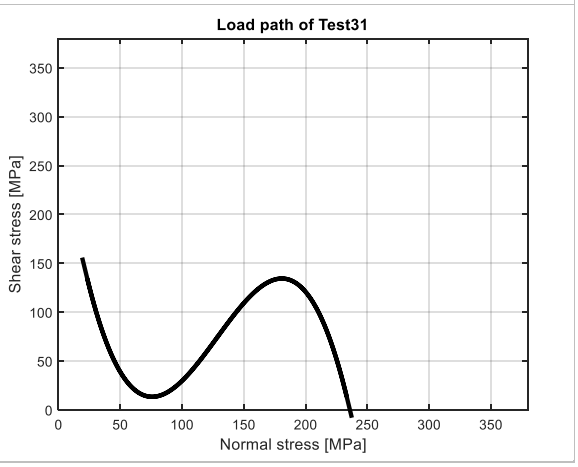
Load path of Test31
Shear stress [MPa]
Normal stress [MPa]

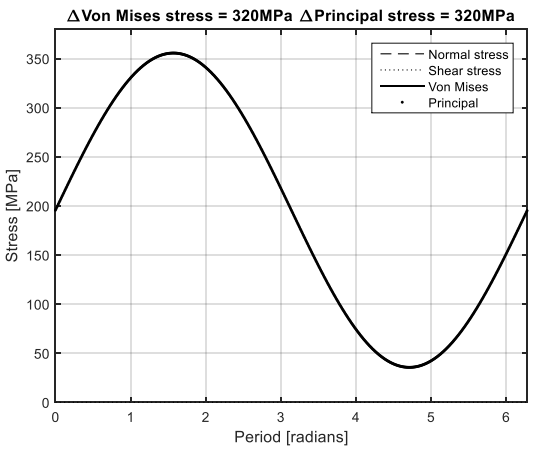
ΔVon Mises stress = 320MPa ΔPrincipal stress = 320MPa
Normal stress
Shear stress
Von Mises
Principal
Stress [MPa]
Period [radians]

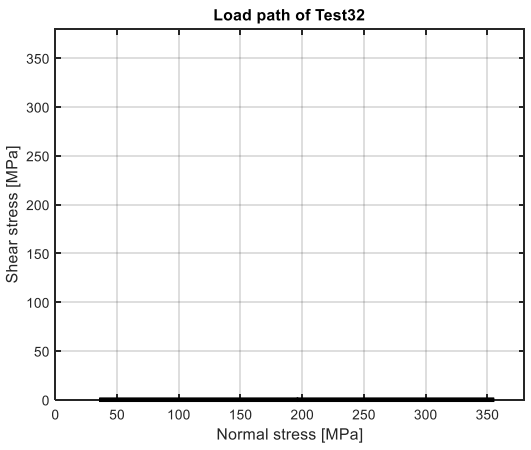
Load path of Test32
Shear stress [MPa]
Normal stress [MPa]

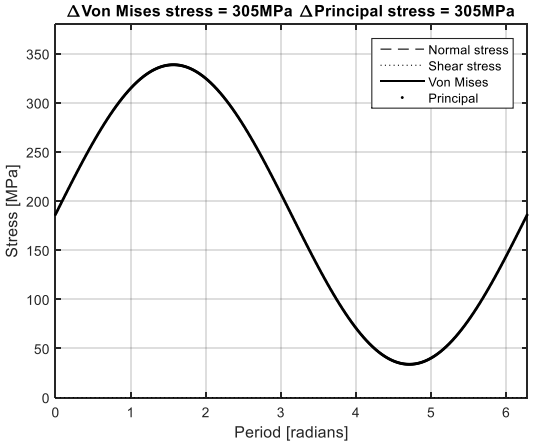
ΔVon Mises stress = 305MPa ΔPrincipal stress = 305MPa
Normal stress
Shear stress
Von Mises
Principal
Stress [MPa]
Period [radians]

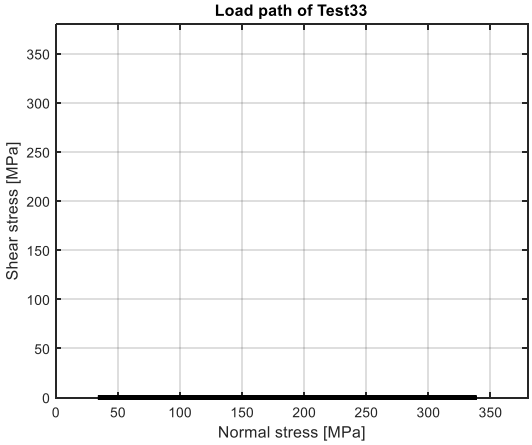
Load path of Test33
Shear stress [MPa]
Normal stress [MPa]

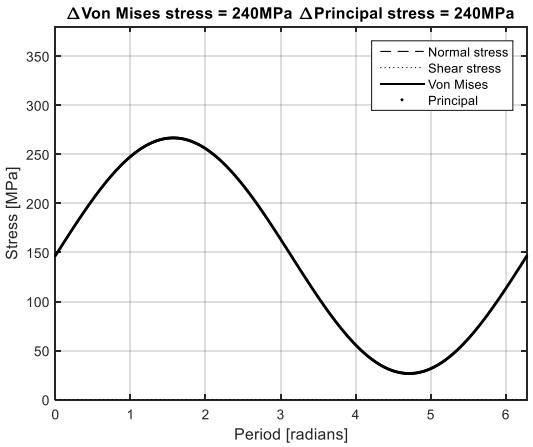
ΔVon Mises stress = 240MPa ΔPrincipal stress = 240MPa
Normal stress
Shear stress
Von Mises
Principal
Stress [MPa]
Period [radians]

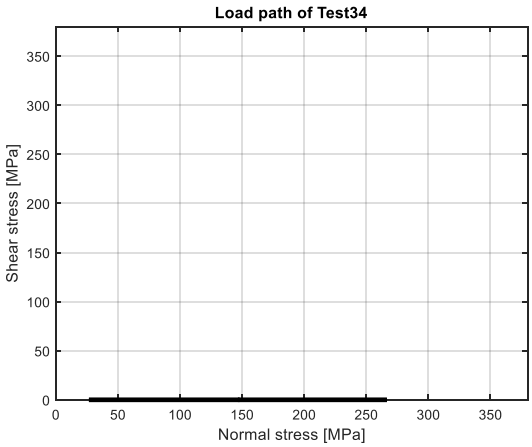
Load path of Test34
Shear stress [MPa]
Normal stress [MPa]

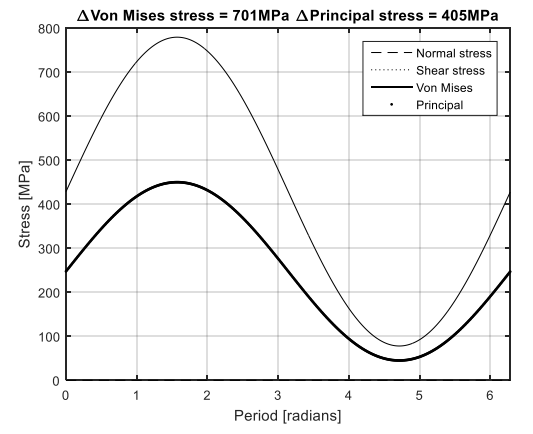
ΔVon Mises stress = 701MPa ΔPrincipal stress = 405MPa
Normal stress
Shear stress
Von Mises
Principal
Stress [MPa]
Period [radians]

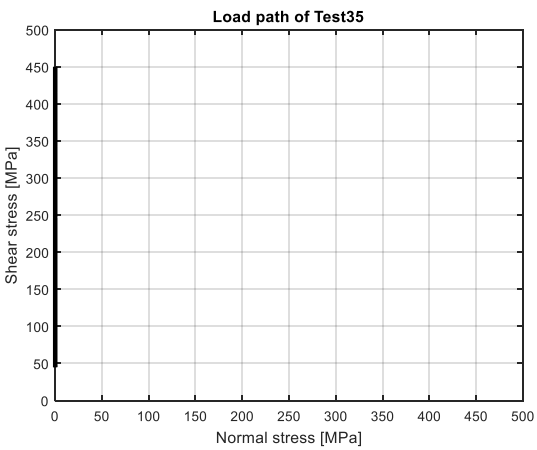
Load path of Test35
Shear stress [MPa]
Normal stress [MPa]

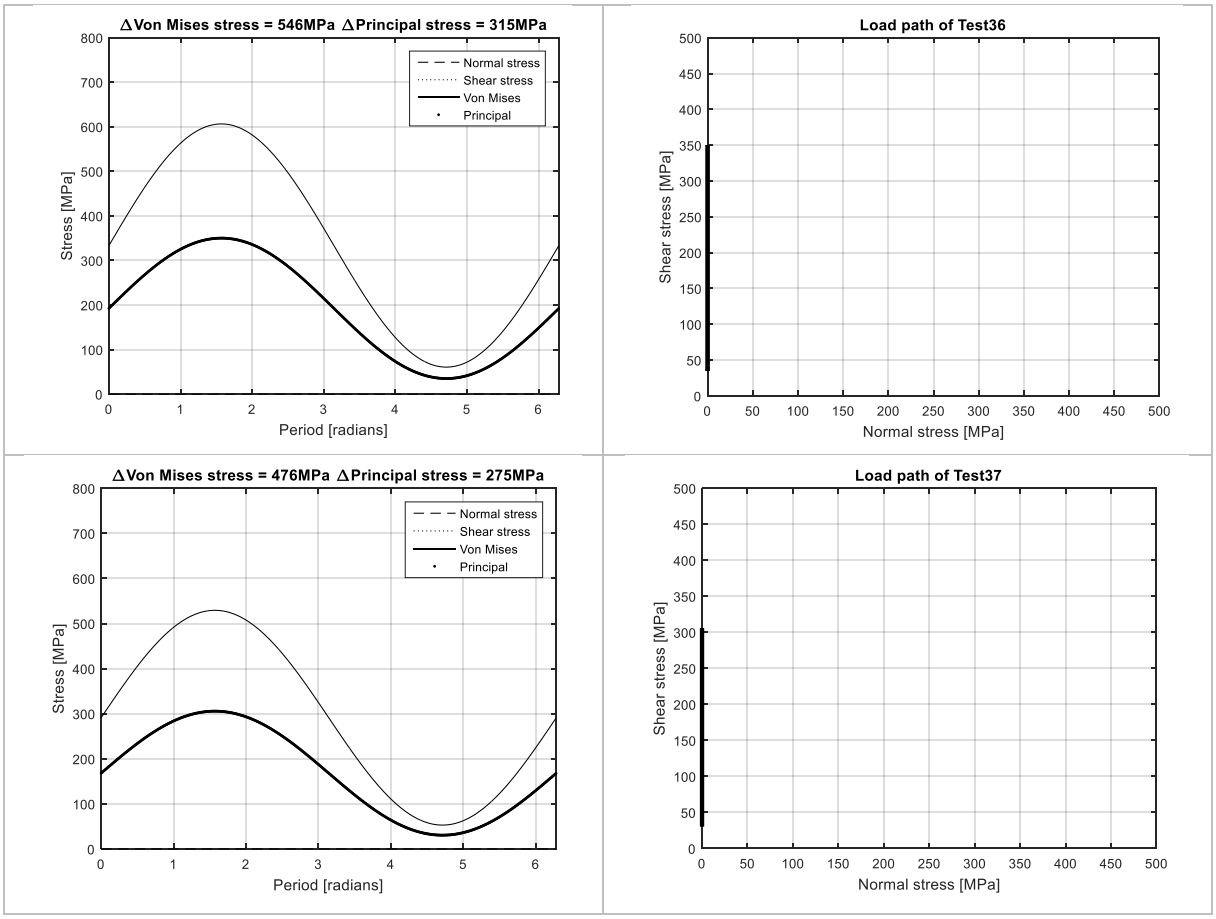
ΔVon Mises stress = 546MPa ΔPrincipal stress = 315MPa
Normal stress
Shear stress
Von Mises
Principal
Stress [MPa]
Period [radians]
Load path of Test36
Shear stress [MPa]
Normal stress [MPa]
ΔVon Mises stress = 476MPa ΔPrincipal stress = 275MPa
Normal stress
Shear stress
Von Mises
Principal
Stress [MPa]
Period [radians]
Load path of Test37
Shear stress [MPa]
Normal stress [MPa]

Source	Material	Loading	Details	Specimen
Yung J.Y. & Lawrence, 1989	ASTM A519	Bending Torsion Combined bending & torsion	$LR = -1$ $\frac{\sigma}{\tau} = \frac{1}{\sqrt{3}}$ As-welded	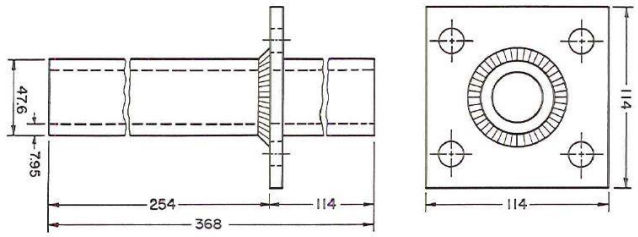
Sonsino & Kueppers, 2001	St E460	Bending Torsion Combined bending & torsion	$LR = -1$ $\sigma/\tau = 1/\sqrt{3}$ As-welded	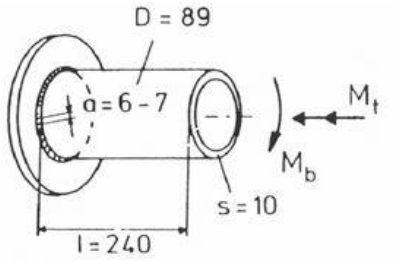
Yousefi, Witt, & Zenner, 2001	ST E460	Bending Torsion Combined bending & torsion	$LR = -1$ $\sigma/\tau = 1/\sqrt{3}$ Stress relief annealed 150 min 540 deg	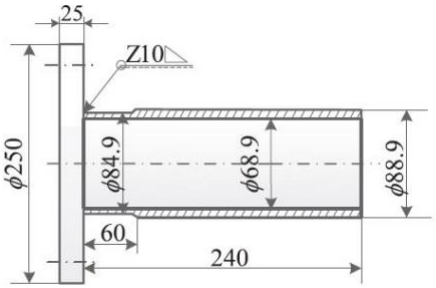

Table 5.8: Overview of the selected experimental reference data from literature

5.7 Test results and failure analysis

For each load case in the test matrix (see Table 5.5) the fatigue lifetime results are shown here. Fatigue failures have been defined as through-thickness failures. A linear least square regression was used to describe the SN curves of the addressed load cases and to extract the fatigue resistance parameters (i.e. inverse slope m and $log(C)$). Because runouts are arbitrarily defined beyond 10 million cycles or more, they can significantly influence the outcome of a linear regression analysis. This can be seen also from the following results where linear regression analysis is applied to data including and excluding runouts. Data analysis in the following sections of this Chapter considers the SN parameters excluding runouts.

5.7.1 Uniaxial loading - Mode I

Uniaxial fatigue tests were performed in pure Mode I loading. Initially, cyclic vertical tension was applied so that the stress distribution remains constant over the cross sectional area. However, this caused the weld start-stop location to become the weakest and fatigue critical location along the circumference. Instead of cyclic tensile loading, cyclic bending was chosen for continuation of the test matrix.

Two sets of fatigue resistance parameters have been determined with the obtained test results in pure Mode I. When all results in pure Mode I are included (i.e. bending and tension), the SN curve is described by $m = 7.7$ and $log(C) = 24.2$. Without consideration of the weld start-stop failures (i.e. the tension tests), these fatigue resistance parameters increase to $m = 10.0$ and $log(C) = 30.0$. See Figure 5.16 versus Figure 5.17.

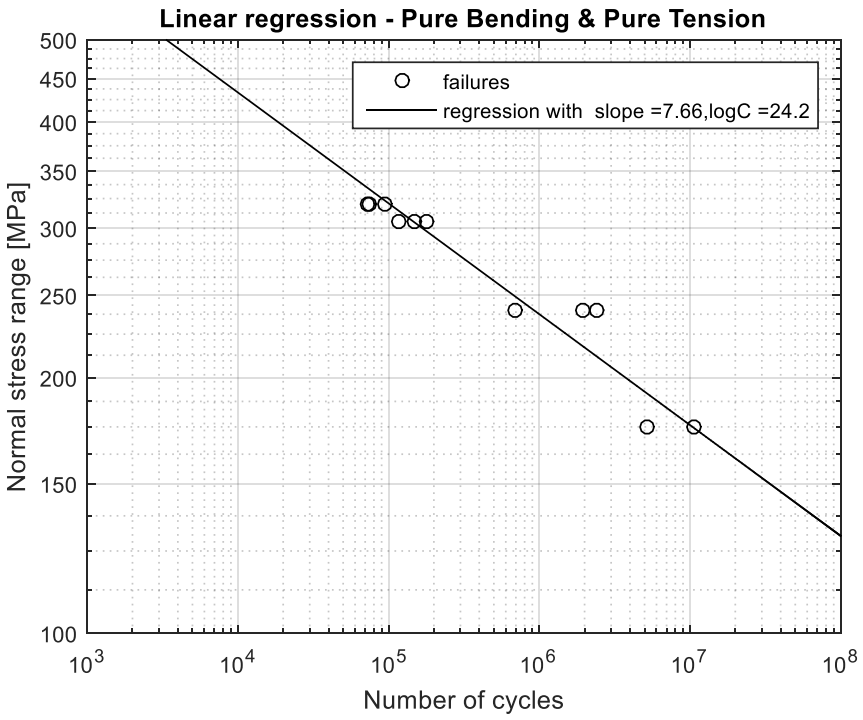

Figure 5.16: Nominal stress based SN-curve based on the linear regression analysis of all test results in pure Mode I

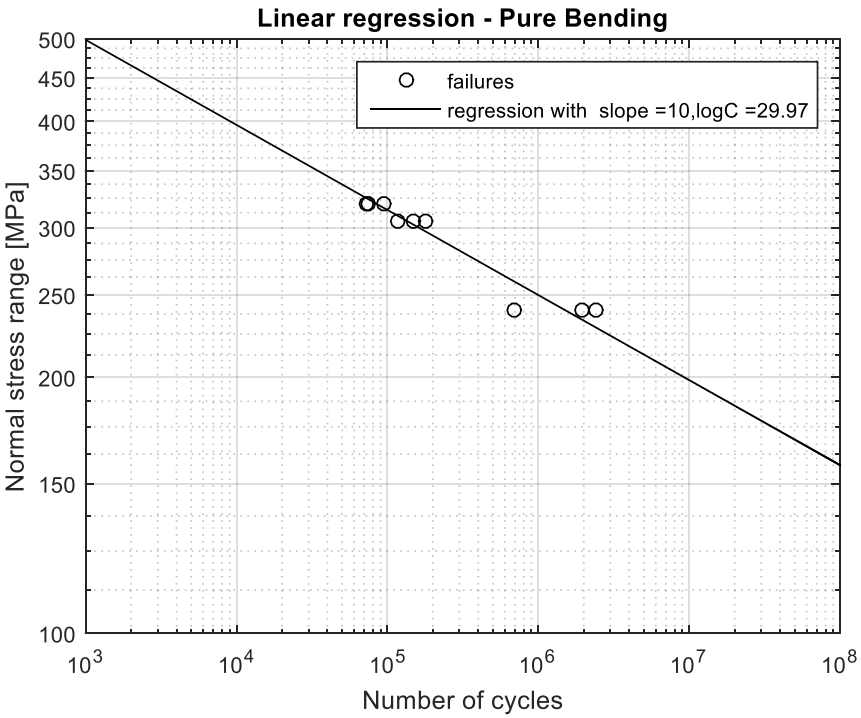

Figure 5.17: Nominal stress based SN-curve based on the linear regression analysis of all results in pure bending

The requirement for the welding quality of the tubular specimen was set to offshore quality standards. An insight can be provided into how this welding quality relates to other welded joints by comparison of the uniaxial fatigue resistance of the welded tubulars to the standardized SN curves in guidelines and recommended practices. In Chapter 4 it has also been discussed how the presence of a welding induced defect can affect fatigue resistance. The Mode I results of the bar specimens with artificial defect (cf. Section 4.4) provide a steeper slope (ranging between $m = 3.4$ and $m = 4$) than the uniaxial fatigue resistance of the tubular specimens in pure Mode I ($m = 7.6$). This demonstrates that the welded tubulars contain smaller defects than what is typically found in welded joints ($< 100\ x\ 400\ \mu m$) and thus confirms the high welding quality. In Figure 5.18 the hexapod results in pure Mode I are compared to the bar specimen results and the base material data in pure Mode I from literature (cf. Section 4.4 and Section 5.5.2). From this figure it can be confirmed that the tubular joints are of high welding quality, i.e. below the base material but above the bar specimen data.

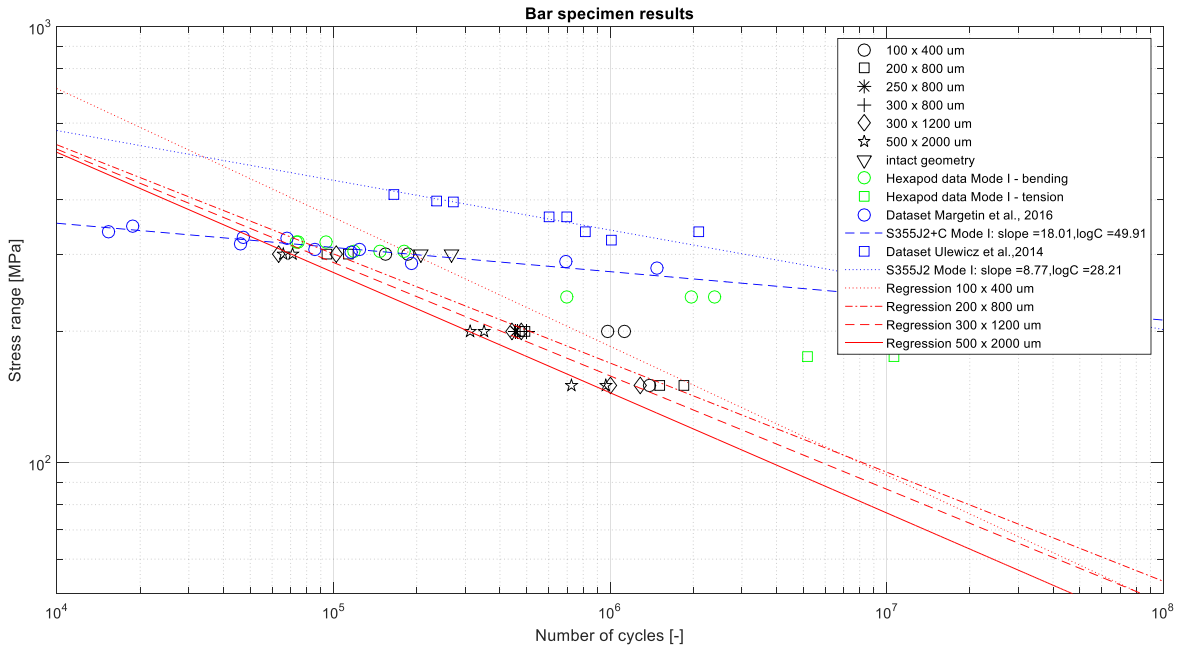

Figure 5.18: : Uniaxial tensile fatigue test results of bar specimens with varying size of elliptically shaped artificial defect, compared to the fatigue lifetime of intact bar specimens from literature and the hexapod results in pure Mode I; Nominal stress based excluding runouts

5.7.2 Uniaxial loading – Mode III

Only a limited number of tests were performed in pure Mode III loading. Within the experimental scope of this dissertation, it was not feasible to perform all fatigue tests in pure Mode III loading (i.e. pure torsion). This had nothing to do with the capabilities of the hexapod but was attributed to problems with sliding of the specimen and operational limitations with testing at a load ratio of 0.1. Eventually, alternative friction disks were used to avoid sliding of the specimen under the applied torsional loads. Furthermore, the tests were performed with a load ratio of -1. The testing frequency that could be achieved under the applied testing conditions was limited and did therefore not allow for the completion of all envisaged torsion tests.

Four torsion tests were perfomed of which three failures and one runout. It should be noted that the runout was obtained under a load ratio of $LR = 0.1$, whilst the three failures were obtained at a load ratio of $LR = -1$. The fatigue resistance parameters that correspond to all data are $m = 6.3$ and $log(C) = 20.8$. See Figure 5.19. When the runout is excluded the SN parameters are $m = 14.6$ and $log(C) = 41.6$. See Figure 5.20.

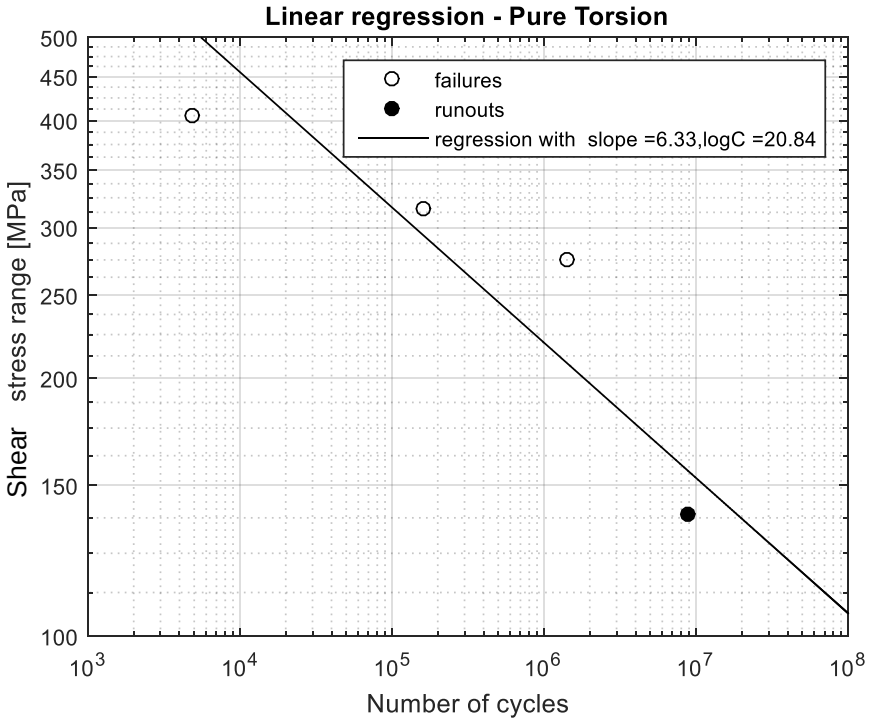

Figure 5.19: Nominal stress based SN-curve based on the linear regression analysis of all test results in pure Mode III

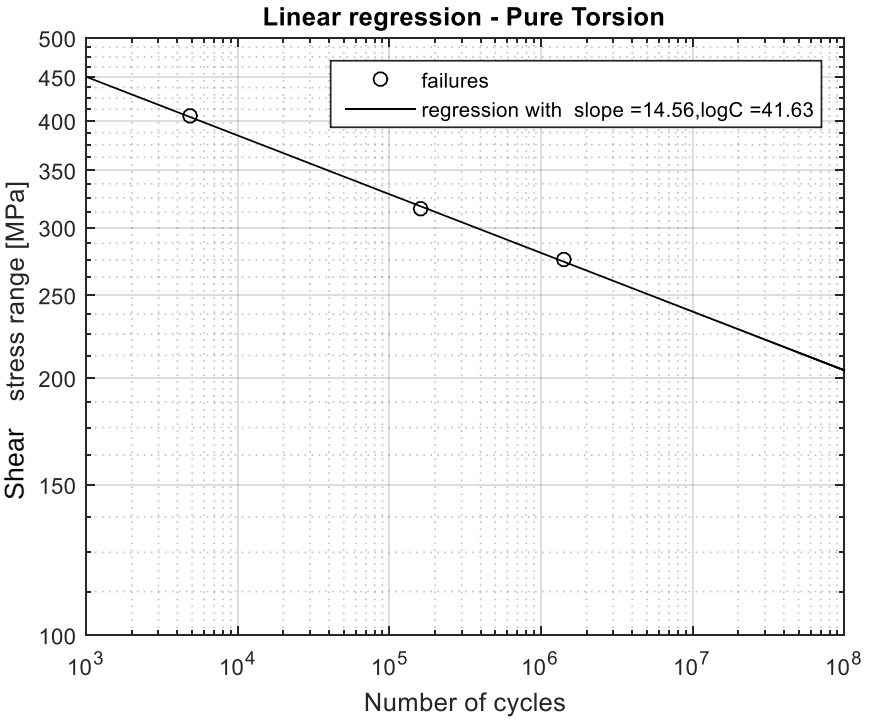

Figure 5.20: Nominal stress based SN-curve based on the linear regression analysis of the test results in pure Mode III excluding runouts

5.7.3 Multiaxial loading – Proportional (IP)

To generate multiaxial loading, cyclic bending was combined with cyclic torsion. The peaks of both sinusoidal load signals occurred in phase, causing proportional multiaxial loading. The fatigue resistance parameters that were experimentally established under this loading condition are $m = 14.1$ and $log(C) = 38.9$ when the runout is included in the linear regression analysis. See Figure 5.21. When the runout is excluded the fatigue resistance parameters are $m = 17.1$ and $log(C) = 46.0$. See Figure 5.22. In comparison to the uniaxial load case (cf. Section 5.7.1), the SN parameters have increased significantly. This demonstrates that proportional multiaxial loading changes the damage mechanism (represented by inverse slope m) and has a detrimental effect on fatigue resistance (represented by $log\ (C)$).

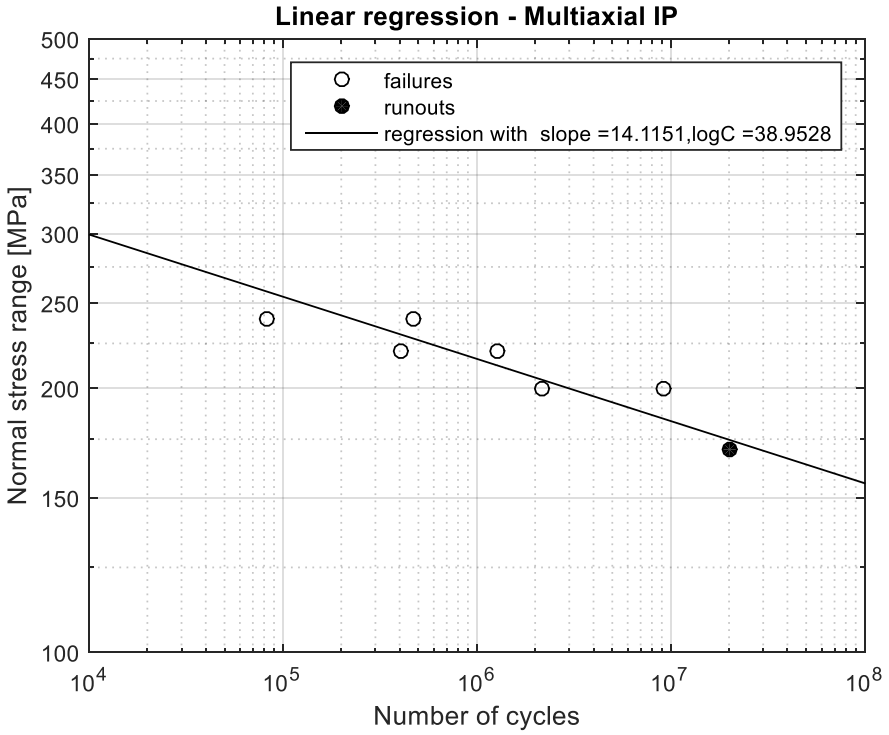

Figure 5.21: Nominal stress based SN-curve based on the linear regression analysis of the results in proportional multiaxial loading (i.e. combined bending and torsion) incl. runouts

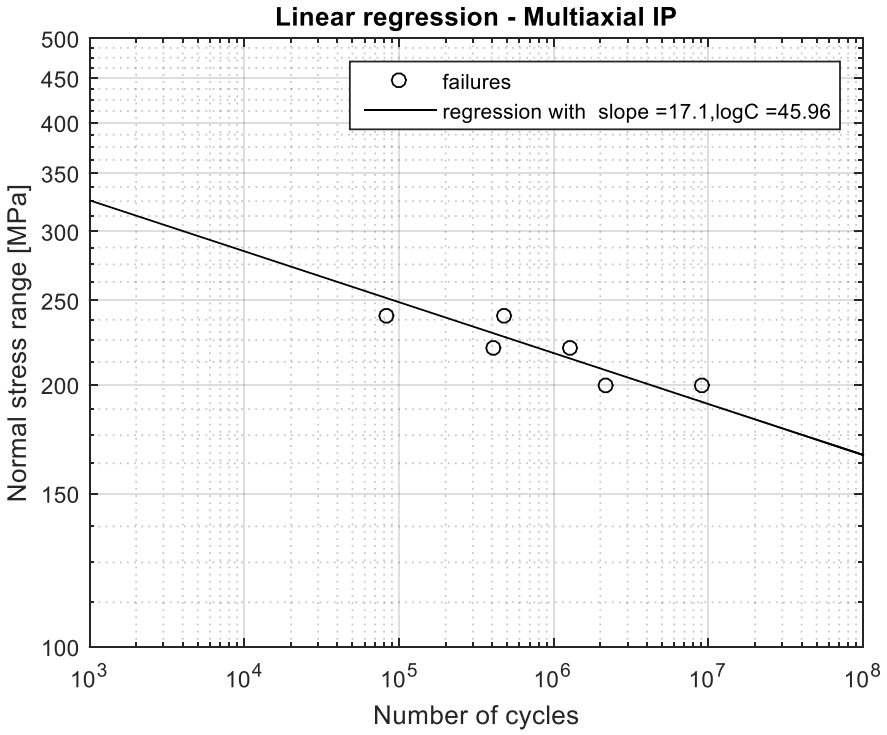

Figure 5.22: Nominal stress based SN-curve based on the linear regression analysis of the results in proportional multiaxial loading (i.e. combined bending and torsion) excl. runouts

5.7.4 Multiaxial loading - Non-proportional (OP)

Non-proportionality can be introduced by two effects: a phase shift between the two sinusoidal load signals, or a frequency difference between the two signals. Both forms of non-proportional multiaxial fatigue have been experimentally investigated in the hexapod. See Figure 5.23 - Figure 5.26.

5.7.4.1 Phase shift induced non-proportionality

Under 90 degrees phase shift induced non-proportional loading, the following SN parameters were found with: $m = 14.4$ and $log(C) = 39.5$ with inclusion of the runout, $m = 15.6$ and $log(C) = 42.4$ with exclusion of the runout. These SN parameters are very close to the values found for proportional multiaxial loading (cf. Section 5.7.2). This demonstrates that proportional and phase shift introduced non-proportional loading introduce the same damage mechanism and fatigue resistance. This is also sensible, considering that proportional loading is a form of phase shift induced non-proportional loading; proportional loading equals 0 degrees phase shift induced non-proportional loading. This is true when normal stress is considered. In following sections also different parameters will be considered.

5.7.4.2 Frequency difference induced non-proportionality

Frequency induced non-proportionality was introduced with a frequency ratio of $1:3$ (i.e. shear stress fluctuated three times faster as the normal stress component). The SN parameters that were experimentally obtained are $m = 16.4$ and $log(C) = 43.7$ with inclusion of runouts and $m = 9.1$ and $log(C) = 26.4$ with exclusion of runouts. These values demonstrate that frequency induced non-

proportionality affects fatigue resistance differently and causes a different damage mechanism than phase shift induced non-proportionality.

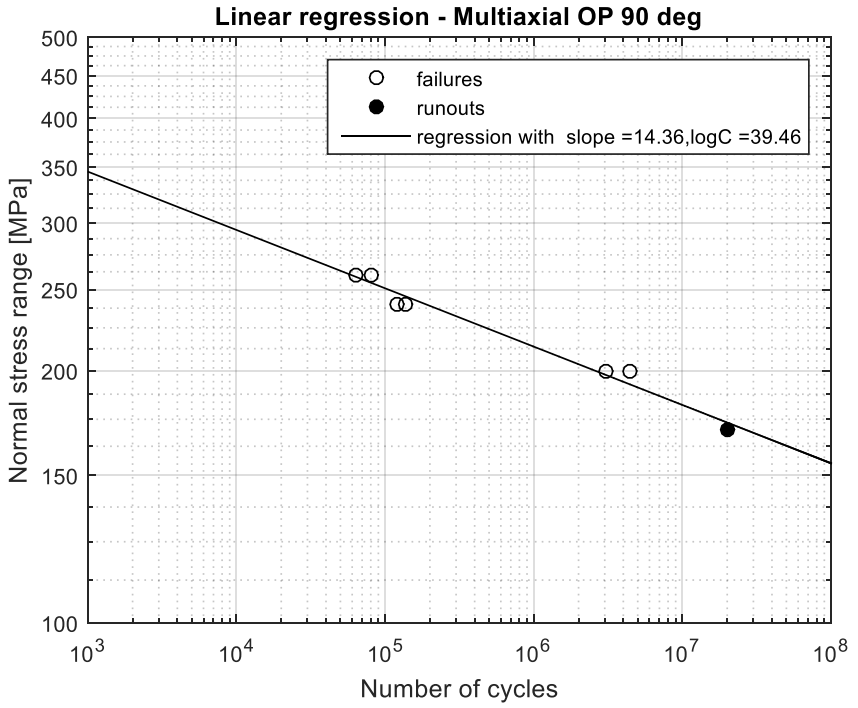

Figure 5.23: Nominal stress based SN-curve based on the linear regression analysis of the results in phase shift induced non-proportional multiaxial loading (i.e. combined bending and torsion) incl. runouts

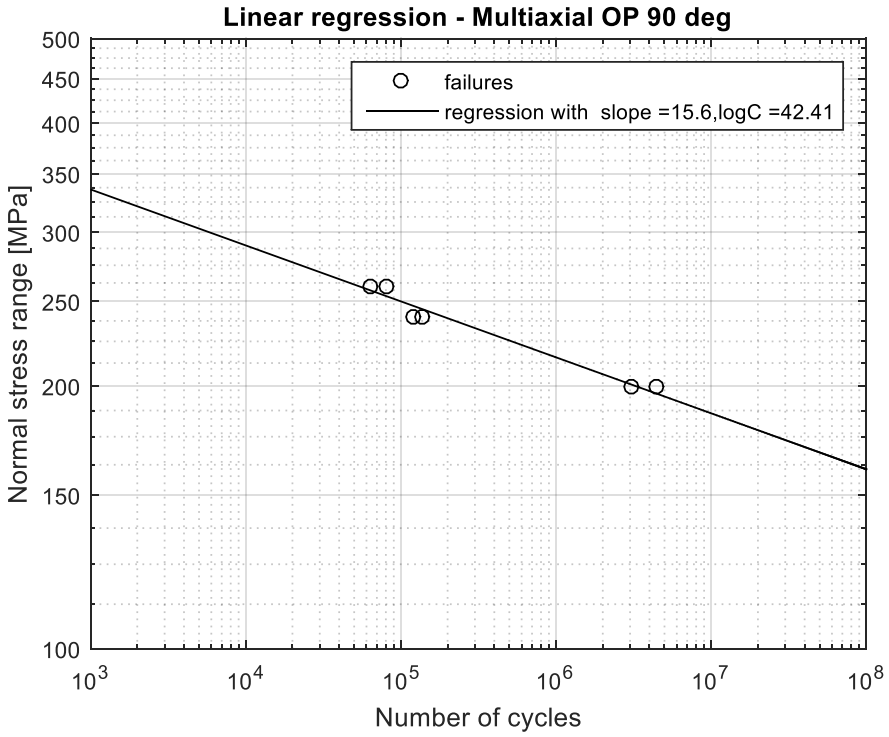

Figure 5.24: Nominal stress based SN-curve based on the linear regression analysis of the results in phase shift induced non-proportional multiaxial loading (i.e. combined bending and torsion) excl. runouts

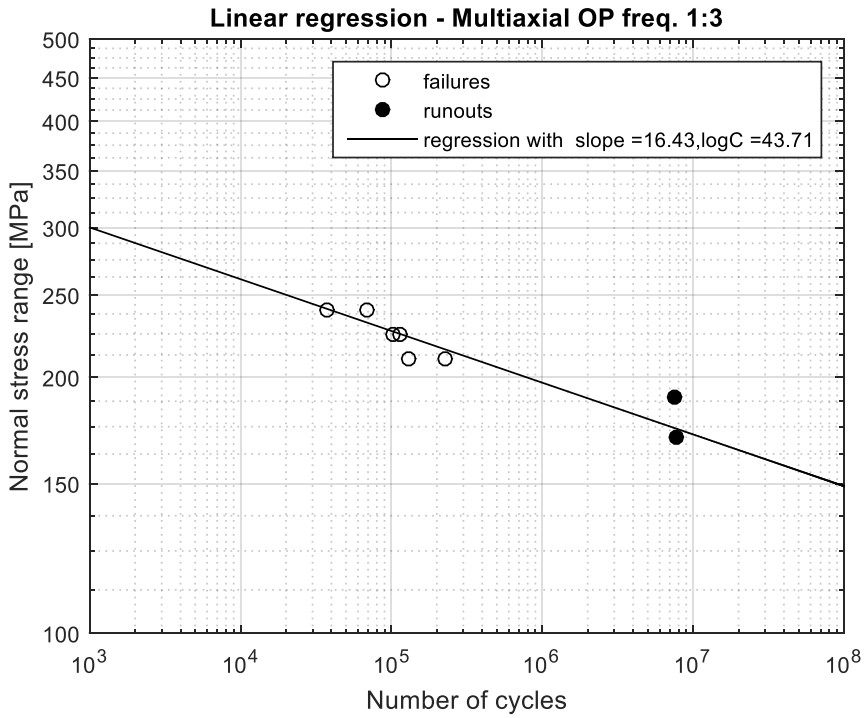

Figure 5.25: Nominal stress based SN-curve based on the linear regression analysis of the results in frequency induced non-proportional multiaxial loading (i.e. combined bending and torsion) incl. runouts

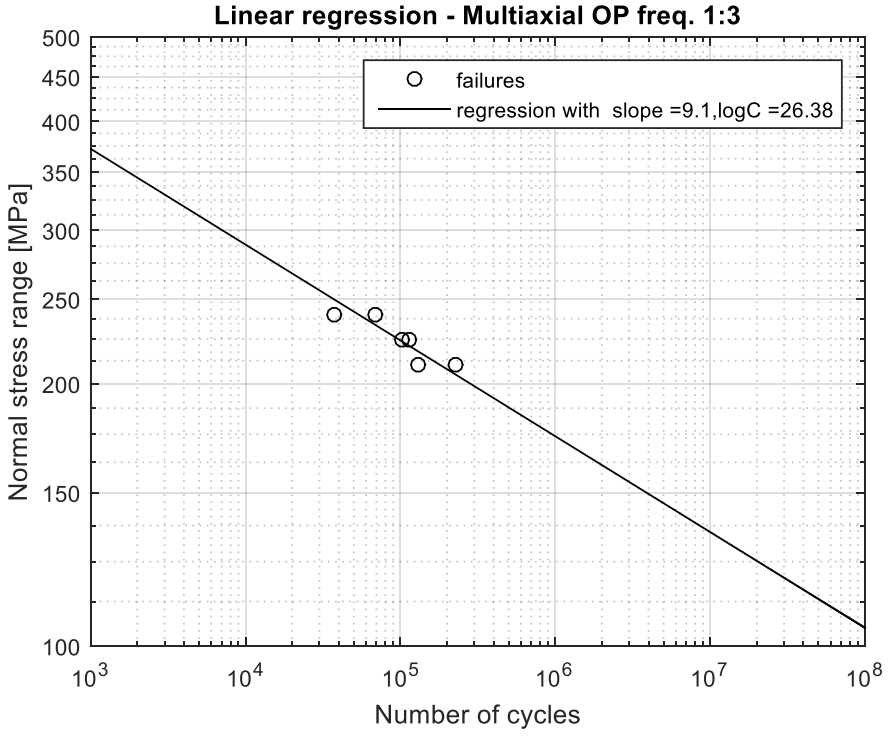

Figure 5.26: Nominal stress based SN-curve based on the linear regression analysis of the results in frequency induced non-proportional multiaxial loading (i.e. combined bending and torsion) excl. runouts

5.7.5 Fatigue resistance analysis

The combined effect of inverse slope m and $log(C)$ determine the overall fatigue resistance. Their values are however dependent on the (equivalent) stress value that is selected for the assessment. In Figure 5.27-5.29 it is shown how the relationship between the tubular test results from different load cases (i.e. uniaxial, multiaxial) changes with the (equivalent) stress that is used for the basis of comparison. Principal stress, Von Mises stress and normal stress have been selected since they are conventionally used in engineering practice. A least squares linear regression is used. As a reference, the mean fatigue resistance curves of the corresponding FAT class (FAT 71) and the tubular base material are included in Figure 5.27-5.29. To correct the recommended FAT design values to mean values a standard deviation of 0.25 was used. Base material data was taken from the data sets presented in Section 4.4. (i.e. S355J2+C and S355J2). Disregarding the basis of comparison, the majority of the hexapod results lay inbetween these reference curves; above the FAT 71 and below the resistance curves of base material. This confirms the offshore quality of the weld and indicates that this quality is better than what would be typically assumed in engineering practice (cf. Section 5.2). At the same time, it shows that the process of welding causes a reduction of the fatigue resistance in comparison to base material.

On the basis of principal stress the clearest distinction is made between the different multiaxial load cases. Figure 5.27 shows that non-proportional loading aggravates the fatigue resistance considerably, in comparison to proportional loading. Furthermore, it demonstrates that in terms of non-proportional loading, frequency induced non-proportionality leads to more fatigue damage than phase shift induced non-proportionality.

When Von Mises stress is used as basis of analysis for the multiaxial test results, it becomes apparent that Von Mises lacks sensitivity to non-proportionality; even when its stress time trace is taken into consideration. See Figure 5.28. The linear regression curve of the data with frequency induced non-proportional loading is almost identical to the one for phase shift induced non-proportional loading. Another interesting finding is that the in-phase proportional loading appears less detrimental than pure Mode I loading.

The normal stress based analysis demonstrates an incapability to capture the distinction between 0 degrees and 90 degrees (non-)proportional loading. Their linear regression curves almost overlap. For frequency induced non-proportionality, the normal stress basis shows an increase in fatigue damage in comparison to phase shift induced non-proporitonality. This finding is in accordance with the findings based on principal stress (Figure 5.27).

Further investigation of the effect of frequency induced non-proportionality on fatigue resistance is required since it depends on the ratio of the frequencies of the individual load components. See also Section 2.2.4.1. The work in this dissertation takes a fixed frequency ratio of $f_\sigma : f_\tau = 1:3$ into consideration. The selection of this ratio is based on the literature study made in Chapter 2. From this study it was assumed that load frequency effects should be reasonably observed at this ratio. From the obtained results, this assumption appears valid. However, the assumption could be refined and stronger supported by additional test results at a variety of frequency ratios.

Table 5.9: SN-parameters of the linear regression curve for the multiaxial data based on principal stress, Von Mises stress and normal stress

Principal stress based		
Load case	$\boldsymbol{m}$	$\boldsymbol{Log(C)}$
Uniaxial Mode I	7.7	24.2
Multiaxial IP	16.6	46.5
Multiaxial OP 90 deg	15.5	41.8
Multiaxial OP freq. 1:3	8.8	25.4
Von Mises stress based		
Load case	$\boldsymbol{m}$	$\boldsymbol{Log(C)}$
Uniaxial Mode I	7.7	24.2
Multiaxial IP	16.7	47.5
Multiaxial OP 90 deg	15.6	42.4
Multiaxial OP freq. 1:3	8.9	26.3
Normal stress based		
Load case	$\boldsymbol{m}$	$\boldsymbol{Log(C)}$
Uniaxial Mode I	7.7	24.2
Multiaxial IP	17.1	46.0
Multiaxial OP 90 deg	15.6	42.4
Multiaxial OP freq. 1:3	9.1	26.4

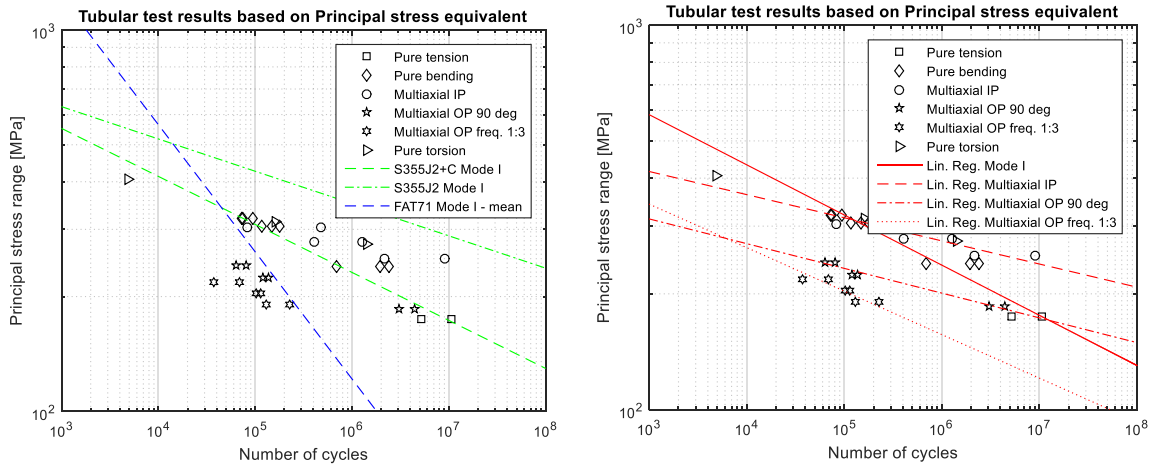

Figure 5.27: Hexapod test results represented based on nominal Principal stress

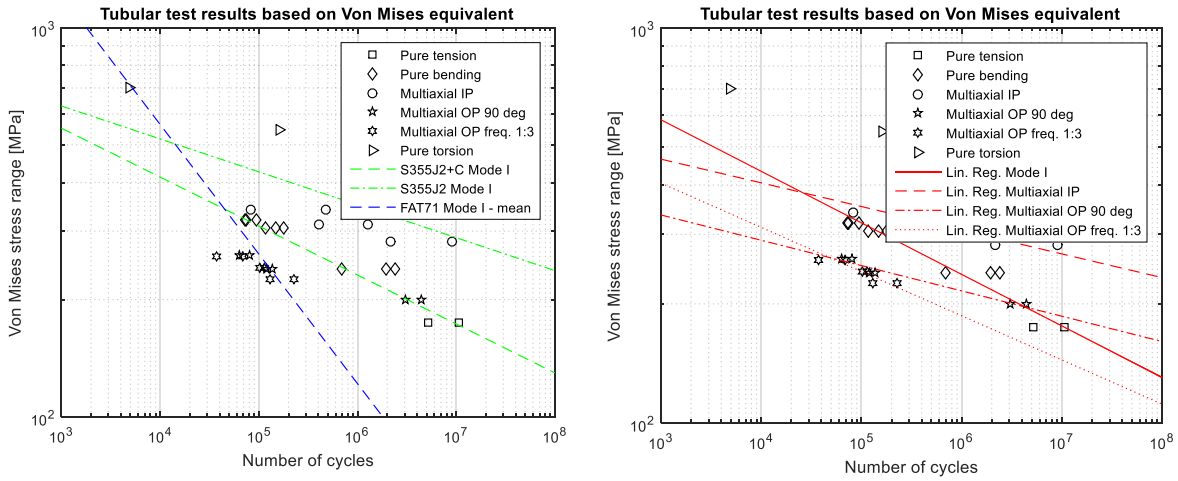

Figure 5.28: Hexapod test results represented based on nominal Von Mises stress

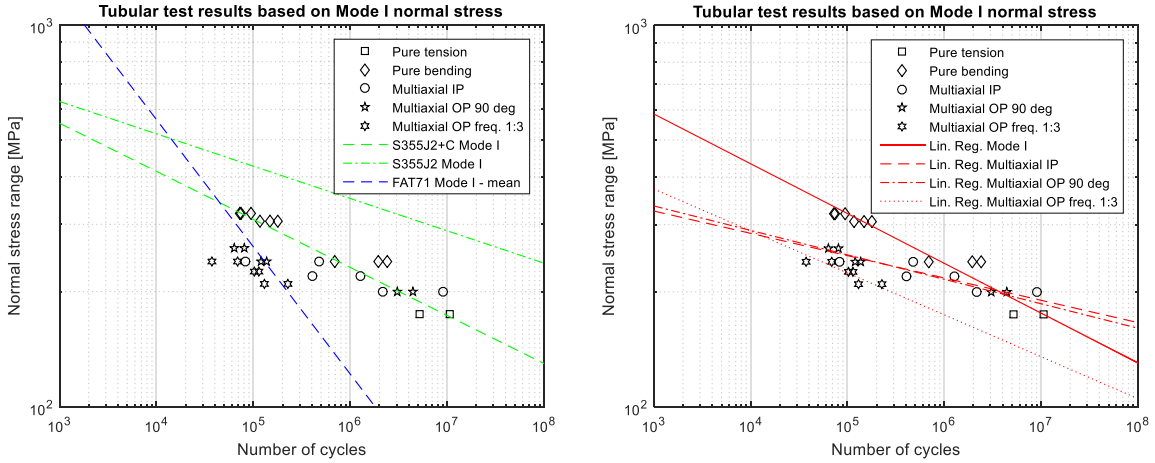

Figure 5.29: Hexapod test results represented based on Mode I nominal normal stress

5.7.6 Fracture surface analysis

A general analysis of the fracture surface was performed by visual inspection. Some insightful observations could be made and will be discussed in this Section. It is recommended to strengthen these observations by further inspection of the existing fracture surfaces once they have all been cut through thickness. Also inspection of additional test results in future research would contribute to an improved understanding of the crack growth behaviour under multiaxial loading.

5.7.6.1 Observations

Pure Mode I tests resulted in a fracture surface that is flat and smooth, with a clear decoloring at the edge of the crack (along the outer circumference of the tubular). See Table 5.10.

Proportional multiaxial loading, results in a saw-tooth shaped fracture surface with variaties in the extremety of this shape. Table 5.11 demonstrates how the different load combinations resulted in varieties of the saw-tooth shaped fracture surfaces.

Non-proportional loading in general, results in a smoother fractures surface. Distinction can however be made between the fracture surface as a result of a 90 degrees phase shift induced non-propotionality and frequency induced non-propotionality.
With a 90 degrees phase shift, the fracture surface is relatively flat. Depending on the load level that is applied, this surface can show grooves initiated at the weld toe at the outer circumference of the tube. Unlike the propotional fatigue failures, these grooves do not tend to grow through thickness (resulting into a saw-tooth shaped fracture surface). Instead, they transition towards a more flat and smooth fracture surface. See Table 5.12.

Frequency induced non-proportionality leads to a different fracture mechanism. Unlike the other load cases, this load case results into a curved fracture surface. The fracture surface is no longer flat and straight but shows curvature in the through thickness profile of the crack. See Table 5.13 for clarification.

5.7.6.2 Explanation of observations

Multiaxiality introduces an interaction between different damage mechanism. The combined effect of these damage mechanisms, over time, is of influence on the eventual manifestation of the fatigue crack. Mode I crack growth is governed by the normal stress (imposed bending) and Mode III crack growth is governed by the shear stress (imposed torsion).

When the normal and shear stress peaks occur simultaneously, the material is exposed to a loading which has its critical fracture plane at a 45 degrees angle (cf. Section 2.2.1). Crack growth is facilitated since a maximum crack opening is introduced at the same instant. This explains the clear saw-tooth shaped fracture surface under proportional multiaxial loading.

Table 5.10: Mode I fracture surfaces

Mode I	
Pure bending	*Pure tension*
	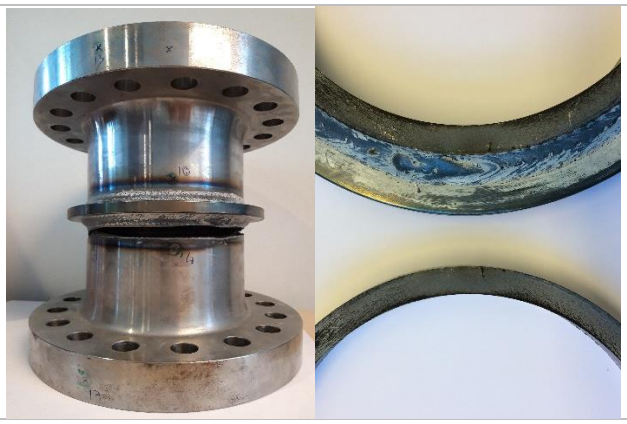
Test 1	Test 3
$\Delta\sigma = 175\ MPa$	$\Delta\sigma = 320\ MPa$

With phase shift induced non-proportionality, the maximum shear stress and normal stress occur sequentially. In addition, when either one reaches its maximum value the other stress component is at its neutral (mean) value. Therefore, the fracture mechanisms also occurs sequentially. By definition, the crack is initiated at the weld toe. Initiation and early crack growth are governed by shear which explains the grooves at the outer circumference of the tubular. When the crack is growing

through thickness, the governing crack growth mechanism changes to Mode I (crack opening). This explains the transition from a grooved fracture surface at the outer edge towards a more smooth and flat fracture surface at the inner edge.

Frequency induced non-proportionality introduces several fluctuations between the governing fracture mechanism, during one load cycle. In contrast to phase shift induced non-proportionality, where the damage mechanism is changing ones per load cycle, the selected frequency difference between the two load components introduced a changing orientation of the fracture surface over time. This lead to the observed curvature in the through thickness of the fatigue crack.

Table 5.11: Fracture surfaces resulting from combined in-phase loading (Mode I & Mode III)

Mode I & Mode III Multiaxial in-phase			
			
Test 16	Test 28	Test 24	Test 19
$\Delta\sigma = 240\ MPa$	$\Delta\sigma = 200\ MPa$	$\Delta\sigma = 220\ MPa$	$\Delta\sigma = 200\ MPa$
$\Delta\tau = 139\ MPa$	$\Delta\tau = 115\ MPa$	$\Delta\tau = 127\ MPa$	$\Delta\tau = 115\ MPa$

Table 5.12: Fracture surfaces resulting from combined out-of-phase loading with 90 deg. phase shift (Mode I & Mode III)

Mode I & Mode III Multiaxial out-of- phase $\delta = 90\ deg$	
	
Test 21	Test 7
$\Delta\sigma = 260\ MPa$	$\Delta\sigma = 240\ MPa$
$\Delta\tau = 150\ MPa$	$\Delta\tau = 139\ MPa$

Table 5.13: Fracture surfaces resulting from combined out-of-phase loading with freq. Difference (Mode I & Mode III)

Mode I & Mode III **Multiaxial frequency ratio $f_\sigma : f_\tau = 1:3$**		
		
Test 30	Test 31	Test 29
$\Delta\sigma = 210\ MPa$	$\Delta\sigma = 210\ MPa$	$\Delta\sigma = 225\ MPa$
$\Delta\tau = 121\ MPa$	$\Delta\tau = 121\ MPa$	$\Delta\tau = 130\ MPa$

5.7.6.3 Conclusion

The discussed observations allude that analysis of the fracture surface provides information about the endured load combination and level of multiaxiallity. This require further investigation and validation but appears a worthwhile finding to pursue. Such knowledge can be used to improve designs and validate design assumptions. It could provide a means to identify critical structural details from inspection of marine structures. Insight into the level of multiaxiallity is also valuable, since this dissertation has demonstrated its significant effect on fatigue resistance reduction.

5.8 Comparative study

For application of multiaxial fatigue methods, uniaxial fatigue resistance curves of the individual stress components are required. Most methods use this uniaxial resistance as a reference case in the model formulation for mixed Mode I and Mode III. Pure Mode I and pure Mode III tests were included in the test matrix of the tubular specimens, cf. Section 5.7.1 and 5.7.2. In the comparative study that follows the shear fatigue resistance curve from Figure 5.20 is used. The validity of using a Mode III SN curve based on such a limited number of data was checked by establishing an artificial shear fatigue resistance curve by scaling the experimentally obtained Mode I SN curve (cf. Section 5.5.1). Due to the apparent high welding quality of the tubular specimens it was decided to consider the least conservative SN curve (including test results in pure bending and pure tension).

For a fillet welded tube-to-flange connection, FAT 71 (σ) and FAT 80 (τ) are advised by IIW and Eurocode 3. The ratios between slope m and $log\ C$ of these SN curves have been used to scale the Mode I hexapod data to an artificial Mode III SN curve. The used scaling ratios are 1.7 and 1.3 for slope m and $log(C)$ respectively. In Table 5.14 the SN parameters of this artificially determined Mode III SN curve are listed and compared to the SN parameters of the other experimentally deterimed SN curves.

Table 5.14: SN-parameters of the Mode I and Mode III reference curves that were established within this dissertation, highlighting the considered reference SN-curves for the data analysis

SN - curve	m	$Log(C)$
FAT 71 (Mode I) – mean values	3	12.3
FAT 80 (Mode III) – mean values	5	16.2
Hexapod data Mode I		
hexapod tests incl. bending and tenstion	7.7	24.2
hexapod tests incl. bending	10.0	30.0
Hexapod data Mode III		
hexapod tests incl. runout	6.3	20.8
Hexapod tests excl. runout	14.6	41.6
Scaled reference SN	12.7	32.3

5.8.1 Recommendations and guidelines

Recommendations and guidelines from IIW, Eurocode and DNV-GL are widely accepted approaches in engineering practice. To demonstrate their performance under multiaxial conditions, a variety of comparisons have been made.

5.8.1.1 Analysis based on literature data

First, lifetime estimates were generated in accordance with IIW, Eurocode and DNV-GL and compared with the reference data as presented in Section 5.5.1. This data includes fatigue resistance under uniaxial mode I loading, uniaxial mode III loading, multiaxial in-phase loading and multiaxial out-of-phase loading (i.e. 90 degrees phase shift). For lifetime estimation, reference SN curves were established through linear regression analysis of the selected data (cf. Figure 5.14). This data was corrected for $LR = 0.1$. See Figure 5.30 for the outcome of this comparison. The effect of using these FAT class deviating linear regression curves as reference SN curves, was demonstrated by determining the lifetime estimates with the mean FAT based SN curves. See Figure 5.31.

It can be observed that the IIW recommendation provides rather conservative results under non-proportional loading. This can be attributed to the advised reduction of the Critical Value (i.e. CV value) from 1.0 to 0.5 for non-proportional loading (cf. Section 2.3.3.2). Therefore, the comparisons were also performed without consideration of this CV reduction. See Figure 5.32 and Figure 5.33. An improved correspondence was found between the lifetime estimates and the experimental results, confirming the level of conservatism introduced by consideration of this CV reduction.

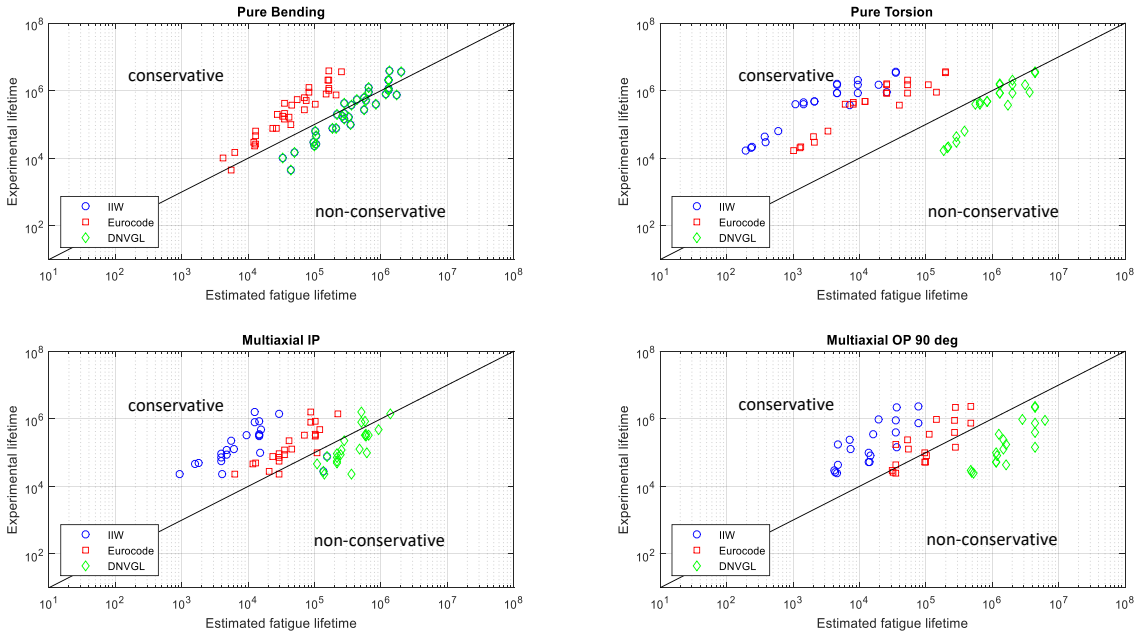

Figure 5.30: Comparison of the lifetime estimates in accordance with IIW, Eurocode and DNV-GL versus experimental lifetime of the multiaxial fatigue data set from literature (cf. Section 5.5.1); Nominal stress based considering the recommended SN reference curves.

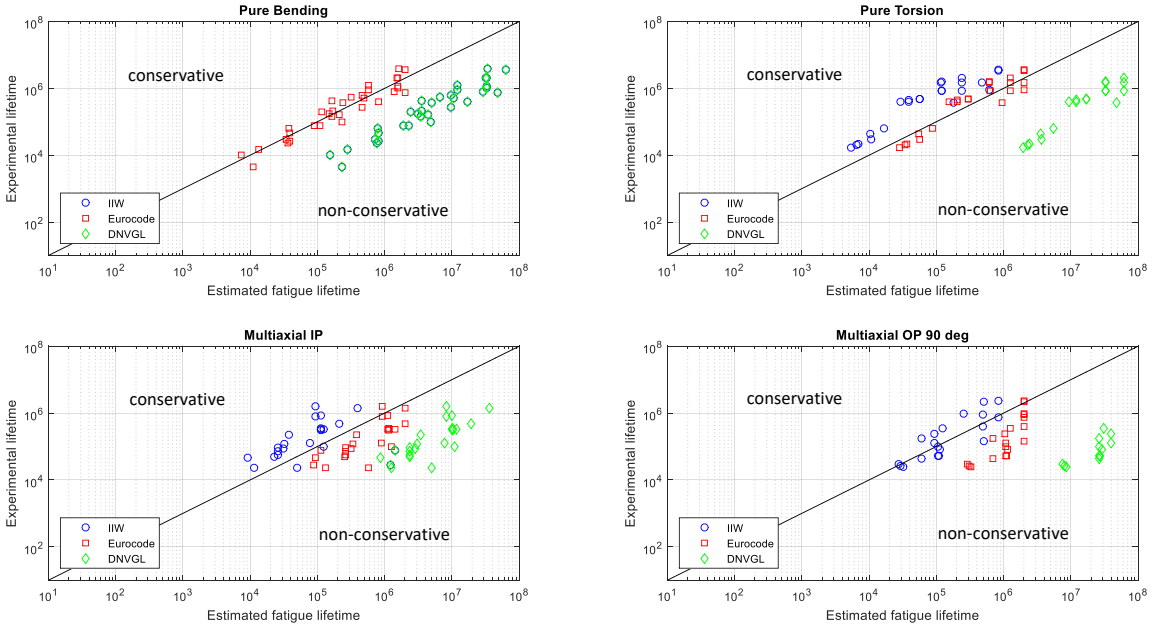

Figure 5.31: Comparison of the lifetime estimates in accordance with IIW, Eurocode and DNV-GL versus experimental lifetime of the multiaxial fatigue data set from literature (cf. Section 5.5.1); Nominal stress based considering SN reference curves based on linear regression analysis of the literature data.

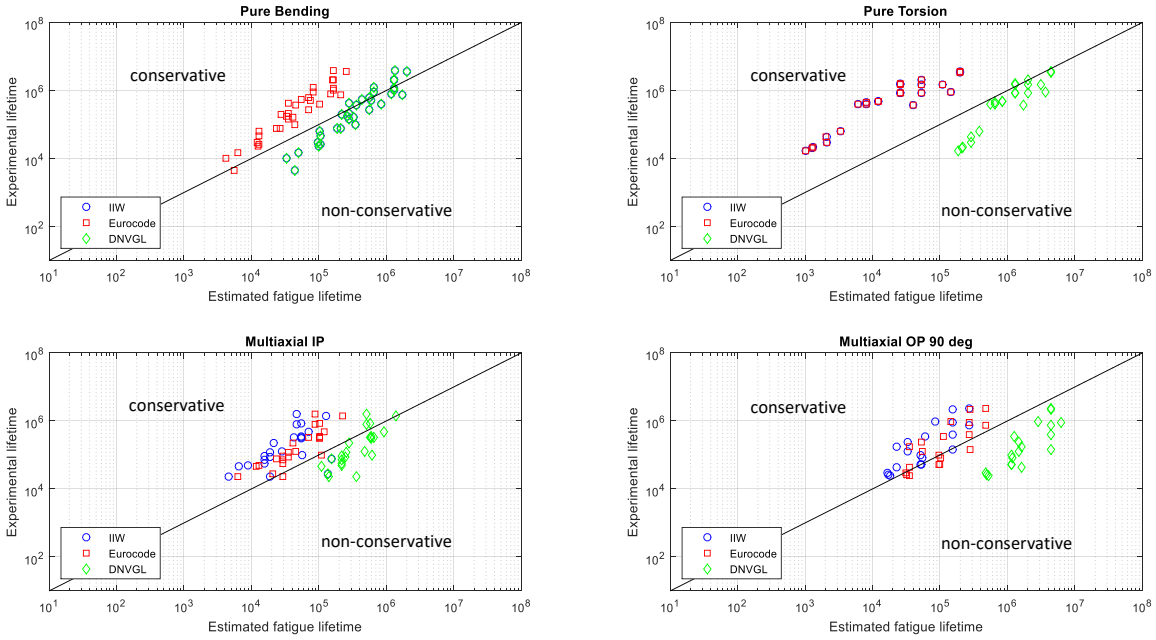

Figure 5.32: Comparison of the lifetime estimates in accordance with IIW, Eurocode and DNV-GL versus experimental lifetime of the multiaxial fatigue data set from literature (cf. Section 5.5.1); Nominal stress based considering the recommended SN reference curves and uncorrected CV value (CV=1) for non-proportional loading.

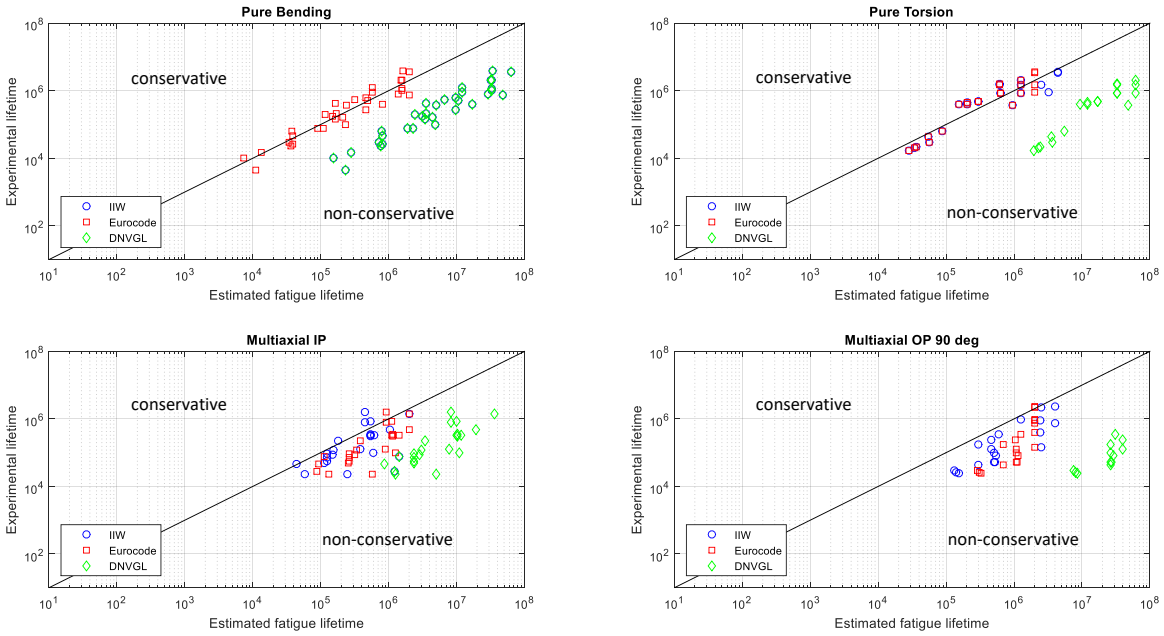

Figure 5.33: Comparison of the lifetime estimates in accordance with IIW, Eurocode and DNV-GL versus experimental lifetime of the multiaxial fatigue data set from literature (cf. Section 5.5.1); Nominal stress based considering SN reference curves based on linear regression analysis of the literature data and uncorrected CV value (CV=1) for non-proportional loading.

5.8.1.2 Literature data based conclusions

A variety of conclusions could be drawn from analysing the in Section 5.5.1 selected data set in accordance with the recommendations and guidelines from IIW, Eurocode and DNV-GL:

- DNV-GL consistently provides the most under-conservative lifetime estimates and IIW the most conservative.
- For the non-proportional load case Eurocode provides the best agreement with the data.
- For the pure bending (Mode I) data the lifetime estimates from IIW and DNV-GL are the same due to the fact that they both assess lifetime based on principal stress under these conditions.
- IIW makes a conservative assumption by reducing the CV value from 1.0 to 0.5 for non-proportional load cases. Disregarding this CV reduction provides lifetime estimates that are less conservative and with a better correspondence to the selected experimental data.
- When linear regression based SN curves are used for lifetime estimation, the fatigue lifetime estimates become less conservative as with the recommended SN curves. This demonstrates that there are discrepancies between the selected data from literature and the data that was used to establish these guidelines. It could indicate that the selected data set from literature originates from the upper bound of the larger data set that was used to generate these guideline/code recommended SN curves.

5.8.1.3 Analysis based on hexapod results

To get an understanding of the performance of the recommended practices and guidelines in relation to the hexapod data, similar analyses as in Section 5.8.1.1. have been performed. Instead of making use of the reference data set from literature, the experimentally obtained hexapod data was used.

Lifetime estimates were generated in accordance with IIW, Eurocode and DNV-GL and compared to the experimental results obtained in the hexapod. See Figure 5.34 for the outcome of this comparison. The hexapod results do not include a sufficient amount of pure mode III data but an additional non-proportional multiaxial load case is included (i.e. frequency induced non-proportionality). For lifetime estimation, the used reference curves are the experimentally obtained SN curve for Mode I loading and the experimentally obtained SN curve for Mode III (cf. Section 5.7.1 and 5.7.2). The effect of using these FAT class deviating linear regression curves as reference SN curves, was demonstrated by also determining the lifetimes with the recommended FAT based mean SN curves. See Figure 5.35.

The lifetime estimates in accordance with IIW were obtained through consideration of a CV (Critical Value) reduction under non-proportional loading (cf. Section 2.3.3.2). This is a conservative recommendation. Therefore, the comparison has been repeated with exclusion of this consideration, i.e. $CV = 1$ under non-proportional loading. See Figure 5.36 and Figure 5.37. Just like in Section 5.8.1.1., an improved correspondence between lifetime estimates and experimental results was found.

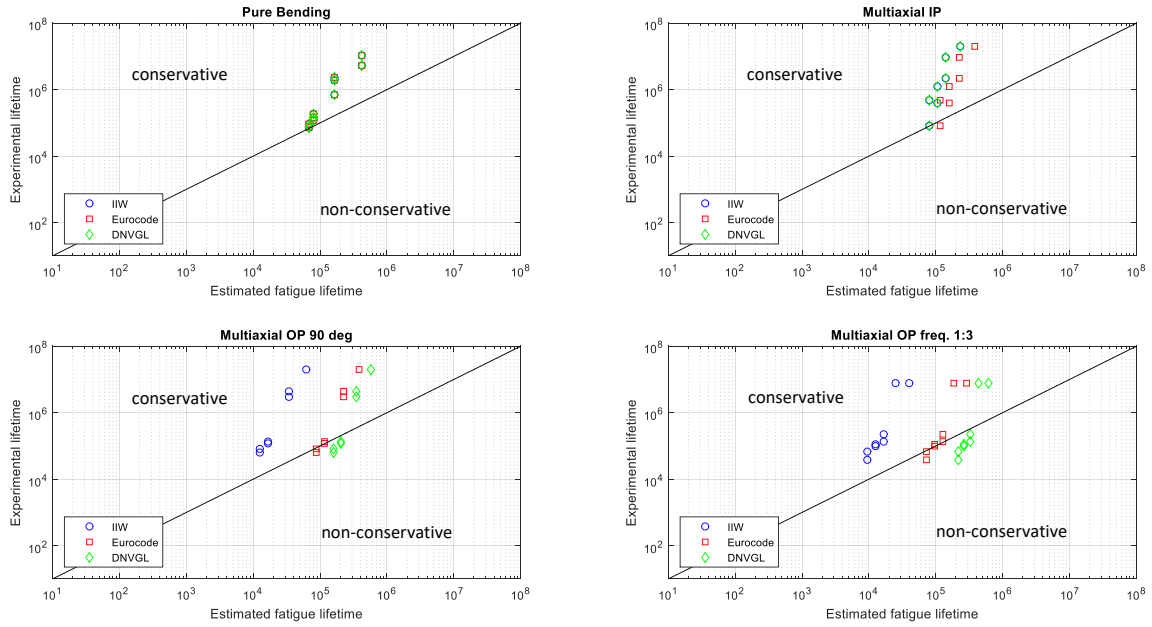

Figure 5.34: Comparison of the lifetime estimates in accordance with IIW, Eurocode and DNV-GL versus experimental hexapod results; Nominal stress based considering the recommended SN reference curves.

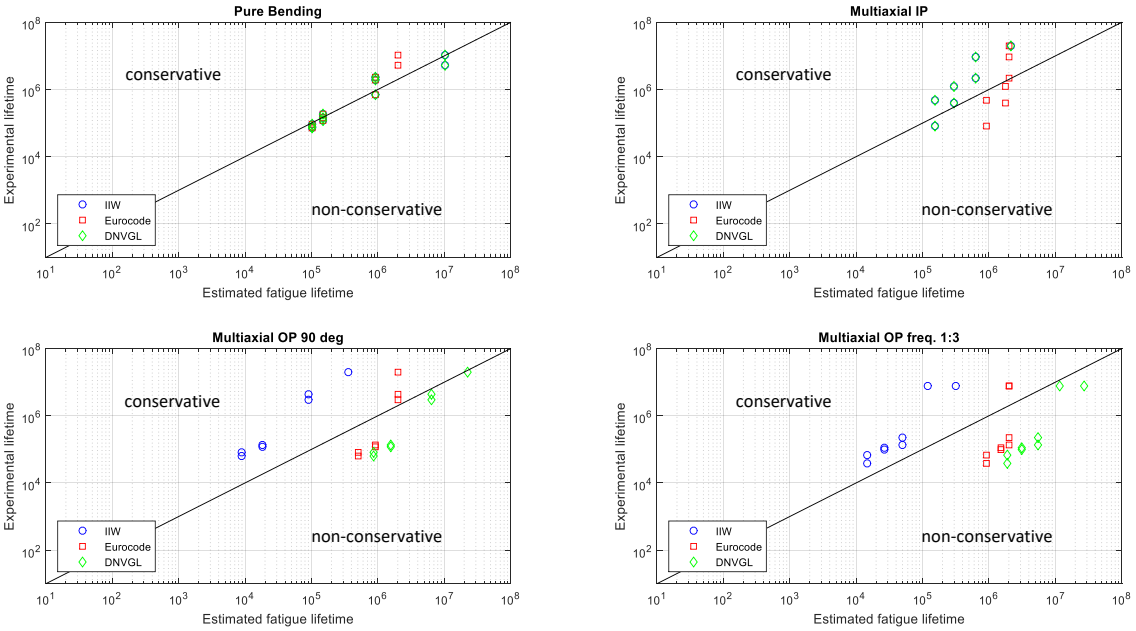

Figure 5.35: Comparison of the lifetime estimates in accordance with IIW, Eurocode and DNV-GL versus experimental hexapod results; Nominal stress based considering SN reference curves based on linear regression analysis of the hexapod data.

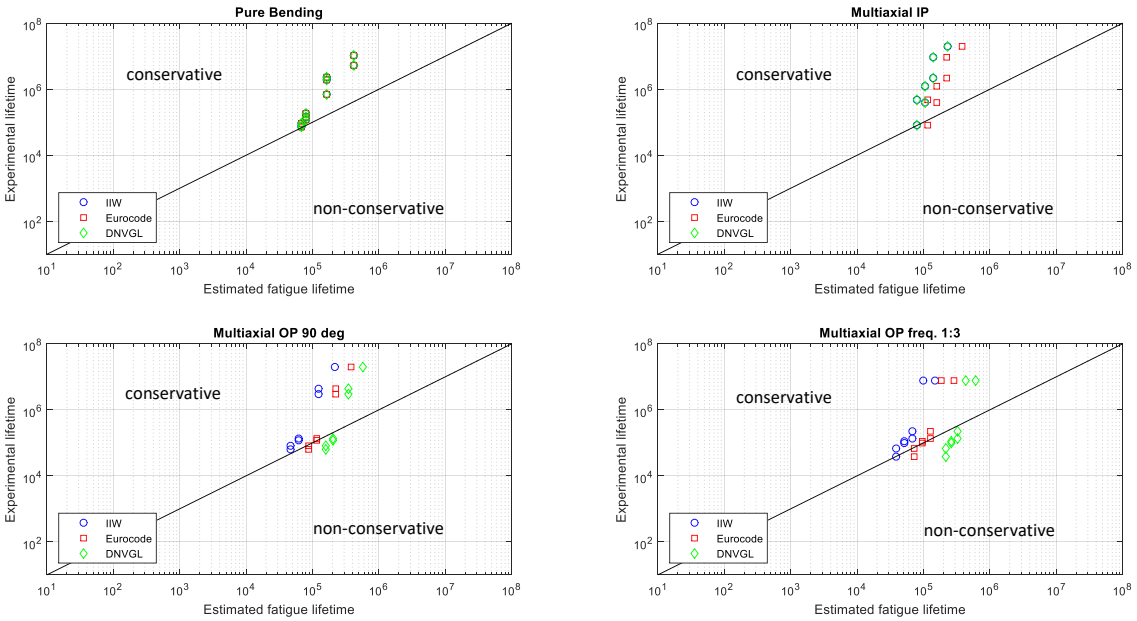

Figure 5.36: Comparison of the lifetime estimates in accordance with IIW, Eurocode and DNV-GL versus experimental hexapod results; Nominal stress based considering the recommended SN reference curves and uncorrected CV value (CV=1) for non-proportional loading.

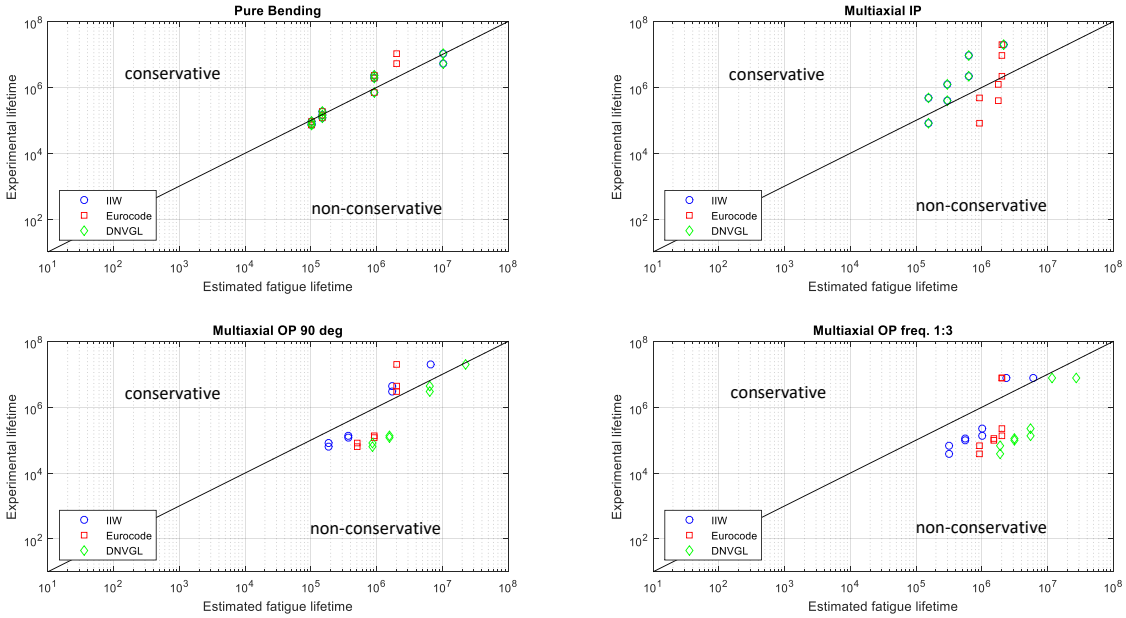

Figure 5.37: Comparison of the lifetime estimates in accordance with IIW, Eurocode and DNV-GL versus experimental hexapod results; Nominal stress based considering SN reference curves based on linear regression analysis of the hexapod data and uncorrected CV value (CV=1) for non-proportional loading.

5.8.1.4 Hexapod data based conclusions

The tests that were completed in the hexapod include a rare additional non-proportional load case considering frequency induced non-proportionality. Apart from the interest in how recommended guidelines and codes account for this type of non-proportionality, there is an interest in benchmarking the obtained hexapod data. Recommended guidelines and codes use reference SN curves that were once established with a large set of experimental data, compiled from different sources. From the analysis discussed and presented in Section 5.8.1.3 the following conclusions could be drawn:

- The correlation between lifetime estimate and experimental fatigue life improves when the reference SN curves are based on the considered data set. This demonstrates that the reference SN curves recommended in the considered guidelines/codes are not representative for the hexapod data set. This can be attributed to the significantly high welding quality of the tubular specimens which affects the slope of their SN curve.
- For the non-proportional load cases, the differences in lifetime estimates of the three considered guidelines/codes become larger when the reference SN curves are based on linear regression analysis of the data.
- IIW makes a conservative assumption by reducing the CV value from 1.0 to 0.5 for non-proportional load cases. Disregarding this CV reduction provides lifetime estimates that are less conservative and with a better correspondence to the selected experimental data.
- The relationship between experimental fatigue life and estimated lifetime shows a clear discrepancy for the comparisons using the code/guideline recommended SN curves. This is the result of the significantly higher slopes of the reference fatigue SN curves in comparison to the slopes of the reference SN curves that are based on the hexapod data.
- IIW consistently provides conservative lifetime estimates and DNV-GL under-conservative lifetime estimates for the non-proportional load cases. Under non-proportional loading, Eurocode provides the best correspondence with the considered data.

5.8.2 Multiaxial fatigue models

A selection of multiaxial fatigue models (cf. Section 5.1) has been compared to the in Section 5.5 presented experimental data from literature, and to the hexapod data presented in Section 5.7. More background information about the selected models can be found in Chapter 2. The objective of this comparison was to identify to what extend the lifetime estimates from the selected multiaxial fatigue models match the experimental results.

In order to apply the selected multiaxial fatigue models some interval and limit values had to be set. Henceforth, the presented MWCM results were obtained with a ρ_{lim} set to 1.7. For the critical plane search an interval of 15 degrees was used. This applies to the MWCM, MCSM and SSCP method. For the data from literature, the SCFs are set to $k_\sigma = 3.9$ in pure Mode I and $k_\tau = 1.9$ in pure Mode III. Their corresponding SSCFs are in pure Mode I $K_\sigma = 1.6$ and in pure Mode III $K_\tau = 1.1$. These values correspond with the tubular specimen from Sonsino & Kueppers, 2001 (cf. Table 5.8). For the hexapod data, the SCFs are set to $k_\sigma = 2.1$ in pure Mode I and $k_\tau = 1.8$ in pure Mode III. Their corresponding SSCFs are $K_\sigma = 1.2$ and $K_\tau = 1.1$.

5.8.2.1 Analysis based on literature data

The selection of experimental data from literature is based on test results that are widely accepted and used within the community of fatigue and fracture mechanics. Therefore, the lifetime estimates

from the selected multiaxial fatigue models are first compared to this data set. The comparison considers SN reference curves based on the literature data. See Figure 5.38.

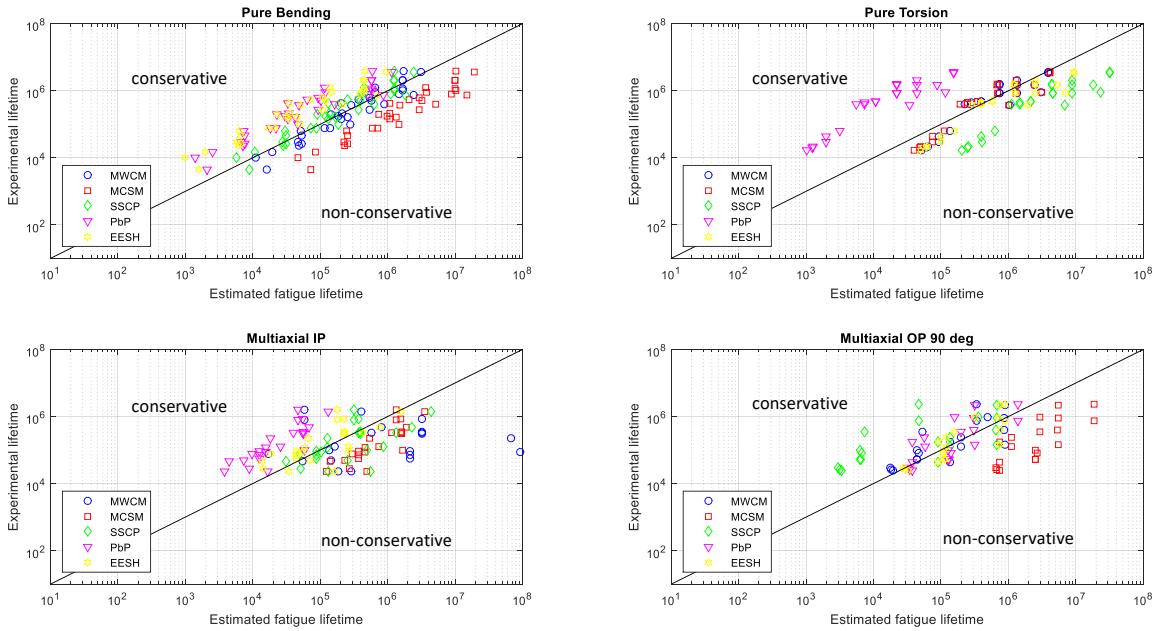

Figure 5.38: : Comparison of the lifetime estimates of the selected multiaxial fatigue models in comparison to the selected reference data from literature (cf. Section 5.5.1)

5.8.2.2 Literature data based conclusions

Several observations and conclusions could be drawn from the analysis presented in Figure 5.38:

- In pure bending, the lifetime estimates show the best agreement with the selected data from literature. The MCSM consistently provides under-conservative lifetime estimates whilst the PbP method and EESH provide consistently conservative lifetimes.
- For the uniaxial pure torsion load cases the MCSM, MWCM and EESH provide very similar lifetime estimates in close correspondence with the literature data. The SSCP method provides under-conservative lifetime estimates whilst the PbP method provides significantly conservative.
- Overal, the EESH shows the best results which is not surprising since a large part of the considered data set was used to develop this model.
- Under non-proportional multiaxial loading the discrepancies between lifetime estimates and test results increase significantly for the MWCM. The correlation between lifetime estimate and experimental results seems to have changed in comparison to the other load cases. This could be attributed to the critical plane definition.
- The selected models show significant discrepancies amongst each other under proportional and non-proportional multiaxial loading. Under proportional loading the PBP method provides most conservative lifetime estimates and MWCM most under-conservative. Under non-proportional loading the most conservative lifetime estimates are provided by the SSCP method and the most under-conservative by the MSCM.

5.8.2.3 Analysis based on hexapod results

The hexapod results that were obtained under various multiaxial loading conditions were compared to the lifetime estimated from the selected multiaxial fatigue models. The outcome of this comparison is shown in Figure 5.39.

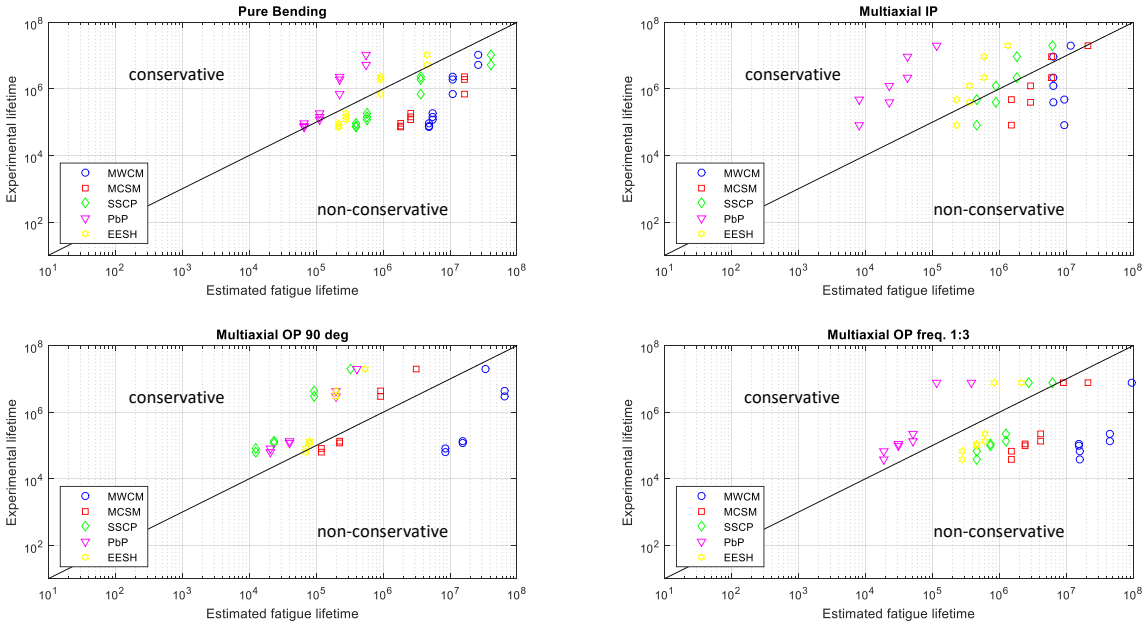

Figure 5.39: Comparison of the lifetime estimates of the selected multiaxial fatigue models in comparison to the hexapod results (cf. Section 5.7).

5.8.2.4 Hexapod data based conclusions

The following conclusions could be drawn from comparison of the hexapod results with the lifetime estimates of the selected multiaxial fatigue methods:

- A significant scatter, similar to the scatter with the literature data, is observed between the lifetime estimates of the various considered multiaxial fatigue models and the hexapod data. For pure bending, the scatter is least whilst for frequency induced non-proportional loading the scatter is largest.
- For all considered load cases, the PbP method provides conservative lifetime estimates.
- The MWCM applied to the multiaxial proportional (IP) load cases, shows hardly any variation in the estimated fatigue lives. The correlation between lifetime estimate and experimental result has changed in comparison to the other cases of multiaxiality. Such a change in correlation between lifetime estimate and experimental result, was also observed with the literature data (cf. 5.8.2.1, 5.8.2.2).

5.9 Discussion and Conclusions

The comparative study with the collected data and selected multiaxial fatigue methods resulted in various main observations which will be discussed here.

The correlation between lifetime estimate and experimental fatigue life improves when the reference SN curves are based on the considered data set. The reference SN curves recommended in the considered guidelines/codes are not representative for the hexapod data set. This can be

attributed to the significantly high welding quality of the tubular specimens which affects the slope of their SN curve.

Considering the hexapod data, IIW consistently provides conservative lifetime estimates and DNV-GL under-conservative lifetime estimates for the non-proportional load cases. Under non-proportional loading, Eurocode provides the best correspondence with the experimental data.

When the reference SN curves are based on the selected literature data, the fatigue lifetime estimates become less conservative as with the recommended SN curves from guidelines. This demonstrates that there are discrepancies between the selected data from literature and the data that was used to establish the recommended curves in the guidelines. It indicates that the selected data set from literature originates from the upper bound of the data set that was used to generate these guideline/code recommended SN curves.

Comparison of the selected models to the selected literature data shows that the EESH provides the best agreement between lifetime estimate and experimental data. This is however not surprising since a large part of the considered data set was used to develop this model.

Considering the literature data, the selected models show significant discrepancies amongst each other under proportional and non-proportional multiaxial loading. The PBP method provides consistently conservative lifetime estimates and MWCM under-conservative. Under non-proportional multiaxial loading the discrepancies between lifetime estimates and test results increase significantly for the MWCM. The correlation between lifetime estimate and experimental results seems to have changed in comparison to the other load cases. This could be attributed to the critical plane definition.

Both considered data sets show a significant scatter between the lifetime estimates of the various considered multiaxial fatigue models. For pure bending, the scatter is least whilst for frequency induced non-proportional loading the scatter is largest.

In Section 5.5.2 the interesting observation was made that the slope ratio (m_τ/m_σ) (i.e. the damage mechanisms between Mode I and Mode III) of the base material reference data and guidelines for welded joints from IIW and Eurocode shows a similar value. The base material reference data has a slope ratio of $18.01/13.23 = 1.4$. IIW and Eurocode recommend a slope ratio of $5/3 = 1.7$. The experimentaly tested tubular specimens in pure Mode I and pure Mode III also show this behaviour (cf. Section 5.8). If only pure bending tests are considerd the slope ratio of the hexapod data is $14.6/10 = 1.5$. Considering both the results in pure bending and tension, this ratio changes to $14.6/7.7 = 1.9$. From this observation it could be concluded that the data and guidelines are consistent amongst each other and describe the same type of the damage mechanisms in pure Mode I and pure Mode III.

The IIW recommendations introduce a large level of conservatism by reduction of the CV value from 0.5 to 1.0 for non-proportional load cases. This correction could be reconsidered since all analysed results within this study remained on the conservative side without consideration of this CV correction.

Since the SSF method requires a polynomial fit with experimental data to obtain the SSF function, this method is not included in the comparative study. This polynomial curve fitting requires a set of non-proportional multiaxial fatigue data from the material and joint of interest, including various phase angles. Both in the considered literature data and the hexapod data this information is lacking, which leads to exclusions of this method from the comparative study. This need for empirical curve fitting is a downside of the SSF method.

The SSCP method follows a combined approach, integrating the MWCM and MCSM. The MWCM and the MCSM define the critical plane differently (cf. Section 2.4.1.1 and Section 2.4.1.2). The

critical plane defines the (normal and shear) stress components that are eventually used in the fatigue criterion. The multiaxiallity factor ρ that is used to determine the modified Wöhler curve (in accordance with MWCM), is based on the stress components that are defined in accordance with the MCSM. This merge of models results in a different agreement of the fatigue lifetime estimates with the considered data. With exception of the torsion data from literature, the SSCP method provides more conservative lifetime estimates than the MWCM. In comparison to the literature data the SSCP method provides less conservative results than the MCSM and more conservative results in comparison to the hexapod data. This indicates a consistent discrepancy and could be attributed to the significant difference between the resistance behaviour of the considered data and the data that has been used to develop this method.

PDMR multiaxial cycle counting (cf. Section 2.5.4) and the MLP equivalent stress formulation (cf. Section 2.6.5) have been specifically developed for variable amplitude loadings. Their features come to show to their advantage when applied to variable amplitude load cases. Such load cases were initially part of the scope of work for this dissertation but eventually removed due to restrictions on time and resources within the project. Therefore, this dissertation only covers constant amplitude loading. Although the procedures were developed, incorporation of PDMR multiaxial cycle counting and the MLP equivalent stress formulation are redundant in this comparative study.

5.10 References

Busby, J. T., Hash, M. C., & Was, G. S. (2005). The relationship between hardness and yield stress in irradiated austenitic and ferritic steels. *Journal of Nuclear Materials*, *336*(2–3), 267–278. https://doi.org/10.1016/j.jnucmat.2004.09.024

DNV-GL. (2005). *Fatigue design of offshore steel structures*. *Recommended Practice*.

European Standard. (2005). *Eurocode 3: Design of steel structures - Part 1-9: Fatigue*.

Hobbacher, A. (2015). *Recomendations for Fatigue Design of Welded Joints and Components*. *IIW document IIW-2259-15 ex XIII-2460-13/XV-1440-13* (Second Edi). https://doi.org/10.1007/978-3-319-23757-2

Margetin, M., Ďurka, R., & Chmelko, V. (2016). Multiaxial fatigue criterion based on parameters from torsion and axial S-N curve. *Frattura Ed Integrita Strutturale*, *10*(37), 146–152. https://doi.org/10.3221/IGF-ESIS.37.20

Sonsino, C. M., & Kueppers, M. (2001). Multiaxial fatigue of welded joints under constant and variable amplitude loadings. *Fatigue and Fracture of Engineering Materials and Structures*, *24*, 309–327.

Verreman, Y., & Nie, B. (1996). Early development of fatigue cracking at manual fillet welds. *Fatigue and Fracture of Engineering Materials and Structures*, *19*(6), 669–681. https://doi.org/10.1111/j.1460-2695.1996.tb01312.x

Yousefi, F., Witt, M., & Zenner, H. (2001). Fatigue strength of welded joints under multiaxial loading: experiments and calculations. *Fatigue and Fracture of Engineering Materials and Structures*, *24*, 339–355.

Yung J.Y., & Lawrence, F. V. (1989). *Predicting the fatigue life of welds under combined bending and torsion*. *Biaxial and Multiaxial Fatigue*.

6 Conclusions

"One is never afraid of the unknown, one is afraid of the known coming to an end."
– Jiddu Krishnamurti

From the work presented in this dissertation various observations were made leading to the following conclusions:

- Proportional multiaxial fatigue data shows more scatter than multiaxial non-proportional loading, whether it be phase shift induced or frequency induced. This could be explained by the fact that proportional loading results in only one most critical location/plane whilst non-proportional loading results in a moving critical location/varying criticial plane orientation; This distribution of probabilities of failure leads to a reduced data scatter. This would mean that in engineering practice, multiaxial proportional loading should be considerd more critical or governing as a result of a lower probability of fatigue failure.
- Multiaxial frequency induced non-proportional loading shows a stronger damage mechanism than phase shift induced non-proportional loading on the basis of Von Mises stress, principal stress and normal stress.
- One could say that $logC$ represents the fatigue strength/sensitivity/severity/intensity of multiaxial fatigue and the slope m the load-path dependent damage mechanism. Considering the different load cases with respect to these two different aspects shows that $logC$ has the highest value for proportional multiaxial loading, followed by non-proportional loading (90 degrees phase shift and then frequency induced) and pure Mode I loading. Slope m is steepest for proportional and phase shift induced non-proportional loading (they show equal slopes), followed by frequency induced non-proportionality and pure Mode I loading.
- From the results with experimentally tested tubular specimens under multiaxial constant amplitude loads a variety of conclusions could be drawn:
    - There is a distinct fatigue damage mechanism between phase shift induced non-proportional loading and frequency induced non-proportional loading.
    - In-phase proportional loading is a form of phase shift induced non-proportional loading and corresponding to the same damage mechanism.
    - The slope ratio (m_τ/m_σ) of the base material reference data shows a similar ratio as the recommended reference SN curves in the considered guidelines, and the experimentally tested tubular specimens. From this observation it can be concluded that the results are consistent amongst each other and describe the same type of damage mechanism in pure Mode I and pure Mode III loading.
- From the analysed guidelines/codes and multiaxial fatigue methods it could be concluded that:
    - When dealing with non-proportionality, DNV-GL consistently provides the most under-conservative lifetime estimates and IIW the most conservative.
    - For the pure bending (Mode I) data the lifetime estimates from IIW and DNV-GL are the same due to the fact that they both assess lifetime based on principal stress under these conditions.

- The relationship between experimental fatigue life and estimated lifetime shows a clear discrepancy for the comparisons using the guidelines/codes recommended SN curves. This is the result of the significantly higher slopes of the reference fatigue SN curves in comparison to the slopes of the reference SN curves that are based on the hexapod data.
- The EESH shows the best agreement with the literature data. This is not surprising since a large part of the considered data set was used to develop this model.
- The selected multiaxial fatigue models show significant discrepancies amongst each other under proportional and non-proportional multiaxial loading. The PbP method provides most conservative lifetime estimates and MWCM most under-conservative.
- IIW makes a conservative assumption by reducing the CV value from 1.0 to 0.5 for non-proportional load cases. Disregarding this CV reduction provides lifetime estimates that are less conservative and with a better correspondence to the selected experimental data.
- The correlation between lifetime estimate and experimental fatigue life improves when the reference SN curves are based on the considered data set. This demonstrates that the reference SN curves recommended in the considered guidelines/codes are not representative for the hexapod data set. This can be attributed to the significantly high (offshore) welding quality of the tubular specimens which affects the damage mechanism.

7 Recommendations for future research

"I tell myself that anyone who says he has finished a canvas is terribly arrogant."
– Claude Monet

The work presented in this dissertation is a stepping stone to better understanding of multiaxial fatigue. The findings and learnings from the performed experimental work provide insights into the phenomenon of multiaxial fatigue in welded marine structures, whilst the comparative study provides insights into the assessment of multiaxial fatigue lifetime for such structures.
Scientific research is however perpetual and therefore several recommendations will be given here for improvement and further investigation:

- One of the most essential features of marine structures is their exposure to stochastic and variable amplitude loading. It is therefore of essence to extend the presented work by adding experimental data that was exposed to representative loadings of marine structures or marine structural details.
- Time domain fatigue assessment methods were selected for the in this dissertation presented comparative study. In the spectral domain difficulties are encountered when facing non-proportional constant amplitude loading. It can have however various advantageous (cf. Section 2.3.1), particularly when variable or stochastic loadings are being considered. Recent developments also show multiaxial fatigue methods that are modified for application in the spectral domain.
- From the test results with the welded tubular specimens it is demonstrated that welding quality has a significant effect on fatigue resistance. The welding quality, governed by welding procedure and welding parameters, is of significant influence and should ideally be incorporated in the fatigue lifetime assessment.
- The with the hexapod generated Mode III fatigue resistance curve is based on a statistically insufficient number of test results (cf. Section 5.7.2). The generated fatigue resistance curve should be verified by performing additional tests at the three considered load levels.
- Extending the experimental tubular data set with additional test results, would improve the accuracy of the generated fatigue resistance curves. It would enable to perform a more refined statistical analysis and reinforce the drawn conclusion in this work.
- Due to restrictions in testing frequency, few data has been collected in the high cycle fatigue region ($1 \cdot 10^7$ cycles or higher). From the results that were collected (experimentally and from literature), a changing slope could be observed towards this high cycle fatigue region. Collecting more experimental data for this region would support the development of methods that provide more accurate fatigue lifetime estimates within this region. Due to the limited amount of data, unnecessary conservatism is typically observed in the lifetime estimates within this region.
- The number of bar specimens that were tested with an intact geometry were insufficient to make a linear regression of their fatigue resistance (cf. Section 4.3). In this dissertation, literature data of intact geometries is compared to the bar specimen data with artificial defects. A distinct slope change is observed between these two data sets. It is assumed that

this change is caused by a change in damage mechanism (due to the presence or absence of a surface defect). This should be verified by collecting additional tests results with intact bar specimens such that a linear regression of its fatigue resistance can be made.

- It was initially planned to include pure Mode III tests with bar specimens in the work of this dissertation. Difficulties were however experienced with plastic deformations of the specimen and availability of a suitable test bench. Therefore, it was decided to first complete the test results under pure Mode I loading. Time and resources did not allow to continue with pure Mode III tests afterwards. It would however add valuable information; not only since pure Mode III data is scare, but also since it would provide Mode I and Mode III data of three distinct conditions of the same joint geometry and material (i.e. intact bar, bar with artificial elliptically shaped surface defect, welded tubular).
- Stress values close to yield and the fatigue limit are not very suitable for linear regression analysis. The presented results in this work can be improved by the use of more refined models for data analysis (e.g. fatigue limit model). This refinement can be achieved and increased by adding more test results to the data set.

8 Acknowledgements

"Educating the mind without educating the heart is no education at all."
– Aristotle

This work is the physical remaining of a huge process that I have been going through over the past few years; Personally and professionally. My reasons for pursuing a PhD have been the search for personal and professional growth in an environment that allows for liberty and autonomy when going through this process. It resulted in experiences of high peaks and low troughs of which some people are more aware than others. Going through all these moments has taught me the art of transformation, persistence, and overcoming challenges. I am very grateful for the support, guidance, help, efforts, patience and feedback that I received from some people in particular. I would like to dedicate this Section to expressing them my sincere gratitude and acknowledgement.

Without the enthusiasm, efforts and qualities of my promoter Professor Mirek Kaminski the 4D-Fatigue project would not have been materialized, and the Technical University Delft would not have procured the unique and impressive beast of a Hexapod. He gave me the honour to become the first PhD candidate that used this test rig for multiaxial fatigue testing purposes; But not only that; He involved me in the entire process, from setting up the design requirements to procurement, engineering, installation and testing. This involvement has given me valuable teachings and experiences, which I would not have attained without his trust. Apart from a very pleasant professional relationship, I have enjoyed the true personal contact he makes. I have really enjoyed his company and lively spirit during our meetings, travels, conferences and other undertakings. Mirek has a true talent for creating a team with a team spirit. I am very grateful for everything he has given me.

Next in line would be my co-promotor Henk den Besten from whom I have received a generous amount of intellectual support. His meticulous and critical mind has provided me with constructive advice, suggestions and insightful comments. His calm and sincere personality have been very pleasant to work with and have given me an environment where I could express myself openly, also when moments were tough.

The work presented in this dissertation, contains a significant amount of experimental test results obtained with the hexapod. Without the hard work, dedication and muscle power of Gabriele Bufalari we would not have managed to complete this significant number of tests. He made enormous contributions to the activities related to the installation and operation of the hexapod. I want to express him my deep appreciation for all he has done. Not only to collect the experimental data but also to achieve a good working relationship with the lab of Civil Engineering and an optimal hexapod performance, considering the significant restrictions we had in executing the envisioned tests.

Special thanks go to all the 4D-Fatigue participants and their representatives. First of all, for their financial support but also for their technical advice, moral support, trust and patience throughout all the developments in this project.

Since this research involved a large experimental scope of work, I have been in close contact with the Material Science department (TU Delft) and the Stevin Lab of Civil Engineering (TU Delft). At the Material science department I would like to thank Ton Riemslag en Elise Reinton for their willingness and cooperation to use the MTS fatigue test bench in their lab. Special thanks go also to Vera Popovich who has been so kind to spend some of her valuable time on assisting me with the analysis of the weld quality of the tubular specimens. At the department of Civil Engineering I would like to thank Peter de Vries and John Hermsen in particular, for their intensive involvement in facilitating and operating the hexapod in harmony with the surrounding offices and test setups.

During the final year of my PhD, I have been facilitated by Allseas, who offered me a part-time working position in the Hydro-Structural department while I was facing delays in the collection of experimental data. I would like to express my appreciation for the willingness and flexibility of André Steenhuis and Marijn Dijk in accommodating this solution.

Without the support, discussions, distractions and moments of distress and joy with family, friends and colleagues I would have never reached the point where I am now. I consider the personal growth throughout this entire PhD research as one of the most significant end results.

I would like to express a deep gratitude to my parents for always wanting the best for me and for making extensive efforts in providing me with the tools to achieve my goals. The chances and opportunities that they provided to me, all derive back to their love, care and interest in my well-being. Also my sister Iris and brother Jasper, each in their own way, have made efforts to support me and engage with me during this process.

This PhD project has been a bumpy ride and particularly in the difficult moments I have been able to lean on some of my close friends and seek their advice. They provided me a sounding board, mirror and listening ear. In particular, I would like to express my gratitude to Ermelinde, Dirk, Theresa, Eelco, Yari, Christien and Kiki. Not only for their heart-warming friendship but also for their support and contribution to my growth and development in the broadest sense of the word.

My colleagues, both at TU Delft and in the Hydro-Structural department of Allseas, have been of great help to put things into perspective and to remind me of the differences between an academic scene and engineering practice. Apart from work related discussions, I have really enjoyed our lunches and coffee breaks. They have contributed to fresh new thoughts and insights, combined with a good dose of fun.

9 Curriculum Vitae

9.1 Academic qualifications

- 2014 – 2019 | *PhD Candidate*
  Delft University of Technology

- 2012 – 2014 | *Master Offshore and Dredging Engineering*
  Delft University of Technology
  Specialisation: Ship and Offshore Structures

  Graduation project in collaboration with Total S.A. and NOV (APL)
  "Multiaxial fatigue analysis of a wheel-rail turret bearing for an FPSO offloading buoy"
  Cum Laude
  Nominated for Best Graduate award KIVI Offshore Technology 2014

- 2009 – 2012 | *Bachelor Mechanical Engineering*
  Delft University of Technology
  Minor: Management of Industrial Production

  Bachelor Research Project in collaboration with Nuclear Research & consultancy Group (NRG)
  "Irradiation embrittlement of nuclear reactor pressure vessel steels"
  Top Track 2012

  Energy project in collaboration with Tata Steel IJmuiden
  "Waste heat utilization at Tata Steel IJmuiden"
  Top Track 2011

- 2008 – 2009 | *Propaedeutic Industrial Design Engineering*
  Delft University of Technology

9.2 Working experience

- July 2019 – current | *Projectmanager*
  TNO - Structural Dynamics (BI&M unit)

- January 2018 – July 2019 | *R&D Engineer*
  Allseas Engineering B.V. – Hydrostructural (Innovations Department)

- 2014 – 2019 | *4D-Fatigue PhD research*
  Delft University of Technology
  PhD internship: École Normale Supérieure (ENS) de Cachan

- November 2013 – May 2014 | *MSc Graduation project*
  Under employment of Total S.A. and in collaboration with Bureau Veritas and APL NOV Norway

- August – October 2013 | *MSc Internship*
  Under employment of Total S.A. and in collaboration with Bureau Veritas and PD Technologies

10 Scientific contributions

10.1 Publications

"Validation of the corrected Dang Van multiaxial fatigue criterion applied to turret bearings of FPSO offloading buoys"
P.S. van Lieshout, J.H. den Besten, M.L. Kaminski
Ships and Offshore Structures 12(4):1-9, 2016
DOI:10.1080/17445302.2016.1182461

"Comparative study of multiaxial fatigue methods applied to welded joints in marine structures"
P.S. van Lieshout, J.H. den Besten, M.L. Kaminski
Conference paper ICMFF 11 2016
Frattura ed Integrità Strutturale 10(37):173-192, 2016
DOI: 10.3221/IGF-ESIS.37.24

"Numerical comparative study of multiaxial fatigue methods applied to welded joints in a container vessel"
G. Bufalari, M.L. Kaminski, P.S. van Lieshout, J.H. den Besten
Conference paper SoSDiD 2017

"Multiaxial Fatigue Assessment of Welded Joints in Marine Structures – Literature Overview of Progresses in Academia and Engineering Practice- "
P.S. van Lieshout, J.H. den Besten, M.L. Kaminski
International Shipbuilding Progress 65(4):1-43, 2017
DOI: 10.3233/ISP-170141

10.2 Conference contributions

- ICMFF11 June 2016
- DIG-It! Research Event 2017
- Teknowlogy Event November 2017
- ONR Navy Program Review 2017
- 34th – 42nd FPSO JIP Week

10.3 Media

TU Delft: https://www.youtube.com/watch?v=VrCiwrYaqsA&feature=youtu.be
TU Delft TV: https://www.youtube.com/watch?time_continue=138&v=z6vScQft8Qo

11 Propositions

1. Testing multiaxial fatigue with a hexapod overcomes limitations in degrees of freedom but capitulates under weaknesses in its foundation.

2. Even though strength comes in many forms and ways it is typically only acknowledged when it is expressed in a dominant and oppressing way.

3. The misconception about attracting more women in technology is that they would require an environment where they can behave like men.

4. Social media appear to connect us with the rest of the world whilst it disconnects us from our inner self, causing a disconnect with the world around us.

5. In modern society, being intelligent is typically associated with the recollection of facts, figures and conditioned behaviours whilst true intelligence features everything but such knowledge.

6. In academia, politics are always in the way of true synergy and cooperation.

7. Foreseeing the unforeseeable is what management demands when they ask you to make and stick to planning and budget.

8. Failing and exploration of what is unsuccessful beholds the core of success.

9. Great things are not achieved by people that are realistic, they are achieved by the 'crazy' visionary optimists.

10. Practice will always supersede theoretical understanding.

11. Frequency induced non-proportional loading introduces a distinct fatigue damage mechanism in comparison to phase shift induced non-proportional loading, with a more detrimental effect on fatigue lifetime.

12. In-phase proportional loading is a form of phase shift induced non-proportional loading and therefore shows the same damage mechanism.

13. Welding quality and material finish significantly affect fatigue resistance behaviour.